NATIONAL CENTER FOR EARTHQUAKE ENGINEERING RESEARCH
Headquartered at the State University of New York at Buffalo

ISSN 1088-3800

PB97-159552

Evaluation, Prevention and Mitigation of Pounding Effects in Building Structures

by

R.E. Valles and A.M. Reinhorn
State University of New York at Buffalo
Department of Civil Engineering
Buffalo, NY 14260

Technical Report NCEER-97-0001

February 20, 1997

This research was conducted at the State University of New York at Buffalo and was supported in whole or in part by the National Science Foundation under Grant No. BCS 90-25010 and other sponsors.

NOTICE

This report was prepared by the State University of New York at Buffalo as a result of research sponsored by the National Center for Earthquake Engineering Research (NCEER) through a grant from the National Science Foundation, and other sponsors. Neither NCEER, associates of NCEER, its sponsors, the State University of New York at Buffalo, nor any person acting on their behalf:

a. makes any warranty, express or implied, with respect to the use of any information, apparatus, method, or process disclosed in this report or that such use may not infringe upon privately owned rights; or

b. assumes any liabilities of whatsoever kind with respect to the use of, or the damage resulting from the use of, any information, apparatus, method, or process disclosed in this report.

Any opinions, findings, and conclusions or recommendations expressed in this publication are those of the author(s) and do not necessarily reflect the views of NCEER, the National Science Foundation, or other sponsors.

NATIONAL CENTER FOR EARTHQUAKE ENGINEERING RESEARCH
Headquartered at the State University of New York at Buffalo

Evaluation, Prevention and Mitigation of Pounding Effects in Building Structures

by

R.E. Valles[1] and A.M. Reinhorn[2]

Publication Date: February 20, 1997
Submittal Date: January 31, 1996

Technical Report NCEER-97-0001

NCEER Task Numbers 94-5101A and 94-3101A

NSF Master Contract Number BCS 90-25010

1 Research Associate, Department of Civil Engineering, State University of New York at Buffalo
2 Professor, Department of Civil Engineering, State University of New York at Buffalo

NATIONAL CENTER FOR EARTHQUAKE ENGINEERING RESEARCH
State University of New York at Buffalo
Red Jacket Quadrangle, Buffalo, NY 14261

PREFACE

The National Center for Earthquake Engineering Research (NCEER) was established in 1986 to develop and disseminate new knowledge about earthquakes, earthquake-resistant design and seismic hazard mitigation procedures to minimize loss of life and property. The emphasis of the Center is on eastern and central United States *structures*, and *lifelines* throughout the country that may be exposed to any level of earthquake hazard.

NCEER's research is conducted under one of four Projects: the Building Project, the Nonstructural Components Project, and the Lifelines Project, all three of which are principally supported by the National Science Foundation, and the Highway Project which is primarily sponsored by the Federal Highway Administration.

The research and implementation plan in years six through ten (1991-1996) for the Building, Nonstructural Components, and Lifelines Projects comprises four interdependent elements, as shown in the figure below. Element I, Basic Research, is carried out to support projects in the Applied Research area. Element II, Applied Research, is the major focus of work for years six through ten for these three projects. Demonstration Projects under Element III have been planned to support the Applied Research projects and include individual case studies and regional studies. Element IV, Implementation, will result from activity in the Applied Research projects, and from Demonstration Projects.

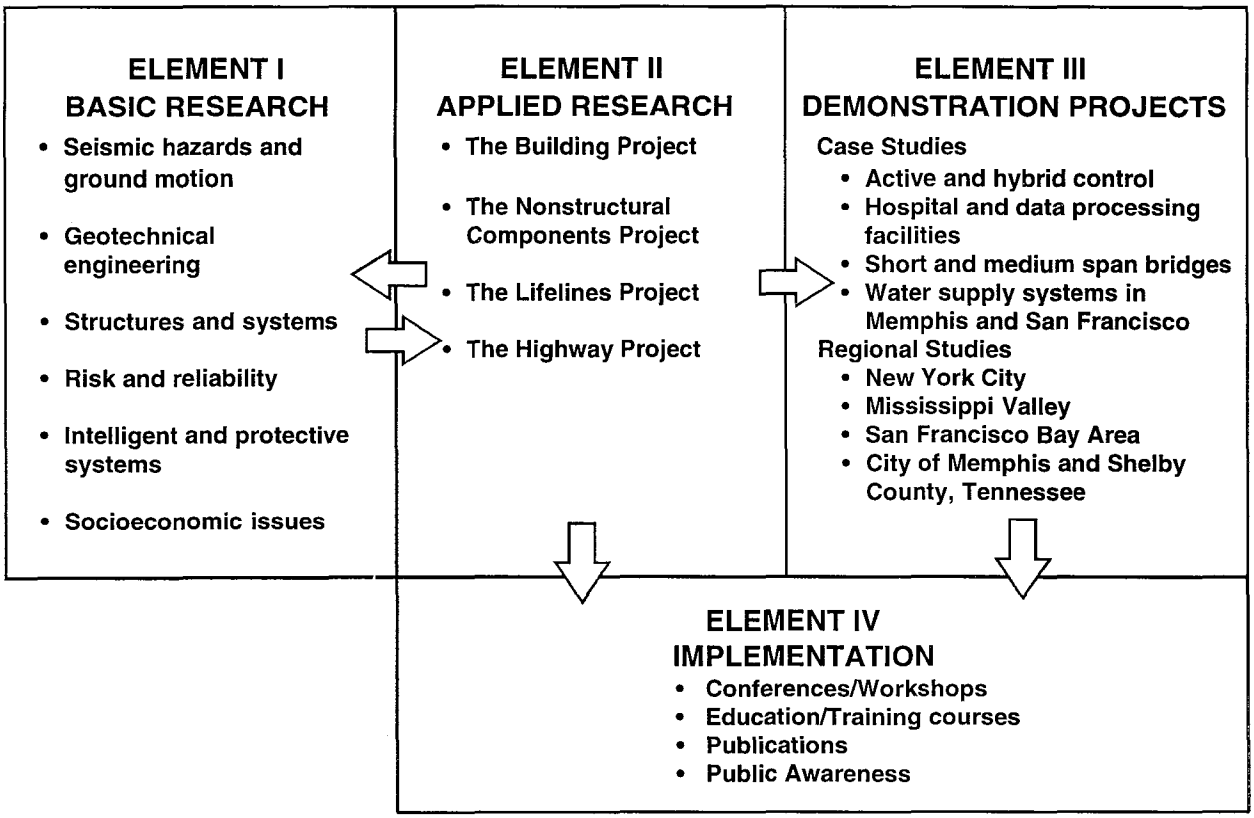

Research in the **Building Project** focuses on the evaluation and retrofit of buildings in regions of moderate seismicity. Emphasis is on lightly reinforced concrete buildings, steel semi-rigid frames, and masonry walls or infills. The research involves small- and medium-scale shake table tests and full-scale component tests at several institutions. In a parallel effort, analytical models and computer programs are being developed to aid in the prediction of the response of these buildings to various types of ground motion.

Two of the short-term products of the **Building Project** will be a monograph on the evaluation of lightly reinforced concrete buildings and a state-of-the-art report on unreinforced masonry. The **structures and systems program** constitutes one of the important areas of research in the **Building Project**. Current tasks include the following:

1. Continued testing of lightly reinforced concrete external joints.
2. Continued development of analytical tools, such as system identification, idealization, and computer programs.
3. Perform parametric studies of building response.
4. Retrofit of lightly reinforced concrete frames, flat plates and unreinforced masonry.
5. Enhancement of the IDARC (inelastic damage analysis of reinforced concrete) computer program.
6. Research infilled frames, including the development of an experimental program, development of analytical models and response simulation.
7. Investigate the torsional response of symmetrical buildings.

The purpose of this report is to investigate the phenomena of pounding. It introduces the concept of a pseudo energy radius to be used as a tool to study pounding between adjacent structures in terms of energy. This pseudo energy radius is then used, along with statistical linearization, to calculate the minimum gap space between structures to avoid pounding. The pseudo energy radius is also used to estimate the effects of pounding and to estimate the effectiveness of different mitigation techniques.

ABSTRACT

Pounding between inelastic structures is investigated using an energy approach. A comprehensive state of the art review, summarizing previous approaches used to model pounding, and important results and conclusions from previous studies, is presented. The main characteristics of the pounding problem are identified and formulated in terms of energy. The Pseudo Energy Radius concept is introduced to study: (*i*) the minimum gap size to avoid pounding, (*ii*) the amplifications due to pounding, and, (*iii*) the evaluation of different pounding mitigation techniques, including the use of supplemental damping devices and shock absorbers. A simple formulation, based on the Pseudo Energy Radius and statistical linearization, was developed to calculate the minimum gap to avoid pounding. Pounding effects in the response of structures were studied, and a simple methodology based on the Pseudo Energy Radius was developed to estimate these effects. Possible pounding mitigation techniques using energy dissipation devices, such as damper links, shock absorbers, or supplemental damping in the structure, are described. The use of the Pseudo Energy Radius is suggested to estimate mitigation effectiveness. The formulations presented are then summarized to provide structural engineers with simple design/evaluation procedures to solve pounding problems.

Building code considerations for pounding are reviewed. Critical gap to avoid pounding is usually specified in terms of the sum of the maximum displacements, or as a percentage of the height, or as a fixed quantity, or as a SRSS combination of the response. Making use of the improved correlation coefficient based on the above mentioned Pseudo Energy Radius, the Double Difference Combination rule may be used to calculate the critical gap to avoid pounding. The formulation can be extended to determine more rational critical gap formulations in seismic codes.

ACKNOWLEDGMENTS

This research was cosponsored by a Fulbright-CONACyT scholarship, and by NCEER grants 94-5101A and 94-3101A. This support is greatly appreciated.

TABLE OF CONTENTS

TABLE OF CONTENTS (cont'd)

TABLE OF CONTENTS (cont'd)

LIST OF FIGURES

LIST OF FIGURES (cont'd)

FIGURE **TITLE** **PAGE**

LIST OF FIGURES (cont'd)

LIST OF FIGURES (cont'd)

LIST OF TABLES

SECTION 1
INTRODUCTION

1.1 Pounding of Buildings

In the past, major earthquakes affecting large metropolitan areas have induced severe pounding damage. In some cases, the additional forces generated by the impact interactions have lead to structural collapse. In other cases, the buildings presented minor local damage, but indicating that pounding may be a serious threat to the structures if a stronger earthquake takes place. Pounding damage has been identified in previous earthquakes, for example, in the Olive View Hospital, during the 1971 San Fernando earthquake, where pounding between the emergency stair towers and the main building occurred, and evidence of the main building colliding against the retaining wall below grade was also detected. Pounding-related damage was also reported during the 1964 Alaskan earthquake, when parts of the Anchorage-Westward Hotel pounded against each other. A greater number of pounding incidents were identified during the 1985 Mexico City earthquake, in which pounding was listed as a major contributing factor to the observed damage patterns.

Pounding between two structures occurs when, due to their different dynamic parameters, the structures oscillate out of phase, and the separation is not sufficient to accommodate the relative displacements. Therefore, a sufficient separation between the bodies would avoid the problem, however, in large metropolitan areas the need for space has lead to small separations, often leading to structures likely to pound during a strong earthquake. The problem is complicated by the fact that, in general, adjacent buildings belong to different owners, and in most cases are built with different materials, at different times, according to different building code specifications, and designed with different functional objectives that translate into different dynamic characteristics.

Base isolated buildings may experience pounding when the gap between the main structure and the surrounding retaining walls is not sufficient. USC Hospital's performance during the

Northridge California earthquake is an example of such an occurrence. Moreover, other types of pounding may be observed in these buildings when a fail-safe mechanism is activated, like the boundary of the Friction Pendulum System (FPS), or the supports in a rubber bearing system. Pounding was also observed between bridge segments, and between the bridge and the abutment, during the recent Northridge earthquake.

Studies on the effects of pounding were done by the nuclear power industry, since some impact may occur during the maximum credible seismic event. The studies emphasized that impact originates a stress concentration that has to be considered in the design. To reduce the local effects of pounding, some elastic link elements were proposed. Nevertheless, since nuclear power plants are designed to withstand missile impacts, some level of pounding is not hazardous to the integrity of the system. Earlier studies of impact by the nuclear power industry concentrated on the response of fuel rods in a reactor core when they interact, or when motion limiting constraints are used.

The negative effects that pounding impose in a structure have been acknowledged by building codes. In general, the approach taken has been to either, fully connect the structures, or to built them separate enough to avoid contact during vibration. Only one building code was found that allowed some level of pounding if the effects do not jeopardize the integrity of either construction. However, no procedure was outlined to indicate how the collision effects are to be calculated. In some cases, the code specified gap is not sufficient, and in others, some construction debris has reduced the actual gap. At present, there is an important number of buildings in major metropolitan areas, and regions of active seismicity, that do not have adequate separation, and are prone to pounding damage.

The pounding problem has some complications inherent to the strong non-linearity that occurs when two structures come in contact. Besides the complexities in the mathematical formulations, some uncertainties are introduced to the model due to differences in the design philosophies, structural systems, building owners, etc. of the structures. Therefore, due to the unavoidable uncertainties that a structural engineer may face when assessing the likelihood of

pounding between two structures, the variation in the response due to some degree of error in the model parameters must be accounted for.

In recent years, research has being done to outline a criteria under which existing buildings can be evaluated, and if necessary, retrofitted. Pounding has been included in the list of important areas to be checked during a seismic evaluation, but in general, the engineer does not have much information on how to evaluate the effects of pounding, nor how to reduce them. The motivation to study pounding came when the seismic capacity of an existing building in the eastern United States was being estimated, and pounding was deemed likely to occur (Valles et al., 1992).

1.2 Scope of Study

The scope of this report is to: ***(i)*** Provide a comprehensive state of the art review, that summarizes previous approaches to model the pounding phenomenon, and present important results and observations from previous studies; ***(ii)*** Identify and formulate the main characteristics of the pounding problem, and introduce the concept of a Pseudo Energy Radius as a simple tool to study pounding between adjacent structures in terms of energy; ***(iii)*** Develop a simple formulation, using the Pseudo Energy Radius and statistical linearization, to calculate the minimum gap to avoid pounding in inelastic structures; ***(iv)*** Study the effects of pounding in the response of structures, and introduce a simple methodology, based on the Pseudo Energy Radius, to estimate these effects; ***(v)*** Summarize possible pounding mitigation techniques, including supplemental damper elements or shock absorbers, and introduce the use of the Pseudo Energy Radius to estimate the effectiveness of different mitigation techniques; and ***(vi)*** Summarize the different methods presented for critical gap computation, for pounding effects estimation, and for the evaluation of mitigation techniques, and explain the procedure using a sample study.

1.3 Organization of Report

To investigate pounding phenomenon, the current state of the art was studied. Section 2 presents an extended review of research in the field. The concepts and observations included in this section provided a solid background for this study. The state of the art is summarized to complement the studies presented in later sections, and for further use by other researchers.

Using the concepts learned during the state of the art review, preliminary observations and studies were carried, and the structural problem was identified (see Section 3). Four major research objectives were identified: (a) estimate the minimum gap (critical gap), to avoid pounding, (b) estimate amplification effects in structures separated by a gap less than critical, (c) evaluate possible pounding mitigation techniques for structures with undesirable amplifications, and, (d) summarize the results in a concise and simple format to guide structural engineers to evaluate, prevent or mitigate pounding damage. The concept of a Pseudo Energy Radius was introduced as a simple tool to study each of the research objectives. A separate section is used to present the development for each of the research objectives, Sections 4 to 7, respectively. Finally, a summary of relevant findings and conclusions of this study are presented in Section 8.

SECTION 2
STATE OF THE ART REVIEW

2.1 Observed Damage due to Pounding

Pounding damage has been reported in most of the recent earthquakes affecting large metropolitan areas. Some of the early observations on structural pounding include the McKinley building during the 1964 Alaskan earthquake, the Misawa Commercial High School during the 1968 Tokachi-oki earthquake, and the Kuju Lakeside Hotel by the 1975 Oita earthquake (Wada et al., 1984).

During the 1971 San Fernando earthquake, some level of pounding was detected between the Olive View Hospital main building and the stairtowers (Mahin et al., 1976). Three of the four towers collapsed due to lack of adequate shear reinforcement (Bertero and Collins, 1973), but did not exhibit significant hammering. However, severe pounding damage was evident in the fourth of them, tower "C". After the earthquake, the main building had a 16.6 inches permanent drift, between the first and second floors, towards tower "C". Therefore, the 0.4 inches of construction gap was insufficient to accommodate for the difference in displacements, and tower "C", although it did not collapse, had a permanent tilting of 1/12.

During the 1985 Mexico City earthquake, about 40% of the damaged structures experienced some level of pounding, 15% of them leading to structural collapse (Rosenblueth and Meli, 1986). Damage tables indicate that structures from 9 to 12 stories were the most damaged constructions (Rosenblueth and Meli, 1986). Studies on the building foundations reveal that most of these buildings are on friction piles (Mendoza and Auvinet, 1988). Friction piles in the downtown area of the city are commonly designed to settle at the same rate as the clay consolidation, that is, the safety factor used for pile design is close to one. This design philosophy has lead to flexible foundations, some of which, after the 1985 earthquake, exhibited sudden differential settlements. Although no table is available to indicate the type of foundation that the structures subjected to pounding had, it is likely that a flexible foundation may have

promoted impact during the earthquake. Furthermore, Rosenblueth and Meli (1986) suggest that a low modulus of elasticity, stiffness deterioration, strength degradation, torsion, and P-δ effects lead to the high percentage of pounding related damage during an earthquake. The Mexico City earthquake was the first to cause a large amount of damage due to impact.

During the 1989 Loma Prieta earthquake, over 200 pounding occurrences were observed at sites over 90 km from the epicenter (Kasai and Maison, 1991b). Pounding was mostly observed in multistory masonry and wood structures, built prior to 1930, with a small gap between them, or sometimes in contact with each other. Parts of the building on 11th Street in the Oakland city center were subjected to pounding, as evidenced in the slabs on the upper floors (Kasai and Maison, 1991a), but did not suffer any structural damage, as opposed to observed pounding damage between different structures. Nonetheless, high-frequency lateral accelerations were generated during the pounding interactions that probably was the cause of the shift of heavy building equipment on the penthouse, the shifted and turned over computer equipment, and the fallen windows. More cases of structural pounding have been observed during the 1994 Northridge earthquake.

Observations from pounding damage that occurred during previous earthquakes have identified the following factors that greatly influence the occurrence of pounding and pounding related damage:

- Inelastic deformations (ductile response).
- Foundation rotation.
- Damage is less severe when the structures are part of the same complex.
- High frequency pulses may damage sensitive equipment.

2.2 Modeling of Impact/Contact Effects

The modeling formulations for impact problems may be classified as: stereomechanical impact, and piece-wise impact. The former one considers only the macroscopic response of the colliding

bodies, while the latter one activates a linear, or nonlinear, element between the bodies when they become in contact.

2.2.1 Stereomechanical Impact

The stereomechanical theory of impact is the classical formulation to the problem of impacting bodies. The original theory considered the impacting bodies as rigid, later a correction factor to account for energy losses was introduced. The formulation has practically remained unchanged since then (Goldsmith, 1960). The theory concentrates on determining the final velocities of two impacting bodies depending on their initial velocities and a coefficient of restitution (e) to account for plasticity during impact. Due to the macroscopic approach to the problem, the theory does not consider transient stresses and deformations in the impacting bodies. Permanent deformation of the bodies is implicitly accounted for by the coefficient of restitution (e). Fig. 2.1 presents the assumed deformation history during a stereomechanical impact. Furthermore, the part of the initial kinetic energy that is transformed into post-impact vibrations in one of the impacting bodies is assumed to be negligible.

The final velocities when two non-rotating bodies impact (see Fig. 2.2), when the contact point and the center of mass of the bodies lie in the same line (central impact), are given by:

$$v_1' = v_1 - (1+e)\frac{m_2(v_1 - v_2)}{m_1 + m_2} \tag{2.1a}$$

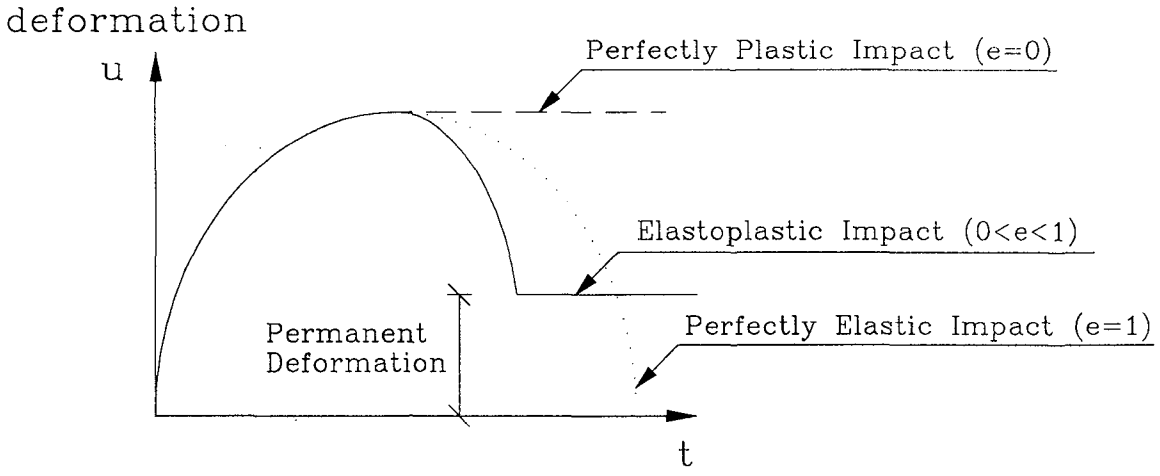

Fig. 2.1 History of deformations during stereomechanical impact (adapted from Goldsmith, 1960).

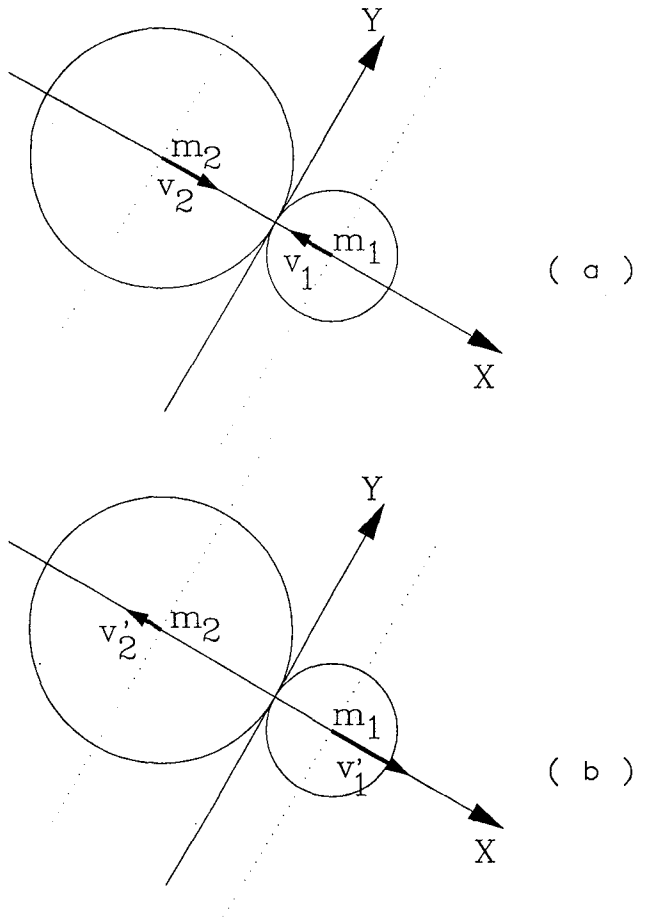

Fig. 2.2 Stereomechanical impact of two non-rotating bodies: (a) onset of pounding, (b) post impact conditions.

$$v_2' = v_2 + (1+e)\frac{m_1(v_1 - v_2)}{m_1 + m_2} \tag{2.1b}$$

Where v_1 and v_2 are the initial velocities of the bodies at the onset of impact, m_1 and m_2 are the masses, and e is the coefficient of restitution:

$$e = \frac{v_1' - v_2'}{v_1 - v_2} \tag{2.2}$$

The loss of kinetic energy is:

$$\Delta T = \frac{1}{2}\left(\frac{m_1 m_2}{m_1 + m_2}\right)(1 - e^2)(v_1 - v_2)^2 \tag{2.3}$$

Therefore the maximum loss of kinetic energy, for perfectly plastic impacts, is:

$$\Delta T_{\max} = \frac{1}{2}\left(\frac{m_1 m_2}{m_1 + m_2}\right)(v_1 - v_2)^2 \tag{2.4}$$

Traditionally the value of the coefficient of restitution was assumed to depend only on the material properties (Goldsmith, 1960), however, the influence of the mass, the shapes, and the relative velocities has being recognized. The coefficient of restitution is traditionally determined from observations of rebound height (h^*), when a sphere is dropped from a height h on a massive plate of the same material:

$$e^2 = \frac{h^*}{h} \tag{2.5}$$

When two spheres of different materials collide, the coefficient of restitution may be estimated from:

$$e_{12} = \frac{e_{11}E_2 + e_{22}E_1}{E_1 + E_2} \tag{2.6}$$

Where e_{11} and e_{22} are the coefficient of restitution for a sphere impacting a plate of the same material, and E_1 and E_2 are the elasticity moduli from each sphere.

The formulas presented for a central impact have been widely used by some researchers to model pounding between buildings (Papadrakakis et al., 1991). The theory of stereomechanical impact

can estimate the post-impact velocities of bodies in three-dimensional motion, and eccentric impact.

Load time response curves may be generated for elastic, perfectly plastic, and elastoplastic models. For an elastic impact, the contact force (f_c) may be calculated using (van Mier et al., 1991):

$$f_c = K_e \delta^{3/2} = -\frac{m_1 m_2}{(m_1 + m_2)} \frac{d^2\delta}{dt^2} \tag{2.7}$$

where δ corresponds to the deformation in the contact zone k_e is a contact parameter that depends on the material properties and the specific contact surface geometry, m_1 and m_2 are the effective masses. The boundary conditions for the problem are:

$$\frac{d\delta}{dt} = v_0 \text{ at } \delta = 0 \tag{2.8a}$$

$$\frac{d\delta}{dt} = 0 \text{ at } \delta = \delta_{max} \tag{2.8b}$$

The maximum contact force, the maximum deformation, and the time at which the maximum force occurs are:

$$f_{max} = \left(1.25 \alpha v^2 K_e^{2/3}\right)^{3/5} \tag{2.9}$$

$$\delta_{max} = \left(1.25 \alpha \frac{v^2}{K_e}\right)^{2/5} \tag{2.10}$$

$$t_{max} = 1.47 \left(1.25 \frac{\alpha}{v^{0.5} K_e}\right)^{2/5} \tag{2.11}$$

where:

$$\alpha = \frac{m_1 m_2}{m_1 + m_2} \tag{2.12}$$

For plastic impact, the contact force may be calculated according to Meyer's law (van Mier et al., 1991):

$$f_c = K_p \delta^n \tag{2.13}$$

For the case of a rigid sphere and a deformable plane n is one, and the maximum contact force, the maximum deformation, and the time at which the maximum force occurs, are given by:

$$f_{c\max} = v\left(\alpha K_p\right)^{1/2} \tag{2.14}$$

$$\delta_{\max} = v\left(\frac{\alpha}{K_p}\right)^{1/2} \tag{2.15}$$

$$t_{\max} = \frac{\pi}{2}\left(\frac{\alpha}{K_p}\right)^{1/2} \tag{2.16}$$

The author proposed a simple elastoplastic model for impact that depends on four parameters: the contact parameter K_e for the elastic phase, the critical stress and the critical size of the contact surface, and the unloading stiffness. Fig. 2.3 presents the proposed load vs. time response of the system in three stages. The initial loading rate (c_1) is determined using K_e to calculate the maximum load and contact time from an elastic impact. The loading rate c_2 depends on the material characteristics, for strain hardening materials, or if the contact plastic contact area increases $c_2 > 0$. And, the elastic restitution coefficient corresponds to c_3.

2.2.2 Piece-wise Impact.

The second approach to model impact phenomenon has been to consider a contact element that is activated when the gap between the structures closes. Four types of contact elements has been used in the past: Linear solid, nonlinear solid, Kelvin solid, and the Hertz contact law.

The simplest contact element consist of a linear elastic element (see Fig. 2.4). The force in the contact element may be expressed according to:

$$f_c = k(u_1 - u_2 - g_p)\,\mathrm{U}[u_1 - u_2 - g_p] \tag{2.17}$$

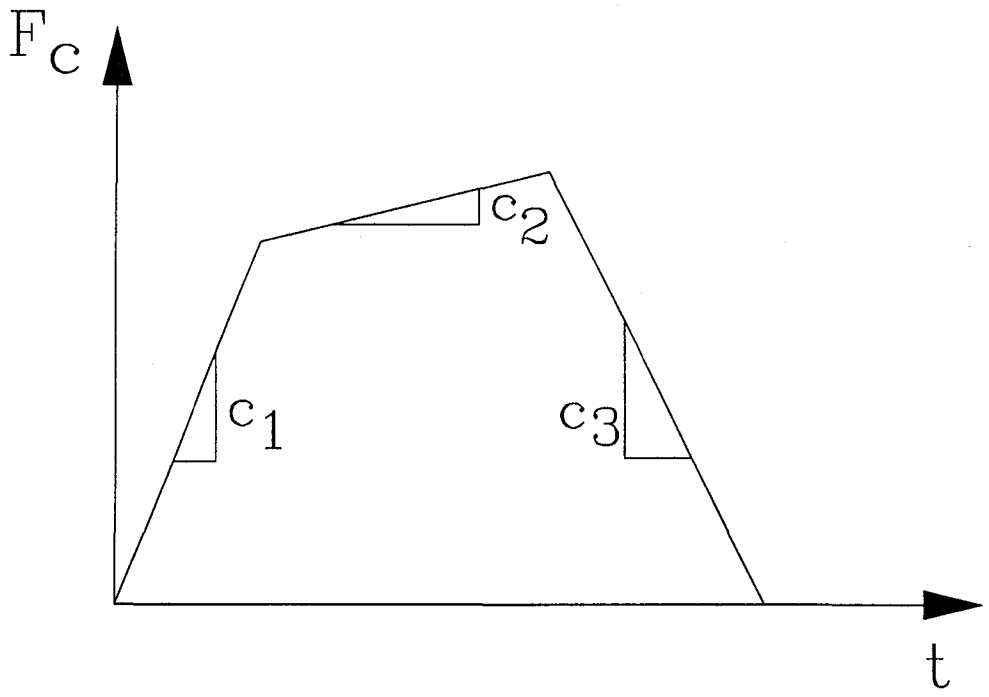

Fig. 2.3 Simple elasto-plastic load time-history model for impact (adapted from van Mier et al., 1991).

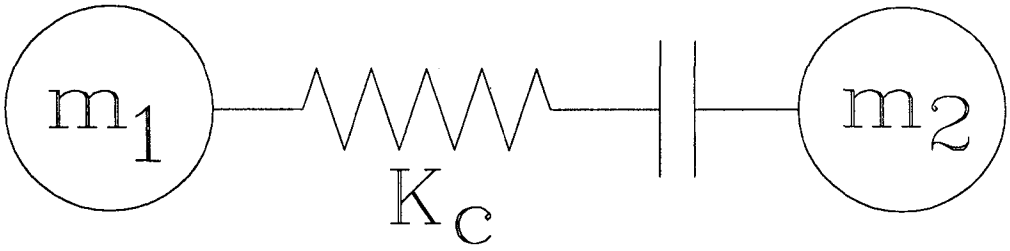

Fig. 2.4 Piece-wise linear spring contact element.

Where u_1 and u_2 are the displacements of the impacting bodies, g_p is the static separation between the structures, and, U[x] corresponds to the unit step function of x. The present model for impact has been used by Kasai et al. (1990, 1991c), Maison and Kasai (1990, 1992), Den Hartog and Heiles (1936).

A generalization to the piece-wise linear stiffness contact element has been to consider nonlinear stiffness for the contact element. The simplest of the models proposed considers two stiffness, an approaching stiffness k_i and a higher stiffness for separation k_f (see Fig. 2.5). The force in the contact element can be expressed as:

$$f_c = \left(k_i (u_1 - u_2 - g_p)\,\mathrm{U}[\dot{u}_1 - \dot{u}_2] + k_f (u_1 - u_2 - g'_p)\,\mathrm{U}[\dot{u}_2 - \dot{u}_1] \right) \mathrm{U}[u_1 - u_2 - g_p] \quad (2.18)$$

The present model includes some energy dissipation due to hysteretic behavior at the impact element.

Another widely used piece-wise model to study impact has been to consider a Kelvin model (see Fig. 2.6) that is activated when the structures come in contact (Anagnostopoulos, 1988; Anagnostopoulos and Spiliopoulos, 1990 and 1992; Wolf and Shrikerud, 1980). The forces in the contact element may be calculated from:

$$f_c = \left(k_c (u_1 - u_2 - g_p) + c_c (\dot{u}_1 - \dot{u}_2) \right) \mathrm{U}[u_1 - u_2 - g_p] \quad (2.19)$$

where k_c and c_c are the spring and dashpot constants of the element. Considering two impacting masses, a relationship may be found between the dashpot constant and the coefficient of restitution (e) during a stereomechanical impact (Anagnostopoulos, 1988):

$$c_c = 2\xi_i \sqrt{k_c \frac{m_1 m_2}{m_1 + m_2}} \quad (2.20)$$

$$\xi_i = \frac{-\ln e}{\sqrt{\pi^2 + (\ln e)^2}} \quad (2.21)$$

Note that a variation of the Kelvin model may include a nonlinear spring, and a contact element that only contributes for positive loading, as discussed in Section 3.4.

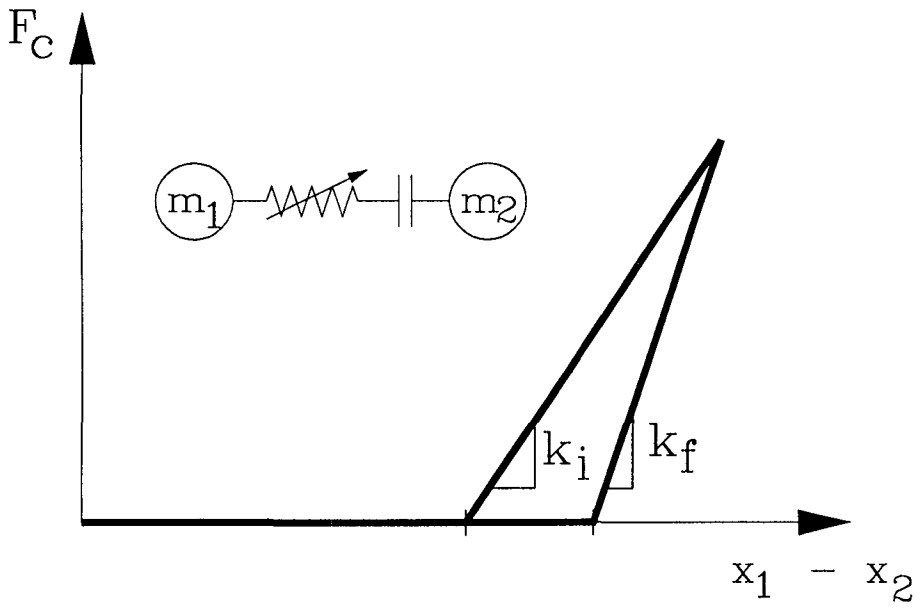

Fig. 2.5 Piece-wise linear contact element with different loading and unloading branches.

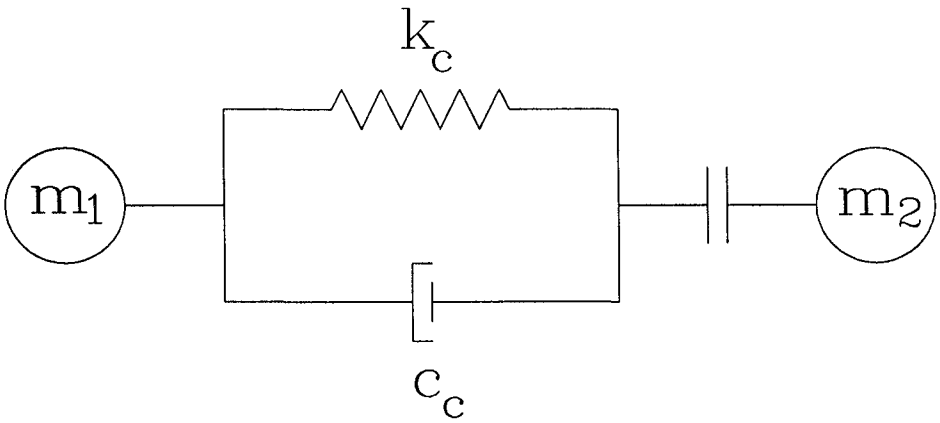

Fig. 2.6 Piece-wise linear Kelvin model for contact problems.

The fourth type of piece-wise element adopted by researchers to model impact uses the Hertz contact law, where the force in the contact element may be expressed as:

$$f = k_c\left(u_1 - u_2 - g_p\right)^{3/2} \mathrm{U}[u_1 - u_2 - g_p] \tag{2.22}$$

The Hertz contact law corresponds to the solution of static contact of two elastic bodies. Nonetheless, the formula has been extrapolated to the cases of dynamic contact problems (Goldsmith, 1960). The Hertz contact law, considering elastic bodies, is incapable of taking into account dissipation during the impact phenomenon. However, the formula has been widely used since it appears to predict the impact parameters that can be determined experimentally (Goldsmith, 1960). Several of the researchers studying pounding have adopted the Hertz contact law to model pounding (Soong, 1983; Jing and Sheu, 1990; Jing and Young, 1991; Davis, 1992)

2.3 Analytical SDOF Studies

A number of studies have been published for single degree of freedom systems subjected to pounding. A brief summary of the major studies, and their relevant conclusions are presented below.

2.3.1 Time Harmonic Excitation

Some early studies on pounding of adjacent structures were performed by the nuclear power industry (Wolf and Shrikerud, 1980). Due to insufficient gap when retrofitting nuclear power plants, and an increase in the seismic requirements for nuclear power plants, studies for pounding evaluation were performed. Furthermore, the performance of nuclear power plants is carefully examined when subjected to the maximum credible earthquake in the site, for which pounding is likely to occur.

Studies carried by Wolf and Shrikerud (1980) investigated two and one sided impact of a single degree of freedom structure (see Fig. 2.7). The authors studied pounding using a

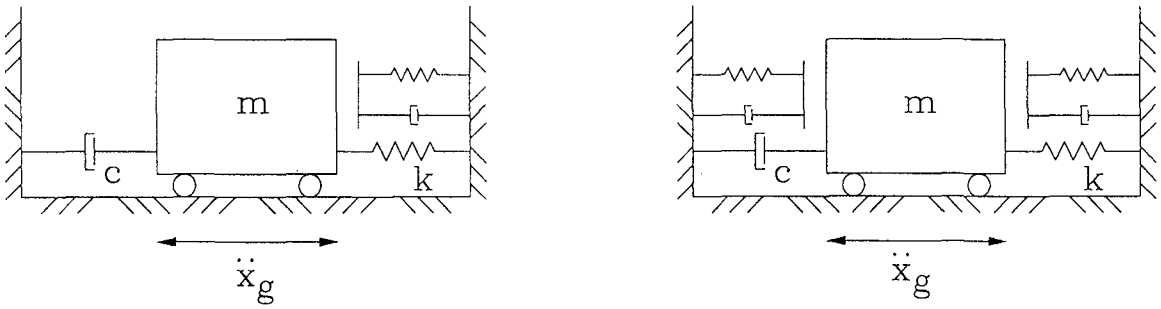

Fig. 2.7 One and two sided impact of a single degree of freedom structure.

piece-wise linear spring for the contact element, extrapolating the studies by Den Hartog and Heiles (1936) and Timoshenko et al. (1974), to the case of one sided impact. The study focused on elastic impact, but the effect of energy dissipation in the impact process was not investigated. Depending on the ratio of the exciting frequency to the natural frequency of the structure (ω_g / ω), and the stiffness of the contact spring (k_c), peaks in the displacement response spectrum, for the zero gap case, were identified for the hyperharmonic response ($\omega_g / \omega = 1$ for $k_c \to \infty$), harmonic response ($\omega_g / \omega = 2$ for $k_c \to \infty$), and subharmonic response ($\omega_g / \omega = 3, 4, 5...$ for $k_c \to \infty$).

Some conclusions can be derived from the simple model considered by Wolf and Skrikerud (1980): an increase in the response is observed for flexible structures, whereas stiff structures may experience a reduction in forces. An important stress concentration is observed in the neighborhood of the impact. The impact force has a high frequency component, and since it acts on a small area, it may excite higher modes of vibration. Note however, that the model studied considers the impact of a SDOF structure with a structure that moves with the ground. As noted by Davis (1992), the other extreme cases would be when the adjacent structure is very flexible, and therefore is not affected by the ground excitation. Davis studied both limit cases using a SDOF with the Hertz contact law to model impact. Using the impact velocity spectrum, one may detect the excitation frequencies at which the response is amplified or deamplified, or even the frequency ranges where chaotic impacts occur. In the spectra, the harmonic and subharmonic response peaks may be easily detected. Results are congruent with the solutions by Wolf and Skrikerud (1980).

Miller (1980) derived close form solutions for the response of two impacting SDOF systems. The solution is valid only for the case of a single impact per cycle. The equations of motion for the system are:

$$\ddot{x} + x = (\Omega - 1) y_1 \tag{2.23a}$$

$$\ddot{y}_1 + \Omega y_1 = \eta \delta \cos(\eta^{1/2} \tau + \alpha) \tag{2.23b}$$

Where:

$$x = y_2 - y_1 \tag{2.24}$$

and y_1 and y_2 are the displacements of each structure. The boundary conditions for the problem are, that at time τ_p:

$$x(\tau_p^-) = -1 \tag{2.25a}$$

$$\dot{x}(\tau_p^-) = -\dot{x}(0^+)/e \tag{2.25b}$$

$$y_1(\tau_p^-) = y_1(0^+) \tag{2.25c}$$

$$\dot{y}_1(\tau_p^-) = \dot{y}_1(0^+) + \frac{\mu(1+e)}{e(1+\mu)}\dot{x}(0^+) \tag{2.25d}$$

Where:

$$\mu = m_2 / m_1 \tag{2.26}$$

$$\tau_p = \frac{2\pi}{\eta^{1/2}} \tag{2.27}$$

The solution to the problem satisfies the system of equations:

$$\dot{x}(0^+) = \left(b_1 + c_1\cos\alpha + d_1\sin\alpha\right)/a_1 \tag{2.28a}$$

$$\dot{y}_1(0^+) = -\frac{(1+e)\mu}{2e(1+\mu)}\dot{x}(0^+) + \frac{\eta^{2/3}\delta\sin\alpha}{\eta-\Omega} \tag{2.28b}$$

$$y_1(0^+) = -\frac{(1+e)\mu}{2e(1+\mu)}\frac{\sin\theta}{\Omega^{1/2}(1-\cos\theta)}\dot{x}(0^+) - \frac{\eta\delta\cos\alpha}{\eta-\Omega} \tag{2.28c}$$

$$x(\tau) > -1 \quad \forall \ 0 < \tau < \tau_p \tag{2.28d}$$

where α, a_1, b_1, c_1, d_1 and θ are determined as a function of the frequency of excitation, the coefficient of restitution, and the mass ratio. Miller indicates that inelastic impacts may protect both structures if they oscillate close to resonance.

2.3.2 Earthquake Excitation

Anagnostopoulos, (1988) used actual earthquake records to study the trends in the response of SDOF systems with pounding. The project focused on the response of a series of bilinear single-degree-of-freedom systems. Two distinct periods are considered in the structures: one for the

external structures, and a different one for the interior structures. The analysis of the systems for different period ratios was performed when subjected to five actual earthquake records.

The effect of the ratio between the periods, the period of the structures, the seismic gap, and the number of buildings was studied. The results indicate that the displacement of exterior constructions may be considerably amplified, while interior structures may experience amplification or deamplification, depending on the ratio of structural periods. The results show that the effects of pounding diminish as the gap increases, and that inelastic and linear structures have a similar response due to pounding. The author notes that the relative masses of the buildings have an important effect in the response, being greater the amplification in the structure with smaller mass. Other parameters, like the stiffness of the contact element, play a minor role in the response.

Anagnostopoulos suggests that the use of a viscoelastic material to fill the gap may reduce the effects of pounding, although the effect will not be as beneficial when the displacements are considered. The results of this study corroborate the observed greater damage that corner buildings experience, while interior buildings may exhibit a deamplification in the response.

2.3.3 Zero Mean Gaussian Stationary Input

Soong (1983) studied the response of a single-degree-of-freedom vibrating between two elastic reflectors due to a zero mean Gaussian white noise input. The study was intended for the design of restraining systems. The system is solved by separating the solution in two distinct phases: before and during impact, for which the solutions are known. The solution of the combined system is then obtained by equating the energy consumption during impact to the kinetic energy in the system. The probability density function of the maximum impact acceleration, Rayleigh type, is found to depend only on the variance of the velocity, the mass ratios and the impact parameters. However, the density function is independent of the gap size, or the stiffness of the oscillator.

The author then calculates the likelihood of pounding using the assumption that the extreme points follow a Poisson process, that is, that the maximums are uncorrelated. The likelihood of pounding may then be calculated from the parameters of the structure, or, the gap for a given allowable likelihood of pounding may be found. By combining the Likelihood of pounding and the density function for the maximum impact acceleration, a rational design of the clear distance may be made.

Jing (Jing and Young, 1990; Jing and Sheu, 1990) studied the response of a SDOF system to a zero mean Gaussian input. The solution to the governing Fokker-Planck equation was found, and the joint probability density function for the displacement and velocity of the system was derived in closed form solution. The probability density function for the steady state solution was then obtained as a limiting form of the joint density function, and it was observed that the density function for the velocity was still Gaussian, while the density function for the displacements was not. The level crossing with positive slope of the displacement was obtained, and the probability of peaks for a given amplitude was then obtained.

Later Jing and Young (1991) extended their studies to the case of two single-degree-of-freedom systems subjected to a zero mean white noise input. The equations of motion of the system to be studied are:

$$m_1\ddot{x}_1 + c_1\dot{x}_1 + k_1x_1 + \eta g(x_1, x_2) = F_1(t) \tag{2.29a}$$

$$m_2\ddot{x}_2 + c_2\dot{x}_2 + k_2x_2 + \eta g(x_1, x_2) = F_2(t) \tag{2.29b}$$

where $g(x_1, x_2)$ is the contact force according to a Hertz contact law. For this problem, the resulting Fokker-Planck equation is considerably more complicated, and closed form solutions are not possible for an arbitrary set of parameters since the displacements are coupled. The authors found the exact solution for the case when:

$$\frac{S_1}{S_2} = \frac{c_1}{c_2} \tag{2.30}$$

A closed form solution for the joint probability density function for displacements and velocities was derived. The probability of impact was determined as:

$$P_{impact} = \sum_{n=0}^{\infty}\sum_{m=0}^{\infty}(-1)^n \frac{m!}{n!}\left(\frac{1}{2}\right)^{n-m}\binom{2n}{2m}k_{12}^{2m}A^{2n-2m} \tag{2.31}$$

where k_{12} is the square root of the ratio of stiffness, and A is the gap. Then, the clearance for a single-degree-of-freedom system is:

$$a_{\min} = \sigma_0 \sqrt{2\left|\ln(P_{impact})\right|} \tag{2.32}$$

and for two vibration systems, the approximate formula is:

$$a_{\min} = \sigma_1 \sqrt{2(1+k_{12}^2)\left|\ln(P_{impact})\right|} \tag{2.33}$$

where σ_1 is the greater variance of the two corresponding linear systems.

2.3.4 Stability and Bifurcation Studies for the Harmonic Excitation Case

Some studies have investigated the stability and bifurcation of oscillators that experience pounding (Nastsiavas, 1990; Li et al., 1990). The studies were intended to study the response of mechanical systems with motion limiting constraints. However, the results are not as useful for buildings subjected to pounding.

2.4 Analytical Case Studies for MDOF Systems

A reduced number of researchers have studied the response of multi-degree-of-freedom structures subjected to pounding. Due to the number of parameters involved, in general, the studies have used actual buildings, and the effects of varying the structural parameters have been investigated.

2.4.1 Pounding between Flexible and Rigid Structures

The first analysis of a building pounding against a rigid structure was the study of the Olive View Hospital (Mahin et al., 1976). The two dimensional model of the structure, using ANSR, included a piece-wise linear spring element that is activated when the displacement of the structure exceeds the 4" gap. The contact element was included to model pounding interactions between the main building and the one story warehouse. The model did not include the stairtower buildings, although evidence of significant pounding was detected in one of them. The report only indicates that a large value for the stiffness of the contact element was used, but no further comments are made in that regard.

Later, Maison and Kasai (1990 and 1988) developed a post-processor of the SuperETABS (SLAM) to analyze the response of a building that pounds against a rigid structure. However, pounding is assumed to occur only at one level. The impact phenomenon was modeled using a piece-wise linear spring. The solution is carried out using two distinct states: when the structure vibrates by itself, and when it vibrates in contact with its neighboring structure. The governing equation of motion for state 1 is:

$$\mathbf{M}\ddot{\mathbf{u}} + \mathbf{C}\dot{\mathbf{u}} + \mathbf{K}\mathbf{u} = -\mathbf{M}\mathbf{r}\ddot{x}_g \tag{2.34}$$

where $\mathbf{r}$ is the earthquake influence coefficients. The equation of motion for state 2 is:

$$\mathbf{M}\ddot{\mathbf{u}} + \overline{\mathbf{C}}\dot{\mathbf{u}} + \overline{\mathbf{K}}\mathbf{u} = -\mathbf{M}\mathbf{r}\ddot{x}_g + \mathbf{b} \tag{2.35}$$

where $\overline{\mathbf{K}}$ is the stiffness matrix of the structure including the contribution from the contact element, $\overline{\mathbf{C}}$ is the damping matrix of the structure assumed as a linear combination of the mass and stiffness matrices, and $\mathbf{b}$ is a vector with the preload forces from the contact springs.

The governing equations for the motion of the building for each state are solved in the modal space by numerically calculating Duhamel's integral, and checking for a change in state at each time step of analysis. Adjustment of the time step of analysis is incorporated in the program to minimize overshooting and undershooting for the change in dynamic state of the structure. For state 2, the modal solution of the system is separated into static and dynamic solutions:

$$Z_i = Z_i^s + Z_i^d \tag{2.36}$$

where the static solution is:

$$Z_i^s = \frac{B_i}{\omega_i^2} \tag{2.37}$$

and the dynamic solution is obtained by numerically calculating the Duhamel's integral.

The program models the response of the structure in three dimensions, allowing for an eccentric position for the impact spring. The displacement, including rotation of the floor slab is:

$$\mathbf{w} = \mathbf{u}_x - \mathbf{u}_\theta y \tag{2.38}$$

Considering the total displacement $\mathbf{w}$, two set of boundary conditions are specified in the modal coordinates for each state. When the structure changes from state 2 to state 1, release of the contact spring, the initial conditions are:

$$Z_i(t') = \phi_i^t \mathbf{M}\mathbf{u}(t') \tag{2.39a}$$

$$\dot{Z}_i(t') = \phi_i^t \mathbf{M}\dot{\mathbf{u}}(t') \tag{2.39b}$$

When pounding occurs at time t', change from state 1 to state 2, the initial conditions are:

$$Z_i^d(t') = \phi_i^t \mathbf{M}\mathbf{u}(t') - Z_i^s \tag{2.40a}$$

$$\dot{Z}_i^d(t') = \phi_i^t \mathbf{M}\dot{\mathbf{u}}(t') \tag{2.40b}$$

Using the program SLAM, Maison and Kasai (1990) studied the response of the University of California Medical Center building in San Francisco, under a hypothetical scenario. The 15-story steel moment resisting frame is assumed to be adjacent to a rigid structure without any separation, with the maximum contact level being the eighth story. The stiffness for the contact element was set equal to the in-plane axial stiffness of the concrete slab. The response of the system was studied under a free vibration (snap-back test), and a forced vibration according to the 1940 El Centro earthquake.

From the results of the analysis, the following conclusions were drawn: Large shears were observed at the stories immediately above and below the contact level, creating a shear wave that travels through the structure, increasing the maximum base and top shears in the structure. Peak lateral displacements were smaller than the no pounding results, while the observed trend for the maximum story drifts was a decrease at the stories below the pounding level, and an increase for

the stories above the pounding level. A 290% increase was observed at the top of the structure. Overturning moments exhibit a trend similar to that observed for interstory drifts.

Some parametric studies, using the snap-back numerical simulation, were carried out to study the effects of pounding location, building separation, stiffness of the contact spring, and initial sway amplitude. The trends observed in the results indicate that the maximum base shear increases for higher pounding location elevation, while no clear trend is observed in the maximum displacements. As the gap size is increased, the results approach the no pounding maximums, therefore, a decrease in the peak parameters is observed. The stiffness of the contact spring has a minor influence on the peak displacement, drift and overturning moments, but a somewhat larger influence on the maximum shears observed. The effect of initial sway exhibit an almost linear influence on the maximum response parameters.

Note that the results obtained are valid for the combination of building period (1.13 sec), and the earthquake predominant frequencies, and one should be careful when trying to extrapolate the results to other characteristic frequencies. A different combination of periods may lead to an increase in displacements. Furthermore, the analysis did not study the response of the shorter, stiffer building.

2.4.2 Prediction of Peak Response

A method for predicting the peak displacement of the structures subjected to pounding was proposed by Kasai et al. (1990). The method considers that the maximum kinetic energy of a structure subjected to pounding may be expressed as a linear variation of the maximum kinetic energy for the no pounding case:

$$KE_{np} \approx \frac{1}{2} m S_v^2 (T_{np}, \xi) \tag{2.41}$$

and the maximum kinetic energy of the structure with the contact spring connected to it (continuous contact):

$$KE_{fs} \approx \frac{1}{2} m S_v^2 (T_{fs}, \xi) \tag{2.42}$$

The authors indicate that the maximum kinetic energy for the pounding case may be calculated according to:

$$KE \approx \frac{(1-\beta)}{2}\left(KE_{np} + KE_{fs}\right) + \beta KE_{np} \tag{2.43}$$

where β is the normalized gap size:

$$\beta = \frac{g_p}{u_{np}} \tag{2.44}$$

The authors indicate that the linear variation of the kinetic energy for the pounding solution was obtained from extensive numerical studies using the program SLAM.

The maximum positive and negative displacements may be estimated by considering:

$$u^- = \alpha u_{np} \tag{2.45a}$$

$$u^+ = \beta u_{np} + \gamma u_{fs} \tag{2.45b}$$

after some algebra, and considering that the kinetic energy of the fixed spring system is greater than the kinetic energy in the no pounding case, some bounds may be calculated for the maximum deformations:

$$u_{np}\sqrt{\frac{1+KE_{fs}/KE_{np}}{2}} \le \left|u^-\right| \le u_{np}, \quad \text{for } 0 \le \beta \le 1 \tag{2.46a}$$

$$u_{np}\sqrt{\frac{1+KE_{fs}/KE_{np}}{2}}\left(\frac{T_{fs}}{T_{np}}\right) \le u^+ \le u_{np}, \text{ for } 0 \le \beta \le 1 \tag{2.46b}$$

According to the bounds in the previous formulas, the maximum displacements of a system with pounding, is always smaller than the no pounding response. These results seems to contradict, for some ground dominant frequency to structural frequency ratios, the observations by other researchers presented earlier.. The assumption of linear variation of the kinetic energy, derived from studying pounding against a infinitely stiff structure, may not be extrapolated to other combinations of characteristic periods.

2.4.3 Pounding between two Flexible Buildings

Maison and Kasai (1992) extended the methodology presented earlier to study the response of two flexible buildings pounding against each other. In the present formulation, the dynamic properties of the two structures are conveniently placed using matrices that include both structures. The solution of the augmented system is once again carried out in the modal space coordinates. A new post-processor for SuperETABS, named SLAM-2 (Maison and Kasai, 1990), was developed.

Using the computer program SLAM-2, the response of the University of California Medical Center Building, with a fundamental mode of 1.13 sec, was determined when pounding occurs with a hypothetical 8-story adjacent structure, with a fundamental period of 0.8 sec. The floor masses of the hypothetical building are four times the floor masses that corresponds to the Medical Center Building. The response of the structures is studied under the 1940 El Centro earthquake, considering no initial separation between the structures. Results indicate an important increase in displacements, story drifts, story shears and overturning moments for the Medical center building, while reductions in the response of the 8-story structures were observed.

A parametric study was carried out by the authors to study the influence in the response of the building masses, the gap, and the stiffness and damping of the contact element. The study was carried out using three artificial earthquakes representative of a deep cohesionless soil (S2), according to the SEAOC recommended provisions. The response of the taller structure becomes larger when the mass of the shorter structure increases, while the response of the shorter structure is hardly influenced by the variation in this parameter. An increase of the separation between the structures reduces the maximum response of the taller structure, while in the shorter structure a decrease in the response away from the pounding side is observed. A response increase is observed in the upper stories of the taller structure for a decrease in the separation. The results indicated that, for the structures considered, the stiffness and damping of the contact element had little influence on the response parameters being studied, but the authors recognize that the acceleration response may be greatly influenced by the contact element stiffness.

After the 1989 Loma Prieta earthquake, Kasai et al. (1991c) performed an analysis of the buildings that experienced pounding. The buildings on Mission Street in San Francisco, a 10 story building and a 5 story building, experienced significant torsional response at the stories above pounding level. The two buildings on 15th Street at the Oakland city center that were subjected to pounding damage were also studied. The results of the analysis agree with the observed structural damage.

A number of researchers have studied alternative methods to calculate the contact forces that develop between adjacent structures. Stavroulakis and Abdalla (1991) studied the contact forces between adjacent structures subjected to static lateral loads. The authors note that the problem of determining the solution for the static load case is equivalent to a quadratic programming problem, and the solution corresponds to the minimization of potential or complementary energy of the structure. The authors propose the method to estimate the required seismic gap to keep the contact forces within some allowable limit, or, estimate the contact forces given an existing gap.

A Lagrange multiplier solution was proposed (Papadrakakis et al., 1991) to enforce geometric compatibility when pounding occurs. The Lagrange multiplier method is, along with the penalty method and the mixed (hybrid) method, one of the three approaches commonly used to solve contact problems in finite elements, based on a variational formulation. For the dynamic contact problem, involving linear elastic structures, the equations of motion are transformed to:

$$\begin{bmatrix} \mathbf{M} & \mathbf{0} \\ \mathbf{0} & \mathbf{0} \end{bmatrix} \begin{Bmatrix} \ddot{\mathbf{u}} \\ \mathbf{0} \end{Bmatrix} + \begin{bmatrix} \mathbf{C} & \mathbf{0} \\ \mathbf{0} & \mathbf{0} \end{bmatrix} \begin{Bmatrix} \dot{\mathbf{u}} \\ \mathbf{0} \end{Bmatrix} + \begin{bmatrix} \mathbf{K} & \mathbf{K}_\lambda^t \\ \mathbf{K}_\lambda & \mathbf{0} \end{bmatrix} \begin{Bmatrix} \mathbf{u} \\ \lambda \end{Bmatrix} = \begin{Bmatrix} \mathbf{P}(t) \\ \delta \end{Bmatrix} \tag{2.47}$$

Where δ_i corresponds to the initial gap between the two structures at story "*i*", λ is the vector of nodal contact forces, and $\mathbf{K}_\lambda$ is a contact matrix that enforces no penetration:

$$\left[\mathbf{K}_\lambda\right] \begin{Bmatrix} \mathbf{u}_1 \\ \mathbf{u}_2 \end{Bmatrix} = \{\delta\} \tag{2.48}$$

The solution is carried out by iterations. The method was developed by minimizing the potential function subjected to the no penetration geometric constraint, which was transformed to the unconstrained optimization problem of a Lagrangian functional.

Papadrakakis et al. (1991) also studied the influence of the Newmark-Beta integration parameters (β and γ) on the post-impact solutions. The authors derived the conditions to observe separation after one time step:

$$\beta = \frac{1}{1+e}\frac{v_1 - v_2 - \delta/\Delta_t}{v_1 - v_2} \tag{2.49}$$

$$\gamma > \frac{(3-e)(v_1 - v_2) - 2\delta/\Delta_t}{2(1+e)(v_1 - v_2)} \tag{2.50}$$

Where e is the coefficient of restitution, v_1 and v_2 are the velocities at the onset of contact, δ is the initial gap size, and Δ_t the time step in the analysis. However, changing the numerical integration parameters is not desirable, since it is better to choose them based on numerical stability conditions. The authors therefore, proposed to calculate the velocities of the structure when they come in contact, enforcing compatibility conditions using the Lagrange multipliers, and using the formulas for stereomechanical pounding, impose the calculated separation velocities as initial conditions for the next time step. The value of accelerations are set equal to their values before the bodies came into contact. The authors indicate that by imposing the post impact conditions, inaccuracies due to the translation of the masses before separation are avoided. Numerical simulations using the developed methodology indicated an amplification of the response in the less excited structure, while a decrease in the peak responses was observed in the structure near resonance.

2.4.4 Pounding of Buildings in Series

Anagnostopoulos and Spiliopoulos (1990) extended their original studies on a series of single-degree-of-freedom systems (Anagnostopoulos, 1988), to the case of multi-degree-of-freedom systems. The buildings were modeled as a lumped mass, shear type, structure with a bilinear force deformation characteristic. Furthermore, the structural models include foundation compliance by means of a linear spring for translational and rotational motions, and a Kelvin solid is used as the contact element. The numerical integration of the equations of motion is carried out using a central difference scheme, considering two different time steps for the structures vibrating free or in contact.

Anagnostopoulos and Spiliopoulos (1992) performed some parametric studies to determine the influence in the response of the system configuration, buildings of unequal height, seismic separation, relative mass size, and the properties of the contact elements. The constants for the foundation springs were determined considering a spread footing foundation on a stiff soil. Yield levels for the inelastic solution were calculated using the 1988 UBC code. The damping constant of the contact element was calculated to yield a coefficient of restitution of 0.5. The model consisted of three buildings in series.

The results indicate that pounding interaction amplifies the response when the adjacent structure is more flexible, while a reduction of the response is observed when the adjacent structure is stiffer. For the combination of periods used, one-sided pounding produced comparable amplifications to the two-sided cases, except for the case when the ratio of fundamental period of the structure to the fundamental period of the adjacent one is 0.6. When studying the influence of different heights of the impacting structures, the authors found that the taller structure pushed the smaller one, increasing the plastic deformation of the smaller one, while the displacements of the taller one remained almost unchanged. However, the authors compared only lateral displacements, so the trends in shear forces may differ.

The response of the structures with separations according to the UBC, and the Eurocode No. 8 was studied. The results indicated that the Eurocode requires more conservative gap sizes. The results indicate that a reduction of the mass of the center building reduces the effect of pounding in the corner buildings, while an increase in the mass of the center building will demand higher ductility in the corner buildings. The parametric studies on the contact element stiffness indicated that the ductility demands are not sensitive to this parameter, while some sensitivity is observed on the response from variation of the coefficient of restitution. The authors note that their observations were based on displacements, and not on accelerations.

2.5 Pounding Damage Mitigation Techniques

Several methods have been proposed to avoid pounding induced collapse of buildings. The methods may be classified according to their approach to the problem of pounding: methods to avoid pounding, methods to strengthen structures to withstand pounding, and techniques to reduce pounding effects in the structures. A brief summary of research by previous investigators is presented.

2.5.1 Methods to Avoid Pounding of Structures

Three methods may be considered to avoid pounding interactions between adjacent constructions: connecting the buildings, calculating the minimum gap size to avoid pounding, and reducing the lateral deformation of the structures. Connecting adjacent buildings is the simplest form of eliminating pounding. This option is generally suggested by building codes if the new constructions may be prone to pounding.

Providing a sufficient gap has been the commonly accepted strategy adopted by building codes throughout the world. Jeng, Kasai and Maison (1992) proposed a spectral difference method to calculate the minimum gap to avoid pounding for linear structures. The method was named Double Difference Combination rule (DDC):

$$g_p = \sqrt{u_1^2 + u_2^2 - 2\rho_{12} u_1 u_2} \tag{2.51}$$

Where the correlation coefficient (ρ_{12}) is calculated according to the simplified formulas derived by Der Kiureghian (1980) for white noise input:

$$\rho_{12} = \frac{8\sqrt{\xi_1 \xi_2}\left(\xi_2 + \xi_1 T_2/T_1\right)\left(T_2/T_1\right)^{3/2}}{\left[1-\left(T_2/T_1\right)^2\right]^2 + 4\xi_1\xi_2\left[1+\left(T_2/T_1\right)^2\right]\left(T_2/T_1\right) + 4\left(\xi_1^2+\xi_2^2\right)\left(T_2/T_1\right)^2} \tag{2.52}$$

Later, the proposed combination rule was extended for nonlinear structures using a shift in the fundamental mode of vibration, and using an equivalent damping coefficient (Kasai and Jagiasi, 1993a). For a bilinear oscillator, the effective period and damping coefficients are:

$$T^* = T\left[1 + 0.09(\mu - 1)\right] \tag{2.53a}$$

$$\xi^* = \xi + 0.084(\mu - 1)^{1.3} \qquad (2.53b)$$

A more detailed description of the rules proposed for building separation is presented in Section 5.

Reducing the lateral deflections of the structures is another form of pounding retrofit. The reduction in the displacements may be accomplished, for some period ranges, by stiffening the structures, or adding passive or active energy dissipation devices. An effective method to reduce the relative deformation between the structure is to add supplemental damping in the structures, since, the response of the constructions tend to respond in phase with high damping (Jeng et al. 1992). Kasai and collaborators (1993b) studied the response of two structures, 10-story and 6-story, inelastic structures with supplemental damping. The 3M viscoelastic dampers used for the study were placed in both structures. The results of the study shown a beneficial effect since displacements and ductility demands in the structures were reduced, in-phase response of the structures was promoted, and some of the energy during impact was absorbed by the dampers.

2.5.2 Methods to Strengthen Structures to Withstand Pounding Effects

Provisions for strengthening the structure to adequately perform during pounding interactions are suggested by the Greek building code (Anagnostopoulos and Spiliopoulos, 1992).

2.5.3 Techniques to Reduce Pounding Effects in the Structures

In the early studies on pounding by Wolf and Skrikerud (1980), the effect of link elements between the structures was studied. The link elements, or tuning devices, studied include tuning springs without tension, tensioned, and with preload. The numerical analysis showed a reduction in the response of the structures, for some ranges of the tuning device stiffness, and of the preload value. Furthermore, the high frequency response induced by pounding is eliminated.

Earlier, in 1962, Rosenblueth and Esteva (Newmark and Rosenblueth, 1986) introduced a pounding protection device, made of wood, to reduce the impact forces. Westermo (1989) studied the effect of a linear elastic link between the structures. Based on the results of time

harmonic and earthquake response, he noted that the presence of the link reduces the relative deflection of the structures, and increases the absolute displacement and base shear of the stiffer structure. The results indicate that the link connecting structures with similar dynamic properties will prevent them from oscillating out of phase. When the link connects buildings with significantly different dynamic properties, the forces in the link element are of the order of the smaller base shear when the structures are not connected.

Filiatrault and Folz (1991) studied the effect of linking two multi-degree-of-freedom inelastic steel structures. The structures studied are similar to the ones studied by Westermo (1989). The response of the structures was obtained using DRAIN-2D, for the San Fernando earthquake (1971), El Centro earthquake (1940), and the Romanian earthquake (1977). The response comparisons include the uncoupled system, an elastic coupling, and coupling of the structures using a friction damper. The optimum properties of the structural links were determined via parametric studies. The parametric study of the optimum slip load indicate that a better performance is achieved when the period of both structures is longer than the predominant period of the ground motion. Studies on the code specified separation indicate that the provisions may be overly conservative or unconservative.

Sues et al. (1991) presented the first phase of a two phase research project, funded by the National Science Foundation, to study the optimal device to reduce seismic structural pounding. In the first phase, a review of the pounding damage potential in the United States was made, the possible passive energy dissipation devices were listed, some notes on the installation of the energy dissipation devices were made, and some preliminary studies on the effectiveness of the devices were performed. The pounding reduction devices investigated were classified in five groups: metallic devices, viscoelastic materials, frictional devices, fluidic damping devices, and magnetic damping devices.

The authors note some of the possible challenges in installation in the devices that may be encountered: difficulty when placing a device between two buildings that are too close together, connecting the device to structural elements capable of withstanding the concentrated forces carried by the link, some disruption in the functionality of the structures may be necessary when

installing the devices, and the solution should be compatible with the existing structural system to avoid a generalized renovation of the structures.

Numerical simulations were performed incorporating some uncertainties in the earthquake ground motion, and in the structural properties. The structures were analyzed by a deterministic model using a number of artificial earthquakes, then output statistics were calculated from the deterministic results. Global damage measurements were used to determine the effectiveness of the damper: story drift, story acceleration, story shear, beam ductilities, and hysteretic energy dissipation in the beams. A number of local damage measures were also used: maximum impact velocity, sum of squared impact velocities, number of impacts, and floor response spectra.

Several link configurations were considered: bilinear link, bilinear impact, bilinear impact link, and linear dashpot link. For the studies, a 7 story structure adjacent to a three story structure were considered. The numerical simulations indicate a reduction in the high frequency accelerations caused by pounding. Depending on the location of the link, the taller structure tended to deform in a second mode configuration, or higher. An increase of the covariance of the response when the dampers are added was observed, however, an important reduction in the mean damage was attained at the same time. The authors note that the inelastic response was very sensitive to the structural and loading uncertainties.

Some of the results presented by the authors include figures for the variation of the story drift along the height of the structures, and little variation was observed between the no pounding case, the pounding case, and the two configurations of link devices used, suggesting that the combination of periods used for the analysis were not the most critical cases for pounding response.

SECTION 3
FORMULATION OF STRUCTURAL PROBLEM

3.1 Introduction

This section summarizes a number of important observations related to the pounding phenomena. Using concepts and observations from the literature survey presented in Section 2, relevant characteristics of the pounding phenomenon are described. Concepts that are used in the remaining portions of this work are introduced.

Using an energy formulation of the equations of motion, the problem of pounding interactions can be interpreted as sudden energy pulses that are transferred from one structure to the other. Such energy pulses lead to a reduction in the input energy of one structure, and an increase in the other. The amplification effects due to pounding can be measured in terms of energy change. The stereomechanical and piece-wise formulations to study pounding are formulated in terms of energy transfer.

A modified version of the Kelvin element is introduced to study pounding. The impact Kelvin element includes a damper element that is activated only for approaching velocities. The response of the impact Kelvin element to the traditional Kelvin element is compared.

Three approaches to model pounding are briefly described. Later, the effect of the maximum peak ground acceleration on the minimum gap to avoid pounding (critical), and on pounding effects, is studied. From the deterministic non-linear set of equations, it can be proven that the effects under a different peak ground acceleration can be derived from scaling the results from the original motion corresponding to a scaled gap size. This observation indicates that pounding analysis is to be carried for a single peak ground acceleration and different gap sizes only, since the response for other peak ground accelerations may be obtained from that set of analysis.

Finally, the concept of a Pseudo Energy Radius is introduced.

3.2 Energy Transfer during Pounding Interactions

During pounding interactions, a force is transmitted from one structure to the adjacent one. The presence of the force alters the energy level that each structure was subjected to, and a new response was observed. Some energy was transferred during the impact interactions, while a part of the energy was dissipated during contact.

Consider the equations of motion of two linear structures prone to pound:

$$m_1\ddot{u}_1 + c_1\dot{u}_1 + k_1u_1 + f_c = -m_1\ddot{x}_g \tag{3.1a}$$

$$m_2\ddot{u}_2 + c_2\dot{u}_2 + k_2u_2 - f_c = -m_2\ddot{x}_g \tag{3.1b}$$

where f_c is the contact force between the structures. Calculate the relative energy in the system by multiplying each equation by the velocity of each structure, and integrating over time (Uang and Bertero, 1988b and 1990):

$$E_{k1} + E_{\xi 1} + E_{p1} + E_{tr12} = E_{i1} \tag{3.2a}$$

$$E_{k2} + E_{\xi 2} + E_{p2} + E_{tr21} = E_{i2} \tag{3.2b}$$

where:

$$E_{k1} = \frac{m_1}{2}(\dot{u}_1)^2 \tag{3.3a}$$

$$E_{\xi 1} = \int_0^t c_1(\dot{u}_1(\tau))^2 d\tau \tag{3.3b}$$

$$E_{p1} = \frac{k_1}{2}(u_1)^2 \tag{3.3c}$$

$$E_{tr12} = \int_0^t f_c(\tau)\dot{u}_1(\tau)d\tau \tag{3.3d}$$

$$E_{i1} = -\int_0^t m_1\ddot{x}_g(\tau)\dot{u}_1(\tau)d\tau \tag{3.3e}$$

For simplicity, a distinction will be made between the input energy (E_i), the transfer energy (E_{tr}), and the structure energy (E_{s1}):

$$E_{s1} = E_{k1} + E_{\xi 1} + E_{p1} \tag{3.4}$$

The contact force introduces an energy term that transfers energy from one structure to the other. Some preliminary studies were performed to study the energy transfer between structures. Two single degree of freedom systems were studied using the deterministic model described by Valles (1995). The structures were subjected to a sinusoidal excitation (see Fig. 3.1). Figs. 3.2 to 3.4 present histories of displacements, velocities and accelerations for both structures for the no pounding and pounding cases, given a gap of $0.25\,g_{cr}$, where g_{cr} is the minimum gap required to avoid pounding (see Section 4). In Fig. 3.5 the history of the separation between the two structures is presented.

Fig. 3.6 presents the input energy and the structural energy for each structure. Energy transfers reduce the structural energy of structure 2, while the opposite occurs in structure 1. The global effect in structure 2 is that the input and structural energies are reduced, while the input and structural energies for structure 1 are increased. In general, one structure will increase its energy level while the other will experience a reduction.

3.3 Impact/Link Models

As indicated in the literature survey in Section 2, contact problems may be modeled in a macroscopic approach using a stereomechanical or piece-wise linear impact models. Both modeling techniques are discussed, along with the models used for link elements.

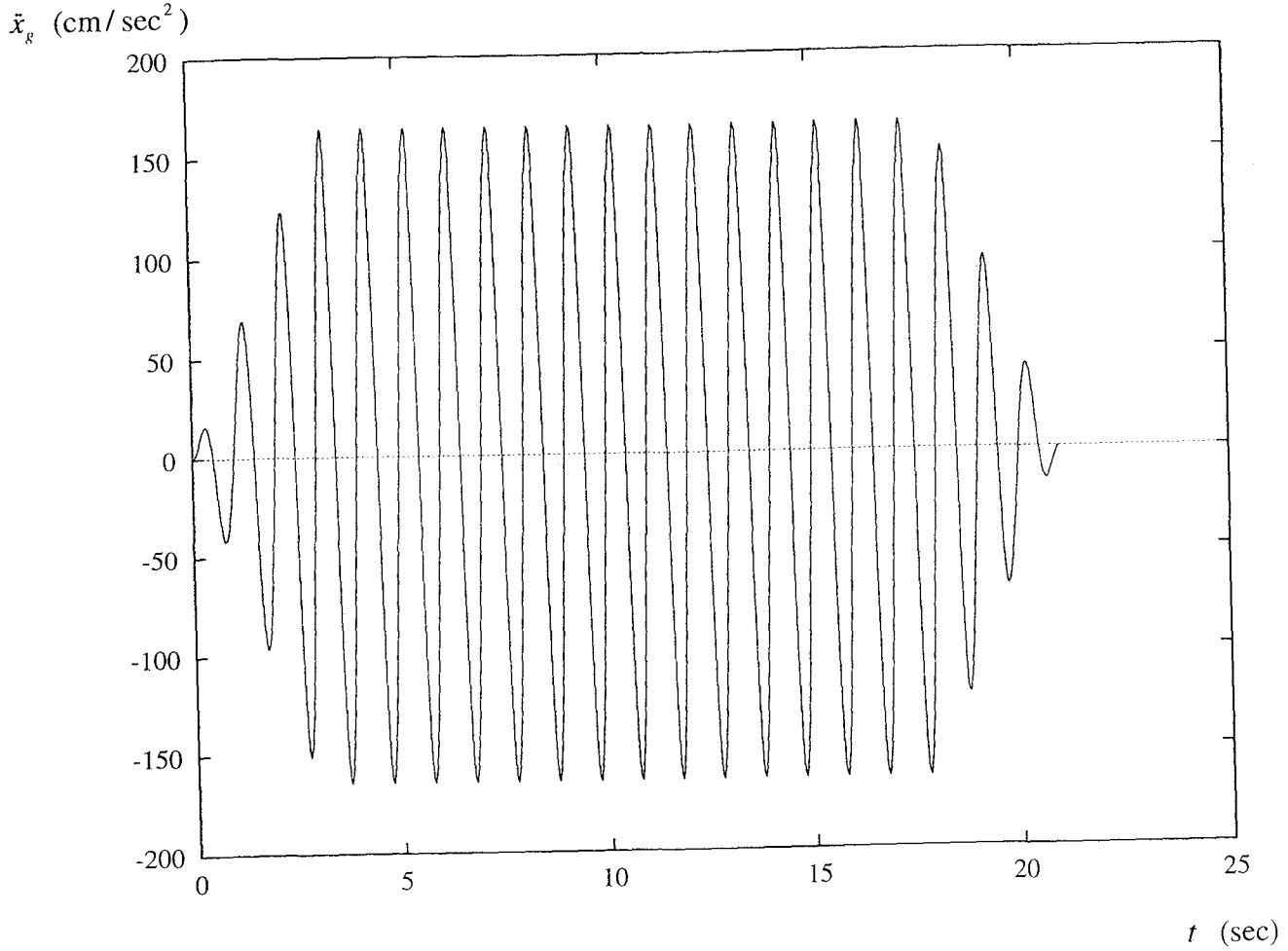

Fig. 3.1 Sinusoidal input motion for energy transfer studies (T_{inp} =1.0 sec).

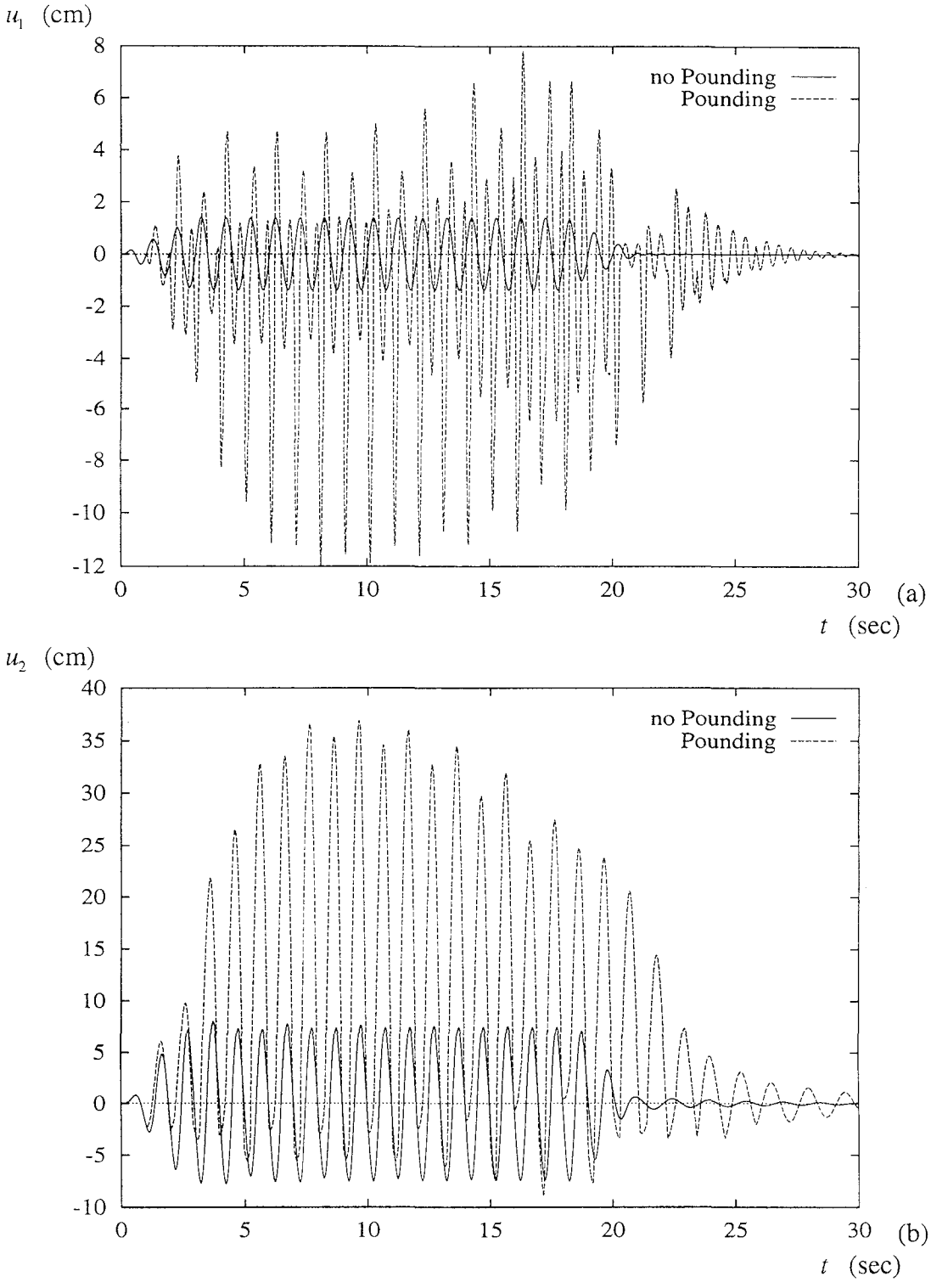

Fig. 3.2 Comparison of pounding vs. no pounding displacements (T_1=0.5 sec, T_2=1.5 sec, g_p=0.25 g_{cr}, PGA=160 cm/sec^2).

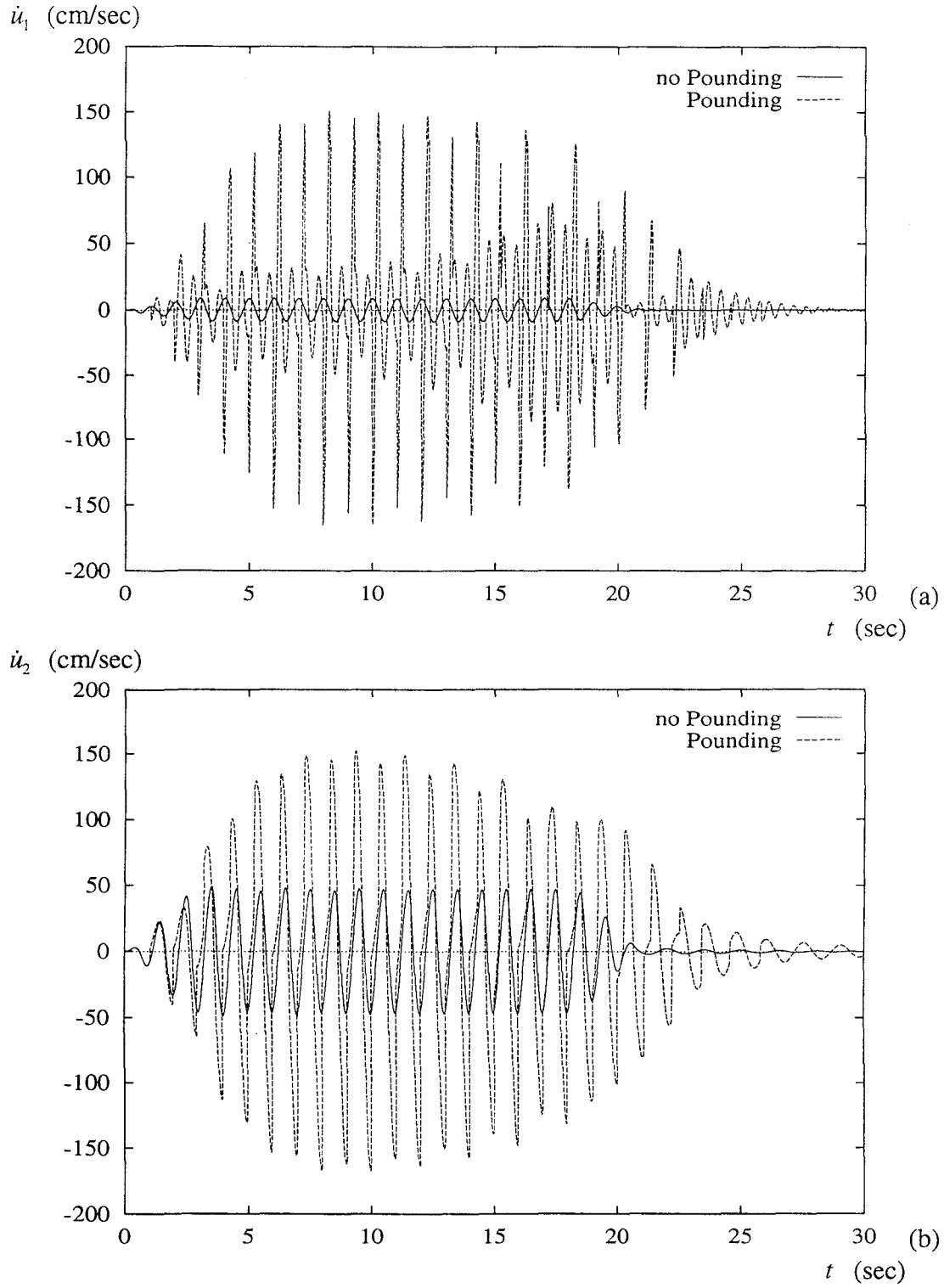

Fig. 3.3 Comparison of pounding vs. no pounding velocities (T_1=0.5 sec, T_2=1.5 sec, g_p=0.25 g_{cr}, PGA=160 cm/sec^2).

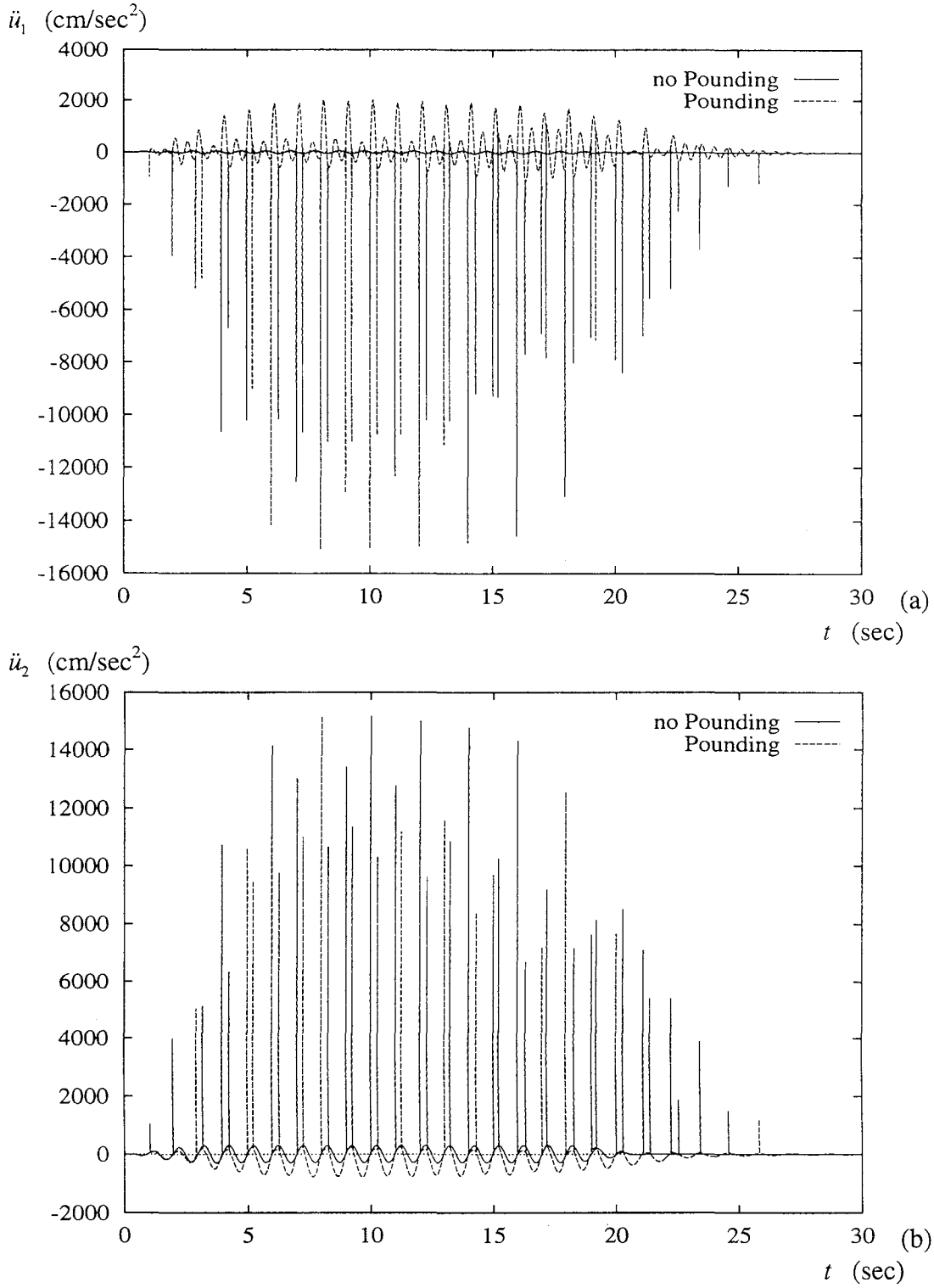

Fig. 3.4 Comparison of pounding vs. no pounding accelerations (T_1=0.5 sec, T_2=1.5 sec, g_p=0.25 g_{cr}, PGA=160 cm/sec^2).

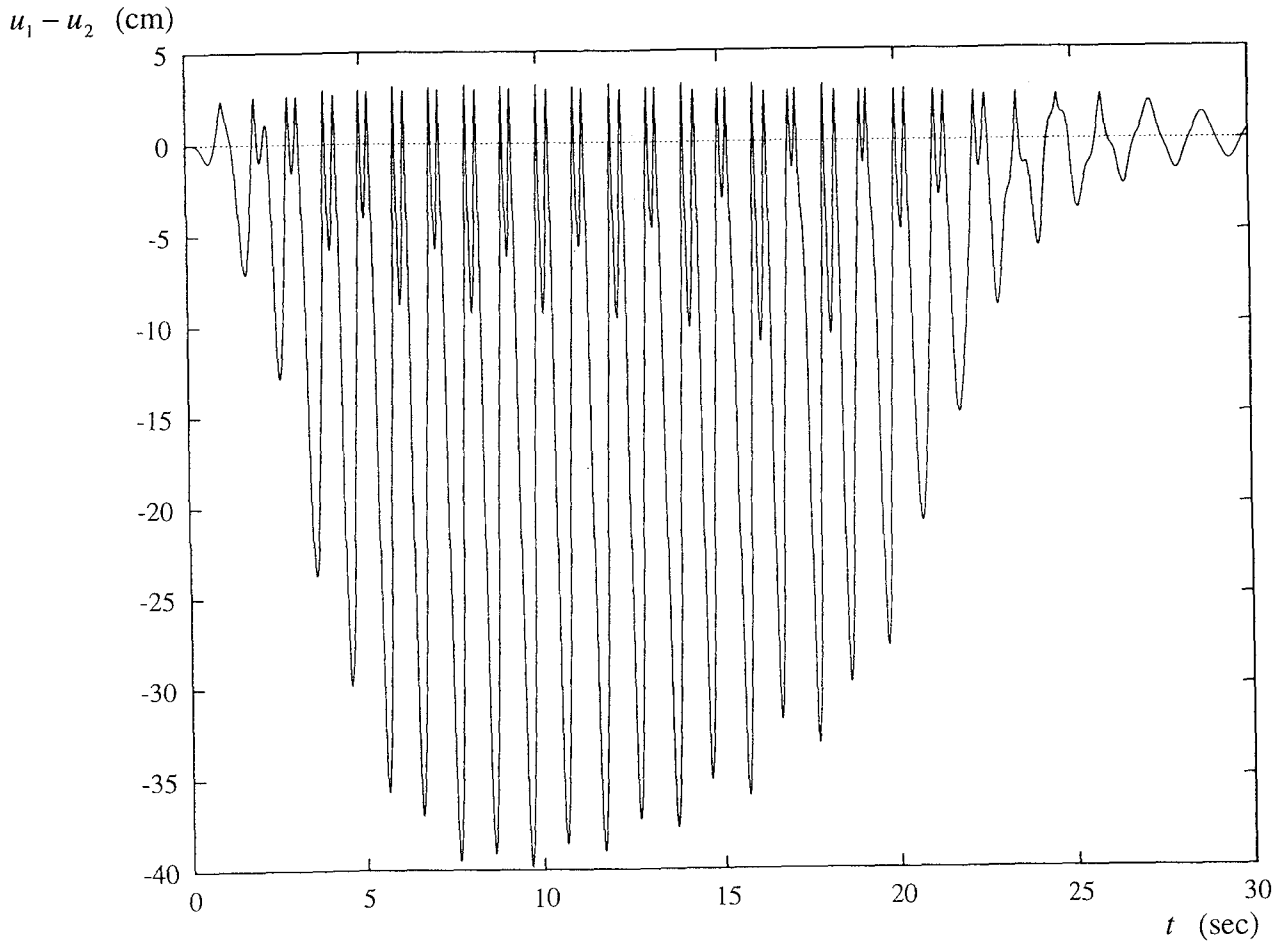

Fig. 3.5 History of separation between the two structures (T_1=0.5 sec, T_2=1.5 sec, g_p=0.25 g_{cr}, PGA=160 cm/sec^2).

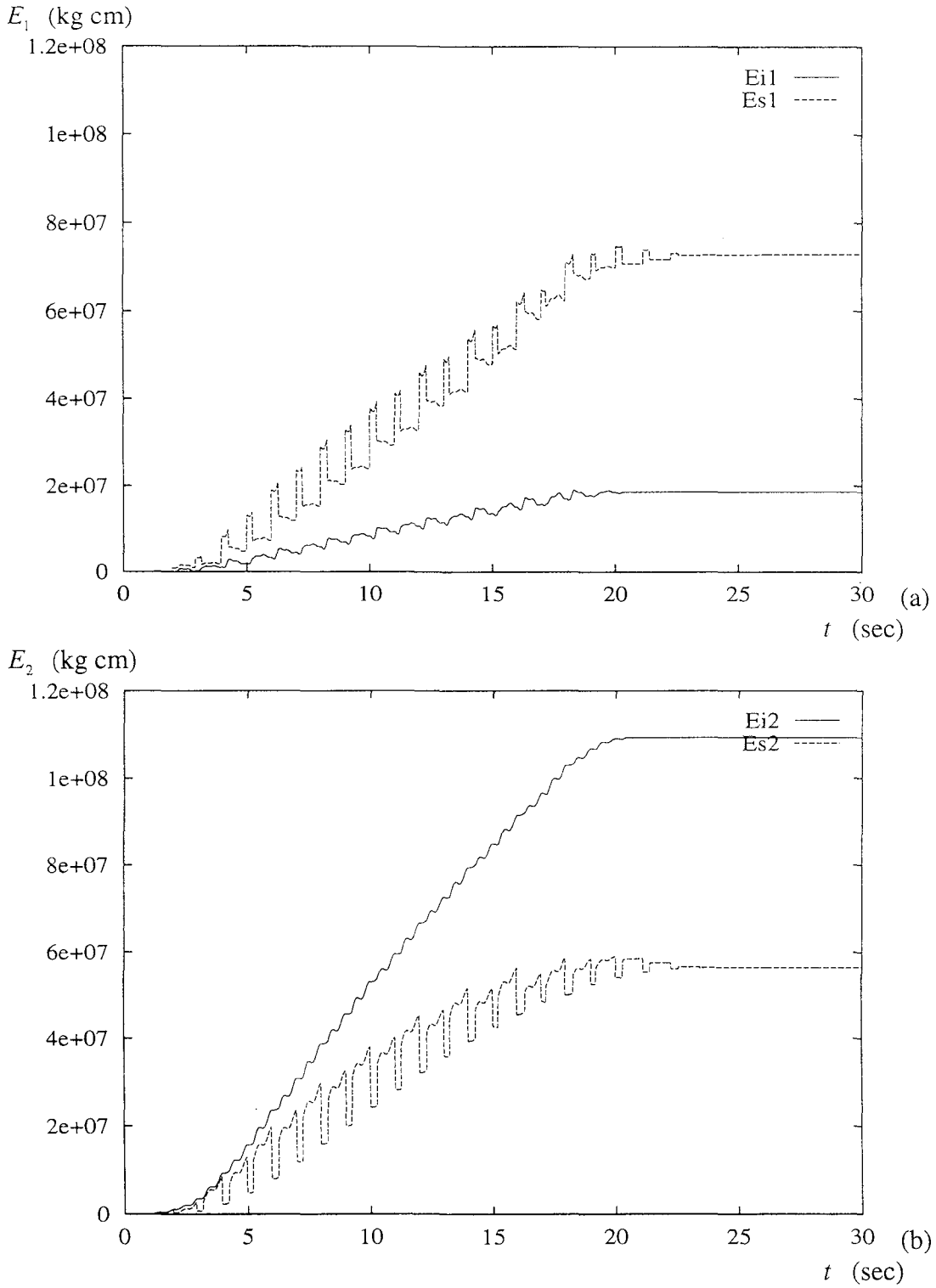

Fig. 3.6 History of input and structural energy for pounding response (T_1=0.5 sec, T_2=1.5 sec, g_p=0.25 g_{cr} , PGA=160 cm/sec^2).

3.3.1 Stereomechanical Impact

Stereomechanical impact is a macroscopic approach to the problem of pounding. The velocity of the impacting bodies is calculated based on the velocities prior to contact, and a coefficient of restitution (e), that takes into account any nonlinearity that may take place during the contact phase. Two bodies approaching each other with velocities v_1 and v_2, prior to impact, will have post impact velocities (v_1' and v_2') according to:

$$v_1' = v_1 - (1+e)\frac{m_2(v_1 - v_2)}{m_1 + m_2} \tag{3.5a}$$

$$v_2' = v_2 + (1+e)\frac{m_1(v_1 - v_2)}{m_1 + m_2} \tag{3.5b}$$

where m_1 and m_2 are the masses of the colliding bodies.

Similarly, when pounding occurs at story "j", the post impact conditions in velocity are:

$$\dot{u}'_{1(j)} = \dot{u}_{1(j)} - (1+e_{(j)})\frac{M_{2(j)}(\dot{u}_{1(j)} - \dot{u}_{2(j)})}{M_{1(j)} + M_{2(j)}} \tag{3.6a}$$

$$\dot{u}'_{2(j)} = \dot{u}_{2(j)} + (1+e_{(j)})\frac{M_{1(j)}(\dot{u}_{1(j)} - \dot{u}_{2(j)})}{M_{1(j)} + M_{2(j)}} \tag{3.6b}$$

Where $\dot{u}_{1(j)}$ and $\dot{u}_{2(j)}$ are the velocities at story "j" at the onset of pounding, $M_{1(j)}$ and $M_{2(j)}$ are the structural masses of the colliding floors, and $e_{(j)}$ is the coefficient of restitution at the interface of story "j".

Note that the relative mass of the structures plays an important part in determining the post impact conditions. Considering elastic impact ($e_{(j)} = 1$), if the masses in the structure are equal, then the magnitude of the velocities will be interchanged, that is:

$$\dot{u}'_{1(j)} = \dot{u}_{2(j)} \tag{3.7a}$$

$$\dot{u}'_{2(j)} = \dot{u}_{1(j)} \tag{3.7b}$$

The new velocity conditions can be calculated using a transformation matrix:

$$\dot{\mathbf{u}}_1' = \left(\mathbf{I} - \mathbf{M}_2\mathbf{T}_{gp}\mathbf{U}_{gp}\right)\dot{\mathbf{u}}_1 + \mathbf{M}_2\mathbf{T}_{gp}\mathbf{U}_{gp}\dot{\mathbf{u}}_2 \tag{3.8a}$$

$$\dot{\mathbf{u}}_2' = \mathbf{M}_1\mathbf{T}_{gp}\mathbf{U}_{gp}\dot{\mathbf{u}}_1 + \left(\mathbf{I} - \mathbf{M}_1\mathbf{T}_{gp}\mathbf{U}_{gp}\right)\dot{\mathbf{u}}_2 \tag{3.8b}$$

Where:

$\mathbf{I}$: Identity matrix.

$\mathbf{T}_{gp}$: Pounding transformation matrix for velocities, of the form:

$$\mathbf{T}_{gp} = \begin{bmatrix} T_{gp(1)} & 0 & \cdots & 0 & 0 & 0 \\ 0 & T_{gp(2)} & \cdots & 0 & 0 & 0 \\ \vdots & \vdots & \ddots & \vdots & \vdots & \vdots \\ 0 & 0 & \cdots & T_{gp(ng-1)} & 0 & 0 \\ 0 & 0 & \cdots & 0 & T_{gp(ng)} & 0 \\ 0 & 0 & \cdots & 0 & 0 & 0 \end{bmatrix} \tag{3.9}$$

The last column and row of zeros depend on the number of degrees of freedom of the structures being studied, that is, according to the matrices being multiplied. The elements in the main diagonal are:

$$T_{gp(j)} = \frac{1 + e_{(j)}}{M_{1(j)} + M_{2(j)}} \tag{3.10}$$

$\mathbf{U}_{gp}$: Diagonal matrix that indicates which contact elements are activated.

Since the contact time is considered small, the displacement configuration of the system would not have changed significantly during pounding, therefore, the post impact displacement are:

$$\mathbf{u}_1' \approx \mathbf{u}_1 \tag{3.11a}$$

$$\mathbf{u}_2' \approx \mathbf{u}_2 \tag{3.11b}$$

However, since the velocities in the system were modified while the displacements were not altered by impact, the accelerations must be recalculated to satisfy the dynamic equilibrium of the system after pounding has taken place:

$$\ddot{\mathbf{u}}_1' = -\ddot{x}_g(t)\mathbf{1} - \mathbf{M}_1^{-1}\mathbf{C}_1\dot{\mathbf{u}}_1' - \mathbf{M}_1^{-1}\mathbf{K}_1\mathbf{u}_1' \tag{3.12a}$$

$$\ddot{\mathbf{u}}_2' = -\ddot{x}_g(t)\mathbf{1} - \mathbf{M}_2^{-1}\mathbf{C}_2\dot{\mathbf{u}}_2' - \mathbf{M}_2^{-1}\mathbf{K}_2\mathbf{u}_2' \tag{3.12b}$$

In matrix notation, the complete post impact state of the system may be calculated according to:

$$\mathbf{U}' = \mathbf{T}_s\mathbf{U} - \ddot{x}_g(t)\mathbf{L}_s \tag{3.13}$$

Where:

$$\mathbf{U}^t = \left\{\mathbf{u}_1^t \quad \mathbf{u}_2^t \quad \dot{\mathbf{u}}_1^t \quad \dot{\mathbf{u}}_2^t \quad \ddot{\mathbf{u}}_1^t \quad \ddot{\mathbf{u}}_2^t\right\} \tag{3.14}$$

$$\mathbf{T}_s = \begin{bmatrix} \mathbf{1} & \mathbf{0} & \mathbf{0} \\ \mathbf{0} & \mathbf{1} & \mathbf{0} \\ \mathbf{0} & \mathbf{0} & (\mathbf{I}-\mathbf{M}_2\mathbf{T}_{gp}\mathbf{U}_{gp}) \\ \mathbf{0} & \mathbf{0} & \mathbf{M}_1\mathbf{T}_{gp}\mathbf{U}_{gp} \\ -\mathbf{M}_1^{-1}\mathbf{K}_1 & \mathbf{0} & -\mathbf{M}_1^{-1}\mathbf{C}_1(\mathbf{I}-\mathbf{M}_2\mathbf{T}_{gp}\mathbf{U}_{gp}) \\ \mathbf{0} & -\mathbf{M}_2^{-1}\mathbf{K}_2 & -\mathbf{M}_2^{-1}\mathbf{C}_2\mathbf{M}_1\mathbf{T}_{gp}\mathbf{U}_{gp} \end{bmatrix}$$

$$\begin{bmatrix} \mathbf{0} & \mathbf{0} & \mathbf{0} \\ \mathbf{0} & \mathbf{0} & \mathbf{0} \\ \mathbf{M}_2\mathbf{T}_{gp}\mathbf{U}_{gp} & \mathbf{0} & \mathbf{0} \\ (\mathbf{I}-\mathbf{M}_1\mathbf{T}_{gp}\mathbf{U}_{gp}) & \mathbf{0} & \mathbf{0} \\ -\mathbf{M}_1^{-1}\mathbf{C}_1\mathbf{M}_2\mathbf{T}_{gp}\mathbf{U}_{gp} & \mathbf{0} & \mathbf{0} \\ -\mathbf{M}_2^{-1}\mathbf{C}_2(\mathbf{I}-\mathbf{M}_1\mathbf{T}_{gp}\mathbf{U}_{gp}) & \mathbf{0} & \mathbf{0} \end{bmatrix} \tag{3.15}$$

$$\mathbf{L}_s^t = \left\{\mathbf{0}^t \quad \mathbf{0}^t \quad \mathbf{0}^t \quad \mathbf{0}^t \quad \mathbf{1}^t \quad \mathbf{1}^t\right\} \tag{3.16}$$

Note that using the stereomechanical transformation matrix $\mathbf{T}_s$ is not computationally as efficient as the transformations of velocity and acceleration using Eqs. 3.8 and 3.12, respectively. Nevertheless, the stereomechanical point transformation matrix was presented for completeness, and to express pounding using a similar notation to the matrix formulation of the Newmark-Beta, used in two of the mathematical formulations discussed later.

The stereomechanical impact may be considered as a point transformation that is activated when the gap in one of the stories is closed. The point transformation takes place in a short period of time, and during the numerical computations is considered instantaneous. Once the new state of the system is obtained, the step by step integration (field transformation) continues.

3.3.2 Piece-wise Linear Impact

During piece-wise linear impact the equations of motion of the structures become suddenly coupled through a contact element. The contact element is considered as Kelvin (see Fig. 3.1a). The force in the contact element at story "*j*" is given by:

$$F_{c(j)} = \left(C_{c(j)}(\dot{u}_{1(j)} - \dot{u}_2) + K_{c(j)}(u_{1(j)} - u_{2(j)} - g_{p(j)})\right) \mathrm{U}[u_{1(j)} - u_{2(j)} - g_{p(j)}] \qquad (3.17a)$$

or as an Impact Kelvin element (see Fig. 3.1b) in which case the contact force is given by:

$$\begin{aligned} F_{c(j)} = &\left(C_{c(j)}(\dot{u}_{1(j)} - \dot{u}_2)\mathrm{U}[\dot{u}_{1(j)} - \dot{u}_{2(j)}]\right. \\ &\left. + K_{c(j)}(u_{1(j)} - u_{2(j)} - g_{p(j)})\right) \mathrm{U}[u_{1(j)} - u_{2(j)} - g_{p(j)}] \end{aligned} \qquad (3.17b)$$

Where:

$C_{c(j)}$: Damping coefficient of pounding element at story "*j*".

$K_{c(j)}$: Stiffness of pounding element at story "*j*".

$\dot{u}_{i(j)}$: Velocity of structure "*i*", at story "*j*".

$u_{i(j)}$: Displacement of structure "*i*", at story "*j*".

$g_{p(j)}$: Initial gap at story "*j*".

U[x]: Unit step function.

The forces in the pounding elements may be expressed in matrix form as:

$$\begin{Bmatrix} \mathbf{F}_c \\ -\mathbf{F}_c \end{Bmatrix} = \begin{bmatrix} \mathbf{C}_c\mathbf{U}_{gp} & -\mathbf{C}_c\mathbf{U}_{gp} \\ -\mathbf{C}_c\mathbf{U}_{gp} & \mathbf{C}_c\mathbf{U}_{gp} \end{bmatrix} \begin{Bmatrix} \dot{\mathbf{u}}_1 \\ \dot{\mathbf{u}}_2 \end{Bmatrix} + \begin{bmatrix} \mathbf{K}_c\mathbf{U}_{gp} & -\mathbf{K}_c\mathbf{U}_{gp} \\ -\mathbf{K}_c\mathbf{U}_{gp} & \mathbf{K}_c\mathbf{U}_{gp} \end{bmatrix} \begin{Bmatrix} \mathbf{u}_1 \\ \mathbf{u}_2 \end{Bmatrix} + \begin{Bmatrix} -\mathbf{K}_c\mathbf{U}_{gp}\mathbf{g}_p \\ \mathbf{K}_c\mathbf{U}_{gp}\mathbf{g}_p \end{Bmatrix} \qquad (3.18)$$

Where $\mathbf{C}_c$ is a diagonal matrix with the damping constants of the contact element at each story:

$$\mathbf{C}_c = \begin{bmatrix} C_{c(1)} & 0 & \cdots & 0 & 0 \\ 0 & C_{c(2)} & \cdots & 0 & 0 \\ \vdots & \vdots & \ddots & \vdots & \vdots \\ 0 & 0 & \cdots & C_{c(ng-1)} & 0 \\ 0 & 0 & \cdots & 0 & C_{c(ng)} \end{bmatrix} \qquad (3.19)$$

$\mathbf{K}_c$ is a diagonal matrix with the stiffness of the contact elements at each story:

$$\mathbf{K}_c = \begin{bmatrix} K_{c(1)} & 0 & \cdots & 0 & 0 \\ 0 & K_{c(2)} & \cdots & 0 & 0 \\ \vdots & \vdots & \ddots & \vdots & \vdots \\ 0 & 0 & \cdots & K_{c(ng-1)} & 0 \\ 0 & 0 & \cdots & 0 & K_{c(ng)} \end{bmatrix} \tag{3.20}$$

And $\mathbf{U}_{gp}$ is a diagonal matrix that indicates which of the contact elements are activated:

$$\mathbf{U}_{gp} = \begin{bmatrix} U_{gp(1)} & 0 & \cdots & 0 & 0 \\ 0 & U_{gp(2)} & \cdots & 0 & 0 \\ \vdots & \vdots & \ddots & \vdots & \vdots \\ 0 & 0 & \cdots & U_{gp(ng-1)} & 0 \\ 0 & 0 & \cdots & 0 & U_{gp(ng)} \end{bmatrix} \tag{3.21}$$

$$U_{gp(j)} = \mathrm{U}[u_{1(j)} - u_{2(j)} - g_{p(j)}] \tag{3.22}$$

Where ng is the maximum story at which pounding may occur.

Note that in general , the number of stories will be different for each structure, and that this number may also differ from ^{ng}. Therefore, special considerations are necessary to perform the matrix manipulations. One solution to the problem would be to consider the same number of degrees of freedom for both structures, knowing that the upper solution for the shorter structure will always be zero. This approach, although simple to program, unnecessarily increases the computation time and the storage requirements. The solution adopted in programming was to dimension the contact matrices ($\mathbf{C}_c$, $\mathbf{K}_c$, and $\mathbf{U}_{gp}$) for the maximum story at which pounding may occur (^{ng}), since higher stories will have no contribution. However, to make the presentation of the formulas in a more straightforward manner, these details will be dealt with under each of the mathematical models.

Therefore, the equations of motion considering piece-wise linear impact may be written as:

$$\begin{bmatrix} \mathbf{M}_1 & \mathbf{0} \\ \mathbf{0} & \mathbf{M}_2 \end{bmatrix} \begin{Bmatrix} \ddot{\mathbf{u}}_1 \\ \ddot{\mathbf{u}}_2 \end{Bmatrix} + \begin{bmatrix} \mathbf{C}_1 & \mathbf{0} \\ \mathbf{0} & \mathbf{C}_2 \end{bmatrix} \begin{Bmatrix} \dot{\mathbf{u}}_1 \\ \dot{\mathbf{u}}_2 \end{Bmatrix} + \begin{bmatrix} \mathbf{K}_1 & \mathbf{0} \\ \mathbf{0} & \mathbf{K}_2 \end{bmatrix} \begin{Bmatrix} \mathbf{u}_1 \\ \mathbf{u}_2 \end{Bmatrix} + \begin{Bmatrix} \mathbf{F}_c \\ -\mathbf{F}_c \end{Bmatrix} = -\begin{bmatrix} \mathbf{M}_1 & 0 \\ 0 & \mathbf{M}_2 \end{bmatrix} \begin{Bmatrix} \mathbf{1} \\ \mathbf{1} \end{Bmatrix} \ddot{x}_g(t) \tag{3.23}$$

3.3.3 Link Element

To retrofit structures that may be prone to severe damage due to pounding, the study includes link elements between the structures. The link elements used consist of a hysteretic spring and a linear dashpot in parallel. The hysteretic spring may be bilinear or a modification of the three parameter model introduced by Park et al. (1987).

Similar to the pounding element, the forces in the link elements are:

$$F_{l(j)} = C_{l(j)}(\dot{u}_{1(j)} - \dot{u}_{2(j)}) + \mathrm{f}_{l(j)}(u_{1(j)} - u_{2(j)}) \tag{3.24}$$

Where:

$C_{l(j)}$: Damping constant of link element at story "j".

$\mathrm{f}_{l(j)}(x)$:Nonlinear force in the contact element at story "j".

Written in matrix notation:

$$\begin{Bmatrix} \mathbf{F}_l \\ -\mathbf{F}_l \end{Bmatrix} = \begin{bmatrix} \mathbf{C}_l & -\mathbf{C}_l \\ -\mathbf{C}_l & \mathbf{C}_l \end{bmatrix} \begin{Bmatrix} \dot{\mathbf{u}}_1 \\ \dot{\mathbf{u}}_2 \end{Bmatrix} + \begin{Bmatrix} \mathbf{f}_l(\mathbf{u}_1 - \mathbf{u}_2) \\ -\mathbf{f}_l(\mathbf{u}_1 - \mathbf{u}_2) \end{Bmatrix} \tag{3.25}$$

Therefore, the equations of motion considering the link elements in the structure are:

$$\begin{bmatrix} \mathbf{M}_1 & \mathbf{0} \\ \mathbf{0} & \mathbf{M}_2 \end{bmatrix} \begin{Bmatrix} \ddot{\mathbf{u}}_1 \\ \ddot{\mathbf{u}}_2 \end{Bmatrix} + \begin{bmatrix} \mathbf{C}_1 & \mathbf{0} \\ \mathbf{0} & \mathbf{C}_2 \end{bmatrix} \begin{Bmatrix} \dot{\mathbf{u}}_1 \\ \dot{\mathbf{u}}_2 \end{Bmatrix} + \begin{bmatrix} \mathbf{K}_1 & \mathbf{0} \\ \mathbf{0} & \mathbf{K}_2 \end{bmatrix} \begin{Bmatrix} \mathbf{u}_1 \\ \mathbf{u}_2 \end{Bmatrix}$$
$$+ \begin{Bmatrix} \mathbf{F}_c \\ -\mathbf{F}_c \end{Bmatrix} + \begin{Bmatrix} \mathbf{F}_l \\ -\mathbf{F}_l \end{Bmatrix} = -\begin{bmatrix} \mathbf{M}_1 & \mathbf{0} \\ \mathbf{0} & \mathbf{M}_2 \end{bmatrix} \begin{Bmatrix} \mathbf{1} \\ \mathbf{1} \end{Bmatrix} \ddot{x}_g(t) \tag{3.26}$$

Note that in the case of stereomechanical impact, the forces from the contact elements are zero, and the transformation to determine the post impact accelerations must consider the link elements:

$$\ddot{\mathbf{u}}_1' = -\ddot{x}_g(t)\mathbf{1} - \mathbf{M}_1^{-1}(\mathbf{C}_1 + \mathbf{C}_l)\dot{\mathbf{u}}_1' + \mathbf{M}_1^{-1}\mathbf{C}_l\dot{\mathbf{u}}_2' - \mathbf{M}_1^{-1}\mathbf{K}_1\mathbf{u}_1' - \mathbf{M}_1^{-1}\mathbf{F}_l \tag{3.27a}$$

$$\ddot{\mathbf{u}}_2' = -\ddot{x}_g(t)\mathbf{1} - \mathbf{M}_2^{-1}(\mathbf{C}_2 + \mathbf{C}_l)\dot{\mathbf{u}}_2' + \mathbf{M}_2^{-1}\mathbf{C}_l\dot{\mathbf{u}}_1' - \mathbf{M}_2^{-1}\mathbf{K}_2\mathbf{u}_2' + \mathbf{M}_2^{-1}\mathbf{F}_l \tag{3.27b}$$

3.3.4 Energy Transfer in Stereomechanical Impact

During impact the structures exchange energy. In stereomechanical impact, the velocities of the systems change according to the post impact conditions. This sudden change in the velocities of the system causes changes to the kinetic energy of the system. The change in the kinetic energies of each structure are the instantaneous energy transfer that pounding imposes in the systems.

Consider that contact at story "j" is observed. The energy transferred to one of the structures may be calculated as the change in kinetic energy in the other. Therefore, the energy transferred by structure 1 is:

$$\begin{aligned} E_{tr1(j)} &= E'_{k2(j)} - E_{k2(j)} \\ &= \frac{1}{2} M_{2(j)} \left(\dot{u}'^{2}_{2(j)} - \dot{u}^{2}_{2(j)} \right) \end{aligned} \tag{3.28a}$$

where $E'_{k2(j)}$ corresponds to the post impact kinetic energy, at story "j", in structure 2. The energy transferred by structure 2 is:

$$\begin{aligned} E_{tr2(j)} &= E'_{k1(j)} - E_{k1(j)} \\ &= \frac{1}{2} M_{1(j)} \left(\dot{u}'^{2}_{1(j)} - \dot{u}^{2}_{1(j)} \right) \end{aligned} \tag{3.28b}$$

Substituting the formulas for the post impact velocities, and after some algebra:

$$\begin{aligned} E_{tr1(j)} = -\frac{1}{2} \frac{\left(1+e_{(j)}\right) M_{1(j)} M_{2(j)}}{\left(M_{1(j)} + M_{2(j)} \right)^2} \Big[& -\left(1+e_{(j)}\right) M_{1(j)} \dot{u}_{1(j)} \\ & + \left(\left(-1+e_{(j)}\right) M_{1(j)} - 2 M_{2(j)} \right) \dot{u}_{2(j)} \Big] \left(\dot{u}_{1(j)} - \dot{u}_{2(j)} \right) \end{aligned} \tag{3.29a}$$

$$\begin{aligned} E_{tr2(j)} = +\frac{1}{2} \frac{\left(1+e_{(j)}\right) M_{1(j)} M_{2(j)}}{\left(M_{1(j)} + M_{2(j)} \right)^2} \Big[& \left(-2 M_{1(j)} + \left(-1+e_{(j)}\right) M_{2(j)} \right) \dot{u}_{1(j)} \\ & - \left(1+e_{(j)}\right) M_{2(j)} \dot{u}_{2(j)} \Big] \left(\dot{u}_{1(j)} - \dot{u}_{2(j)} \right) \end{aligned} \tag{3.29b}$$

For a perfect elastic impact ($e_{(j)} = 1$), the previous equations for the transferred energy simplify to:

$$E_{tr1(j)} = -\frac{M_{1(j)} M_{2(j)}}{\left(M_{1(j)} + M_{2(j)}\right)^2}\left[-2M_{1(j)}\dot{u}_{1(j)} - 2M_{2(j)}\dot{u}_{2(j)}\right]\left(\dot{u}_{1(j)} - \dot{u}_{2(j)}\right) \tag{3.30a}$$

$$E_{tr2(j)} = +\frac{M_{1(j)} M_{2(j)}}{\left(M_{1(j)} + M_{2(j)}\right)^2}\left[-2M_{1(j)}\dot{u}_{1(j)} - 2M_{2(j)}\dot{u}_{2(j)}\right]\left(\dot{u}_{1(j)} - \dot{u}_{2(j)}\right) = -E_{tr1(j)} \tag{3.30b}$$

Therefore, during an elastic impact, energy is conserved during pounding, and the energy transferred by one structure equals the energy received by the other structure. Note that the masses of the structure highly influence the post impact velocities as well as the transferred energy.

For non-linear impacts, only part of the energy is transferred to the other structure, since some energy is dissipated. The dissipated energy may be calculated as the sum of the transferred energies:

$$\begin{aligned} E_{tr1(j)} + E_{tr2(j)} &= \frac{1}{2}\frac{\left(1+e_{(j)}\right) M_{1(j)} M_{2(j)}}{\left(M_{1(j)} + M_{2(j)}\right)^2}\left[\left(-1+e_{(j)}\right)\left(M_{1(j)} + M_{2(j)}\right)\dot{u}_{1(j)}\right. \\ &\quad \left. -\left(-1+e_{(j)}\right)\left(M_{1(j)} + M_{2(j)}\right)\dot{u}_{2(j)}\right]\left(\dot{u}_{1(j)} - \dot{u}_{2(j)}\right) \\ &= \frac{1}{2}\frac{\left(e_{(j)}^2 - 1\right) M_{1(j)} M_{2(j)}}{M_{1(j)} + M_{2(j)}}\left(\dot{u}_{1(j)} - \dot{u}_{2(j)}\right)^2 \end{aligned} \tag{3.31}$$

Note that the dissipated energy is negative, because energy is being removed from the system. A smaller coefficient of restitution will induce larger energy dissipation. Greater relative approach velocities will also induce larger energy dissipation.

The expected energy transferred by each structure is calculated according to:

$$\begin{aligned} E\left\{E_{tr1(j)}\right\} = -\frac{1}{2}\frac{\left(1+e_{(j)}\right) M_{1(j)} M_{2(j)}}{\left(M_{1(j)} + M_{2(j)}\right)^2}\left[-\left(1+e_{(j)}\right) M_{1(j)}\left(E\left\{\dot{u}_1^2\right\} - E\left\{\dot{u}_1\dot{u}_2\right\}\right)\right. \\ \left. +\left(\left(-1+e_{(j)}\right) M_{1(j)} - 2M_{2(j)}\right)\left(E\left\{\dot{u}_1\dot{u}_2\right\} - E\left\{\dot{u}_2^2\right\}\right)\right] \end{aligned} \tag{3.32a}$$

$$E\{E_{tr2(j)}\} = +\frac{1}{2}\frac{(1+e_{(j)})M_{1(j)}M_{2(j)}}{(M_{1(j)}+M_{2(j)})^2}\Big[\Big(-2M_{1(j)}+(-1+e_{(j)})M_{2(j)}\Big)\Big(E\{\dot{u}_1^2\} - E\{\dot{u}_1\dot{u}_2\}\Big) - (1+e_{(j)})M_{2(j)}\big(E\{\dot{u}_1\dot{u}_2\} - E\{\dot{u}_2^2\}\big)\Big] \tag{3.32b}$$

For elastic impact ($e_{(j)} = 1$) the expected energy transfer by each structure is:

$$E\{E_{tr1(j)}\} = -\frac{M_{1(j)}M_{2(j)}}{(M_{1(j)}+M_{2(j)})^2}\Big[-2M_{1(j)}\big(E\{\dot{u}_1^2\} - E\{\dot{u}_1\dot{u}_2\}\big) - 2M_{2(j)}\big(E\{\dot{u}_1\dot{u}_2\} - E\{\dot{u}_2^2\}\big)\Big] \tag{3.33a}$$

$$\begin{aligned} E\{E_{tr2(j)}\} &= +\frac{M_{1(j)}M_{2(j)}}{(M_{1(j)}+M_{2(j)})^2}\Big[-2M_{1(j)}\big(E\{\dot{u}_1^2\} - E\{\dot{u}_1\dot{u}_2\}\big) - 2M_{2(j)}\big(E\{\dot{u}_1\dot{u}_2\} - E\{\dot{u}_2^2\}\big)\Big] \\ &= -E\{E_{tr1(j)}\} \end{aligned} \tag{3.33b}$$

The expected dissipated energy due to non-linear impacts is:

$$E\{E_{tr1(j)} + E_{tr2(j)}\} = \frac{1}{2}\frac{(e_{(j)}^2 - 1)M_{1(j)}M_{2(j)}}{M_{1(j)}+M_{2(j)}}\Big(E\{\dot{u}_{1(j)}^2\} - 2E\{\dot{u}_{1(j)}\dot{u}_{2(j)}\} + E\{\dot{u}_{2(j)}^2\}\Big) \tag{3.34}$$

Note that the expected transfer energy, and the expected dissipated energy are related to the variance and covariance of the response.

3.3.5 Energy Transfer in Piece-wise Linear Impact

To calculate the energy transfer at each story in a piece-wise linear system, multiply the contact forces by the velocity at that story and integrate over time:

$$\begin{aligned} E_{tr1(j)} &= \int \dot{u}_{1(j)}F_{c(j)}dt \\ &= \int\Big[C_{c(j)}U_{gp(j)}\dot{u}_{1(j)}\big(\dot{u}_{1(j)} - \dot{u}_{2(j)}\big) + K_{c(j)}U_{gp(j)}\dot{u}_{1(j)}\big(u_{1(j)} - u_{2(j)} - g_{p(j)}\big)\Big]dt \\ &= E_{tr1(j)}^{C} + E_{tr1(j)}^{K} \end{aligned} \tag{3.35a}$$

$$
\begin{aligned}
E_{tr2(j)} &= -\int \dot{u}_{2(j)} F_{c(j)} dt \\
&= \int \left[C_{c(j)} U_{gp(j)} \dot{u}_{2(j)} \left(\dot{u}_{1(j)} - \dot{u}_{2(j)} \right) + K_{c(j)} U_{gp(j)} \dot{u}_{2(j)} \left(u_{1(j)} - u_{2(j)} - g_{p(j)} \right) \right] dt \\
&= E^{C}_{tr2(j)} + E^{K}_{tr2(j)}
\end{aligned}
\tag{3.35b}
$$

Where the spring contributions to the transfer energy balance:

$$
\begin{aligned}
E^{K}_{tr1(j)} &= \int_{t_0}^{t} \dot{u}_{1(j)} K_{c(j)} \left(u_{1(j)} - u_{2(j)} - g_{p(j)} \right) \mathrm{U}[u_{1(j)} - u_{2(j)} - g_{p(j)}] d\tau \\
&= \int_{u_{2(j)}+g_{p(j)}}^{u_{1(j)}} K_{c(j)} \left(u_{1(j)} - u_{2(j)} - g_{p(j)} \right) du_{1(j)} \\
&= K_{c(j)} \left[\frac{u^2_{1(j)}}{2} - u_{1(j)} \left(u_{2(j)} + g_{p(j)} \right) \right]_{u_{2(j)}+g_{p(j)}}^{u_{1(j)}} \\
&= \frac{1}{2} K_{c(j)} \left(u_{1(j)} - u_{2(j)} - g_{p(j)} \right)^2
\end{aligned}
\tag{3.36a}
$$

$$
\begin{aligned}
E^{K}_{tr2(j)} &= \int_{t_0}^{t} \dot{u}_{1(j)} K_{c(j)} \left(u_{1(j)} - u_{2(j)} - g_{p(j)} \right) \mathrm{U}[u_{1(j)} - u_{2(j)} - g_{p(j)}] d\tau \\
&= \int_{u_{1(j)}+g_{p(j)}}^{u_{2(j)}} K_{c(j)} \left(u_{1(j)} - u_{2(j)} - g_{p(j)} \right) du_{2(j)} \\
&= K_{c(j)} \left[u_{2(j)} \left(u_{1(j)} - g_{p(j)} \right) - \frac{u^2_{2(j)}}{2} \right]_{u_{1(j)}-g_{p(j)}}^{u_{2(j)}} \\
&= -\frac{1}{2} K_{c(j)} \left(u_{1(j)} - u_{2(j)} - g_{p(j)} \right)^2 = -E^{K}_{tr1(j)}
\end{aligned}
\tag{3.36b}
$$

Energy transferred by the linear elastic part of the contact element is therefore conserved. To estimate the transferred energy by each structure from the viscous part of the contact element:

$$
E^{C}_{tr1(j)} = \int_{t_0}^{t} C_{c(j)} \left(\dot{u}_{1(j)} - \dot{u}_{2(j)} \right) \dot{u}_{1(j)} d\tau \tag{3.37a}
$$

$$
E^{C}_{tr2(j)} = -\int_{t_0}^{t} C_{c(j)} \dot{u}_{2(j)} \left(\dot{u}_{1(j)} - \dot{u}_{2(j)} \right) d\tau \tag{3.37b}
$$

The energy dissipated by the piece-wise linear impact may be calculated by adding viscous contribution to the transferred energies by the contact elements:

$$
\begin{aligned}
E_{tr1(j)} + E_{tr2(j)} &= E^{C}_{tr1(j)} + E^{C}_{tr2(j)} \\
&= \int_{t_0}^{t} C_{c(j)} \left(\dot{u}_{1(j)} - \dot{u}_{2(j)} \right)^2 d\tau
\end{aligned}
\tag{3.38}
$$

Note that by performing the integrals in Eqs. 3.36 to 3.38, the total energy transfer and energy dissipated during impact can be determined, and can be compared to Eqs. 3.29 and 3.31 for stereomechanical impact. An equivalent coefficient of restitution (e) can be obtained to produce the same amount of energy transfer and energy dissipation. Conversely, the parameters of a piece-wise element can be derived to model a given coefficient of restitution.

The expected value of the transfer energies is given by:

$$E\left\{E_{tr1(j)}\right\} = \int_{t_0}^{t}\left[C_{c(j)}U_{gp(j)}\left(E\left\{\dot{u}_{1(j)}^2\right\} - E\left\{\dot{u}_{1(j)}\dot{u}_{2(j)}\right\}\right)\right.$$
$$\left. + K_{c(j)}U_{gp(j)}\left(E\left\{\dot{u}_{1(j)}u_{1(j)}\right\} - E\left\{\dot{u}_{1(j)}u_{2(j)}\right\} - g_{p(j)}E\left\{\dot{u}_{1(j)}\right\}\right)\right]d\tau \tag{3.39a}$$

$$E\left\{E_{tr2(j)}\right\} = \int_{t_0}^{t}\left[C_{c(j)}U_{gp(j)}\left(E\left\{\dot{u}_{1(j)}\dot{u}_{2(j)}\right\} - E\left\{\dot{u}_{2(j)}^2\right\}\right)\right.$$
$$\left. + K_{c(j)}U_{gp(j)}\left(E\left\{\dot{u}_{2(j)}u_{1(j)}\right\} - E\left\{\dot{u}_{2(j)}u_{2(j)}\right\} - g_{p(j)}E\left\{\dot{u}_{2(j)}\right\}\right)\right]d\tau \tag{3.39b}$$

The expected energy dissipated during of pounding is:

$$E\left\{E_{tr1(j)} + E_{tr2(j)}\right\} = \int_{t_0}^{t} C_{c(j)}\left(E\left\{\dot{u}_{1(j)}^2\right\} - 2E\left\{\dot{u}_{1(j)}\dot{u}_{2(j)}\right\} + E\left\{\dot{u}_{2(j)}^2\right\}\right)d\tau \tag{3.40}$$

3.3.6 Energy Transfer in Link Elements

Energy transfer in link elements may be calculated using formulas similar to the ones presented for the piece-wise linear impact:

$$\begin{aligned} E_{lk1(j)} &= \int \dot{u}_{1(j)}F_{l(j)}dt \\ &= \iint\left[C_{l(j)}\dot{u}_{1(j)}\left(\dot{u}_{1(j)} - \dot{u}_{2(j)}\right) + K_{l(j)}\dot{u}_{1(j)}\left(u_{1(j)} - u_{2(j)}\right)\right]dt \\ &= E_{lk1(j)}^{C} + E_{lk1(j)}^{K} \end{aligned} \tag{3.41a}$$

$$\begin{aligned} E_{lk2(j)} &= -\int \dot{u}_{2(j)}F_{l(j)}dt \\ &= \iint\left[C_{l(j)}\dot{u}_{2(j)}\left(\dot{u}_{1(j)} - \dot{u}_{2(j)}\right) + K_{l(j)}\dot{u}_{2(j)}\left(u_{1(j)} - u_{2(j)}\right)\right]dt \\ &= E_{lk2(j)}^{C} + E_{lk2(j)}^{K} \end{aligned} \tag{3.41b}$$

The energy dissipated by the link elements may be calculated as:

$$E_{lk1(j)} + E_{lk2(j)} = \int_{t_0}^{t} C_{l(j)}\left(\dot{u}_{1(j)} - \dot{u}_{2(j)}\right)^2 d\tau \tag{3.42}$$

The expected energy transferred by the link elements is therefore:

$$E\{E_{lk1(j)}\} = \int_0^t \left[C_{l(j)} \left(E\{\dot{u}_{1(j)}^2\} - E\{\dot{u}_{1(j)}\dot{u}_{2(j)}\} \right) + K_{l(j)} \left(E\{\dot{u}_{1(j)}u_{1(j)}\} - E\{\dot{u}_{1(j)}u_{2(j)}\} \right) \right] d\tau \tag{3.43a}$$

$$E\{E_{lk2(j)}\} = \int_0^t \left[C_{l(j)} \left(E\{\dot{u}_{1(j)}\dot{u}_{2(j)}\} - E\{\dot{u}_{2(j)}^2\} \right) + K_{l(j)} \left(E\{\dot{u}_{2(j)}u_{1(j)}\} - E\{\dot{u}_{2(j)}u_{2(j)}\} \right) \right] d\tau \tag{3.43b}$$

The expected dissipated energy by the link elements is:

$$E\{E_{lk1(j)} + E_{lk2(j)}\} = \int_0^t C_{l(j)} \left(E\{\dot{u}_{1(j)}^2\} - 2E\{\dot{u}_{1(j)}\dot{u}_{2(j)}\} + E\{\dot{u}_{2(j)}^2\} \right) d\tau \tag{3.44}$$

3.4 Impact Kelvin Element

A number of researchers have adopted the Kelvin element to model contact problems between structures. The force transmitted through a Kelvin element is:

$$f_c = \left(k_c \left(u_1 - u_2 - g_p \right) + c_c \left(\dot{u}_1 - \dot{u}_2 \right) \right) \mathrm{U}[u_1 - u_2 - g_p] \tag{3.45}$$

Where k_c and c_c are the spring and dashpot constants, u_1 and u_2 are the displacements of the structures, and g_p is the initial separation between the two. The element becomes active whenever the gap between the two structures closes, that is, when the unit step function U becomes one. However, it has the disadvantage that the viscous component of the element remains activated when the structures tend to separate, that is, the dashpot in the element opposes the motion of the structure when they come together, but also opposes the motion of the structure as they bounce back. Nevertheless, the Kelvin model has been commonly adopted by researchers in the area (Anagnostopoulos, 1992, Wolf and Skikerud, 1980).

A variation of the Kelvin element is proposed, where the viscous part of the element is only active for positive velocities. Due to its potential applications when studying pounding, the element is referred to as Impact Kelvin element. Restoring forces in the element are according to:

$$f_c = \left(k_c\left(u_1 - u_2 - g_p\right) + c_c\left(\dot{u}_1 - \dot{u}_2\right)\mathrm{U}[\dot{u}_1 - \dot{u}_2]\right)\mathrm{U}[u_1 - u_2 - g_p] \tag{3.46}$$

Fig. 3.7 presents the two models and their idealized dashpot portions response. Fig. 3.8 presents the hysteretic response for each model when used to simulate the response of two colliding masses, for different critical damping ratios of the contact element (ξ_c). Note that the traditional Kelvin model exhibits a portion where the damper will tend to keep the masses together towards the end of the collision, while the Impact Kelvin element disconnects the damper when the bodies are no longer approaching each other.

Fig. 3.9 presents the history of relative displacements, relative velocities and forces in the contact element during the collision of the two bodies, for a critical damping ratio (ξ_c) of 0.5. The response tend to diverge for higher critical damping ratios. Note that the forces in the contact element opposes the separation of the masses when the collision process is near completion. Furthermore, as the critical damping ratio increases, the contact time increases for the Kelvin element, and decreases for the Impact Kelvin element (see Fig. 3.10). Reduced duration of contact for higher critical damping ratios reflects the expected physical response.

For the Impact Kelvin element, the time at which the maximum deformation is observed (approach time) is:

$$t_{\max} = \frac{1}{\omega_d}\tan^{-1}\left(\frac{\omega_d}{\xi_c\omega_c}\right) \tag{3.47}$$

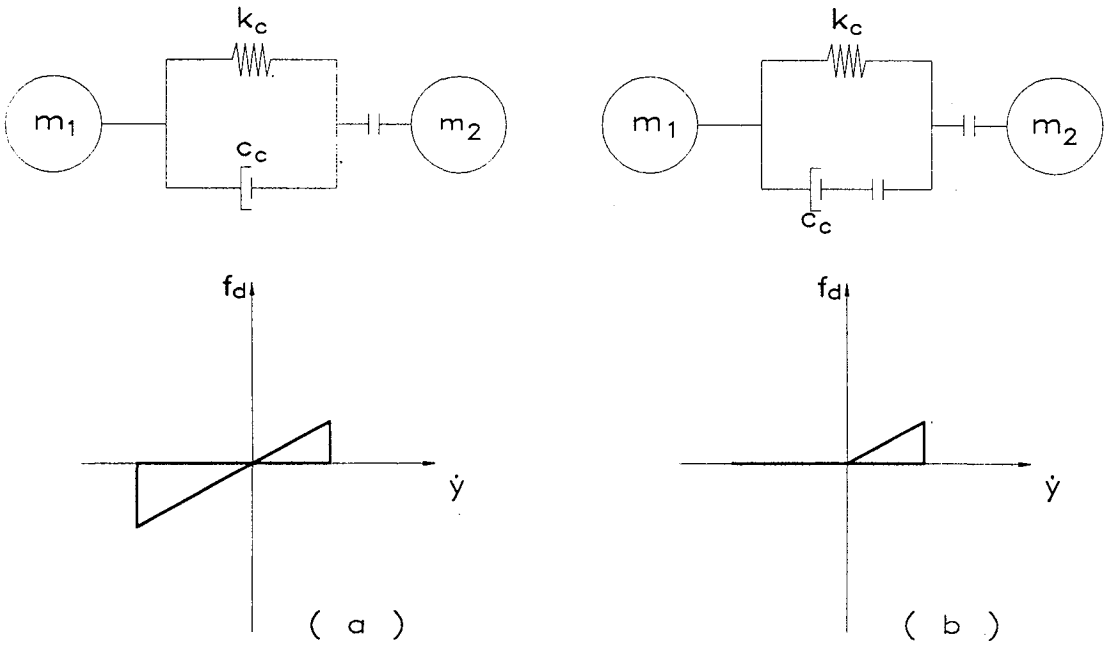

Fig. 3.7 Kelvin element vs. Impact Kelvin element, idealized dashpot response: (a) Kelvin element, (b) Impact Kelvin element.

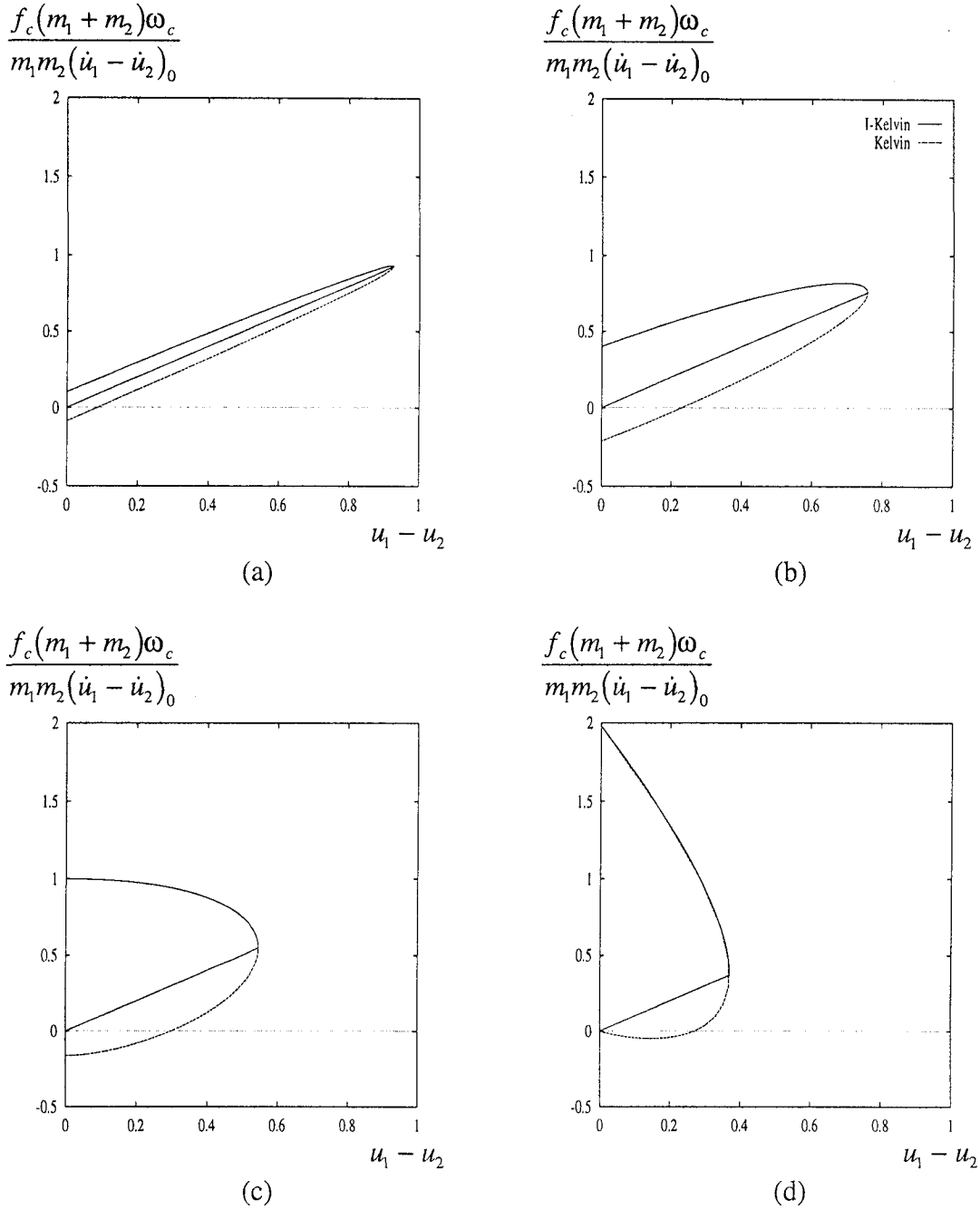

Fig. 3.8 Hysteretic response of Kelvin elements and Impact Kelvin elements for contact problems, for various critical damping ratios: (a) ξ_c=0.05, (b) ξ_c=0.2, (c) ξ_c=0.5, (d) ξ_c=1.0.

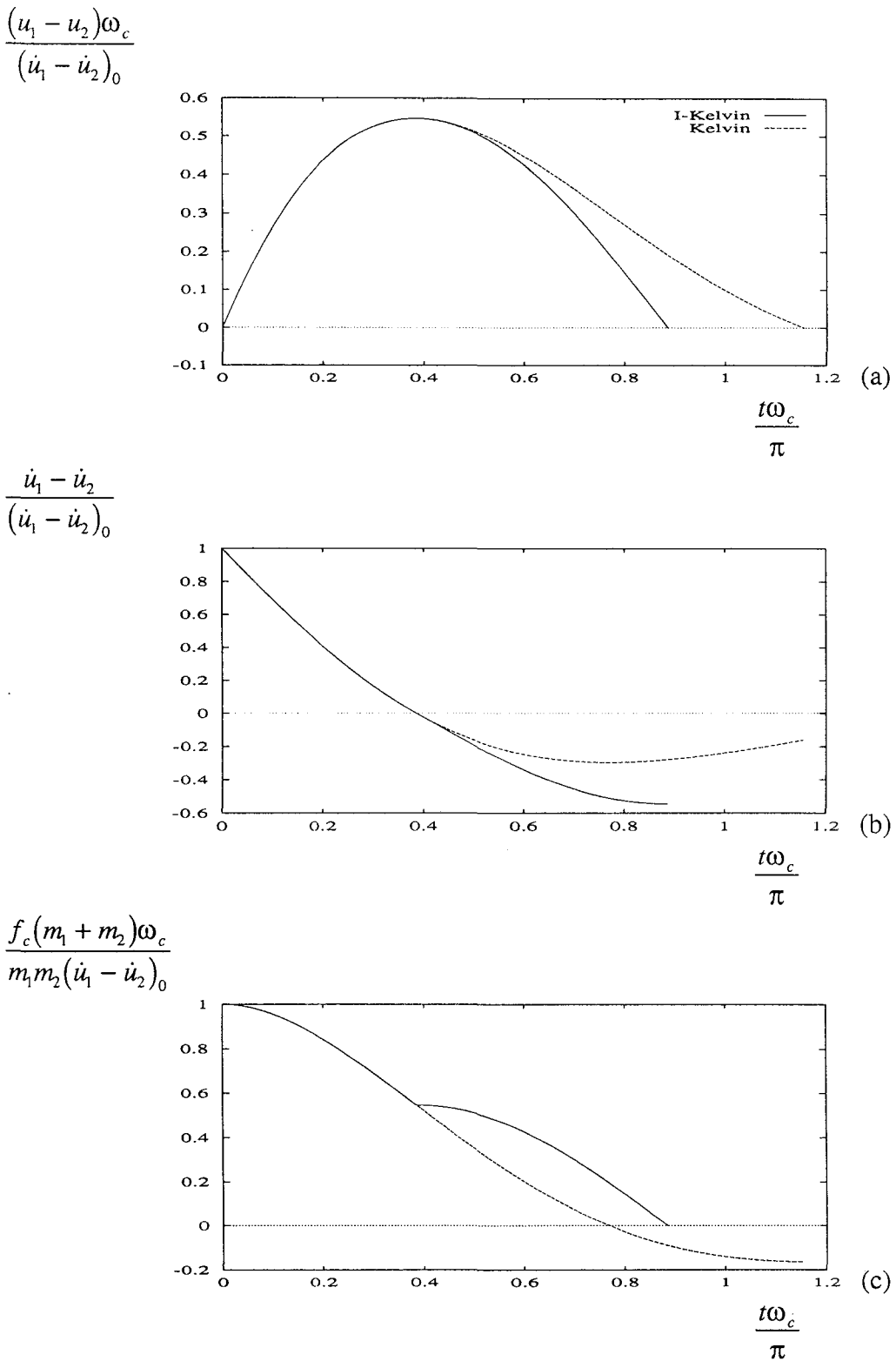

Fig. 3.9 History of deformations, velocities and contact forces for Kelvin and Impact Kelvin elements (ξ_c=0.5).

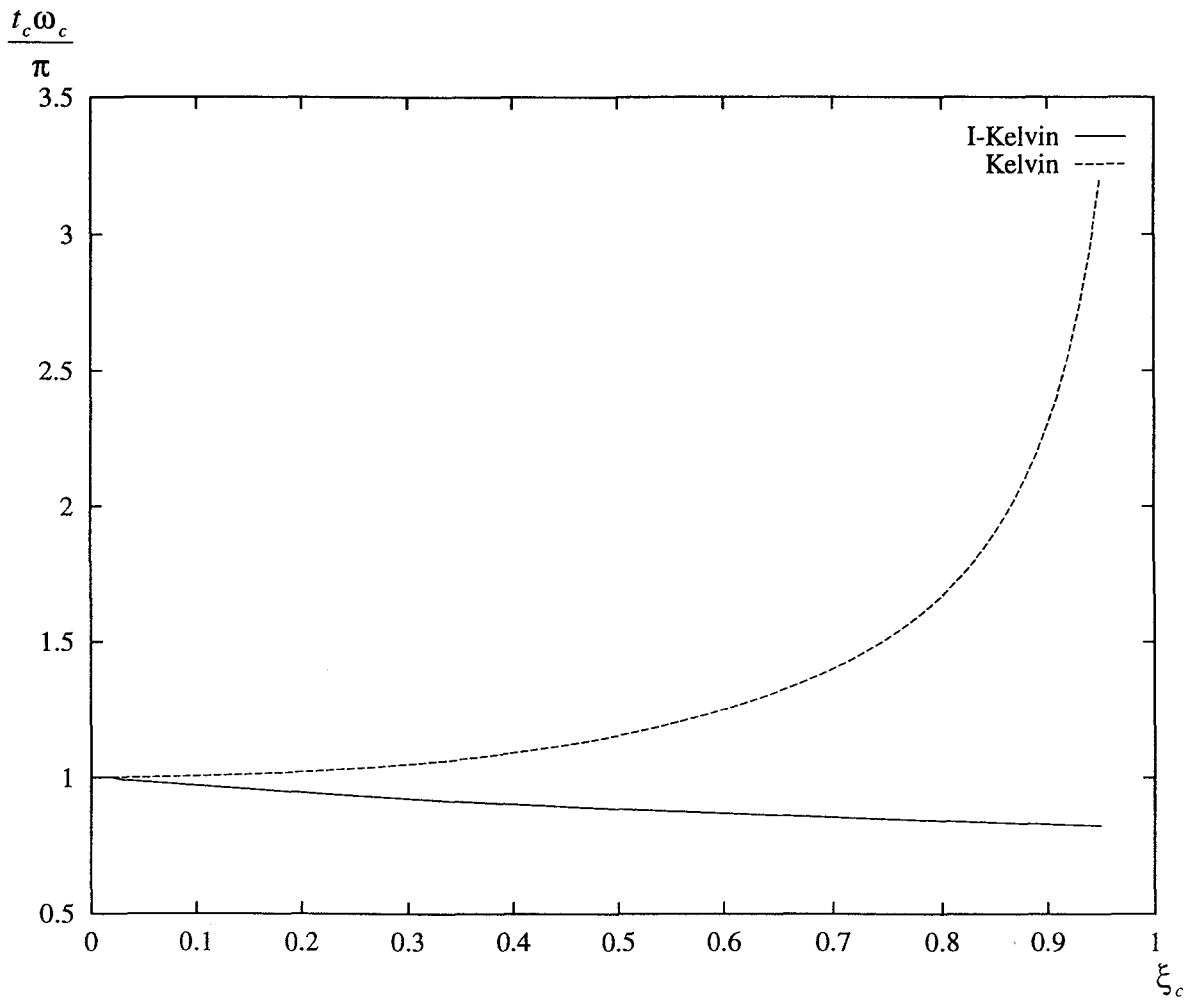

Fig. 3.10 Duration of contact for Kelvin and Impact Kelvin models for different critical damping ratios.

this time t_{max} depends on the parameters of the contact element, and on the masses of the colliding bodies:

$$\omega_c = \sqrt{\frac{k_c(m_1 + m_2)}{m_1 m_2}}; \quad \omega_d = \omega_c \sqrt{1 - \xi_c^2} \tag{3.48}$$

$$\xi_c = \frac{c_c}{2}\sqrt{\frac{m_1 + m_2}{k_c m_1 m_2}} \tag{3.49}$$

After the maximum deformation is observed, the viscous part of the contact element is deactivated, therefore, the total time of contact is:

$$t_{tot} = t_{max} + \frac{\pi}{2\omega_d} \tag{3.50}$$

The final relative velocity of the colliding bodies may be calculated from the relative velocity at the onset of pounding ($\dot{y}_0$), and the equivalent restitution coefficient is:

$$e = \sin(\omega_d t_{max}) \exp(-\xi_c \omega_c t_{max}) \tag{3.51}$$

Fig. 3.11 presents the relation of the critical damping coefficient (ξ_c) to the restitution coefficient (e) from stereomechanical impact.

The use of the Impact Kelvin element is recommended over the traditional Kelvin element, since the presence of a force keeping the structures together when they tend to separate does not seem to have a physical intuitive explanation.

3.5 Models for Structural Pounding

To study pounding response in multi-degree-of-freedom systems, three mathematical formulations were developed: a deterministic model, a probabilistic model, and a hybrid model (Valles, 1995). Figures 3.12 to 3.14 present diagrams of input and output for the three mathematical models developed. The deterministic model considers a given history of accelerations and calculates the response of the structures considering

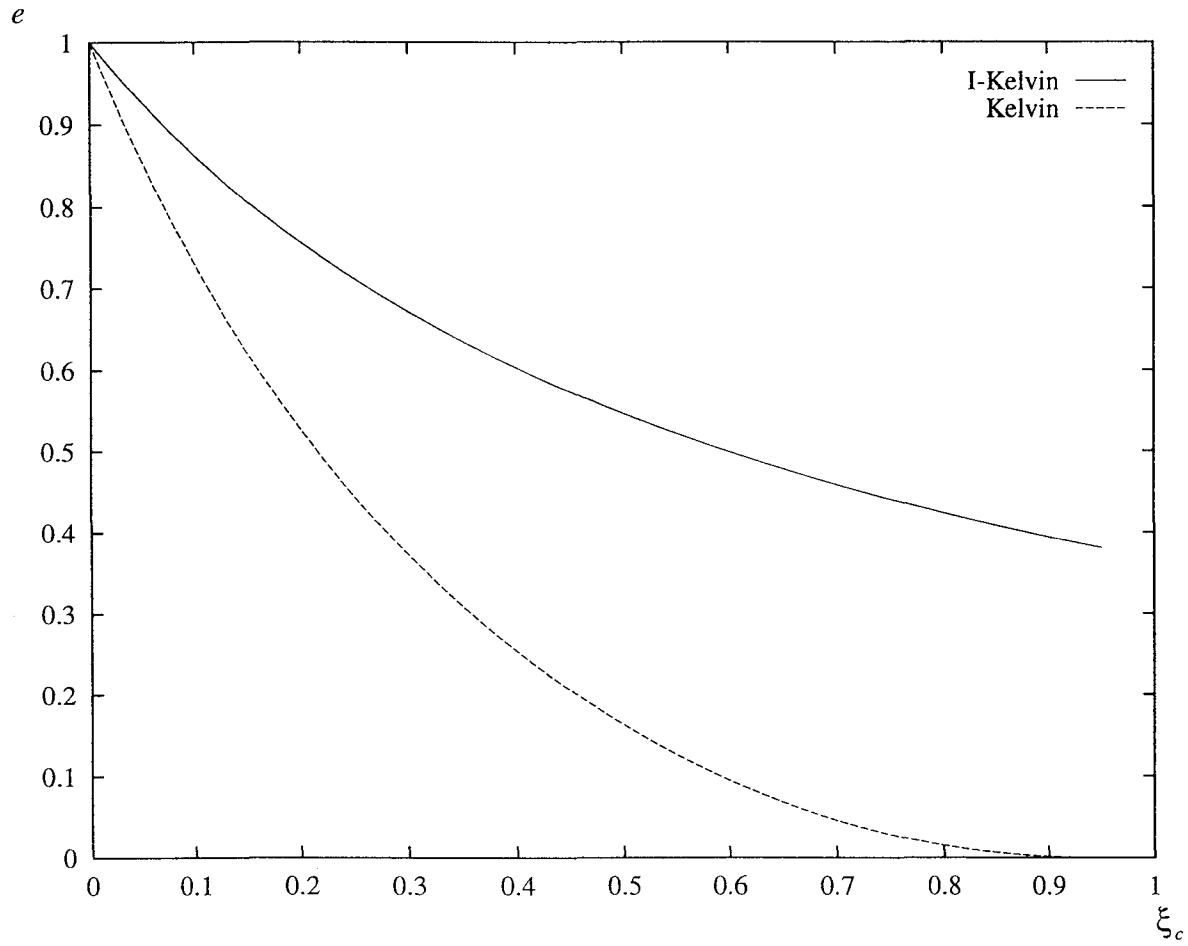

Fig. 3.11 Equivalent coefficient of restitution (e) for different critical damping ratios of the Kelvin and Impact Kelvin elements.

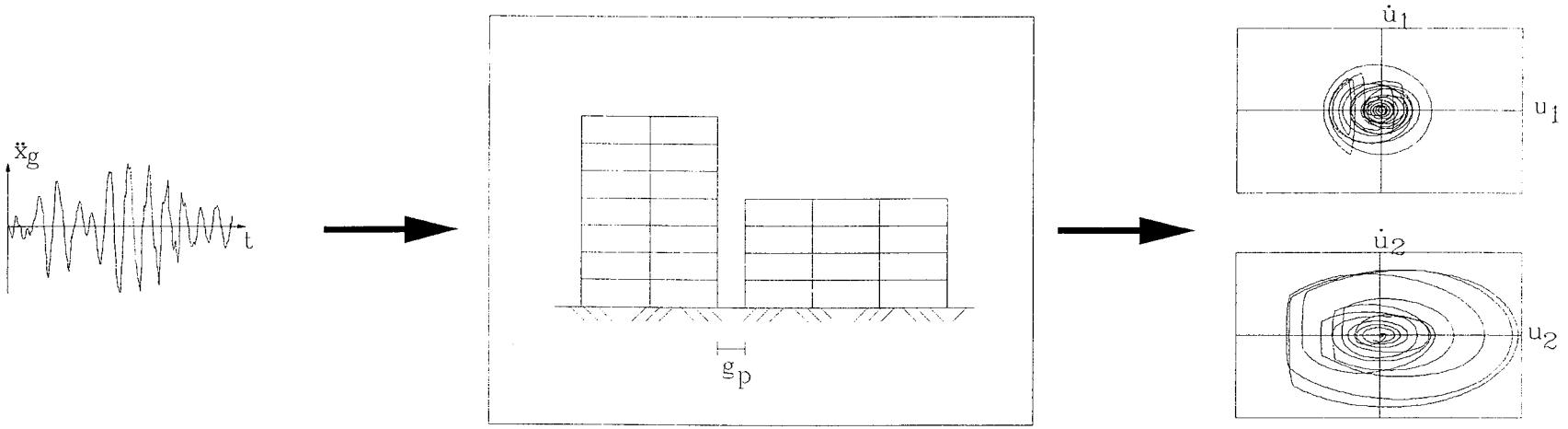

Fig. 3.12 Mathematical model for deterministic studies.

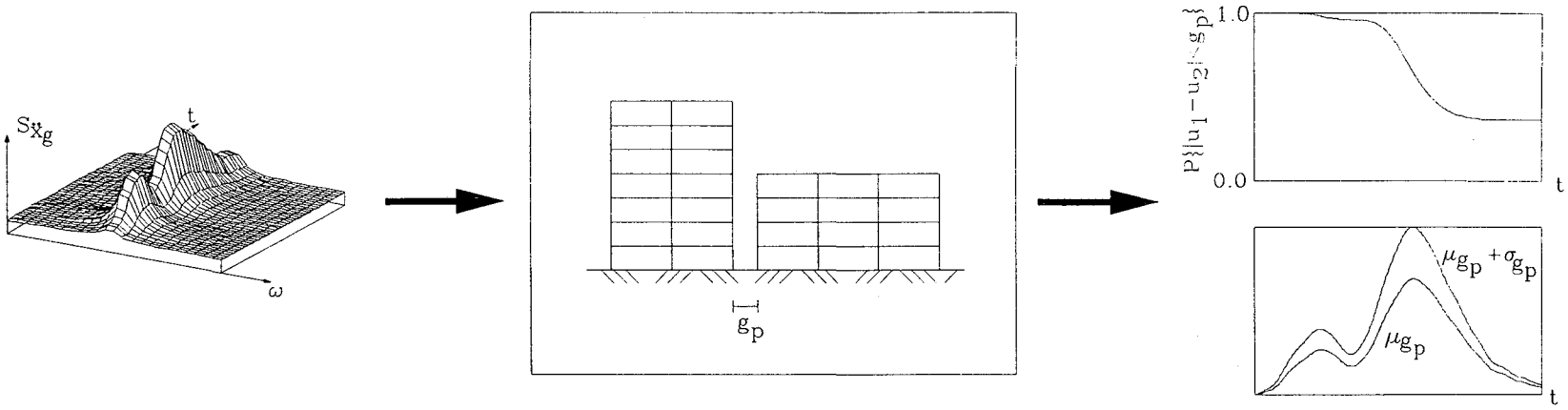

Fig. 3.13 Mathematical model for probabilistic studies.

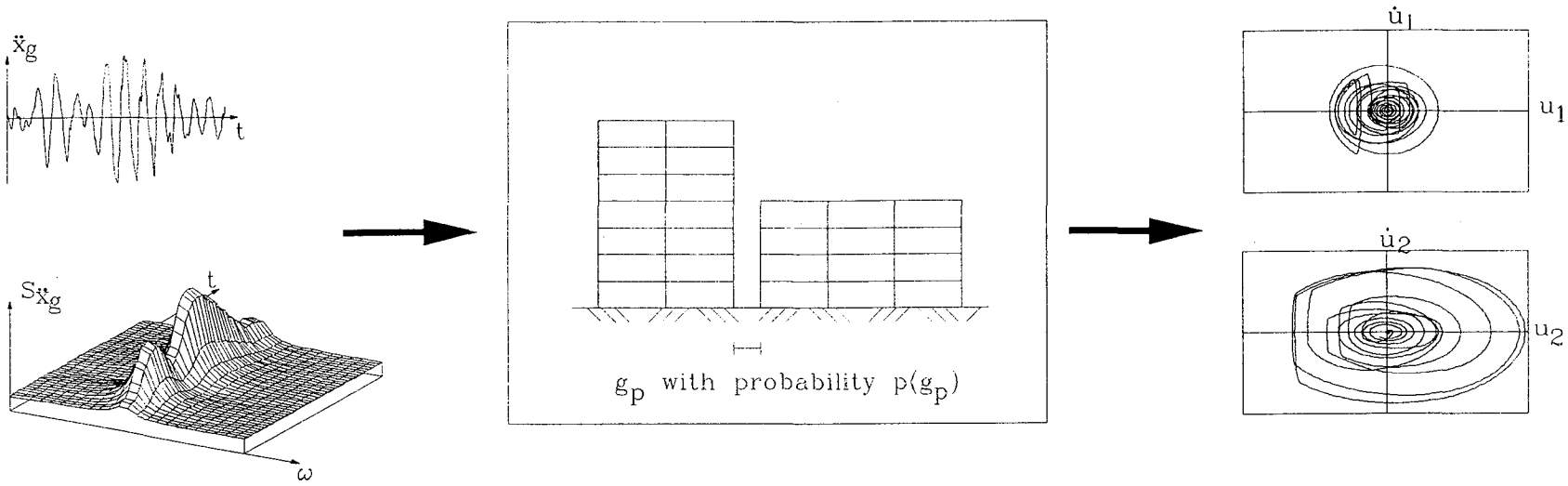

Fig. 3.14 Mathematical model for hybrid studies.

impact between the structures using the stereomechanical or the piece-wise linear pounding approaches. The probabilistic model uses an evolutionary power spectrum to characterize the input, and determines the confidence of no pounding, and the instantaneous probability of pounding. The hybrid model combines a deterministic approach in which pounding is determined in a probabilistic sense. See Valles (1995) for details on each of the mathematical models developed.

3.6 Effect of Peak Ground Acceleration

Because of its nature, pounding is a nonlinear problem. For any given pair of linear structures prone to pound, the equations of motion may be written as:

$$m_1\ddot{u}_1 + c_1\dot{u}_1 + k_1u_1 + f_c(g_0,\alpha_{c1},\alpha_{c2},\ldots,\alpha_{cn}) = -m_1\ddot{x}_g \qquad (3.52a)$$

$$m_2\ddot{u}_2 + c_2\dot{u}_2 + k_2u_2 - f_c(g_0,\alpha_{c1},\alpha_{c2},\ldots,\alpha_{cn}) = -m_2\ddot{x}_g \qquad (3.52b)$$

Where the nonlinear part of the problem is embedded in the contact force f_c, that depends on the separation between the structures (g_0), and a number of other parameters ($\alpha_{c1},\alpha_{c2},\ldots,\alpha_{cn}$).

Given that the solution for the equations of motion is known for any value of the gap (g_0), the solution for a ground acceleration "c_g" times greater than $\ddot{x}_g$ may be obtained by multiplying both sides of the equations of motion by the constant "c_g":

$$m_1c_g\ddot{u}_1 + c_1c_g\dot{u}_1 + k_1c_gu_1 + c_gf_c(g_0,\alpha_{c1},\alpha_{c2},\ldots,\alpha_{cn}) = -m_1c_g\ddot{x}_g \qquad (3.53a)$$

$$m_2c_g\ddot{u}_2 + c_2c_g\dot{u}_2 + k_2c_gu_2 - c_gf_c(g_0,\alpha_{c1},\alpha_{c2},\ldots,\alpha_{cn}) = -m_2c_g\ddot{x}_g \qquad (3.53b)$$

However, if the nonlinearity in the contact forces arises only due to the piece-wise nature of the problem, the system of equations may be rewritten as:

$$m_1\ddot{u}_1' + c_1\dot{u}_1' + k_1u_1' + f_c(g_0/c_g,\alpha_{c1},\alpha_{c2},\ldots,\alpha_{cn}) = -m_1c_g\ddot{x}_g \qquad (3.54a)$$

$$m_2\ddot{u}_2' + c_2\dot{u}_2' + k_2u_2' - f_c(g_0/c_g,\alpha_{c1},\alpha_{c2},\ldots,\alpha_{cn}) = -m_2c_g\ddot{x}_g \qquad (3.54b)$$

in terms of the new variables:

$$u_1' = c_gu_1 \qquad (3.55a)$$

$$u_2' = c_g u_2 \tag{3.55b}$$

That implies that the solution for a different acceleration level ($c_g \ddot{x}_g$) may be calculated by multiplying the response for the original acceleration level ($\ddot{x}_g$) with a gap of g_0 / c_g.

In the present study, most of the models used for the contact element are of the piece-wise linear type, therefore, scaling of the results, with the appropriate scaling of the gap is possible. The response of the structures will be calculated for an arbitrary ground acceleration level, given that the response for any acceleration level may be obtained from the scaling procedure outlined above.

3.7 Research Objectives

Four major research objectives were established from the preliminary studies on pounding. This first is to establish a good and reliable estimate for the critical gap, that is, the minimum gap required for the design earthquake, so that pounding between the structures will not occur (see Fig. 3.15a). A number of parameters influence the calculation of the critical gap, therefore, the influence of these parameters must be assessed.

Previous researchers (Jeng et al., 1992) and building codes have proposed formulas to estimate the minimum gap requirements for structures. However, improvements in the calculations can be made. One of the intended improvements consists of using statistical models to account for the uncertainty inherent in earthquake motions. Another important improvement can be made using statistical linearization to more accurately estimate the response of nonlinear structures.

The second objective established is to determine the amplification effects on structures that are prone to pounding (see Fig. 3.15b), since most of the important metropolitan areas in medium to high seismicity zones have a large number of structures

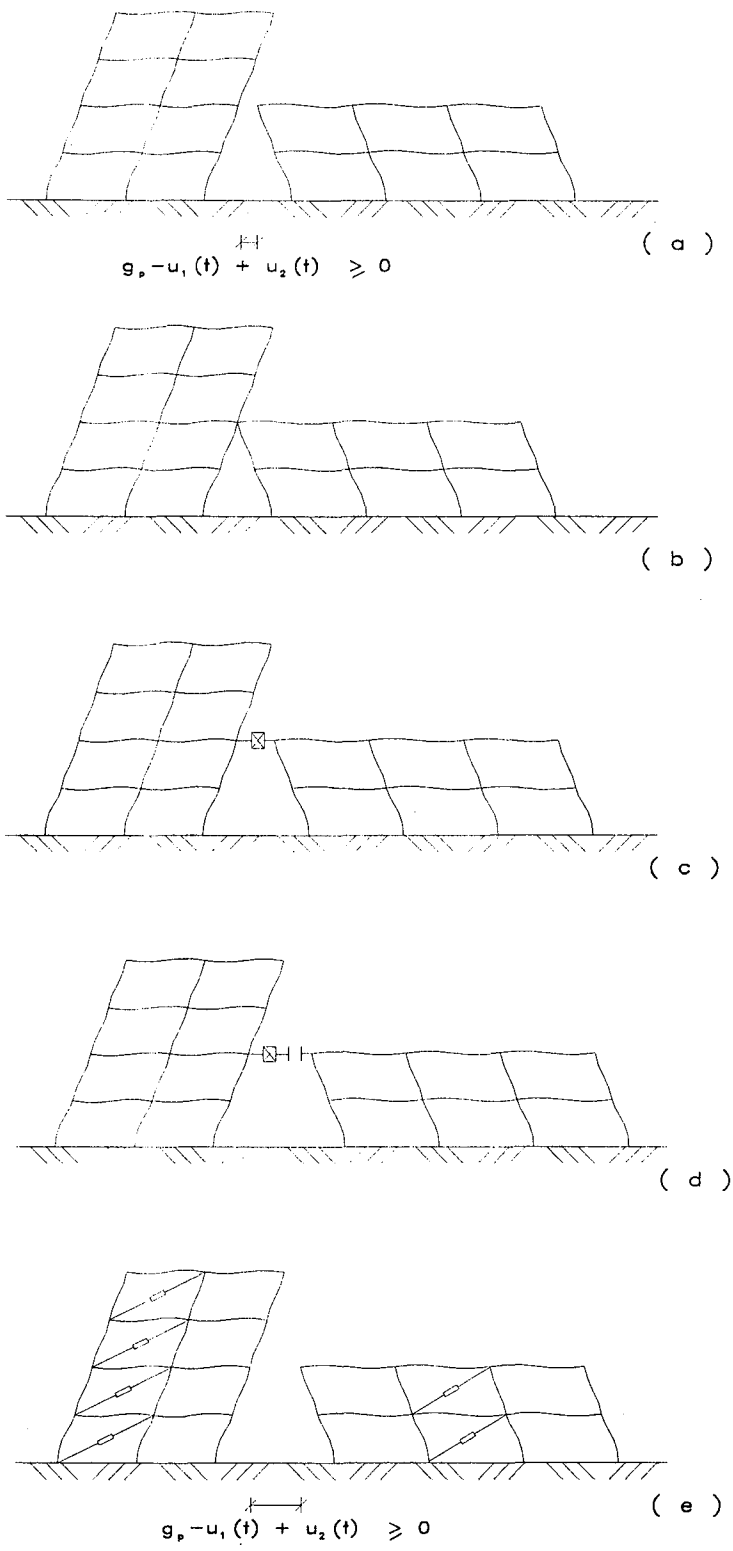

Fig. 3.15 Research objectives: (a) critical gap estimation, (b) evaluation of pounding effects; pounding mitigation techniques: (c) link elements, (d) bumper dampers, and (e) supplemental energy dissipation devices.

with clear gaps smaller than critical. In this situation, determining the magnitude of local impulsive stress concentrations, as well as estimating the change in the global response parameters and demands to the structure, are of interest. Quantifying the change in the response of the structures will identify buildings with high seismic risk due to pounding that need to be strengthened or retrofitted, as well as structures that may pound but with no significant change in the safety level of both structures.

The third objective consists of studying possible pounding mitigation techniques when pounding effects pose a serious threat to the safety of the constructions (see Fig. 3.15c to 3.15e). Possible mitigation techniques will be investigated and simple preliminary design guidelines will be developed.

The fourth objective is to combine all the observations from the previous findings and outline design/evaluation recommendations that could be applied by a design engineer. Charts or formulas that would help the designer calculate the critical gap, estimate the demands imposed on the structure if pounding is observed, and evaluate the effectiveness of linking the structures to reduce to allowable limits, or eliminate, damage due to pounding will be developed.

3.8 Pseudo Energy Radius

The Pseudo Energy Radius (PER) was introduced by Valles (1995) to study and solve pounding related problems. The applications of the Pseudo Energy Radius in calculating the critical gap to avoid pounding in inelastic structures (Section 4), in estimating amplification effects when pounding occurs (Section 5), and to estimate the effectiveness of various mitigation techniques (Section 6) are described in the following sections of this report. The development and theory of the Pseudo Energy Radius is summarized in this section.

Consider a single-degree-of -freedom system, with frequency ω, subjected to an earthquake ground motion. The response of the system can be visualized in the state space plane (see Fig. 3.16), that is, displacement (u) versus the velocity divided by the frequency of the structure

$(\dot{u}/\omega)$. In this graphical representation of the response, the distance r of any point along the response path traced by the system to the origin provides a measurement of the instantaneous elastic structural energy E_e (kinetic plus potential energy):

$$\frac{E_e}{m} = \frac{1}{2}\dot{u}^2 + \frac{1}{2}\omega^2 u^2 \tag{3.56}$$

or:

$$\frac{2E_e}{m\omega^2} = \frac{\dot{u}^2}{\omega^2} + u^2 = r^2 \tag{3.57}$$

Where m corresponds to the mass of the structure.

In this representation, the distance r can be interpreted as the radius of concentric circles defining constant energy levels in the structure:

$$r = \sqrt{\frac{2E_e}{m\omega^2}} \tag{3.58}$$

Using the concept of concentric energy levels of radius r, the response of the structure can be traced as it changes from one energy level to another. When no external load is applied, the damping in the structure will gradually decrease the energy level of the system, and drive it towards the origin of the state space representation, where the system will become static. When an external load is applied to the system, at a given instant in time, the effect can be to increase or decrease the energy level of the structure, depending on the phase between the input motion and the response displacement.

In the present formulation, the maximum experienced distance r (energy level), is referred to as the Pseudo Energy Radius (PER), and can be denoted as r_{PER}. Such value can be determined during the analysis by monitoring the elastic structural energy of the system E_e, and storing its maximum value. Some differences between the Pseudo Energy Radius and the commonly used input and viscous energies can be identified.

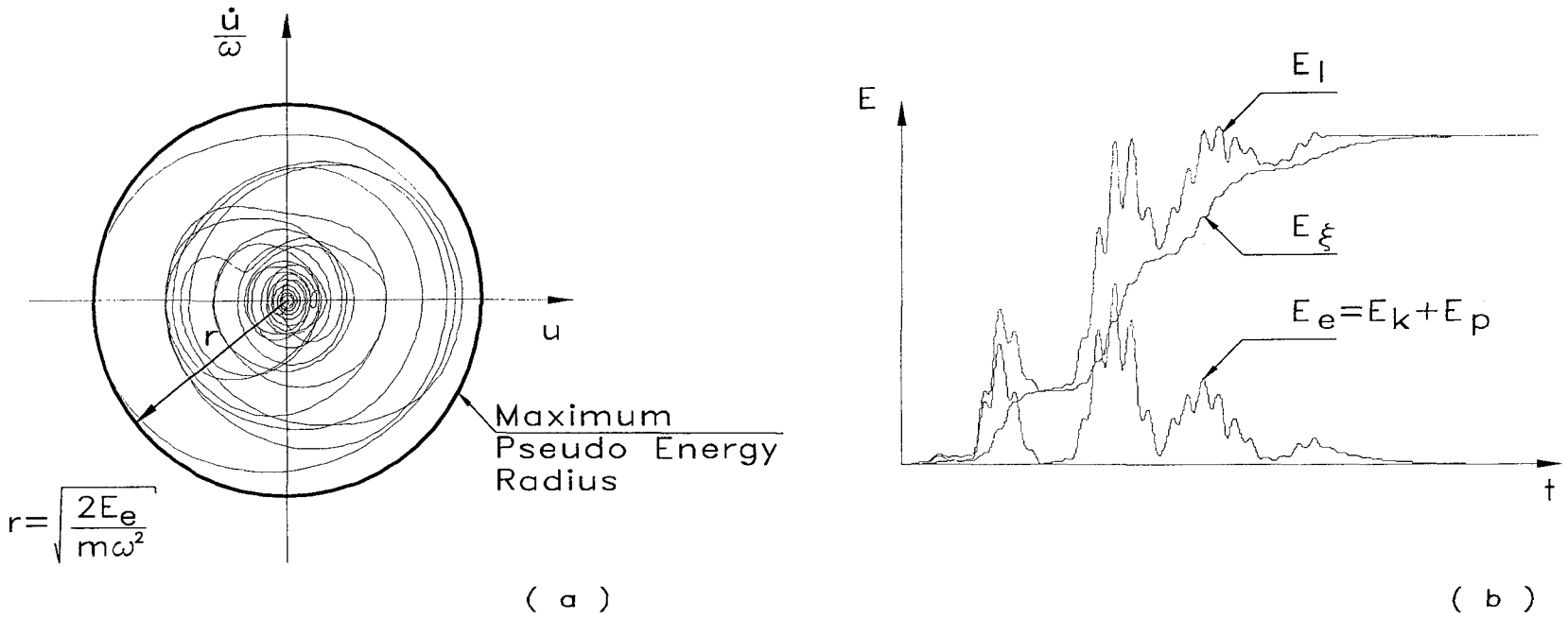

Fig. 3.16 Maximum Pseudo Energy Radius (PSE) from a state space representation.

First, the Pseudo Energy Radius is expressed in units of displacements and not energy. This will prove to be useful to study pounding problems since the radius r can be directly correlated to the critical gap g_{cr}, or the actual gap g_p between two adjacent structures.

The second major difference between the Pseudo Energy Radius and input or viscous energy measurements is that the former measure is directly related to the maximum response of the structure:

$$u_{\max} \approx r_{PER}$$

$$\dot{u}_{\max} \approx \omega r_{PER}$$

while the later ones are not since other parameters such as the duration of the event considerably change these measurements (see Fig. 3.16). Figures 3.17 and 3.18 present the Pseudo Energy Spectrum for the 1985 Mexico City earthquake, and for the Taft earthquake.

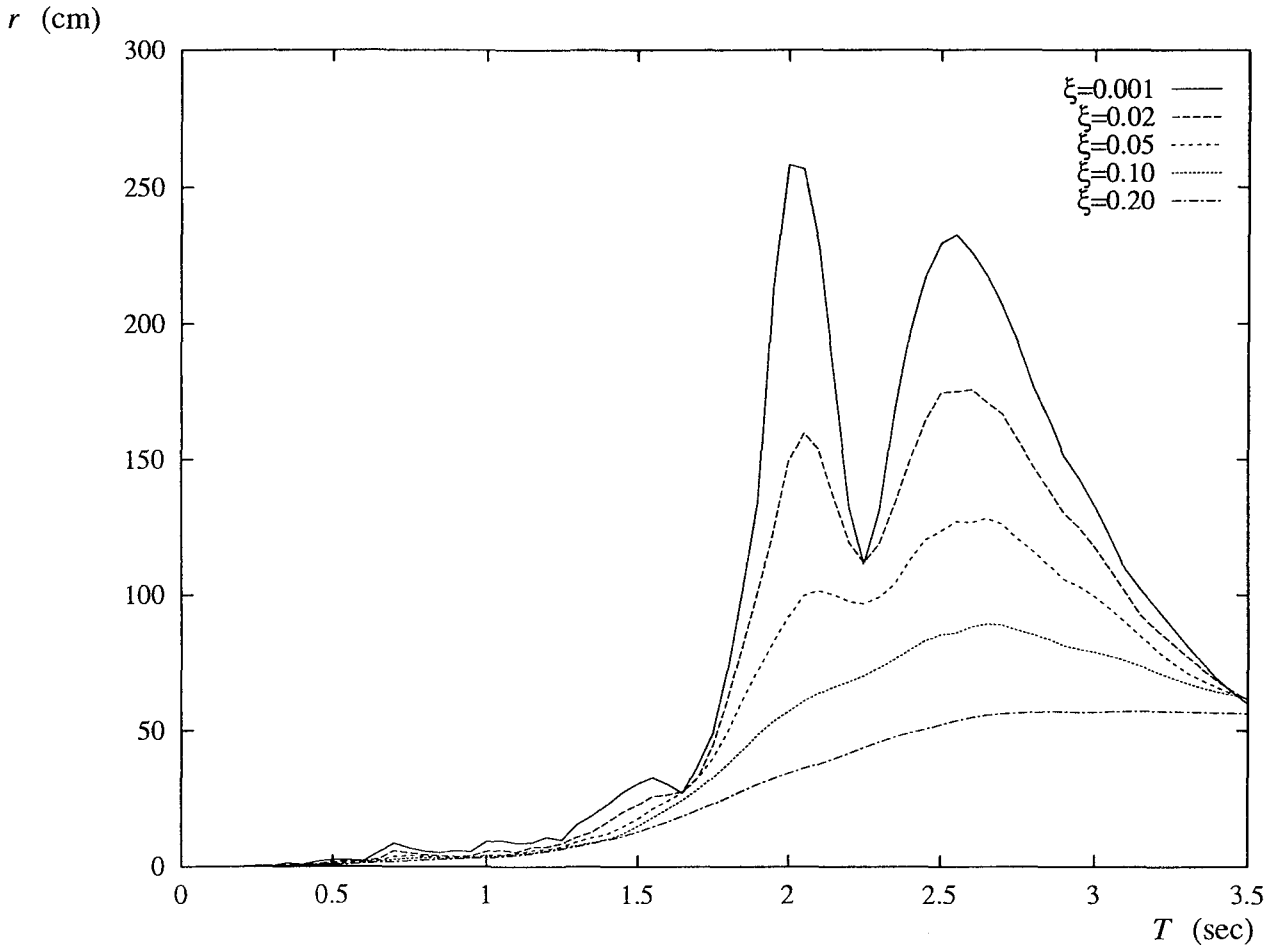

Fig. 3.17 Pseudo Energy Radius (PER) spectrum for 1985 Mexico City earthquake.

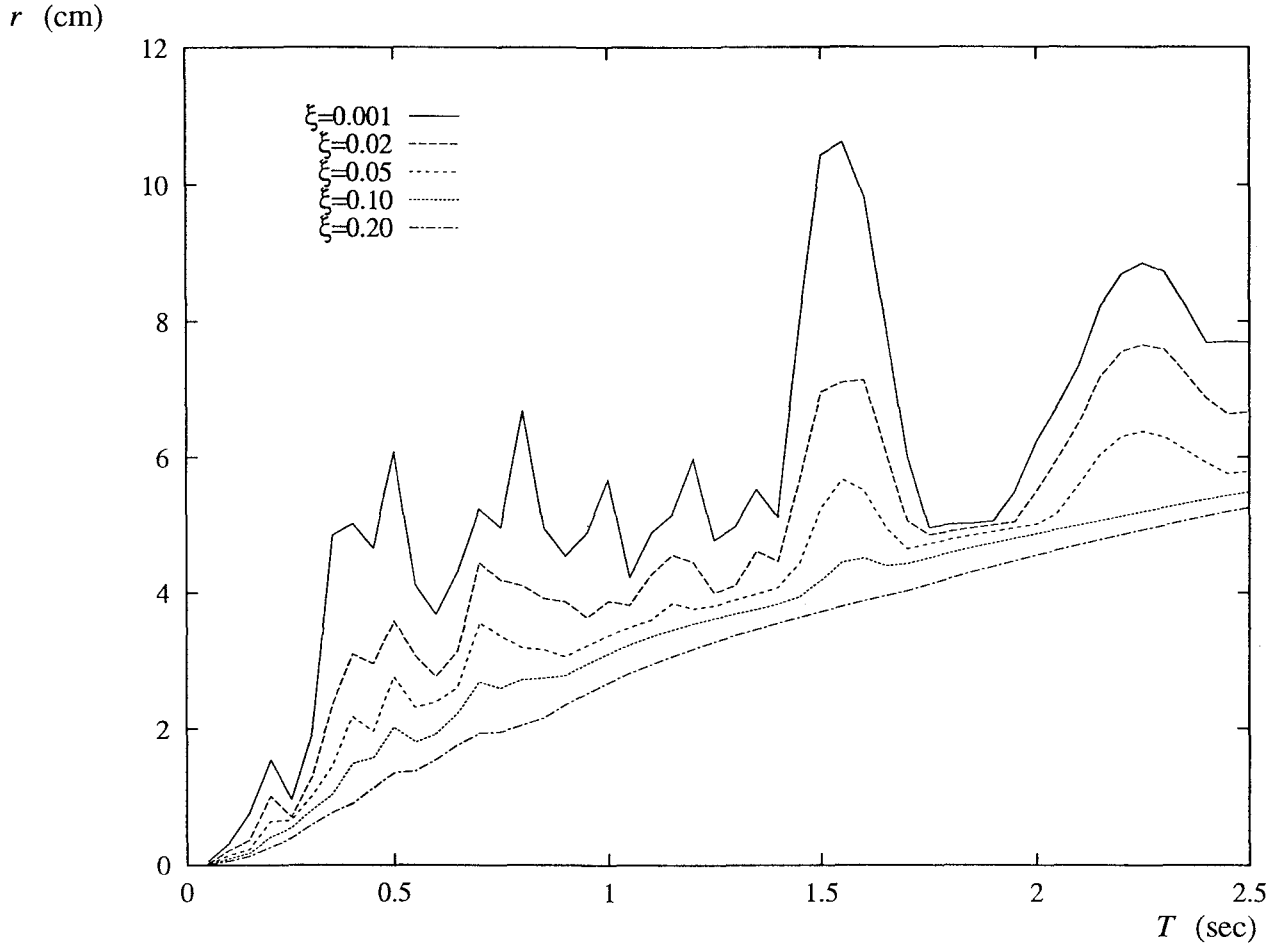

Fig. 3.18 Pseudo Energy Radius (PER) spectrum for Taft earthquake.

SECTION 4
CRITICAL GAP SIZE

4.1 Introduction

Critical gap size between two inelastic structures is defined as the minimum distance between the structures to avoid pounding. In this section some of the building code requirements for minimum gap are reviewed, the Double Difference Combination rule proposed by Kasai to estimate the minimum separation to avoid pounding. The theory of statistical linearization, the estimate for the critical gap for bilinear structures subjected to a filtered white noise input is obtained.

4.2 Building Code Requirements

Building codes in zones of active seismicity around the world have recognized the destructive effects that pounding may induce in constructions. The approach commonly adopted in building codes has been to avoid contact interactions between the structures by providing sufficient separation between them. The provisions from several building codes are summarized by Valles (1995). Each building code considers different design criteria, seismic risk, construction practice, earthquake magnitude, etc. That is, loads, parameters, and displacements involved to calculate the critical gap are likely to differ for each country. Therefore, a direct comparison of the different building codes is not possible since force reduction factors and structural ductility factors are different in each code. However, some observations can be made pertaining to the criteria to avoid pounding used in the codes. In the majority of the building codes reviewed, the adopted criteria has been to specify a minimum separation between the structures so that pounding is not likely to occur. This criterion has been defined using four different expressions:

$$gap \geq factor(sum\ of\ displ) \tag{4.1}$$

$$gap \geq coefficient(height) \tag{4.2}$$

$$gap \geq \text{fixed distance} \tag{4.3}$$

$$gap \geq SRSS(displacements) \tag{4.4}$$

Eq. 4.1 may be considered as equivalent to the absolute sum of maximums (ABS rule), multiplied by an amplification factor. The amplification factor in most cases comes from the increase in displacements due to the inelastic response of the structures, but does not take into account that the maximum displacements in the structures, in general, will not occur at the same time. Eq. 4.2 may be easily justified, since, in general, building codes specify a maximum inelastic drift. Using this approach, the dynamic characteristics of the structures are not relevant to the gap computation, since the lateral deformations are always checked. This approach is the easiest to check by building code officials, and does not involve the calculation of the inelastic response of an adjacent structure which dynamic properties are, in general, unknown. Furthermore, embedded in the coefficient, considerations for amplification of displacements due to rotations at the foundation may be included. Nevertheless, this form of specifying the gap, by not considering the dynamic properties of the adjacent structures, may be overly conservative for buildings that tend to respond in phase. Buildings with high percentages of critical damping, or inelastic buildings for some ratios of frequencies to the characteristic earthquake frequency, belong to this category, as will be discussed later in this section.

Eq. 4.3 is specified for construction considerations, that is, to allow for adequate space to place the formwork for beams and columns, to build masonry walls, or place elements of the facade. A minimum gap, applicable for short structures, should always be specified in building codes. Most of the building codes reviewed clearly state that the gap between structures is to be kept free from debris.

Only Eq. 4.4 takes into account the fact that the maximum displacements in the structures will not occur at the same time. It uses the SRSS modal combination rule, that is it assumes assuming that the input motion is stationary, and that the response of each structure (or mode) is uncorrelated with the others. Therefore, it yields conservative results when the response of the structures are somewhat to perfectly correlated. The CQC combination rule proposed by

Der Kiureghian (1979) may be applied to take into account the correlation in the response, as suggested by Kasai (Jeng et al., 1992), adopting the name Double Difference Combination Rule (DDC), since in this case we are interested in the difference of the displacements, and not on the sum of the response parameters. The Double Difference Combination Rule is discussed in detail in the next subsection.

A combination of Eqs. 4.1 and 4.2 has been adopted in the building code in Mexico City, where the amplification as a function of the building height is introduced to take into account rotations at the foundation, of great significance in the soft soil (lake) zone of the city, where a large number of mid-rise buildings, from 5 to 15 stories, stand on friction piles. Due to the consolidation of the Mexico City clay, and to avoid that a structure would emerge, the friction piles are generally designed using a safety factor of one (Mendoza and Auvinet, 1988). Therefore, the building settles at approximately the same rate as the clay when negative skin friction in the piles is observed. Buildings supported by friction piles have a small rotational stiffness when compared to end bearing piles or spread footings on stiff soil. Therefore, in Mexico City, much of the pounding damage observed may be correlated to the use of friction piles at the foundation.

Of all the building codes reviewed, only the one from Venezuela allows adjacent buildings to abut against each other if the floor levels coincide, and if the interactions will not produce an undesirable response in either of the two. In the rest of the codes, no contact is allowed, in some cases clearly stating that no pounding is to take place, or the buildings should be connected.

None of the building codes studied included some corrective measures if pounding is detected as a problem in a future seismic event. In the ATC-14 for seismic evaluation of existing buildings (1987), pounding is listed as one of the concerns in the checklist. However, no suggested methodology is included to guide the engineer to estimate the effects of pounding in the structure.

4.3 Review of Double Difference Combination Rule

In this subsection a short description of the CQC combination rule proposed by Der Kiureghian (1979 and 1980), a reinterpretation of which lead to the Double Difference Combination Rule (Jeng et al., 1992), is presented.

Der Kiureghian (Wilson et al., 1981) proposed the method now called CQC, where the total response of a structure may be estimated from the weighted contribution of the response from each mode:

$$\overline{R}_{\tau} = \left(\sum_{i} \sum_{j} \rho_{0,ij} \overline{R}_{i\tau} \overline{R}_{j\tau} \right)^{1/2} \tag{4.5}$$

where $\overline{R}_{\tau}$ corresponds to the total response of the structure, $\overline{R}_{i\tau}$ corresponds to the stationary response of mode "*i*", and $\rho_{0,ij}$ is the correlation coefficient between the response of each pair of modes. An approximate expression for the correlation coefficient was obtained by Der Kiureghian (1979) when the structure was subjected to a white noise excitation:

$$\rho_{0,ij} = \frac{8\sqrt{\xi_i \xi_j \omega_i \omega_j}\left(\xi_i \omega_i + \xi_j \omega_j\right)\omega_i \omega_j}{\left(\omega_i^2 - \omega_j^2\right)^2 + 4\xi_i \xi_j \omega_i \omega_j \left(\omega_i^2 + \omega_j^2\right) + 4\left(\xi_i^2 + \xi_j^2\right)\omega_i^2 \omega_j^2} \tag{4.6}$$

Fig. 4.1 presents the variation of the correlation coefficient, for different critical damping ratios, for the response of the structure when the response is stationary and the systems are subjected to a white noise excitation.

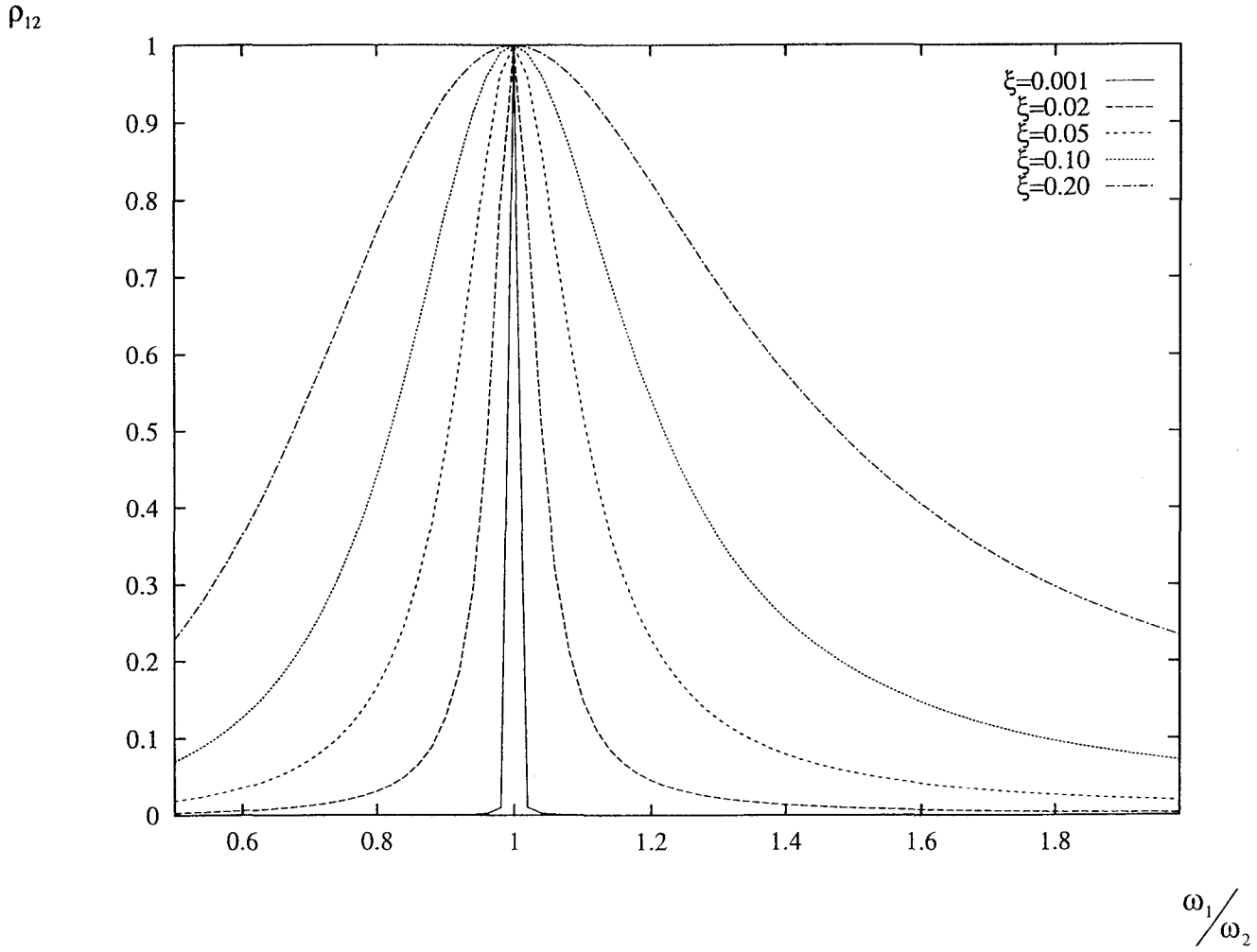

Fig. 4.1 Correlation coefficient for linear oscillators subjected to white noise input proposed by Der Kiureghian (1979).

Using the results obtained by Der Kiureghian, Kasai and other researchers (Van Jeng et al., 1992) introduced the Double Difference Combination rule. In the pounding problem, the response of interest is the absolute difference in displacements:

$$u_{rel}(t) = |u_1(t) - u_2(t)| \tag{4.7}$$

with mean value:

$$E\{u_{rel}(t)\} = |E\{u_1(t)\} - E\{u_2(t)\}| \tag{4.8}$$

and correlation:

$$\begin{aligned} E\left\{\left(u_{rel}(t)\right)^2\right\} &= E\{u_1^2(t)\} - 2E\{u_1(t)u_2(t)\} + E\{u_2^2(t)\} \\ &= E\{u_1^2(t)\} - 2\rho_{12}\sqrt{E\{u_1^2(t)\}E\{u_2^2(t)\}} + E\{u_2^2(t)\} \end{aligned} \tag{4.9}$$

Where the correlation coefficient adopted was the simplification for white noise input derived by Der Kiureghian, Eq. 4.6. Since the input is considered trend free, the response is a zero mean process. Furthermore, Kasai and Jagiasi (1993a) generalized the method for the case of nonlinear structures introducing an effective period and effective critical damping ratio to be used for calculating the correlation coefficient. Using the results from numerical simulations the authors interpolated the formulas:

$$T^* = T(1 + 0.09(\mu - 1)) \tag{4.10}$$

$$\xi^* = \xi + 0.084(\mu - 1)^{1.3} \tag{4.11}$$

for bilinear structures, and:

$$T^* = T(1 + 0.18(\mu - 1)) \tag{4.12}$$

$$\xi^* = \xi + 0.160(\mu - 1)^{0.9} \tag{4.13}$$

for a stiffness degrading model similar to the Takeda model. In the above equations, μ corresponds to the maximum ductility experienced by the structure. Figs. 4.2 and 4.3 present the corresponding correlation coefficient for bilinear and degrading structures for different maximum ductility, as obtained using the modification in period and effective damping suggested by Kasai.

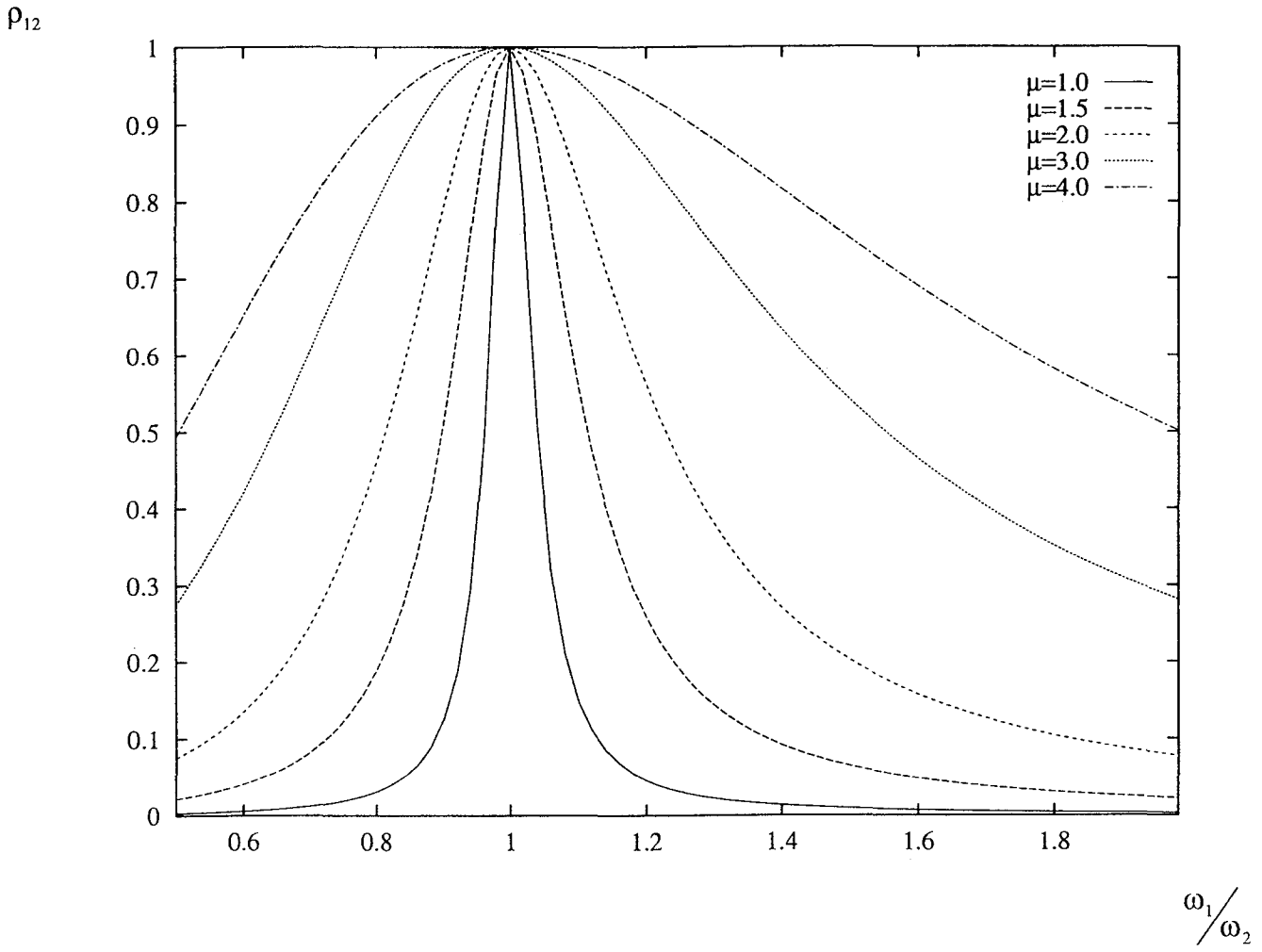

Fig. 4.2 Correlation coefficient for bilinear oscillators, as suggested by Kasai and Jagiasi (1993a).

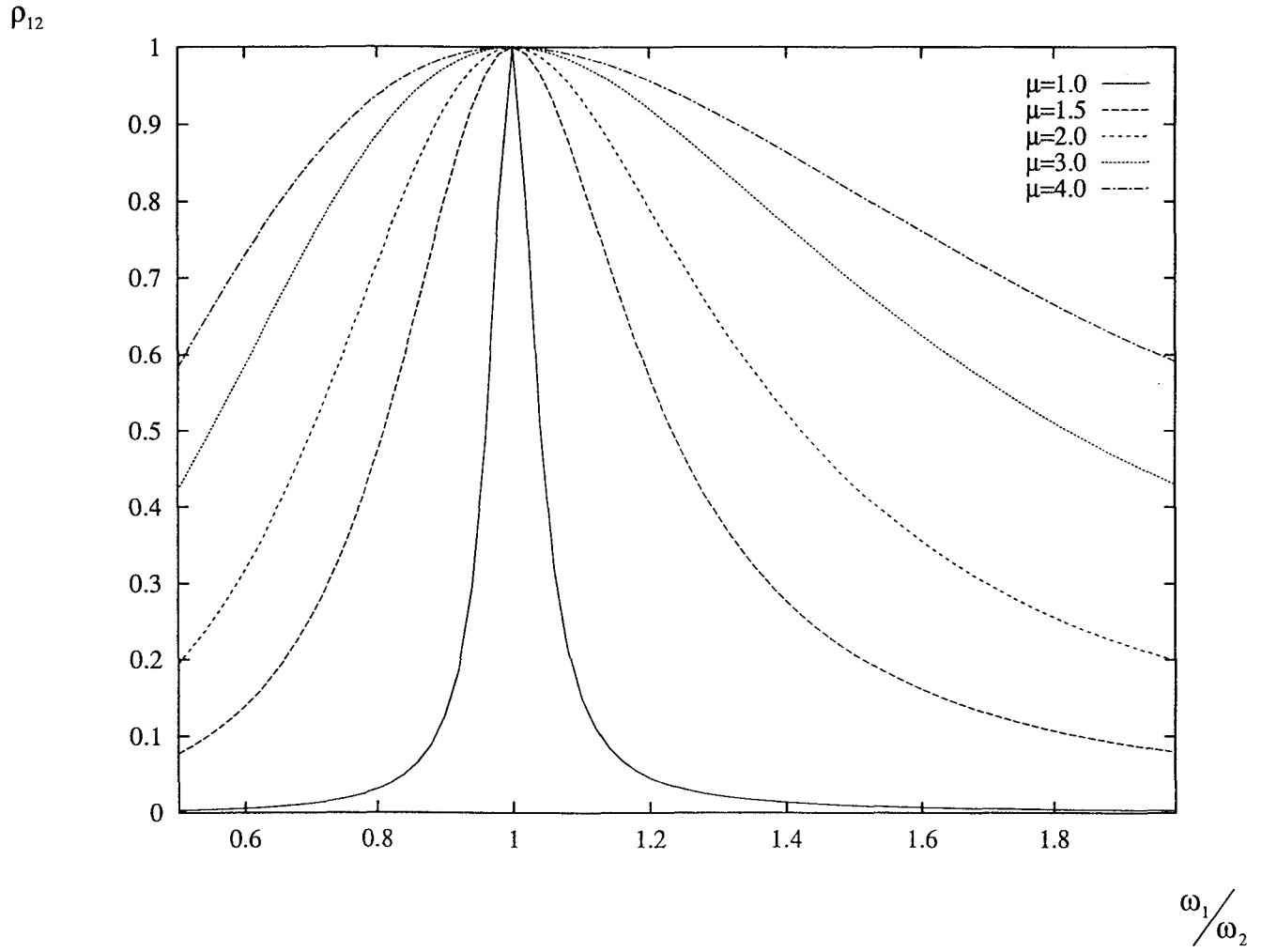

Fig. 4.3 Correlation coefficient for stiffness degrading structures, as suggested by Kasai and Jagiasi (1993a).

The formulation introduced as the Double Difference Combination (DDC) rule offers a simple formula to estimate the minimum gap to avoid pounding. As expected, the simplified formulas for effective period and damping yield a higher correlation coefficient for higher ductility ratios. However, when the predominant frequency of the input motion is considered, a different correlation coefficient may be expected. Furthermore, the simplified formula to calculate the correlation coefficient, as proposed by Der Kiureghian (1979), was derived for a white noise input.

The simplified formulas to calculate the effective damping and period presented by Kasai and Jagiasi (1993a) were determined by curve fitting results from numerical simulations. However, the proposed formulas may have a restricted range of applicability. Therefore, there is a need to determine a more general solution for bilinear structures that will include the characteristic frequency and band width of the input.

The extension of the Double Difference Combination rule to inelastic structures provides only a formula to modify the correlation coefficient, while no change is suggested for the maximum displacements of the structures. While this is commonly accepted for structures in the long period range, constant displacement region of the spectrum, in general, the maximum elastic displacement will differ from the maximum inelastic displacement. The ratio of elastic to inelastic displacement will be a function of the predominant frequency of excitation.

Due to the uncertainties that the Double Difference Combination rule has when inelastic structures are considered, a more detailed study of the critical gap for bilinear structures was deemed necessary.

4.4 Statistical Estimation for Critical Gap

To estimate the critical gap between two bilinear structures, an approach using statistical linearization and the Pseudo Energy Radius was adopted (Valles, 1995). The random process that defines the difference in the displacements of the two structures is:

$$G_p = U_1 - U_2 \tag{4.14}$$

Where the statistics of G_p may be determined from the statistics of U_1 and U_2. The input motion is considered as a zero mean Gaussian process, therefore, the displacements in the structure, and the difference in displacement are also zero mean Gaussian processes.

The variance of the difference in displacements may be obtained from:

$$\begin{aligned} E\{G_p^2\} &= E\{U_1^2\} - 2\rho\sqrt{E\{U_1^2\}E\{U_2^2\}} + E\{U_2^2\} \\ &= \sigma_{u1}^2 - 2\rho\sigma_{u1}\sigma_{u2} + \sigma_{u2}^2 = \sigma_{gp}^2 \end{aligned} \tag{4.15}$$

Because the input motion is zero mean Gaussian, the difference in displacements is also a zero mean Gaussian process if the structures respond linearly. Therefore, the first two moments completely describe the process G_p in a probabilistic sense. The probability of G_p exceeding an actual gap value may be determined, or, conversely, the minimum gap for an acceptable probability of being exceeded may be found. The former approach may be used when an actual gap is observed between two structures, while the latter is useful to estimate an allowable gap for a new edification.

Eq. 4.15 may be rewritten as:

$$g_{cr} = \sqrt{u_1^2 - 2\rho u_1 u_2 + u_2^2} \tag{4.16}$$

where g_{cr} is the critical gap, u_1 and u_2 are the maximum displacements of structures 1 and 2, respectively, and ρ is the correlation coefficient in displacements:

$$\rho = \frac{E\{U_1 U_2\}}{\sqrt{E\{U_1^2\}E\{U_2^2\}}} \tag{4.17}$$

In this interpretation, the probability level is implicit in the computation of u_1 and u_2. That is, the critical gap calculated according to Eq. 4.16 has the same probability of being exceeded as the maximum displacements u_1 and u_2 have of being greater than estimated. Therefore, the critical gap is calculated considering comparable risk levels as the structural displacements.

The importance of the correlation coefficient is observed (see Fig. 4.4). When the response of the two structures are perfectly correlated ($\rho = 1$), the critical gap becomes the absolute difference of the structural displacements:

$$g_{cr} = |u_1 - u_2| \tag{4.18}$$

However, when the response of the two structures is uncorrelated ($\rho = 0$), the critical gap becomes the square root of the sum of the squares (SRSS rule):

$$g_{cr} = \sqrt{u_1^2 + u_2^2} \tag{4.19}$$

Finally, when the response of the structures is negatively correlated ($\rho = -1$), the critical gap becomes the absolute sum of the standard deviations (ABS rule):

$$g_{cr} = u_1 + u_2 \tag{4.20}$$

The correlation coefficient considerably modifies critical gap. Note that the absolute sum of the displacements is a conservative estimate since a negative correlation between the response of the structures is not common in practice.

Using the Pseudo Energy Radius, the critical gap size and the effect of the correlation coefficient can be easily visualized. Consider two structures with fundamental frequencies ω_1 and ω_2 separated by a distance g_p (see Fig. 4.5). If the distance g_p is greater than the sum of the corresponding Pseudo Energy Radius $r_1 + r_2$, no pounding interactions will take place. Therefore g_p is greater than g_{cr}.

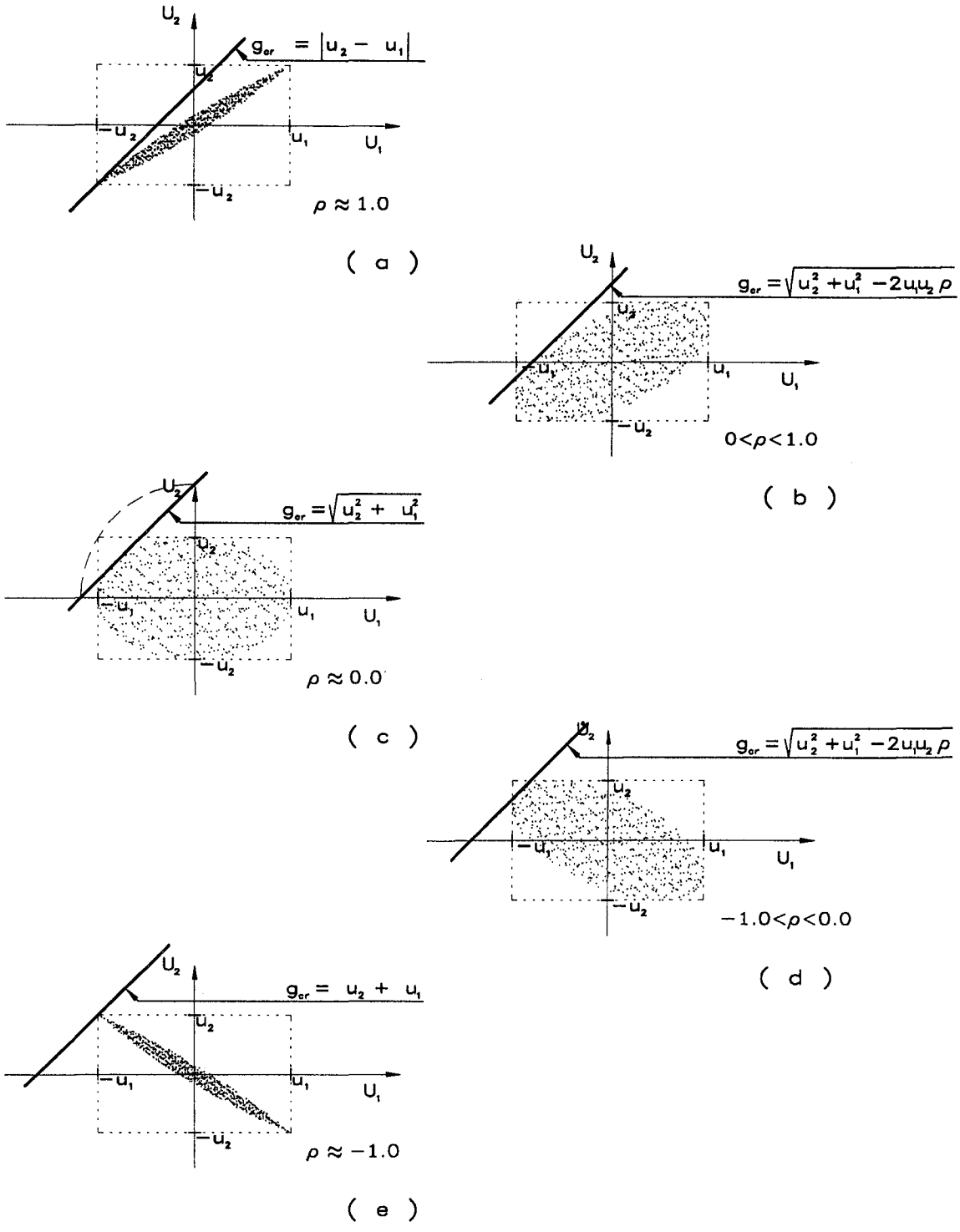

Fig. 4.4 Critical gap for different correlation coefficients.

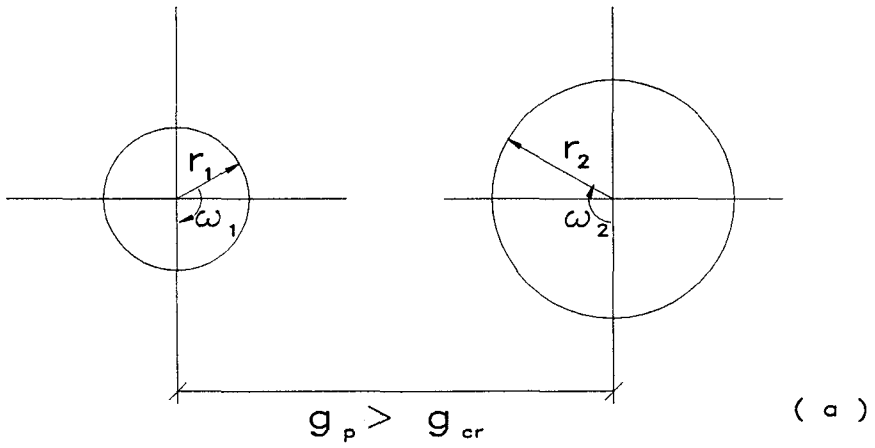

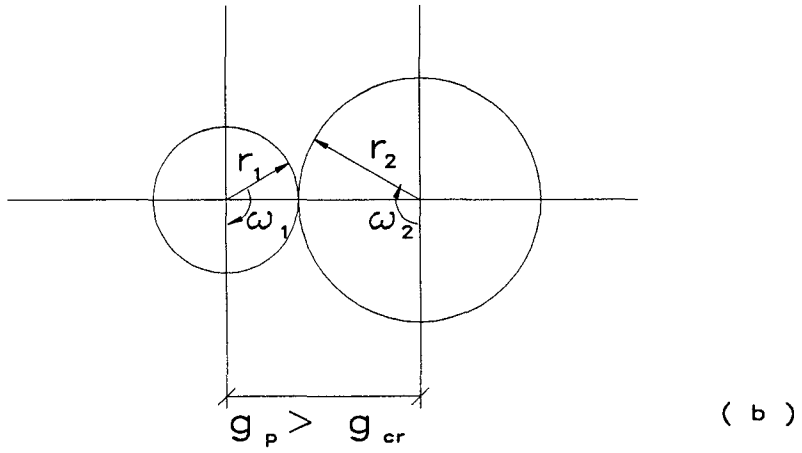

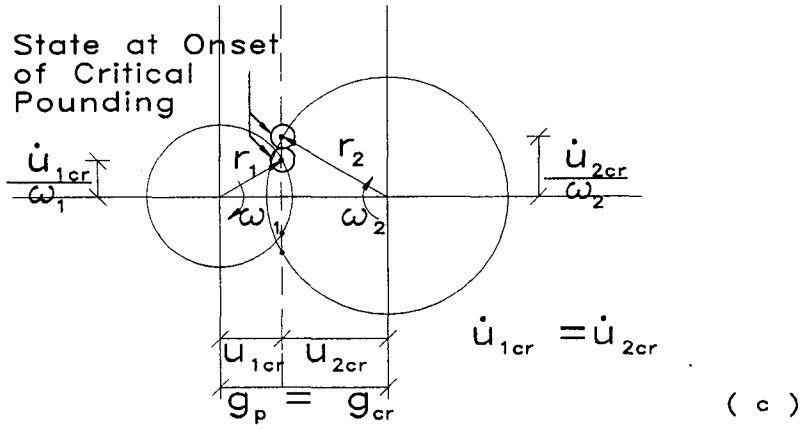

Fig. 4.5 Pseudo Energy Radius (PER) representation for various gap sizes: (a) $g_p >> g_{cr}$, (b) $g_p > g_{pr}$, (c) $g_p = g_{cr}$.

If the distance g_p is equal to the sum $r_1 + r_2$, contact will occur only if the two structures are at the tangent point of the two energy levels at the same instant in time. Nevertheless, pounding effects will not occur since the structure comes in contact with zero relative velocity. When the structures do not cross the tangent point at the same instant in time, the actual critical gap is smaller than the sum $r_1 + r_2$.

If the structures are separated by the critical gap g_{cr} calculated according to Eq. 4.16, considering $u_1 \approx r_1$ and $u_2 \approx r_2$, overlapping of the energy levels is possible without inducing pounding effects since the structures come in contact with zero relative velocity. Note that using the present state space representation u versus $\dot{u}/\omega$ will yield two points that coincide in the horizontal axis, but have different vertical ordinates (see Fig. 4.6). This is due to the difference in the predominant frequencies of the structures that yields two different vertical scales. Note that if the vertical scales were not normalized by the frequency, the points at the onset of pounding would coincide.

The maximum overlapping of the Pseudo Energy Radius without inducing pounding effects is controlled by the correlation coefficient ρ. Fig. 4.7 Presents maximum overlapping without introducing pounding effects for different values of the correlation coefficient. Figures 4.8 and 4.9 show the response traces of buildings with separation g_{cr} subjected to Mexico City and Taft earthquakes.

Next the theory to determine the correlation coefficient for bilinear structures subjected to a filtered white noise is presented.

4.4.1 Statistical Linearization for a Bilinear Oscillator

The response of two bilinear structures subjected to an input f(t) obeys the differential equations:

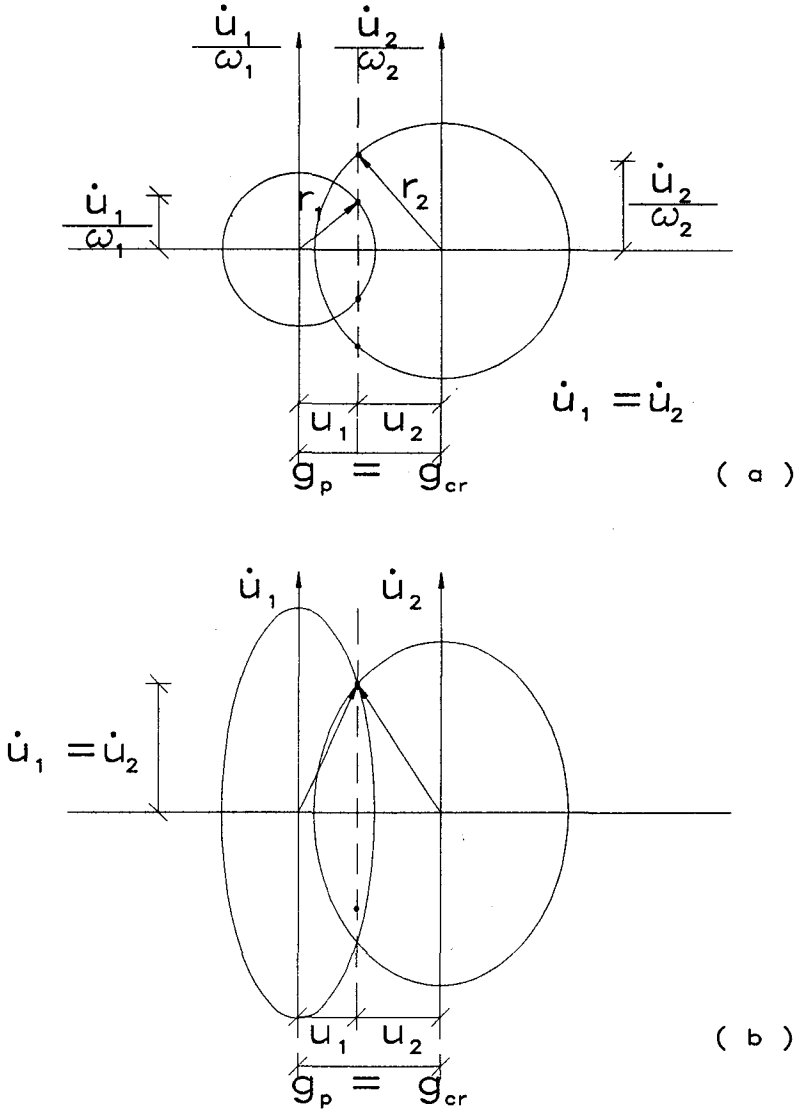

Fig. 4.6 Critical gap separation: (a) representation using the Pseudo Energy Radius (PER), (b) phase plane representation.

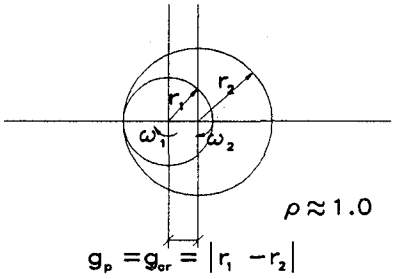

$\rho \approx 1.0$

$g_p = g_{cr} = |r_1 - r_2|$ (a)

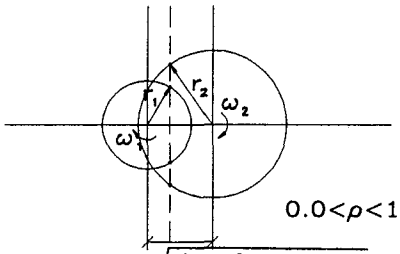

$0.0 < \rho < 1.0$

$g_p = g_{cr} = \sqrt{r_1^2 + r_2^2 - 2r_1\, r_2 \rho}$ (b)

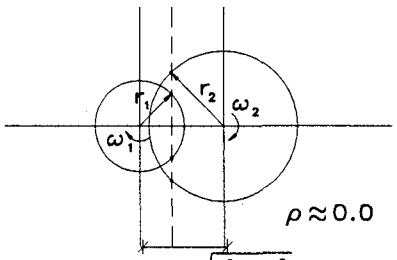

$\rho \approx 0.0$

$g_p = g_{cr} = \sqrt{r_1^2 + r_2^2}$ (c)

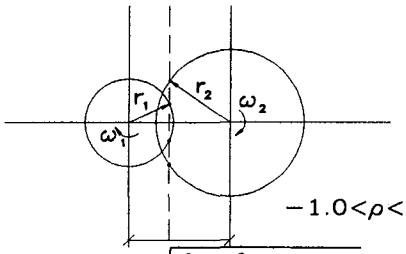

$-1.0 < \rho < 0.0$

$g_p = g_{cr} = \sqrt{r_1^2 + r_2^2 - 2r_1\, r_2 \rho}$ (d)

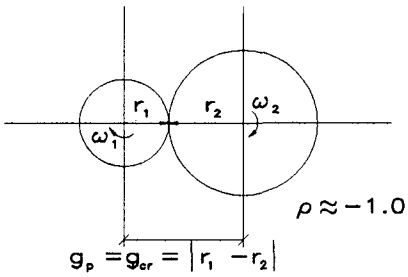

$\rho \approx -1.0$

$g_p = g_{cr} = |r_1 - r_2|$ (e)

Fig. 4.7 Maximum overlapping in the energy levels without inducing pounding effects.

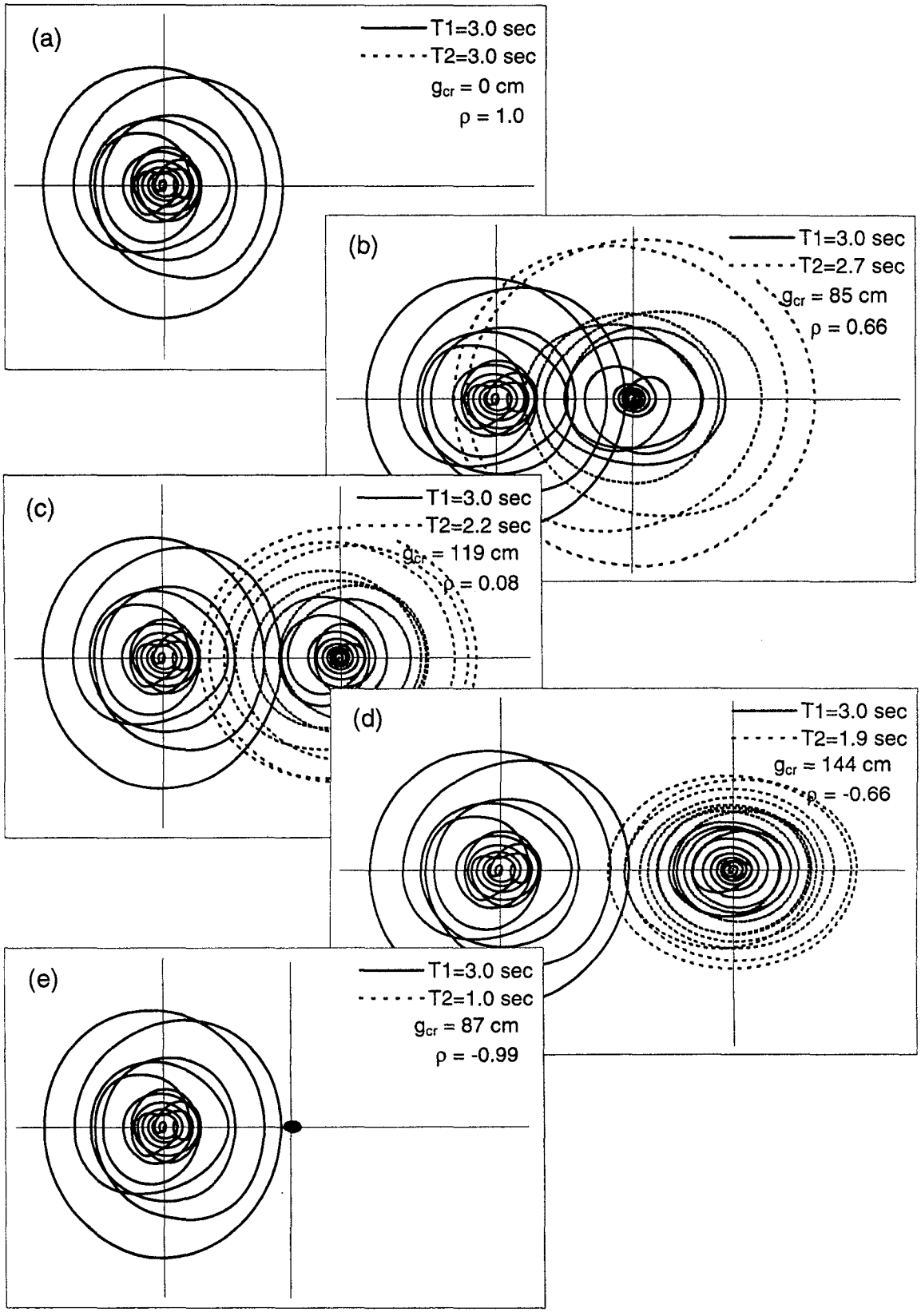

Fig. 4.8 Critical gap for various structural periods, Mexico City earthquake.

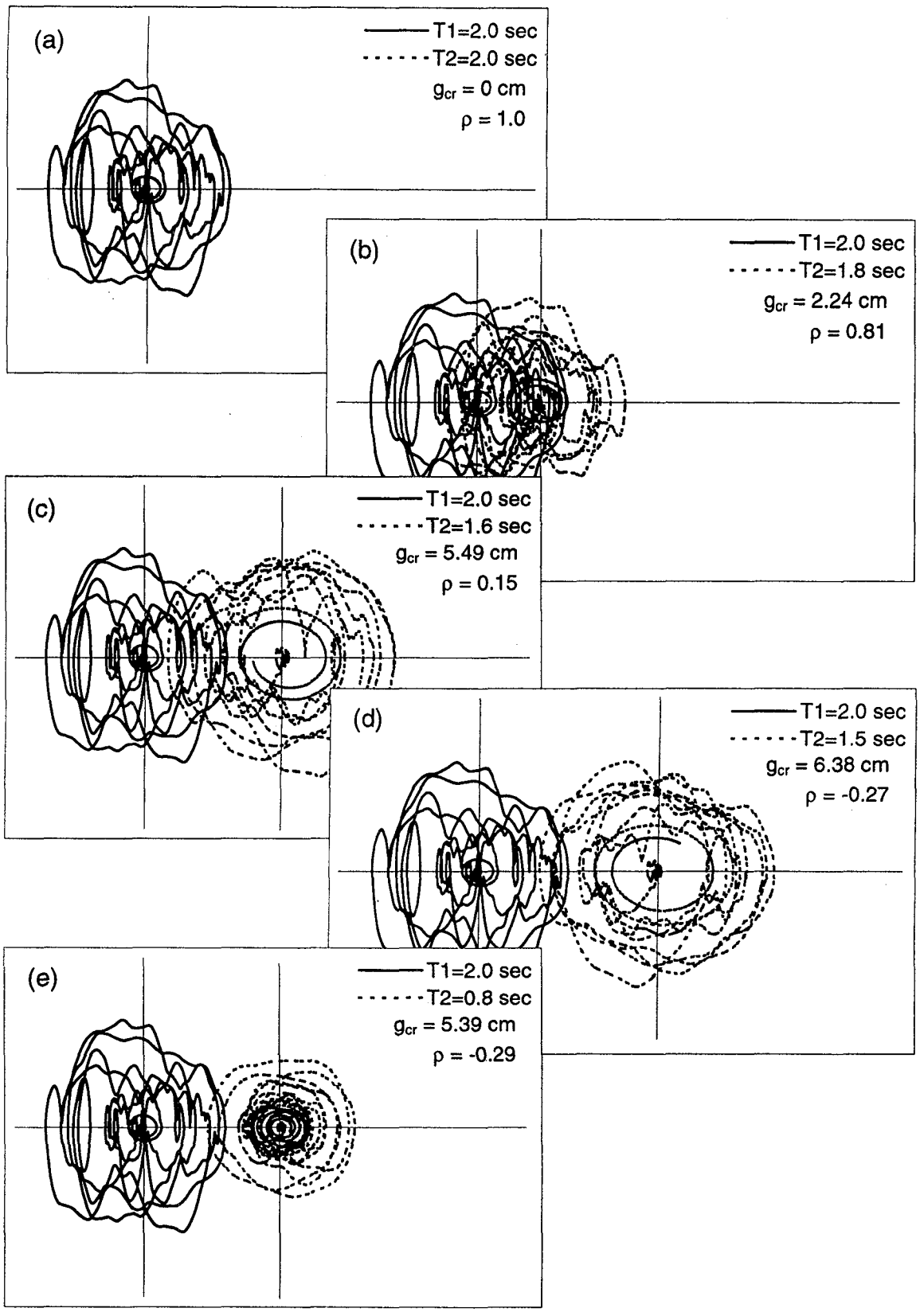

Fig. 4.9 Critical gap for various structural periods, Taft earthquake.

$$\ddot{u}_1 + 2\xi_1\omega_1\dot{u}_1 + \alpha_1\omega_1^2 u_1 + \omega_1^2(1-\alpha_1)z_1' = f(t) \tag{4.21a}$$

$$\ddot{u}_2 + 2\xi_2\omega_2\dot{u}_2 + \alpha_2\omega_2^2 u_2 + \omega_2^2(1-\alpha_2)z_2' = f(t) \tag{4.21b}$$

Where the frequencies correspond to the initial stiffness of the structure, and the parameters α_1 and α_2 corresponds to the ratio of post-yielding stiffness to elastic stiffness. Normalizing the equations of motion with respect to the yield displacements in the structures (u_{y1} and u_{y2}):

$$\ddot{\mu}_1 + 2\xi_1\omega_1\dot{\mu}_1 + \alpha_1\omega_1^2\mu_1 + \omega_1^2(1-\alpha_1)z_1 = f(t)/u_{y1} \tag{4.22a}$$

$$\ddot{\mu}_2 + 2\xi_2\omega_2\dot{\mu}_2 + \alpha_2\omega_2^2\mu_2 + \omega_2^2(1-\alpha_2)z_2 = f(t)/u_{y2} \tag{4.22b}$$

Where:

$$\mu_1 = u_1/u_{y1} \tag{4.23a}$$

$$\mu_2 = u_2/u_{y2} \tag{4.23b}$$

are estimates of the ductility experienced by each of the structures.

For a bilinear oscillator, the functions z_1 and z_2, correspond to an elastoplastic model as introduced by Suzuki and Minai (Roberts and Spanos, 1990), and satisfies the differential equation:

$$\dot{z}_i = G_i(\dot{\mu}_i, z_i) = \dot{\mu}_i\left[1 - \mathrm{U}(\dot{\mu}_i)\,\mathrm{U}(z_i - 1) - \mathrm{U}(-\dot{\mu}_i)\,\mathrm{U}(-z_i - 1)\right] \tag{4.24}$$

where $\mathrm{U}(x)$ denotes the unit step function of x. The study was developed for a bilinear oscillator since only two additional variables, for each structure, are introduced to the problem, namely, the ratio for post yielding stiffness (α_i) and the yield displacements (u_{yi}). A number of other models have been proposed in the literature, among them Wen's model (Wen, 1976), and variations of that model to include degrading and pinching in the hysteretic loops (Baber et al., 1979, 1981, and 1985). The statistical linearization may be calculated with more realistic models, however, an important number of parameters are introduced to the analysis making generalizations of the results dependent on the set of parameters chosen. In the present study, the widely accepted building code approach of bilinear structures has been adopted to study the critical gap between inelastic structures.

The differential equation governing the bilinear response of the structures may be linearized as (Roberts and Spanos, 1990):

$$\dot{z}_i = -c_i^e \dot{\mu}_i - k_i^e z_i \tag{4.25}$$

where the equivalent linearized parameters are:

$$\begin{aligned} c_i^e &= -E\left\{\frac{\partial G(\dot{\mu}_i, z_i)}{\partial \dot{\mu}_i}\right\} \\ &= -1 + \int_1^\infty \int_0^\infty \mathrm{f}(\dot{\mu}_i, z_i) d\dot{\mu}_i dz_i + \int_{-\infty}^{-1} \int_{-\infty}^{0} \mathrm{f}(\dot{\mu}_i, z_i) d\dot{\mu}_i dz_i \end{aligned} \tag{4.26}$$

$$\begin{aligned} k_i^e &= -E\left\{\frac{\partial G(\dot{\mu}_i, z_i)}{\partial z_i}\right\} \\ &= \int_0^\infty \dot{\mu}_i \, \mathrm{f}(\dot{\mu}_i, 1) d\dot{\mu}_i - \int_{-\infty}^{0} \dot{\mu}_i \, \mathrm{f}(\dot{\mu}_i, -1) d\dot{\mu}_i \end{aligned} \tag{4.27}$$

Note that the linearized parameters for the bilinear model need the statistics of the response of the structure, that depend on the linearized parameters for the bilinear model. Therefore, an iterative process is carried out until a desirable convergence criterion has been met. When the first derivative of the ductility and the parameter z_i are modeled as a jointly Gaussian process, the formulas for the equivalent linearized coefficients simplify (see Roberts and Spanos, 1990).

4.4.2 Statistics of the Response

The response of the structures will be investigated when the structures, linear or bilinear, are subjected to a stationary white noise input or filtered white noise input. The formulation presented will include only the bilinear structures subjected to a filtered white noise input, and the derivation for the other cases is included in Appendix A.

For a filtered white noise input, the ground motion satisfies the differential equations:

$$f(t) = \omega_g^2 x_g + 2\xi_g \omega_g \dot{x}_g \tag{4.28}$$

$$\ddot{x}_g + 2\xi_g \omega_g \dot{x}_g + \omega_g^2 x_g = n(t) \tag{4.29}$$

where $n(t)$ corresponds to a stationary white noise process, and, ω_g and ξ_g are the fundamental frequency and damping of the linear ground filter. The input motion has a power spectrum corresponding to what is known as a Kanai-Taijimi spectrum (Soong and Grigoriu, 1992):

$$S_g(\omega) = \frac{1+4\xi_g^2(\omega/\omega_g)^2}{\left(1-(\omega/\omega_g)^2\right)^2+4\xi_g^2(\omega/\omega_g)^2} S_0 \tag{4.30}$$

where S_0 is the power spectrum value for the white noise input.

The equations of motion governing the response of the system may be expressed in the state representation:

$$\dot{\mathbf{X}} = \mathbf{G}\mathbf{X} + \mathbf{B}n(t) \tag{4.31}$$

where:

$$\mathbf{X} = \begin{Bmatrix} \mu_1 \\ \dot{\mu}_1 \\ \mu_2 \\ \dot{\mu}_2 \\ z_1 \\ z_2 \\ x_g \\ \dot{x}_g \end{Bmatrix} = \begin{Bmatrix} u_1/u_{y1} \\ \dot{u}_1/u_{y1} \\ u_2/u_{y2} \\ \dot{u}_2/u_{y2} \\ z_1 \\ z_2 \\ x_g \\ \dot{x}_g \end{Bmatrix} \tag{4.32}$$

$$\mathbf{G} = \begin{bmatrix} \mathbf{G}_{\mu\mu} & \mathbf{G}_{\mu z} & \mathbf{G}_{\mu x} \\ \mathbf{G}_{z\mu} & \mathbf{G}_{zz} & \mathbf{0} \\ \mathbf{0} & \mathbf{0} & \mathbf{G}_{xx} \end{bmatrix} \tag{4.33}$$

$$\mathbf{G}_{\mu\mu} = \begin{bmatrix} 0 & 1 & 0 & 0 \\ -\alpha_1\omega_1^2 & -2\xi_1\omega_1 & 0 & 0 \\ 0 & 0 & 0 & 1 \\ 0 & 0 & -\alpha_2\omega_2^2 & -2\xi_2\omega_2 \end{bmatrix} \tag{4.34a}$$

$$\mathbf{G}_{\mu z} = \begin{bmatrix} 0 & 0 \\ \omega_1^2(\alpha_1 - 1) & 0 \\ 0 & 0 \\ 0 & \omega_2^2(\alpha_2 - 1) \end{bmatrix} \tag{4.34b}$$

$$\mathbf{G}_{\mu x} = \begin{bmatrix} 0 & 0 \\ \omega_g^2/u_{y1} & 2\xi_g\omega_g/u_{y1} \\ 0 & 0 \\ \omega_g^2/u_{y2} & 2\xi_g\omega_g/u_{y2} \end{bmatrix} \tag{4.34c}$$

$$\mathbf{G}_{z\mu} = \begin{bmatrix} 0 & -c_1^e & 0 & 0 \\ 0 & 0 & 0 & -c_2^e \end{bmatrix} \tag{4.34d}$$

$$\mathbf{G}_{zz} = \begin{bmatrix} -k_1^e & 0 \\ 0 & -k_2^e \end{bmatrix} \tag{4.34e}$$

$$\mathbf{G}_{xx} = \begin{bmatrix} 0 & 1 \\ -\omega_g^2 & -2\xi_g\omega_g \end{bmatrix} \tag{4.34f}$$

with the allocation vector:

$$\mathbf{B}_j = \begin{cases} 1 & \text{if } j = 8 \\ 0 & \text{otherwise} \end{cases} \tag{4.35}$$

The variance of the state obeys the differential equation (Roberts and Spanos, 1990):

$$\dot{\mathbf{V}} = \mathbf{G}\mathbf{V}^t + \mathbf{V}\mathbf{G}^t + \mathbf{D} \tag{4.36}$$

because the variance for the white noise input motion is:

$$w_{ff}(\tau) = E\left\{\mathbf{f}(t)\mathbf{f}^t(t+\tau)\right\} = \mathbf{D}\delta(\tau) \tag{4.37}$$

$\delta(\tau)$ being the Dirac delta function, and:

$$\mathbf{D}_{ij} = \begin{cases} 2\pi S_0 & \text{if } i = j = 8 \\ 0 & \text{otherwise} \end{cases} \tag{4.38}$$

The structures start at a deterministic state, or at least uncorrelated with the input, that is, the initial condition for the variance of the structural response starts from zero. On the other hand, the ground filter should have reached its stationary phase before the input motion is transmitted to the structure. The initial conditions for the variance are:

$$\mathbf{V}(0) = \begin{bmatrix} \mathbf{0} & \mathbf{0} \\ \mathbf{0} & \mathbf{V}_{xx}(0) \end{bmatrix} \tag{4.39}$$

The initial conditions for the variance of the ground pre-filter are:

$$\mathbf{V}_{xx}(0) = \begin{bmatrix} \dfrac{\pi S_0}{2\xi_g \omega_g^3} & 0 \\ 0 & \dfrac{\pi S_0}{2\xi_g \omega_g} \end{bmatrix} \tag{4.40}$$

4.4.3 Stationary Solution

When only the stationary solution of the response is of interest, Eq. 4.36 reduces to:

$$\mathbf{G}\mathbf{V}^t + \mathbf{V}\mathbf{G}^t + \mathbf{D} = \mathbf{0} \tag{4.41}$$

that may be rewritten as a system of linear algebraic equations of the form:

$$\mathbf{G}'\mathbf{V}' = \mathbf{D}' \tag{4.42}$$

See Appendix A for the set of linear algebraic equations solved.

For the bilinear case, the system of equations is expressed in terms of the yield displacements u_{y1} and u_{y2}. Once a value for u_{y1} and u_{y2} is provided, the statistics of the response may be determined. The yield displacements were determined for two different cases: to limit within a probability level the maximum experienced ductility (μ), or, to provide a fraction (R) of the probable elastic demand as the yield capacity of the structure.

The former approach will provide the correlation coefficient for a maximum probable ductility level . Since the ductility is a function of the yield displacement, an iterative procedure was implemented. Convergence is achieved when the probability that the ductility μ is exceeded is approximately 5%:

$$P\left\{\left|\frac{U}{u_y}\right| \geq \mu\right\} \approx 0.05 \tag{4.43}$$

where U is the R.V describing the displacement of the structure, u_y is the yield displacement, and μ the maximum ductility with 5% probability of being exceeded. Considering that statistical linearization was used, the output statistics may be approximated using a Gaussian process, therefore, the target standard deviation in the ductility is:

$$\sigma_{\mu} = \frac{\mu}{1.96} \tag{4.44}$$

In the present study five ductility levels were considered: 1.0, 1.5, 2.0, 3.0 and 4.0.

The latter approach, providing a fraction (R) of the probable elastic demand as the yield capacity of the structure, uses the variance of the linear elastic displacement of the structure (σ_{ue}^2) to determine an elastic probable demand. For the present study, the elastic probable demand is determined for a 5% probability of being exceeded:

$$P\{|U_e| \geq u_e\} = 0.05 \tag{4.45}$$

where U_e is the R.V. describing the elastic displacement of the structure, and u_e the probable elastic demand. Since a Gaussian input is being considered, the elastic demand with 5% probability of being exceeded is:

$$u_e = 1.96 \quad \sigma_{ue} \tag{4.46}$$

In the present study five reduction levels were considered: 1.0, 1.5, 2.0, 3.0 and 4.0.

Note that the second approach corresponds to the methodology often adopted by building codes: the structures are designed to withstand only a fraction of the elastic demand, and adequate detailing is provided so that the ductility demand will not exceed the ductility capacity.

A probability level of 5% has been adopted in the present study, however, a different probability level may be selected depending on the allowable risk level for the structure, and the importance of the facility. That is, different probability levels should be used for office buildings and hospitals. The probability level should be set to a level comparable to the risk inherent in the building code design spectra.

The stationary correlation coefficient for a bilinear system with maximum probable ductility μ, is shown in Fig. 4.10 for a broad band (ξ_g=0.6) input, and in Fig. 4.11 for a narrow band (ξ_g=0.05) input. For non-white excitations the ratio of the structural frequencies to the predominant frequency of input is of importance. In this analysis three ratios were considered: 0.5, 1.0 and 2.0. This allows for direct comparison to the correlation coefficient plots in Der

Kiureghian papers (1979 and 1980). As expected, higher correlation coefficients tend to be observed for bilinear systems. Some difference can be observed when comparing to the approximate solution for bilinear systems (see Fig. 4.2). In general, the approximate solution yields higher correlation coefficient, that may lead to an unconservative analysis. Furthermore, the approximate solution does not take into account the predominant period of the input motion, that is determinant on the observed behavior of structures subjected to a narrow band input motion.

Fig. 4.12 to 4.14 presents the correlation coefficient derived from statistical linearization as a three-dimensional surface. The plots correspond to a maximum probable ductility level of 4.0, subjected to white noise, broad band, and narrow band inputs. The horizontal axis correspond to the ratio of the structural periods to the predominant input period. Along with the surface, contour plots for equal correlation coefficient levels are included. Correlation coefficient plots included in Appendix B are presented using contour levels.

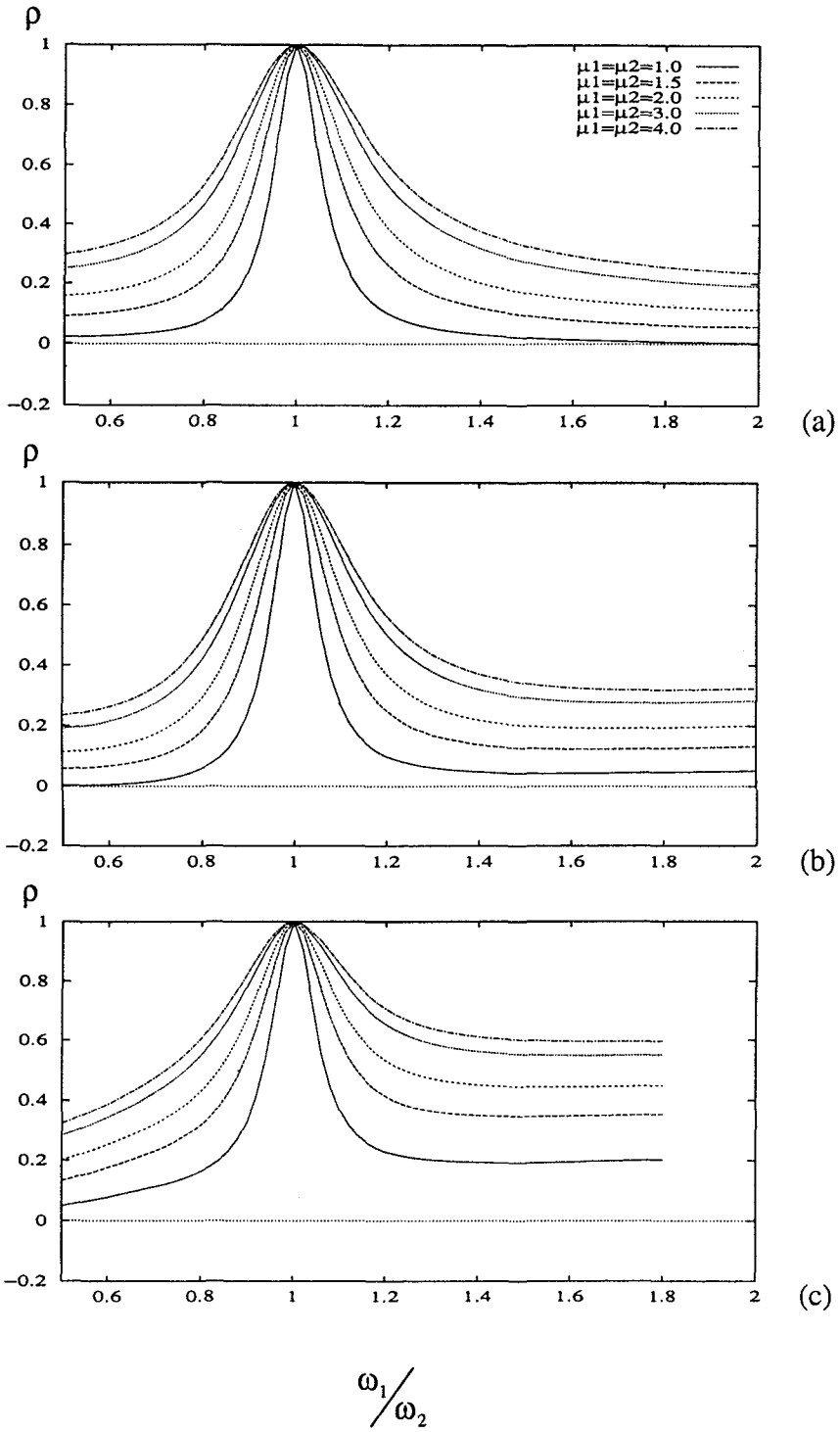

Fig. 4.10 Correlation coefficient for bilinear oscillators and broad band input: (a) $\omega_2 = 0.5\omega_g$, (b) $\omega_2 = \omega_g$, (c) $\omega_2 = 2.0\omega_g$.

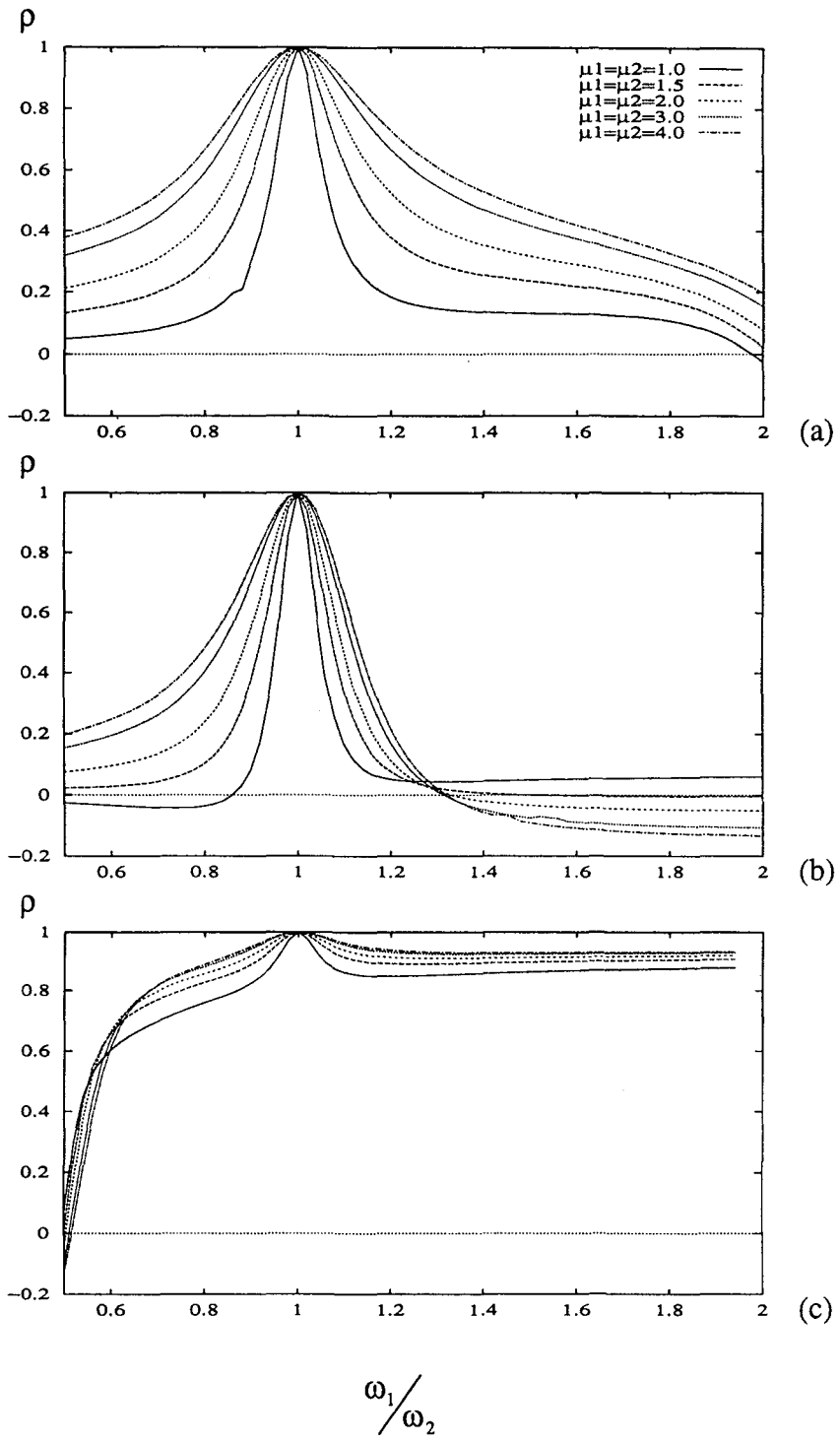

Fig. 4.11 Correlation coefficient for bilinear oscillators and narrow band input: (a) $\omega_2 = 0.5\omega_g$, (b) $\omega_2 = \omega_g$, (c) $\omega_2 = 2.0\omega_g$.

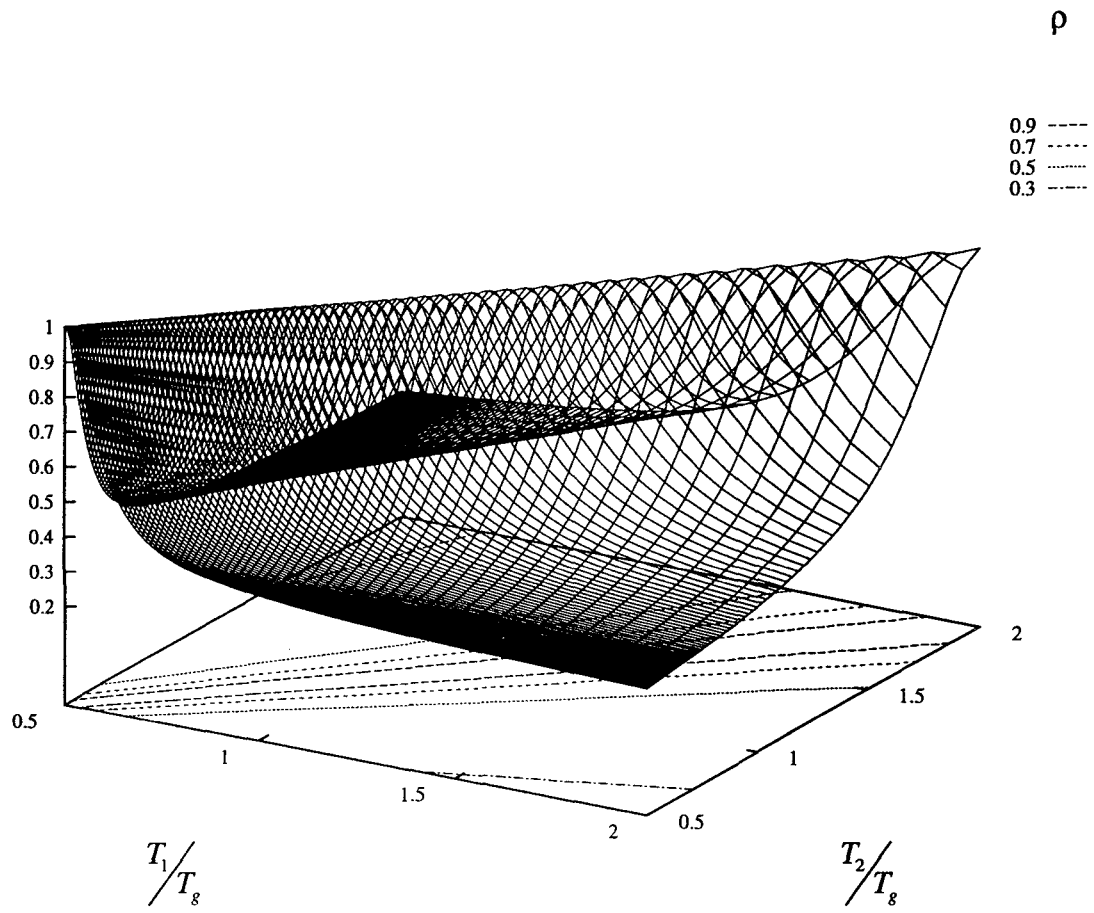

Fig. 4.12 Correlation coefficient surface and contours for bilinear oscillators and white noise input ($\mu_1 = \mu_2 = 4.0$).

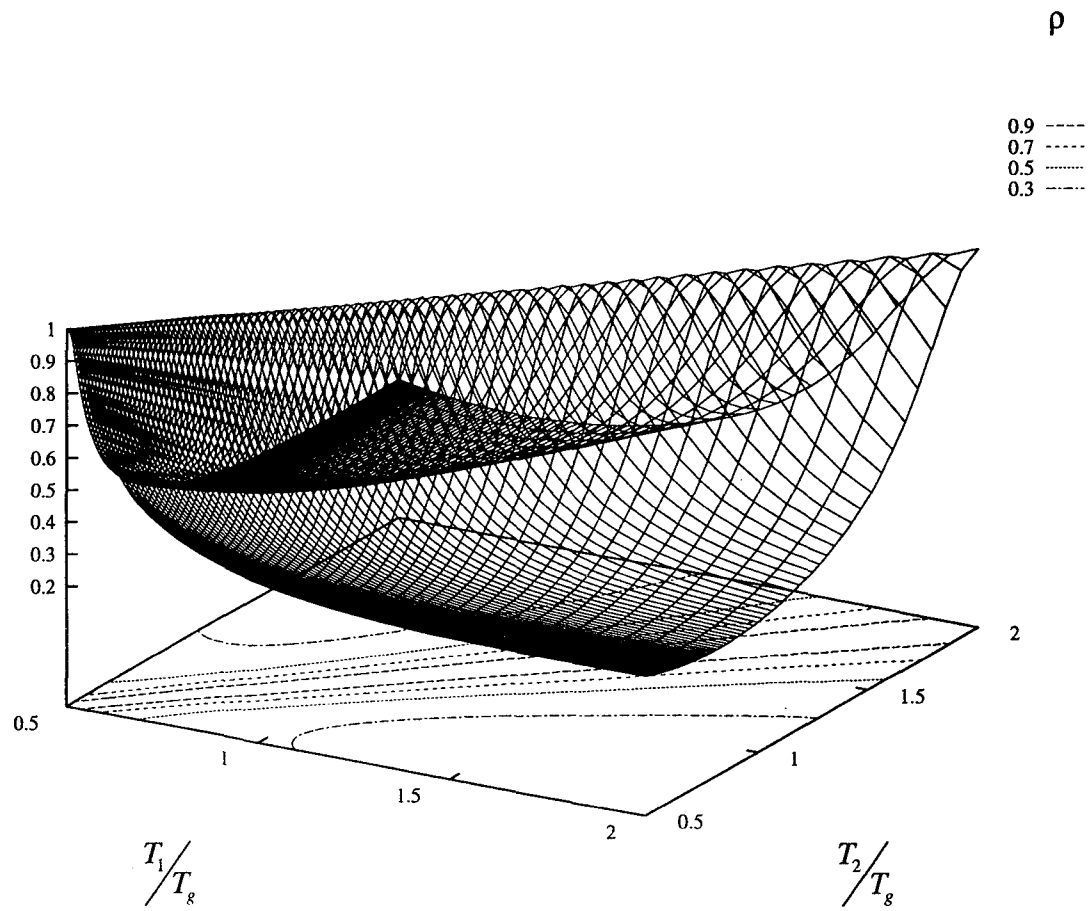

Fig. 4.13 Correlation coefficient surface and contours for bilinear oscillators and broad band input ($\mu_1=\mu_2=4.0$, $\xi_g=0.6$).

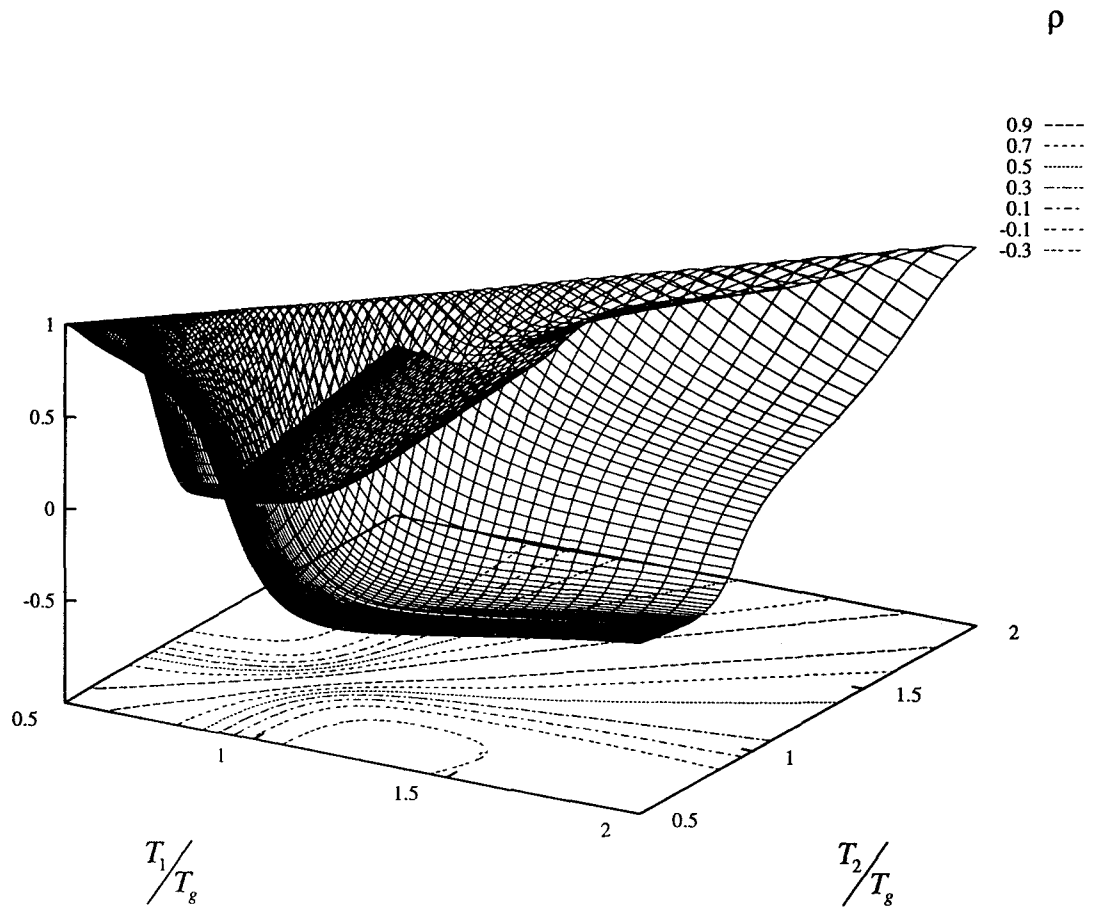

Fig. 4.14 Correlation coefficient surface and contours for bilinear oscillators and narrow band input ($\mu_1=\mu_2=4.0$, $\xi_g=0.05$).

A large number of correlation coefficient plots are included in Appendix B, to cover the most commonly encountered practical situations. In all the plots generated, both structures are assumed to have the same damping characteristics, the same probable ductility level, or the same reduction factor. Often, this may not be true in actual applications. Fig. 4.15 presents the correlation coefficient for bilinear structures with probable target ductility of μ_1=2.0 and μ_2=4.0, subjected to a narrow band input. Note that some degree of asymmetry is introduced due to the difference in the target ductility. A conservative estimate can be obtained considering the same target ductility in both structures being equal to the smaller of the two.

4.4.4 Distribution for the Critical Gap

The probability density function for the extreme of the process G_p, that is, the critical gap (G_{cr}), may be described for a stationary Gaussian process by (Soong and Grigoriu, 1992):

$$f_{G_{rc}}(g_{cr}) = \sqrt{\frac{1-\zeta^2}{2\pi\sigma^2_{g_{cr}}}}\exp\left[-\frac{g^2_{cr}}{2\sigma^2_{g_{cr}}(1-\zeta^2)}\right] + \frac{\zeta g_{cr}}{\sigma^2_{gcr}}\Phi\left(\frac{\zeta g_{cr}}{\sigma_{g_{cr}}\sqrt{1-\zeta^2}}\right)\exp\left[-\frac{g^2_{cr}}{2\sigma^2_{g_{cr}}}\right] \tag{4.47}$$

where:

$$\zeta = \frac{\sigma^2_{\dot{g}_{cr}}}{\sigma_{g_{cr}}\sigma_{\ddot{g}_{cr}}} \tag{4.48}$$

$$\Phi(x) = \frac{1}{\sqrt{2\pi}}\int_{-\infty}^{x} e^{-u^2/2}du \tag{4.49}$$

The parameter ζ is a measure of how broad or narrow is the response of the structure. For broad band response the parameter tends to zero, while for narrow band response, it tends to one.

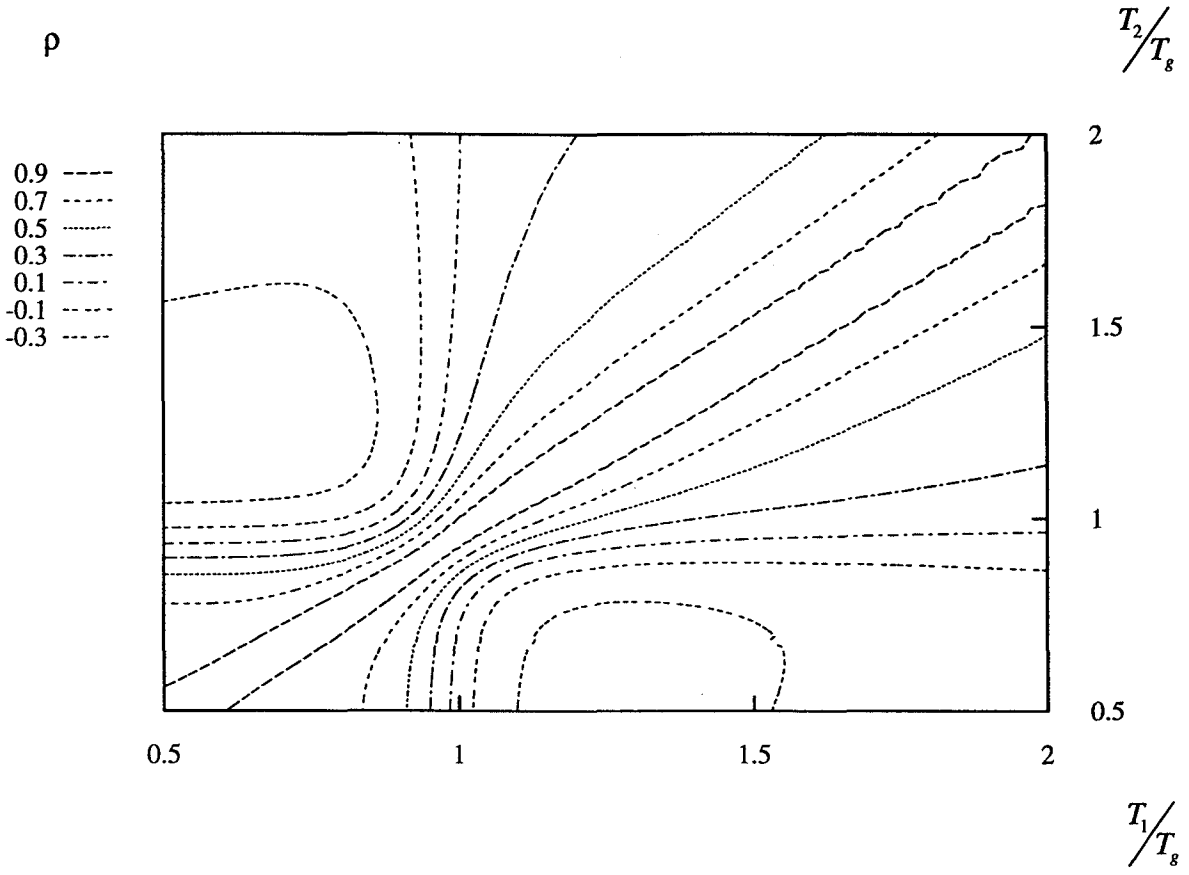

Fig. 4.15 Correlation coefficient contours for bilinear oscillators and narrow band input (μ_1=2.0, μ_2=4.0, ξ_g=0.05).

The variance of the acceleration in the ductility demand may be calculated from equations of the form:

$$R_{\ddot{\mu}_1\ddot{\mu}_1} = -2\xi_1\omega_1 R_{\dot{\mu}_1\ddot{\mu}_1} - \alpha_1\omega_1^2 R_{\mu_1\ddot{\mu}_1} - \omega_1^2(1-\alpha_1)R_{z_1\ddot{\mu}_1} + \frac{\omega_g^2}{u_{y1}} R_{x_g\ddot{\mu}_1}$$
$$+ \frac{2\xi_g\omega_g}{u_{y1}} R_{\dot{x}_g\ddot{\mu}_1} \qquad (4.50)$$

where each correlation involving the acceleration of the response may be calculated from similar expressions in term of known variances. The mean and variance of the critical gap can be then calculated, taking the first moment of the probability density function (Eq. 4.47).

4.5 Critical Gap Computation

Using the results from the previous subsections, a methodology to estimate the critical gap (g_c) to avoid pounding is outlined. The critical gap is determined using the underlying principles of the Double Difference Combination Rule:

$$g_{cr} = \sqrt{u_1^2 + u_2^2 - 2\rho u_1 u_2} \qquad (4.51)$$

where u_1 and u_2 are the maximum inelastic displacements 1 and 2, respectively. The inelastic displacements are calculated using the inelastic amplification factor in Figs. B.1 to B.4, that are a function of the structural period (T), the expected probable maximum ductility (μ), and the width characteristics of the earthquake motion (ξ_g). The correlation coefficient (ρ), determined from statistical linearization analysis of bilinear structures subjected to filtered white noise inputs, is presented in Appendix B, as a function of the structural periods (T_1 and T_2), their relationship to the predominant earthquake period (T_g), the characteristic width of the input motion (ξ_g), and the expected probable maximum ductility levels (μ), or reduction factors (R) in the structures.

4.6 Critical Gap Including Soil-Structure Interaction

Building structures located on soft soil conditions are likely to experience a significant change in the response due to soil-structure interaction. Damage reports from previous earthquakes affecting metropolitan areas where soft soil conditions prevail, like Mexico City, indicate the importance that such interactions can have on the overall performance of the structure. Often, soil-structure interaction will result in larger deflections, therefore, increasing the likelihood of pounding.

The critical gap under these conditions can be calculated, extending the theory developed in Section 4.4, to include rotations at the foundation. The random process that defines the difference in the displacements of the two structures is:

$$G_p = U_1 + \Theta_1 h - U_2 - \Theta_2 h \tag{4.52}$$

where U_1 and U_2 correspond to the random variables describing the relative deformation of the structures, Θ_1 and Θ_2 correspond to the random variables describing the rotation at the foundation, and h is the height at which pounding is likely to occur.

According to this stochastic description, the statistical parameters of the difference in displacements may be determined from the statistics of U_1, U_2, Θ_1,and Θ_2. The input motion in this case will be assumed to be a zero mean Gaussian process. Therefore, the structural displacements and foundation rotations of the linear system will also be zero mean Gaussian processes. Consequently the process G_p is also zero mean Gaussian.

The variance of the difference in displacements may be calculated from:

$$\begin{aligned} E\{G_p^2\} = {} & E\{U_1^2\} + h^2 E\{\Theta_1^2\} + E\{U_2^2\} + h^2 E\{\Theta_2^2\} \\ & + 2hE\{U_1\Theta_1\} + 2hE\{U_2\Theta_2\} - 2E\{U_1U_2\} \\ & - 2hE\{U_1\Theta_2\} - 2hE\{U_2\Theta_1\} - 2h^2 E\{\Theta_1\Theta_2\} \end{aligned} \tag{4.53}$$

that may be rewritten as a function of the correlation coefficients:

$$\rho_{u1u2} = \frac{E\{U_1 U_2\}}{\sqrt{E\{U_1^2\}E\{U_2\}}} \tag{4.54a}$$

$$\rho_{u1\theta1} = \frac{E\{U_1 \Theta_1\}}{\sqrt{E\{U_1^2\}E\{\Theta_1^2\}}} \tag{4.54b}$$

$$\rho_{u1\theta2} = \frac{E\{U_1 \Theta_2\}}{\sqrt{E\{U_1^2\}E\{\Theta_{21}^2\}}} \tag{4.54c}$$

$$\rho_{u2\theta1} = \frac{E\{U_2 \Theta_1\}}{\sqrt{E\{U_2^2\}E\{\Theta_1^2\}}} \tag{4.54d}$$

$$\rho_{u2\theta2} = \frac{E\{U_2 \Theta_2\}}{\sqrt{E\{U_2^2\}E\{\Theta_2^2\}}} \tag{4.54e}$$

$$\rho_{\theta1\theta2} = \frac{E\{\Theta_1 \Theta_2\}}{\sqrt{E\{\Theta_1^2\}E\{\Theta_2^2\}}} \tag{4.54f}$$

according to:

$$\begin{aligned} E\{G_p^2\} = {} & \sigma_{u1}^2 + h^2\sigma_{\theta1}^2 + \sigma_{u2}^2 + h^2\sigma_{\theta2}^2 + 2h\sigma_{u1}\sigma_{\theta1}\rho_{u1\theta1} \\ & +2h\sigma_{u2}\sigma_{\theta2}\rho_{u2\theta2} - 2\sigma_{u1}\sigma_{u2}\rho_{u1u2} - 2h\sigma_{u1}\sigma_{\theta2}\rho_{u1\theta2} \\ & -2h\sigma_{u2}\sigma_{\theta1}\rho_{u2\theta1} - 2h^2\sigma_{\theta1}\sigma_{\theta2}\rho_{\theta1\theta2} \end{aligned} \tag{4.55}$$

Because the process G_p is zero mean Gaussian, the first two moments completely describe the statistics of the response. The probability of a gap g_p being exceeded can be determined from the standard deviation σ_{gp}. Therefore, the critical gap for a given probability of exceedance may be found according to:

$$\begin{aligned} g_{cr}^2 = {} & u_1^2 + h^2\theta_1^2 + u_2^2 + h^2\theta_2^2 + 2hu_1\theta_1\rho_{u1\theta1} \\ & +2hu_2\theta_2\rho_{u2\theta2} - 2u_1u_2\rho_{u1u2} - 2hu_1\theta_2\rho_{u1\theta2} \\ & -2hu_2\theta_1\rho_{u2\theta2} - 2h^2\theta_1\theta_2\rho_{\theta1\theta2} \end{aligned} \tag{4.56}$$

where the maximum probable displacements and rotations are determined from a design spectra as a function of the periods of the structure alone (T_1 and T_2) and the periods of the foundation system with infinitely stiff structures ($T_{\theta1}$ and $T_{\theta2}$). The six correlation coefficients are determined from the charts in Appendix B, using the corresponding periods.

An alternate approach to estimating the critical gap with soil-structure interaction would be to develop a response spectra that includes such effects. In this situation Eq. 5.51 would be used with total displacements u_{t1} and u_{t2}, and the correlation coefficient would be determined as a function of the actual fundamental periods of vibration (T_{t1} and T_{t2}).

4.7 Remarks and Conclusions

Four different formulas to calculate the critical gap by different countries with moderate to high seismicity level have been identified. The survey indicated that a minimum gap separation to avoid pounding interactions is the commonly adopted design philosophy. Only one building code was found to allow for some level of pounding, if the impact interactions did not impose undesirable effects in the response of the structures.

Building codes adopted one of the following four approaches to specify the minimum distance to avoid pounding:

- a factor times sum of maximum
- a SRSS combination of the displacements
- a coefficient times the height
- a fixed distance

The formulations above do not include the effects of the correlation coefficient, and may lead to conservative results for structures with similar periods, or large damping.

The Double Difference Combination rule, introduced by Kasai (Jeng et al., 1992) incorporates the correlation coefficient relating to the displacements of the structures. A formula for the correlation coefficient was adopted from the simplified solution of linear structures subjected to white noise input, as developed by Der Kiureghian (1979). Later, Kasai and Jagiasi (1993a) presented some simple modification to be used for bilinear and degrading structures. Such simple formulations were obtained from curve fitting numerical simulations.

In this section, the Double Difference Combination rule was suggested to compute the critical gap, using a modified value for the correlation coefficient. The derivation by Der Kiureghian was extended for bilinear structures, through the use of statistical linearization, subjected to a filtered white noise input. The results are presented in Appendix B in plots as a function of the structural periods, and the ratio to the predominant ground motion period.

Two frequency band widths were considered: narrow and broad, to simulate the response of Mexico City type and Taft or El Centro type earthquakes, respectively. The improved correlation coefficients were used in the Double Difference formulation to determine the critical gap of the systems.

Soil-structure interaction may amplify the lateral deflections of the structures due to rotation at the foundation. The extension of the Double Difference Combination rule to structures on flexible foundations is presented. For this situation, the maximum relative deflections of the structures and the maximum rotations at the foundations, combined with six correlation coefficients provide an estimate of the critical gap.

The Double Difference Combination rule introduced by other researchers was extended to calculate the critical gap for bilinear structures subjected to narrow band (soft soil conditions), or broad band inputs (stiff soil conditions). In some cases, existing buildings may be found with gaps smaller, or considerably smaller than the critical gap. Pounding is likely to occur in such cases. Section 5 describes the pounding effects that can be expected when buildings are separated by a gap smaller than critical.

SECTION 5
EFFECTS DUE TO POUNDING IN STRUCTURES SEPARATED BY A GAP LESS THAN CRITICAL

5.1 Introduction

The quantification of the amplification effects in structures subjected to pounding interactions is of interest in existing buildings separated by a gap less than critical. These amplification effects may be calculated using the mathematical formulations briefly described in Section 3.5 for a given earthquake input motion.

The amplification effects for single degree of freedom structures is presented under a sinusoidal input, a narrow band earthquake motion (Mexico City), and a broad band earthquake motion (Taft earthquake). While some trends in the amplification may be detected for the sinusoidal and narrow band inputs, the broad band results show no clear trend that will help the engineer to estimate pounding effects.

A simple methodology to estimate pounding effects for gaps slightly smaller than critical is presented. The methodology assumes that a single hit occurs between the structures when they are at the maximum energy level. Determining the onset of critical pounding, and backtracking in the time to the instant when the structures come into contact, yields the state at the onset of pounding. Using the formulas for stereomechanical pounding, the post impact state and energy levels are determined. The methodology offers a simple approach to estimating the maximum effects of pounding for gaps slightly smaller than critical. Furthermore, the results obtained using this methodology have comparable probability of being exceeded as the design spectra.

5.2 Single Story (SDOF) Structures Subjected to a Sinusoidal Input

To identify some of the trends that may be observed during pounding interactions, the response of a pair of single story (SDOF) structures, when subjected to a sinusoidal input, was studied using the deterministic model presented in Valles (1995).

At this first stage in the analysis, the period of the structures was fixed, and the period of the input motion was varied. To study the effects of pounding in the structure the amplification due to pounding in the total input energy of the system was monitored:

$$\frac{E_I}{E_I^0} = \frac{E_{I1} + E_{I2}}{E_{I1}^0 + E_{I2}^0} \tag{5.1}$$

where E_I corresponds to the total input energy considering pounding effects, E_I^0 is the total input energy when pounding effects are not considered. The total input energy was chosen rather than the individual input energies because it provides a global estimate on whether pounding interactions increase or decrease the energy in the system. Note that when the individual input energies are observed, one structure will experience an amplification in its input energy while the other will undergo a reduction in the input energy, making it difficult to assess the actual global effects on the system.

Fig. 5.1 presents a typical set of amplification curves for structural periods of 0.75 and 1.5 seconds, for different ratios of the actual gap (g_p) to the critical gap (g_{cr}). Different combination of periods present the same amplification characteristics but with the peaks of maximum amplification or deamplification at different input periods. The envelope of the amplification curves, for all combinations of periods T_1 and T_2, follow the curve sketched in Fig. 5.2.

The amplification curves exhibit two periods for the input motion at which significant amplification in the response is observed. These periods approximately corresponds to:

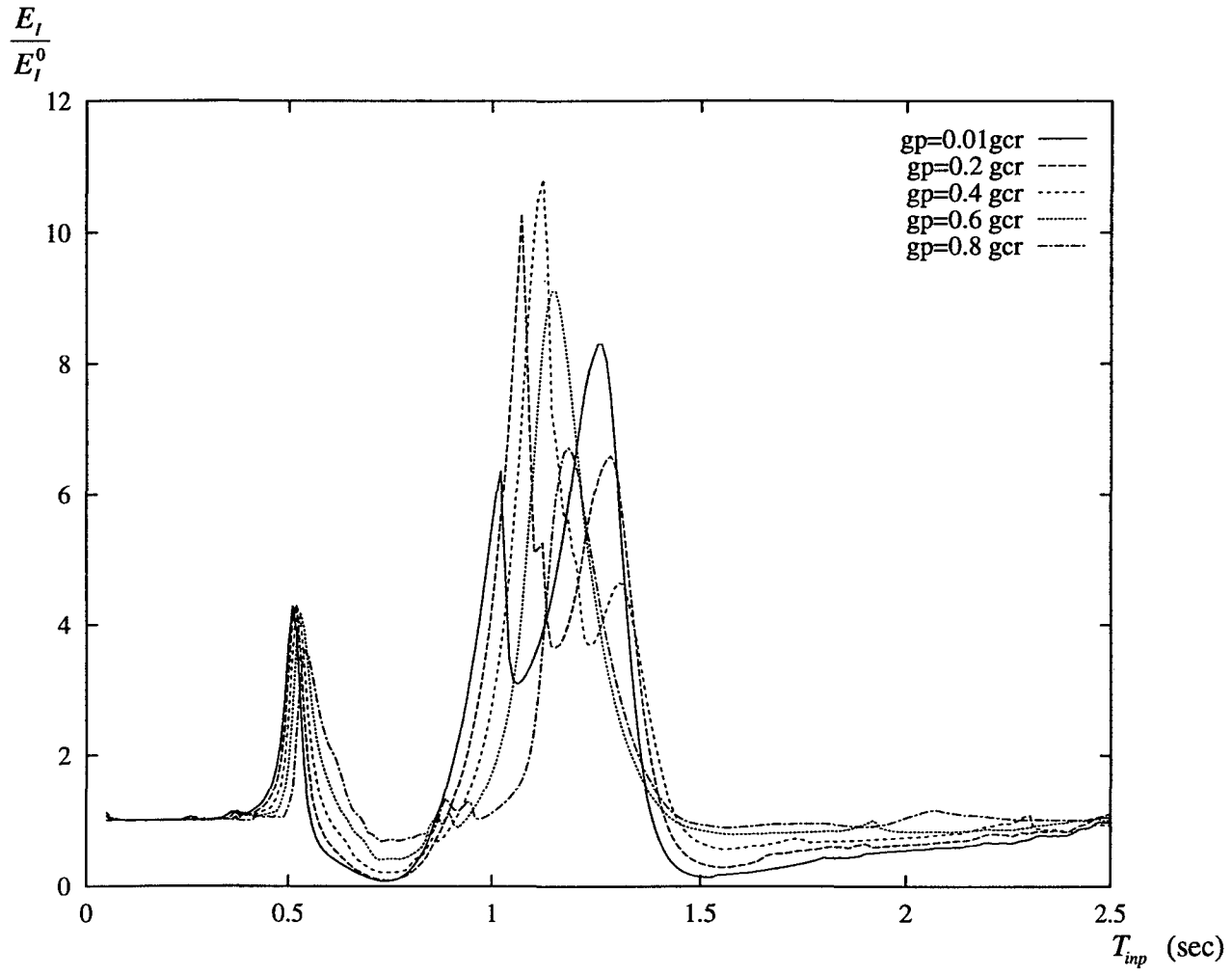

Fig. 5.1 Amplification curves for a sinusoidal input (T_1=0.75 sec, T_2=1.5 sec, PGA=160 cm/sec^2).

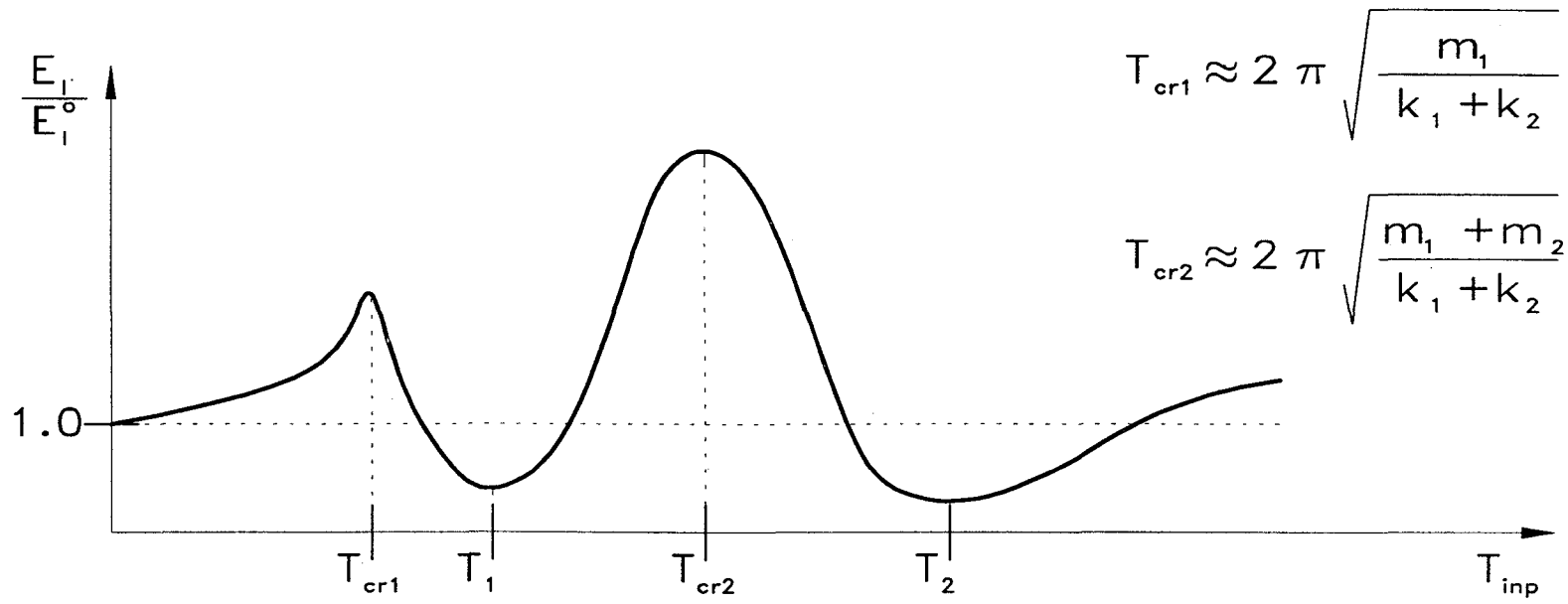

Fig. 5.2 Envelope of amplification curves for a sinusoidal input.

$$T_{cr1} \approx 2\pi\sqrt{\frac{m_1}{k_1 + k_2}} \tag{5.2a}$$

$$T_{cr2} \approx 2\pi\sqrt{\frac{m_1 + m_2}{k_1 + k_2}} \tag{5.2b}$$

The second critical peak (T_{cr2}) corresponds to the period of the system if the structures were connected with a rigid link. The first critical peak corresponds to a higher oscillation frequency in which out of phase motion is promoted between the two structures, therefore, increasing the relative velocity at the onset of pounding.

The amplification curves also present two characteristic periods at which a maximum deamplification is observed. As expected, these periods coincide with the fundamental periods of vibration of the structures. The significant reduction is observed since pounding stops the gradual build-up of energy that would otherwise take one of the structures to resonance. Although a significant energy is transferred to the non-resonating structure, the reduced energy in the otherwise resonating structure is considerably smaller, resulting in a net reduction in the total input energy.

Fig. 5.3 presents the transfer energy in the system; by structure 1, to structure 2:

$$E_{tr12} = E_{I1} - E_{s1} - E_{\xi 1} \tag{5.3}$$

where

$$E_{s1} = E_{k1} + E_{p1} \tag{5.4}$$

and E_{I1} is the input energy of structure 1, $E_{\xi 1}$ is the viscous energy in structure 1, E_{k1} and E_{p1} are the kinetic and potential energies in structure 1, respectively. The results for different ratios of actual to critical gap are normalized to the total no pounding input energy in the system. Although the results are presented for the case when T_1 is 0.75 sec, and T_2 is 1.5 sec, similar patterns were observed for different combination of periods. For the case when T_2 is smaller than T_1, the same curves were observed but with opposite signs.

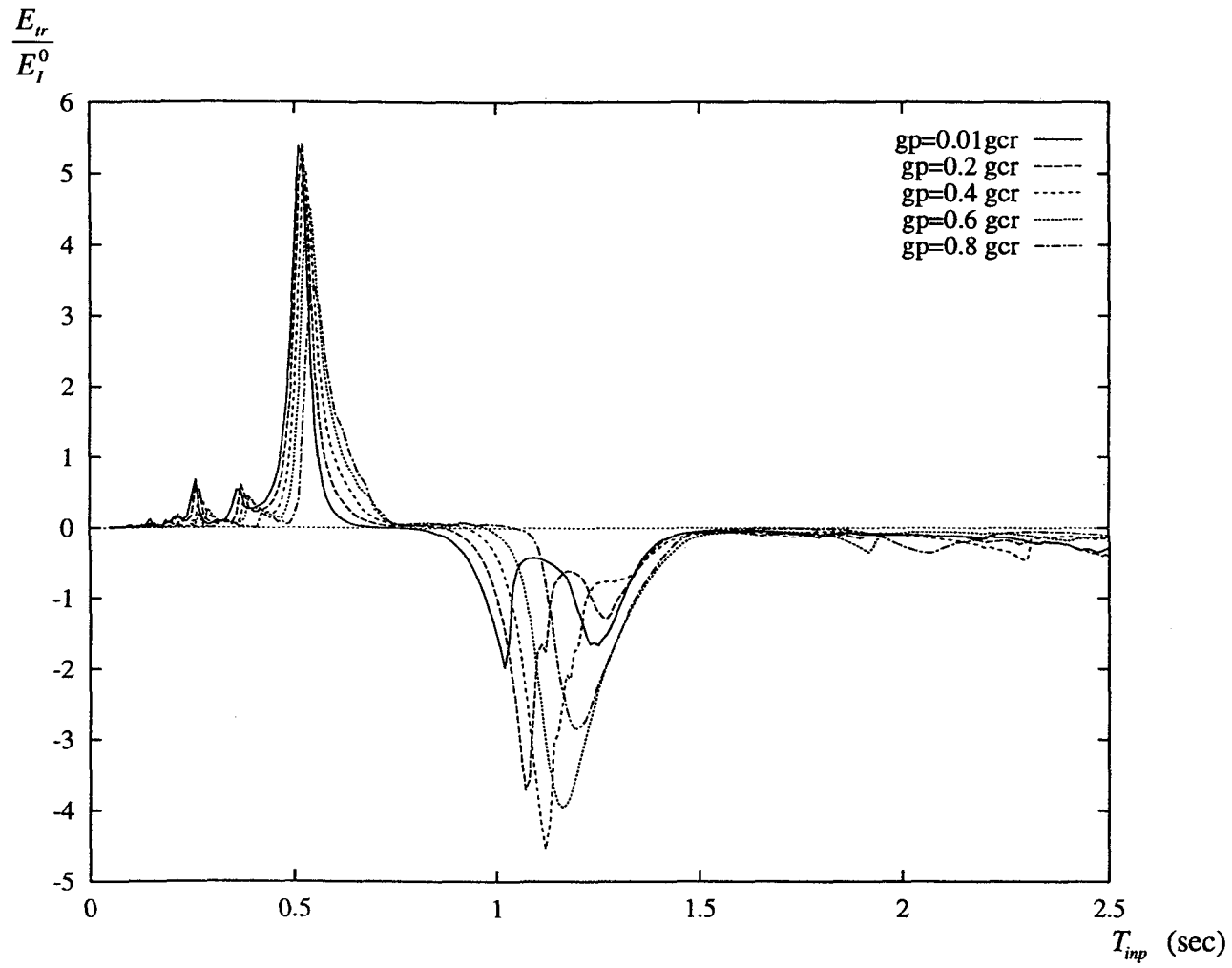

Fig. 5.3 Transfer energy curves for a sinusoidal input (T_1=0.75 sec, T_2=1.5 sec, PGA=160 cm/sec^2).

The envelope curve for the transfer energy from structure 1 to structure 2 is schematically presented in Fig. 5.4. Energy is transferred from the lowest period structure to the highest period structure when the input has a predominant period smaller than both structures, coinciding with the critical period T_{cr1}. On the other hand, energy is transferred from the highest period structure to the lowest period one when the input has a predominant period intermediate to the structural periods. The reason for this trend is due to the energy levels of the structures when subjected to a sinusoidal input of frequency $\overline{\omega}$ (see Fig. 5.5). Note that the structure with higher energy level transfers energy to the one with smaller energy level.

In the next phase of the study, the influence of the gap size on the pounding effects was investigated. Fig. 5.6 presents schematically the four distinct trends in the amplification of the total input energy of the system as the gap size is varied.

The first case studied is typical of the response of structures when the period of the input motion lies between T_1 and T_{cr2}, or between T_{cr2} and T_2. For this situation, a gradual increase in the total input energy is observed, with a maximum at small gap sizes. A greater rate of amplification is observed at smaller gap sizes. Under these conditions a gap slightly smaller than critical will not impose severe effects in the structures, while a small gap size will significantly amplify the response.

The second case studied is observed when the period of the input motion approximately coincides with T_{cr1} or T_{cr2}. For this combination of parameters, the total energy input dramatically increases for gaps slightly smaller than critical. After the peak is reached, a further decrease in the gap size will make the amplification factors smaller, although still greater than one. Under these conditions, a gap slightly smaller than critical will impose severe amplifications in the response of the structures.

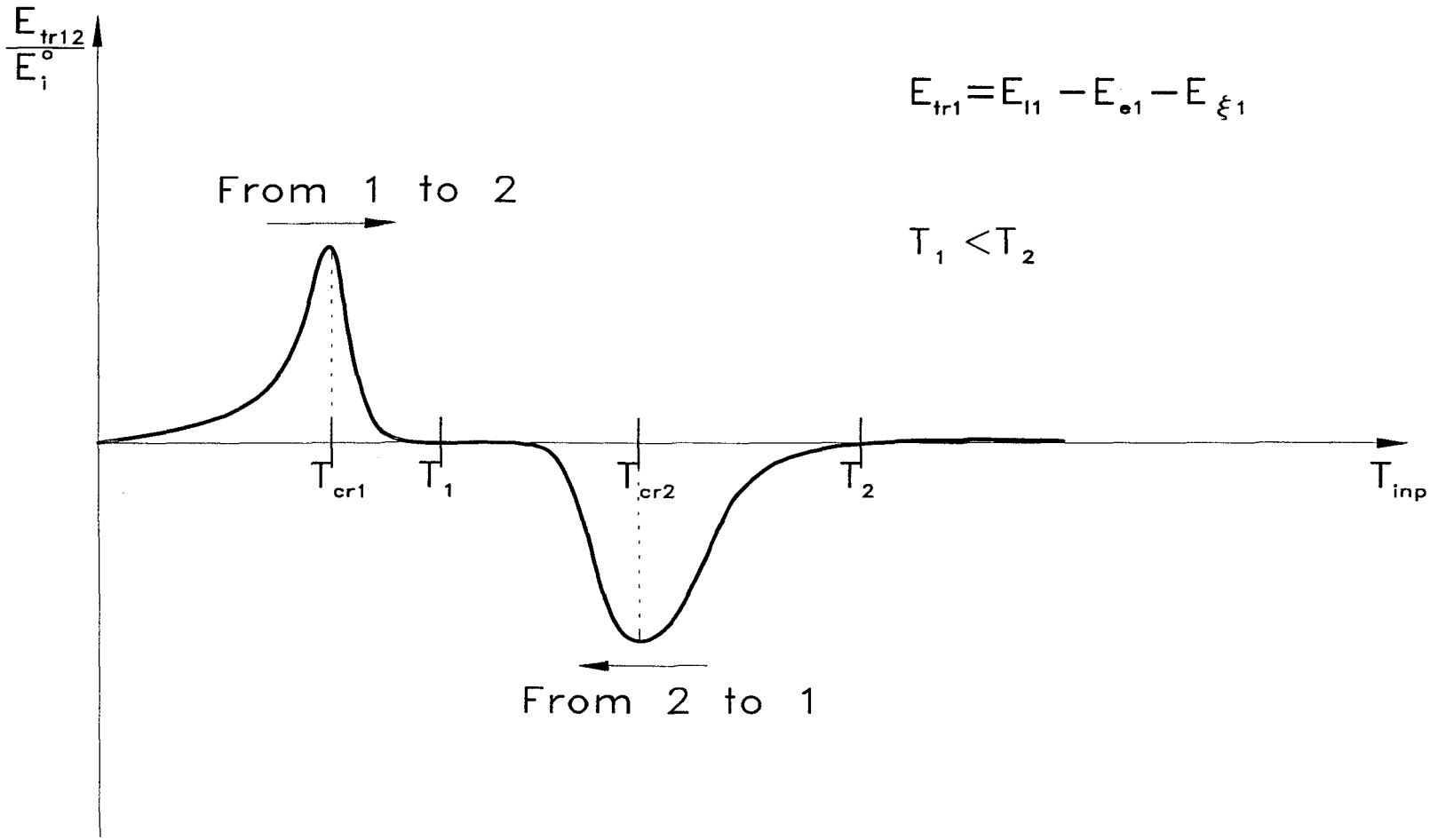

Fig. 5,4 Envelope of transfer energy for a sinusoidal input.

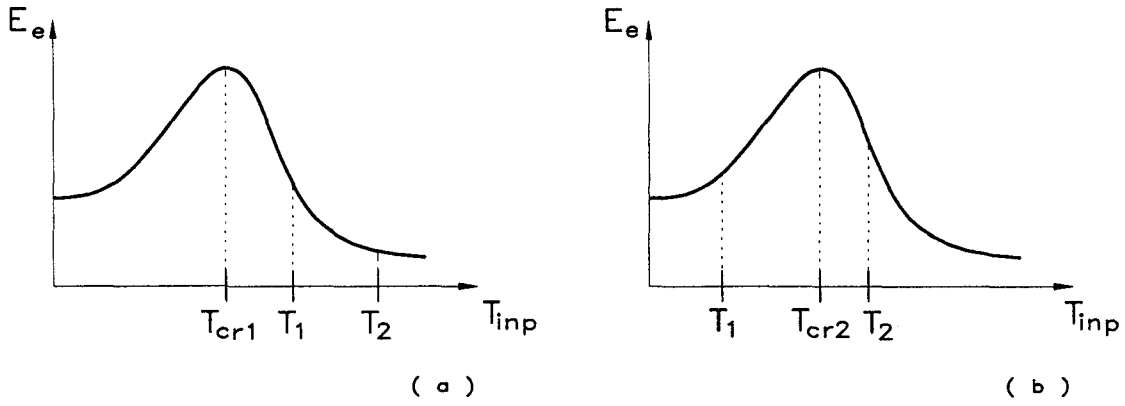

Fig. 5.5 Structural energy for input with critical periods.

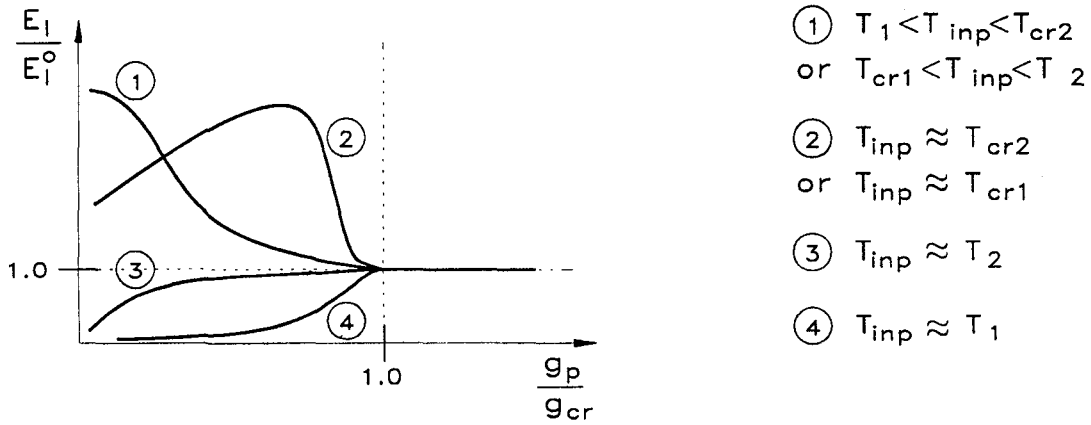

Fig. 5.6 Trends in the amplification factor as a function of the gap size.

The third case studied is observed when the period of the input motion approximately coincides with T_2. For this combination of parameters, a gradual decrease of the total input energy was observed as the gap size was reduced. A greater rate of decrease was observed at smaller gap sizes.

The fourth case studied was observed when the period of the input motion approximately coincided with T_1. For this combination of parameters a reduction in the total input energy of the system was observed as the gap size reduces. The greater rate in the deamplification was observed for gap sizes slightly smaller than critical.

Note that although a reduction in the total input energy of the system was observed in cases three and four, the structure not at resonance will experience an important amplification in the response. If the amplification in kinetic and potential energies is studied, a factor greater than one was observed except when the structure is at resonance if pounding effects are ignored. Furthermore, the non-resonant structure in cases three and four may experience an amplification in displacement and velocity much greater than the one observed in cases one and two, where the nonlinearly coupled system resonates.

The schematic drawings showed in this subsection are intended to show only qualitatively the general trends observed from a large number of numerical simulations, and should not be adopted for design purposes.

5.3 Single Story (SDOF) Structures Subjected to a Narrow Band Input

Using the deterministic model briefly described in Section 3.5, a pair of single story (SDOF) structures were studied. In this subsection the 1985 Mexico City earthquake was used as input motion. The period of both structures was varied from 0.5 to 4.0 seconds. The response was obtained under three different gaps, namely, 25%, 50% and 75% of the critical gap (g_{cr}).

For the analysis elastic impact was considered, being the stiffness and damping constants of the Impact Kelvin element:

$$K_c = 100.0 \quad (K_1 + K_2) \tag{5.5}$$

$$C_c = 0.0 \tag{5.6}$$

where K_1 and K_2 are the stiffness of each structure, respectively.

The response amplification is presented monitoring the change in the structures energy. Furthermore, the analysis was carried out for the mass ratio:

$$\frac{m_1}{m_2} = 1.0 \tag{5.7}$$

Figs. 5.7 to 5.9 present the results using contours of equal amplifications for different combinations of structural periods. Only the amplification response for structure one is presented since the corresponding amplification for structure two may be obtained, in this case, by interchanging the structural periods. For different mass ratios this simplification is not valid, and a different set of graphs for each structure is necessary.

Note that although some peculiarities of the input motion are reflected in the equal amplification curves, trends similar to the ones described in the sinusoidal input case are identifiable. This is due to the similarities between the Mexico City earthquake and a sine curve.

5.4 Single Story (SDOF) Structures Subjected to a Broad Band Input

A similar set of analysis as those described in the previous subsection were performed using the Taft earthquake motion as input. The results from these simulations are presented in Figs. 5.10 to 5.12 in terms of structural energy amplification factors for different combination of structural periods.

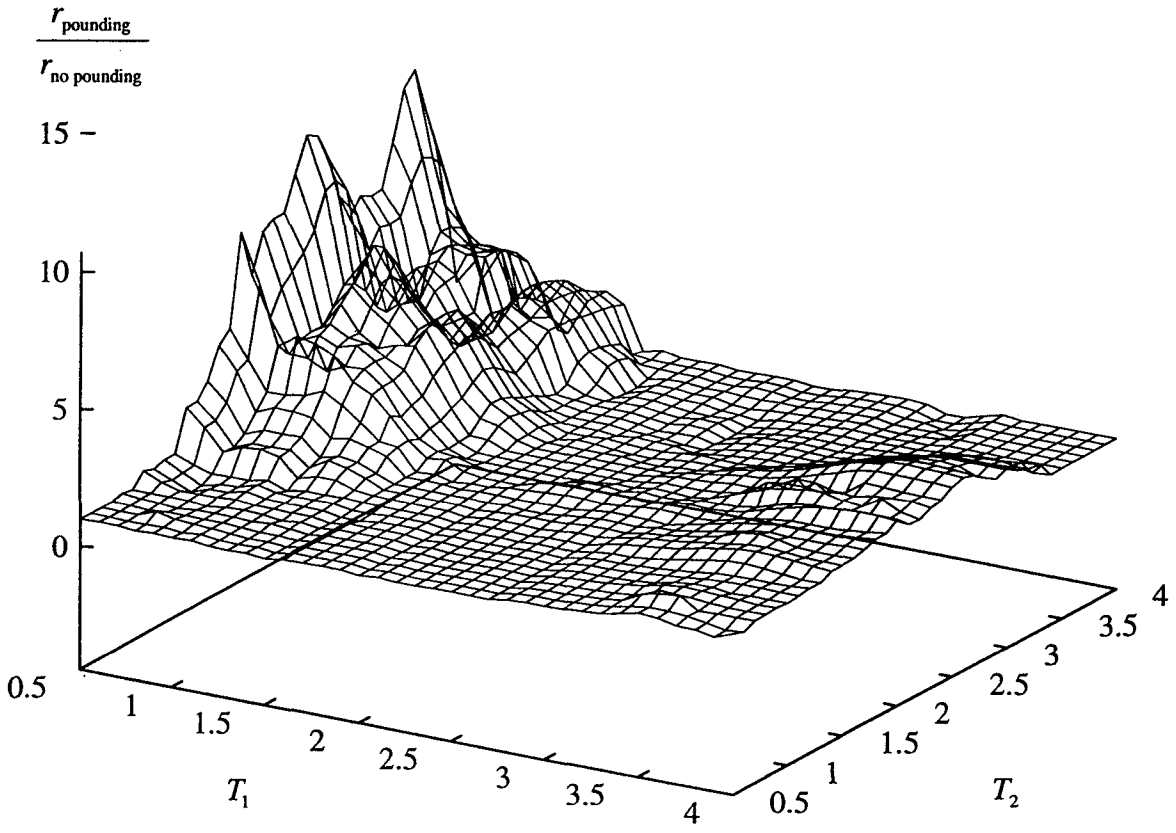

Fig. 5.7 Amplification in the structural Pseudo Energy Radius (Mexico City earthquake, g_p=0.75 g_{cr}, $m_1 = m_2$).

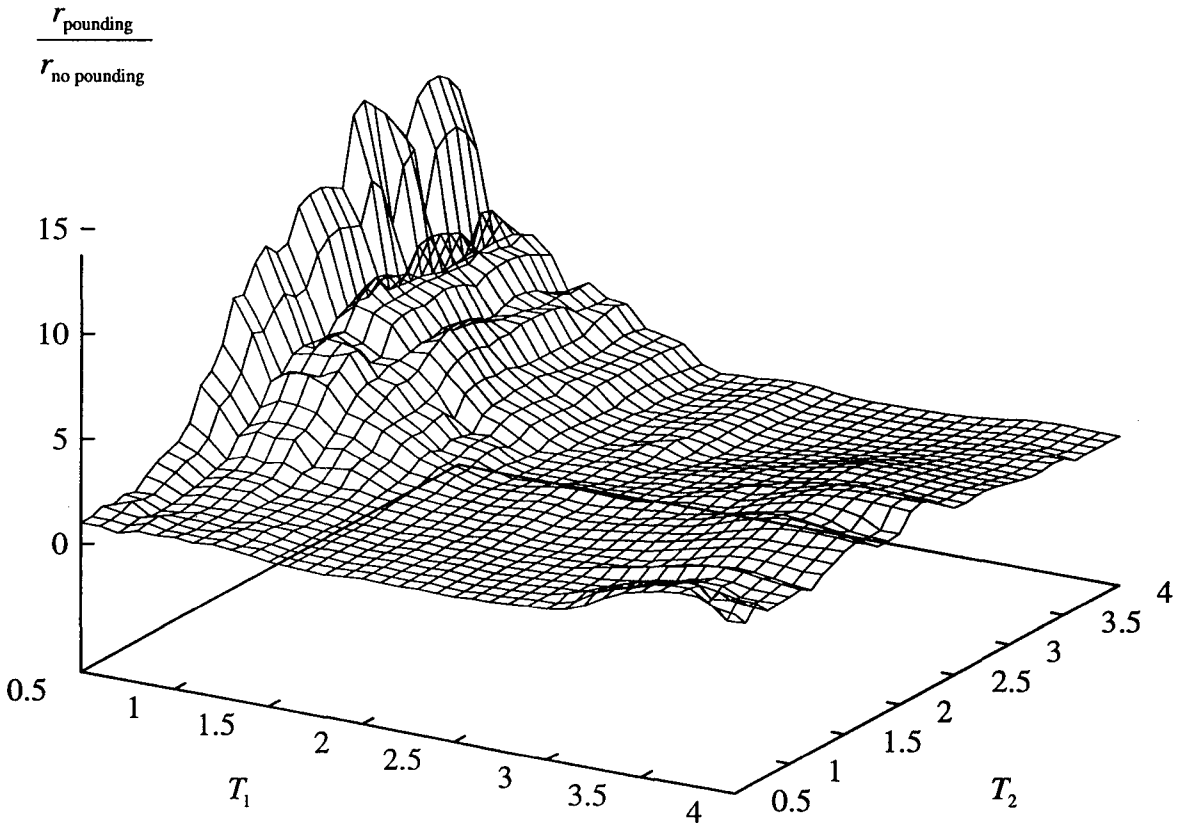

Fig. 5.8 Amplification in the structural Pseudo Energy Radius (Mexico City earthquake, g_p=0.5 g_{cr}, $m_1 = m_2$).

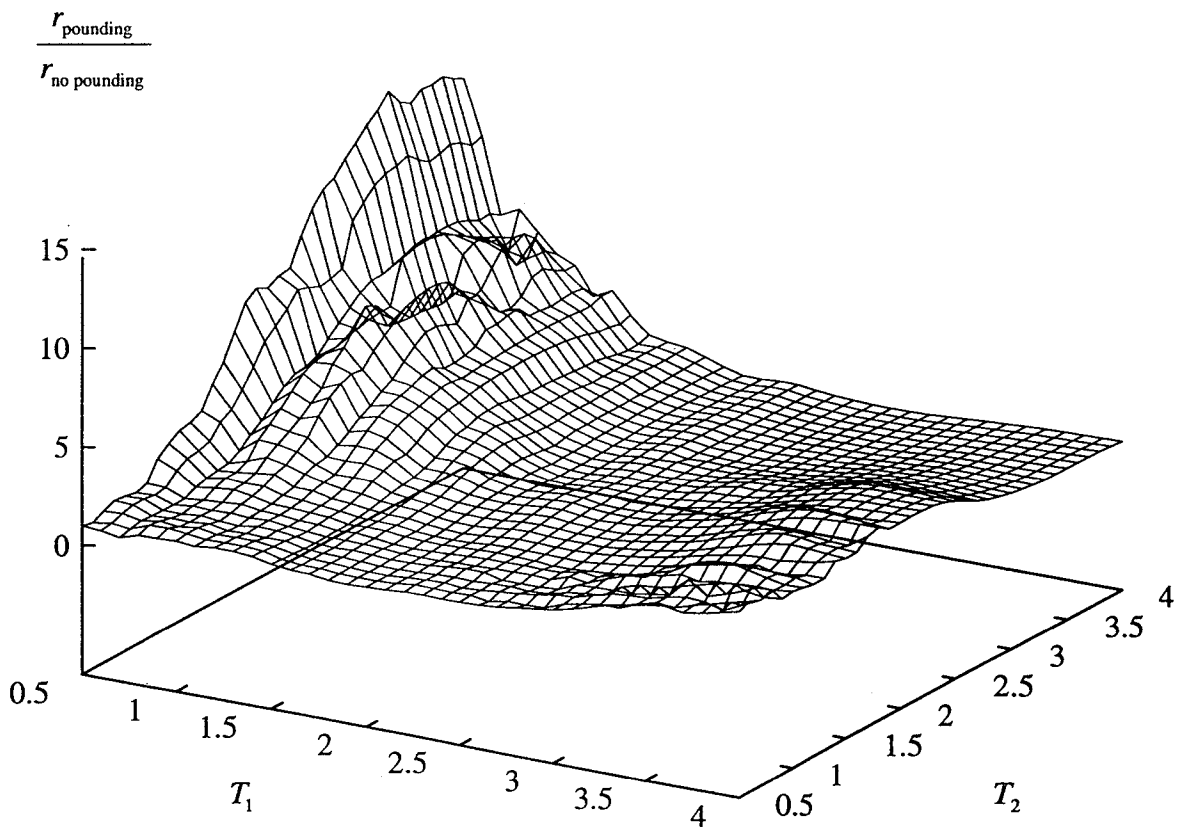

Fig. 5.9 Amplification in the structural Pseudo Energy Radius (Mexico City earthquake, g_p=0.25 g_{cr}, $m_1 = m_2$).

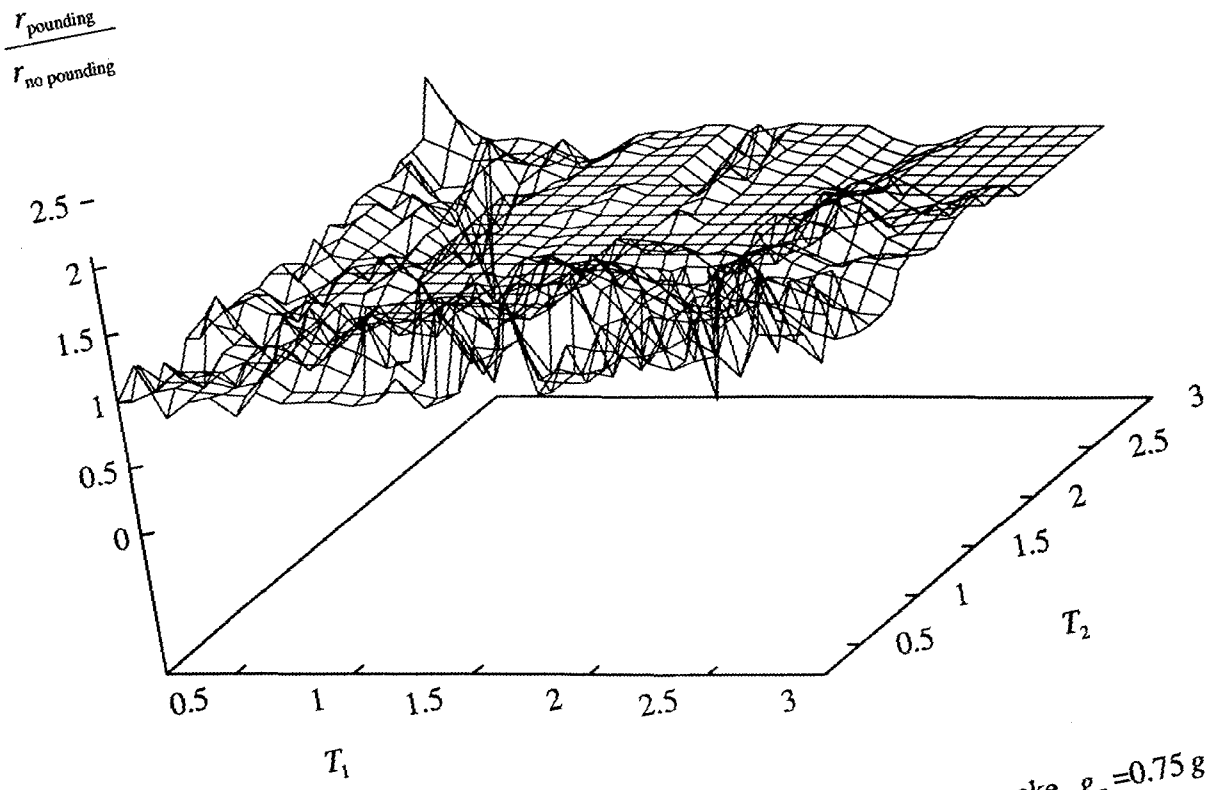

Fig. 5.10 Amplification in the structural Pseudo Energy Radius (Taft earthquake, g_p=0.75 g_{cr}, $m_1 = m_2$).

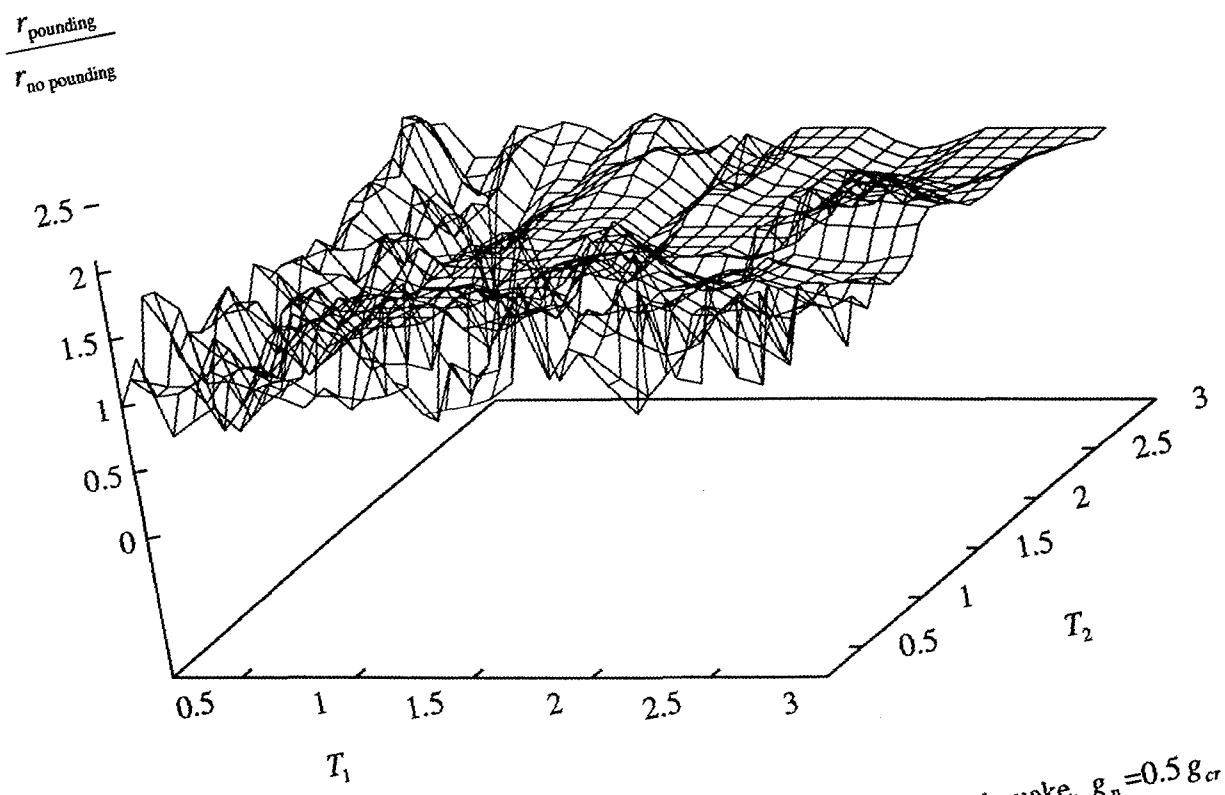

Fig. 5.11 Amplification in the structural Pseudo Energy Radius (Taft earthquake, g_p=0.5 g_{cr}, $m_1 = m_2$).

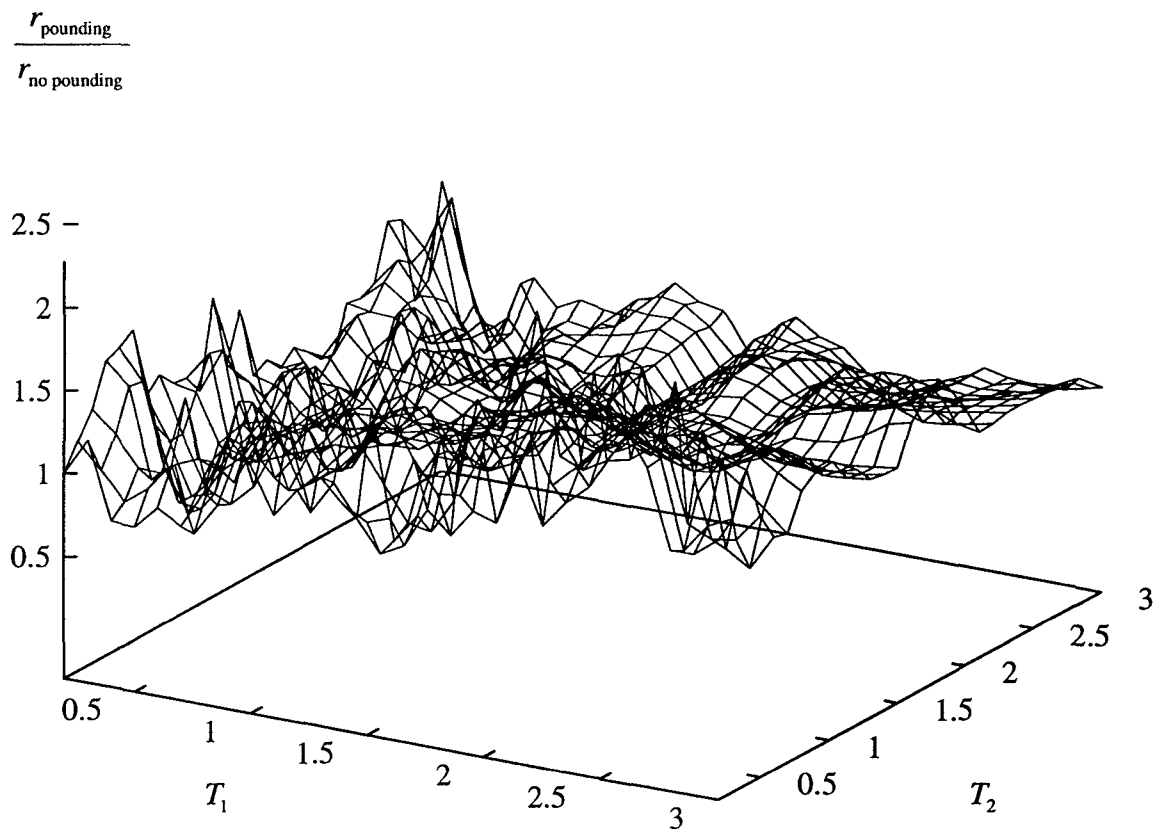

Fig. 5.12 Amplification in the structural Pseudo Energy Radius (Taft earthquake, g_p=0.25 g_{cr}, $m_1 = m_2$).

Note that for this case, due to the bandwidth of the input motion, the amplification curves do not show distinguishable trends that may be used for design guidelines. The observed response is a direct consequence of the lack of a distinguishable trend in the input motion, as opposed to the sinusoidal similarities found in the Mexico City earthquake.

5.5 Estimating Pounding Effects

As shown in the previous subsections, estimating the effects that pounding may impose in a pair of structures, separated by a gap less than critical, is a cumbersome task, that can be undertaken using a computer program. Such effects are dependent on the characteristics of the earthquake motion, the fundamental periods of the structure, damping and hysteretic characteristics, the mass of the colliding floors, the actual gap as a fraction of the critical gap, and the degree of inelastic behavior that can be expected to take place at the pounding interface. The response of the systems will be greatly influenced by the previous six sets of parameters. Although more parameters influencing the response may be identified, these six are often the crucial ones. Therefore, provided that the parameters are known, the amplification effects may be calculated using a nonlinear program with a gap element.

Using the results from computationally extensive, and time consuming analysis, the influence of the parameters can be investigated, and some general trends in the expected response of the structures can be identified. However, their use and range of applicability becomes limited to the chosen combination of values or range of values, of the parameters. Although some amplification plots, of the type shown in Figs. 5.7 to 5.12, may be generated, these plots are specific for the earthquake record used, and the observed trends may not be extrapolated for different earthquake motions. In the previous subsections, two band width characteristics of the input were considered, namely, a broad band input (Taft earthquake), and a narrow band input (Mexico City earthquake). However, these results may not be extrapolated to broad band or narrow band processes. Therefore, a simple method to estimate the effects to the structure imposed by pounding interactions is needed.

5.5.1 Single Hit Event Approach

A simple method based on a single hit event was introduced to estimate pounding effects in adjacent structures (Valles, 1995). Since the method assumes a single hit, occurs at the most unfavorable moment in time, it yields good results for gaps smaller than critical, but close to it, in which case a single hit will take place, or if subsequent hits occur, the overall maximum amplification in the response is still governed by the first hit.

The single hit event approach uses the Pseudo Energy Radius formulation presented in Section 3.8, and the critical gap computation summarized in Section 4.5. Using the concept of concentric energy levels of radius r, the response of the structure may be traced as it changes from one energy level to another. When no external load is applied, the damping in the structure will gradually decrease the energy level of the system, and drive it towards the origin of the state space representation, where the system becomes static. When an external loading is applied in the system, at any instant of time, the effect may be to increase or decrease the energy level of the structure, depending on the phase between the input motion and the response displacement. Pounding between two structures can be modeled as impulsive external loading to the buildings (see Section 3.3.1).

In this analysis, single hit case, it will be conservatively assumed that on the onset of pounding both structures are at their maximum energy level imposed by the earthquake. Therefore, from this point the trajectories described by the systems in the state space plane will be replaced by the circle describing the maximum structure energy level that the system reaches (see Fig. 5.13a). Pounding effects will be calculated based on the assumption that when the structures hit, they are traveling along the maximum energy level. At this point, the energy level of the structures will change according to the formulas for stereomechanical pounding.

Consider a pair of structures with Pseudo Energy Radius (PER) at the onset of pounding of r_1 and r_2, respectively, separated by a gap g_p larger than the sum of pseudo energy levels, and consequently, greater than the critical gap (see Fig. 5.13a). Under these conditions, no

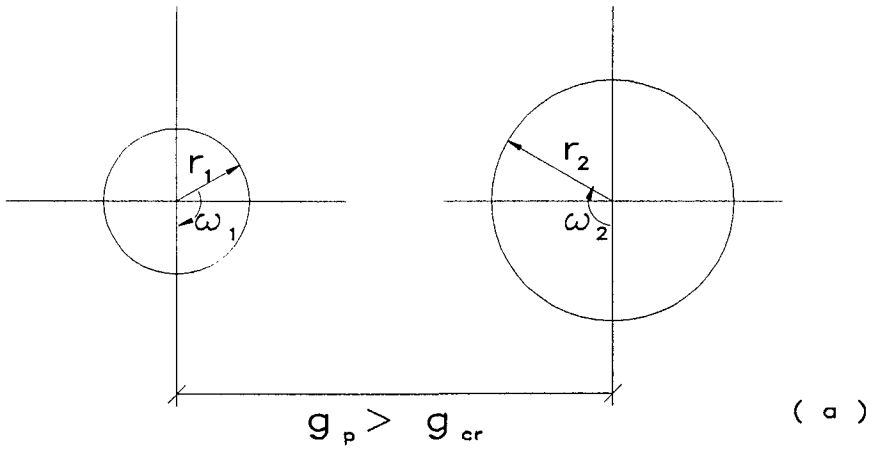

(a)

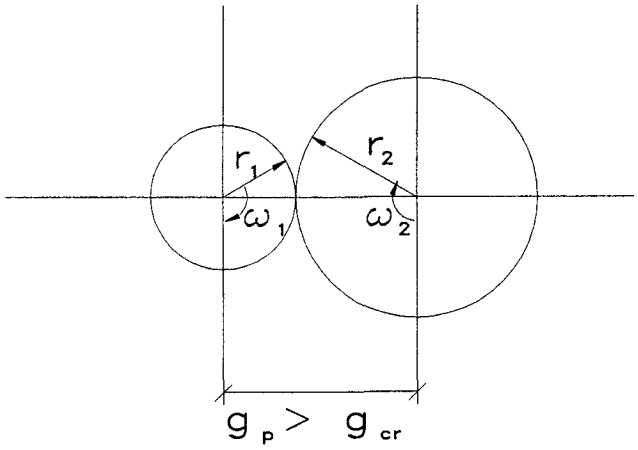

(b)

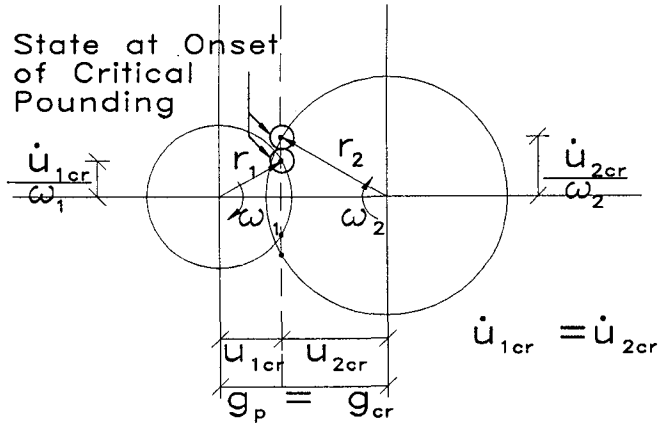

(c)

Fig. 5.13 Pseudo Energy Radius (PER) representation for various gap sizes: (a) $g_p >> g_{cr}$, (b) $g_p > g_{pr}$, (c) $g_p = g_{cr}$.

pounding interactions will take place. Note how the trajectories at the maximum energy levels never cross, implying that the distance between the two structures is always positive.

Consider now the same set of structures separated by a gap equal to the sum of the pseudo energy radius (see Fig. 5.13b):

$$g_p = r_1 + r_2 \tag{5.8}$$

that is, when the energy levels become tangent. In this case pounding will not occur since the gap is smaller than the critical gap, and only equal to it if the correlation coefficient is minus one. Even if the correlation coefficient is one, no pounding effects are observed since the velocity of both structures at the onset of pounding is zero. In view of this situation one may conclude that for pounding to occur some overlapping of the energy levels must take place.

Consider now the same set of structures separated by the critical gap (g_{cr}) (see Fig. 5.13c):

$$g_{cr} = \sqrt{r_1^2 + r_2^2 - 2r_1 r_2 \rho} \tag{5.9}$$

with correlation coefficient ρ determined from Appendix B. In this situation, the overlapping of the energy levels is the maximum possible without inducing pounding interactions. When the gap is equal to the critical gap, the structures will touch each other, however, no pounding interaction will take place because the structures will have the same velocity. This unique pounding condition will be referred to as critical pounding, since it occurs when the gap is at its critical size (critical gap). Using the present state space graphical representation, u versus $\dot{u}/\omega$, will yield two points that coincide in the horizontal axis, but have different vertical ordinates (see Fig. 5.14a). This is due to the difference in the predominant frequencies of the structures, that makes the vertical scales not comparable. If the vertical scales where not normalized by the frequency, the points at the onset of critical pounding would coincide (see Fig. 5.14b). Note that two possible critical pounding conditions are possible, one when both structures meet with positive velocity, and a second one when the structures meet with negative velocity.

It is important to note that some degree of overlapping of the energy levels is possible without inducing pounding effects. The overlapping is a function of the individual pseudo energy levels, and of the correlation coefficient ρ:

$$\rho = \frac{E\{U_1 U_2\}}{\sqrt{E\{U_1^2\} E\{U_2^2\}}} \tag{5.10}$$

a larger correlation coefficient is indicative of an in phase response of the structures, and a larger overlapping in the energy levels is possible without inducing pounding interactions. On the other hand, as the correlation coefficient approaches -1, the response tends to be 180 degrees out of phase, and little overlapping in the energy levels is possible without inducing pounding effects. Fig. 5.15 presents the maximum overlapping, without inducing effects, for different values of the correlation coefficient ρ. See Figures 4.8 and 4.9 for actual response traces of buildings subjected to Mexico City or Taft Earthquakes.

Consider now the case when the energy levels are separated by a distance g_p smaller than the critical gap. Under these conditions, pounding will be observed, since the overlapping in the energy levels is greater, and the structures will eventually meet with different velocities, and pounding will take place. If pounding is ignored, the points corresponding to the state at the onset of critical pounding will occur at the same time, however, the separation between the structure will indicate a negative number, implying that penetration has taken place (see Fig. 5.16a). Assuming that the structures move along the energy level with velocities ω_1 and ω_2, we can backtrack in time to the position where, for the gap g_p, the structures first meet (see Fig. 5.16b), and determine the state of the structures at the onset of pounding, transform the velocities of the structures using the formulas for stereomechanical impact to account for pounding effects, and determine the new, post-impact energy levels of the structures (see Fig. 5.16c). Using the ratio of post-impact to original Pseudo Energy Radius (PER), an estimate of the amplification factor due to pounding is found. Next, the procedure and formulas used to estimated the pounding effects will be presented.

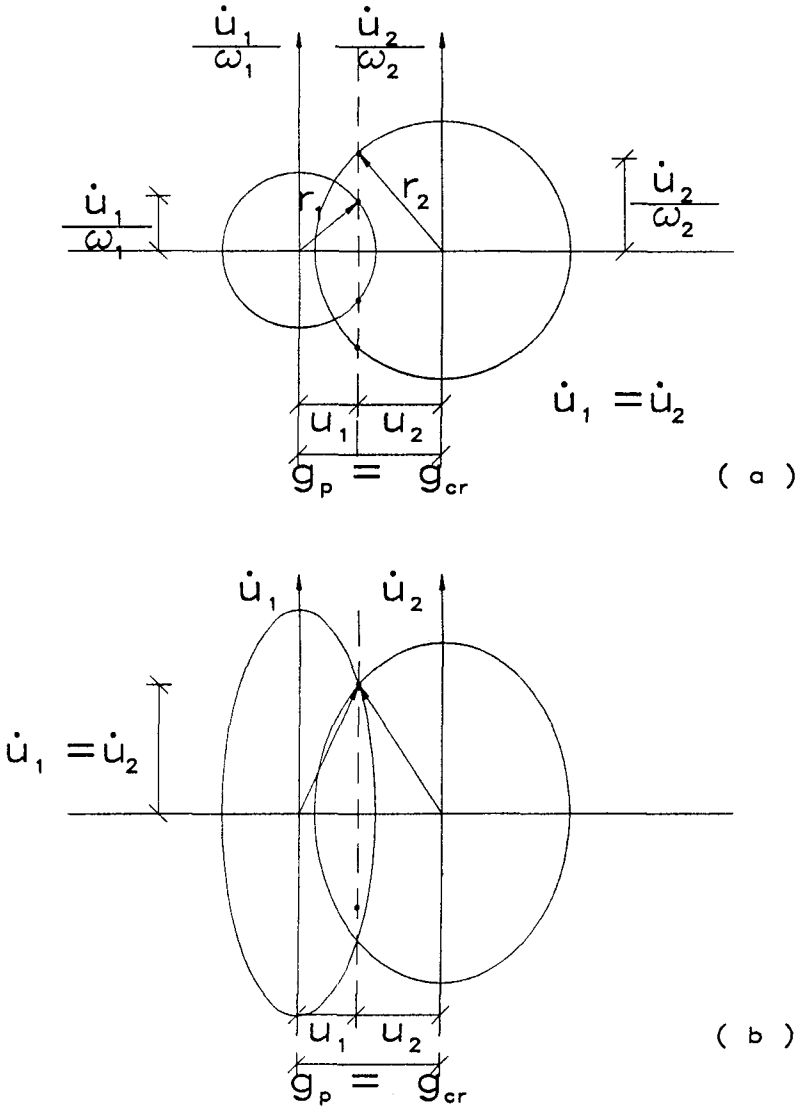

Fig. 5.14 Critical gap separation: (a) representation using the Pseudo Energy Radius (PER), (b) phase plane representation.

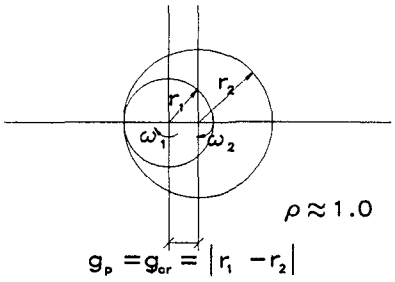

$\rho \approx 1.0$

$g_p = g_{cr} = |r_1 - r_2|$ (a)

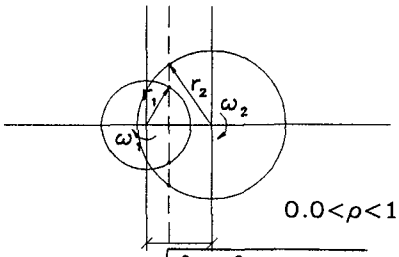

$0.0 < \rho < 1.0$

$g_p = g_{cr} = \sqrt{r_1^2 + r_2^2 - 2 r_1 r_2 \rho}$ (b)

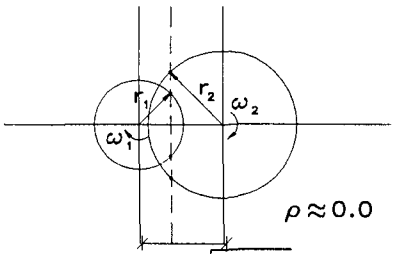

$\rho \approx 0.0$

$g_p = g_{cr} = \sqrt{r_1^2 + r_2^2}$ (c)

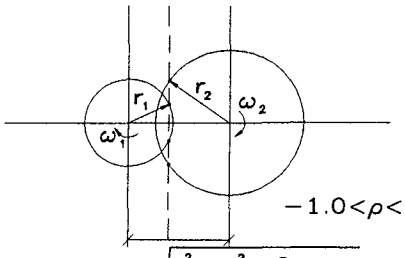

$-1.0 < \rho < 0.0$

$g_p = g_{cr} = \sqrt{r_1^2 + r_2^2 - 2 r_1 r_2 \rho}$ (d)

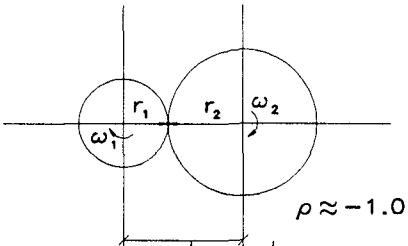

$\rho \approx -1.0$

$g_p = g_{cr} = |r_1 - r_2|$ (e)

Fig. 5.15 Maximum overlapping in the energy levels without inducing pounding effects.

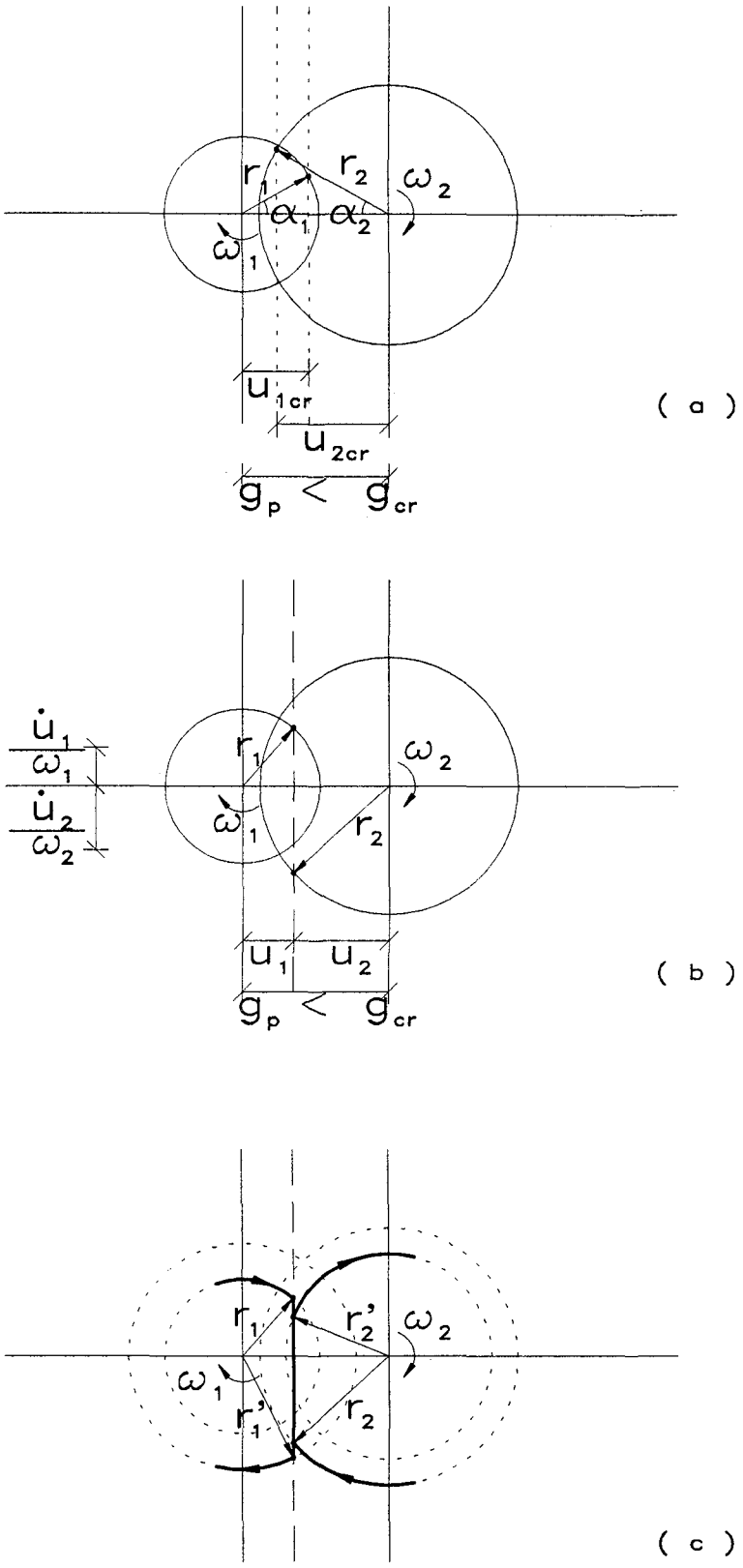

Fig. 5.16 Simplified single hit procedure to estimate pounding effects.

The simplified, one hit procedure to estimate pounding consists of three steps (see Fig. 5.16): **(1)** identify the state of the structures at the onset of critical pounding if the actual gap was the critical gap, **(2)** backtrack in time the motions to the point where they come in contact before penetration takes places, and finally, **(3)** using the state at the onset of pounding and the formulas for stereomechanical pounding, determine the new post-impact states, and post-impact energy levels.

(1) The state of the structures at the onset of critical pounding, if the gap is the critical gap, may be described by identifying the angles α_1 and α_2 shown in Fig. 5.16a. At the onset of critical pounding, displacement and velocity compatibility is to be observed. From displacement compatibility:

$$g_{cr} - u_{1cr} + u_{2cr} = 0$$

$$g_{cr} - r_i \cos\alpha_1 - r_2 \cos\alpha_2 = 0 \tag{5.11}$$

solving for $\cos\alpha_2$:

$$\cos\alpha_2 = \frac{g_{cr}}{r_2} - \frac{r_1}{r_2}\cos\alpha_1 \tag{5.12}$$

From velocity compatibility considerations:

$$\dot{u}_{1cr} = \dot{u}_{2cr}$$

$$r_1\omega_1\sqrt{1-\cos^2\alpha_1} = r_2\omega_2\sqrt{1-\cos^2\alpha_2} \tag{5.13}$$

that may be rewritten as:

$$\frac{r_1^2\omega_1^2}{r_2^2\omega_2^2}\left(1-\cos^2\alpha_1\right) = 1-\cos^2\alpha_2 \tag{5.14}$$

substituting Eq. 5.12 yields a quadratic equation on $\cos\alpha_1$ of the form:

$$\left(\frac{r_1^2}{r_2^2} - \frac{r_1^2\omega_1^2}{r_2^2\omega_2^2}\right)\cos^2\alpha_1 - 2\frac{g_{cr}r_1}{r_2^2}\cos\alpha_1 + \left(\frac{r_1^2\omega_1^2}{r_2^2\omega_2^2} - 1 + \frac{g_{cr}^2}{r_2^2}\right) = 0 \tag{5.15}$$

or:

$$c_a\cos^2\alpha_1 + c_b\cos\alpha_1 + c_c = 0 \tag{5.16}$$

with solution:

$$\cos\alpha_1 = \frac{-c_b + \sqrt{c_b^2 - 4c_a c_b}}{2c_a} \tag{5.17}$$

and α_2 is found from Eq. 5.12. Note that two possible critical pounding onsets are possible, however, the points are symmetric with respect to the zero velocity horizontal line.

(2) To backtrack in time the motion to the point where the structures come in contact, the motion is assumed to follow along the maximum energy level, with clockwise velocities ω_1 and ω_2, respectively. Consider the case when the onset of critical pounding occurs with positive velocities (Case A), the state of the structures may be expressed as:

$$u_1 = r_1 \cos(-\omega_1 t + \alpha_1) \tag{5.18a}$$

$$\dot{u}_1 = r_1 \omega_1 \sin(-\omega_1 t + \alpha_1) \tag{5.18b}$$

$$u_2 = -r_2 \cos(\omega_2 t + \alpha_2) \tag{5.18c}$$

$$\dot{u}_2 = r_2 \omega_2 \sin(\omega_2 t + \alpha_2) \tag{5.18d}$$

where t of zero corresponds to the time at the onset of critical pounding if the gap was the critical gap. The time at the onset of pounding (t_p) may be found by finding the negative root of the function:

$$f_{gp} = g_p - u_1 + u_2$$

$$f_{gp} = g_p - r_1 \cos(-\omega_1 t + \alpha_1) - r_2 \cos(\omega_2 t + \alpha_2) \tag{5.19}$$

closer to zero. Substituting the root t_p in Eqs. 5.18 yields the state of the system at the onset of pounding.

For the case when the onset of critical pounding corresponds to negative velocities (Case B), the state may be expressed as:

$$u_1 = r_1 \cos(\omega_1 t + \alpha_1) \tag{5.20a}$$

$$\dot{u}_1 = -r_1 \omega_1 \sin(\omega_1 t + \alpha_1) \tag{5.20b}$$

$$u_2 = -r_2 \cos(-\omega_2 t + \alpha_2) \tag{5.20c}$$

$$\dot{u}_2 = -r_2 \omega_2 \sin(-\omega_2 t + \alpha_2) \tag{5.20d}$$

and the time at the onset of pounding (t_p) is the negative root of the function:

$$f_{gp} = g_p - r_1 \cos(\omega_1 t + \alpha_1) - r_2 \cos(-\omega_2 t + \alpha_2) \tag{5.21}$$

closer to zero. In this case, the state at the onset of pounding is found by substituting $t = t_p$ in the Eqs. 5.20.

(3) The post impact conditions are determined using the theory of stereomechanical impact:

$$u_1' = u_1 \tag{5.22a}$$

$$\dot{u}_1' = \dot{u}_1 - (1+e)\frac{m_2(\dot{u}_1 - \dot{u}_2)}{m_1 + m_2} \tag{5.22b}$$

$$u_2' = u_2 \tag{5.22c}$$

$$\dot{u}_2' = \dot{u}_2 - (1+e)\frac{m_1(\dot{u}_1 - \dot{u}_2)}{m_1 + m_2} \tag{5.22d}$$

where e is the coefficient of restitution ranging from zero for a perfectly plastic impact, to one for a perfectly elastic impact. Note that the influence of the masses upon the contact process is taken into account. The new post-impact energy levels may be determinate from:

$$r_1' = \sqrt{u_1^2 + \left(\frac{\dot{u}_1'}{\omega_1}\right)^2} \tag{5.23a}$$

$$r_2' = \sqrt{u_2^2 + \left(\frac{\dot{u}_2'}{\omega_2}\right)^2} \tag{5.23b}$$

that describes the Pseudo Energy Radius for the single hit approximation of pounding.

Note that while one structure will increase its energy level, the energy level in the other one will decrease. Opposite tendencies may be observed depending on the point at the onset of critical pounding selected. Since both situations are possible, the maximum post-impact Pseudo Energy Radius from both analysis controls. Although a reduction in the Pseudo Energy Radius will take place in one of the structures, the no pounding maximum has been already observed, and should be used for design. That is, the minimum energy level for design when pounding occurs should be the maximum no pounding energy level.

A comparison of the predicted response amplification calculated using the simplified formulation discussed, and exact results from a time history analysis is shown in Fig. 5.17. Note how a fairly good estimate of the amplification effects was obtained with considerably less computational effort.

The present formulation uses the Pseudo Energy Radius to calculate the critical gap and estimate pounding effects, instead of the maximum displacements. This formulation considers the maximum energy level, that may have been achieved by a maximum displacement or velocity, in any direction of the earthquake being considered.

The simplified, single hit, pounding effect estimation is congruent with the probability of being exceeded contemplated in the design spectra. Note however, that for this formulation the design spectra should be provided, or transformed, to a Pseudo Energy Radius spectra, and later amplified to take into account inelastic effects. The correlation coefficient, ρ, is to be determined from the figures in Appendix B, or derived using the methodology described in the previous section.

The formulation is only intended for the cases when the assumptions are approximately correct, that is, when a single hit occurs, namely, for gaps only slightly smaller than the critical gap. For smaller gaps one may expect multiple hits at smaller energy levels before the structures reach their maximum energy levels, that may increase or decrease considerably the response. For such cases, the simplified methodology mentioned above may not be used.

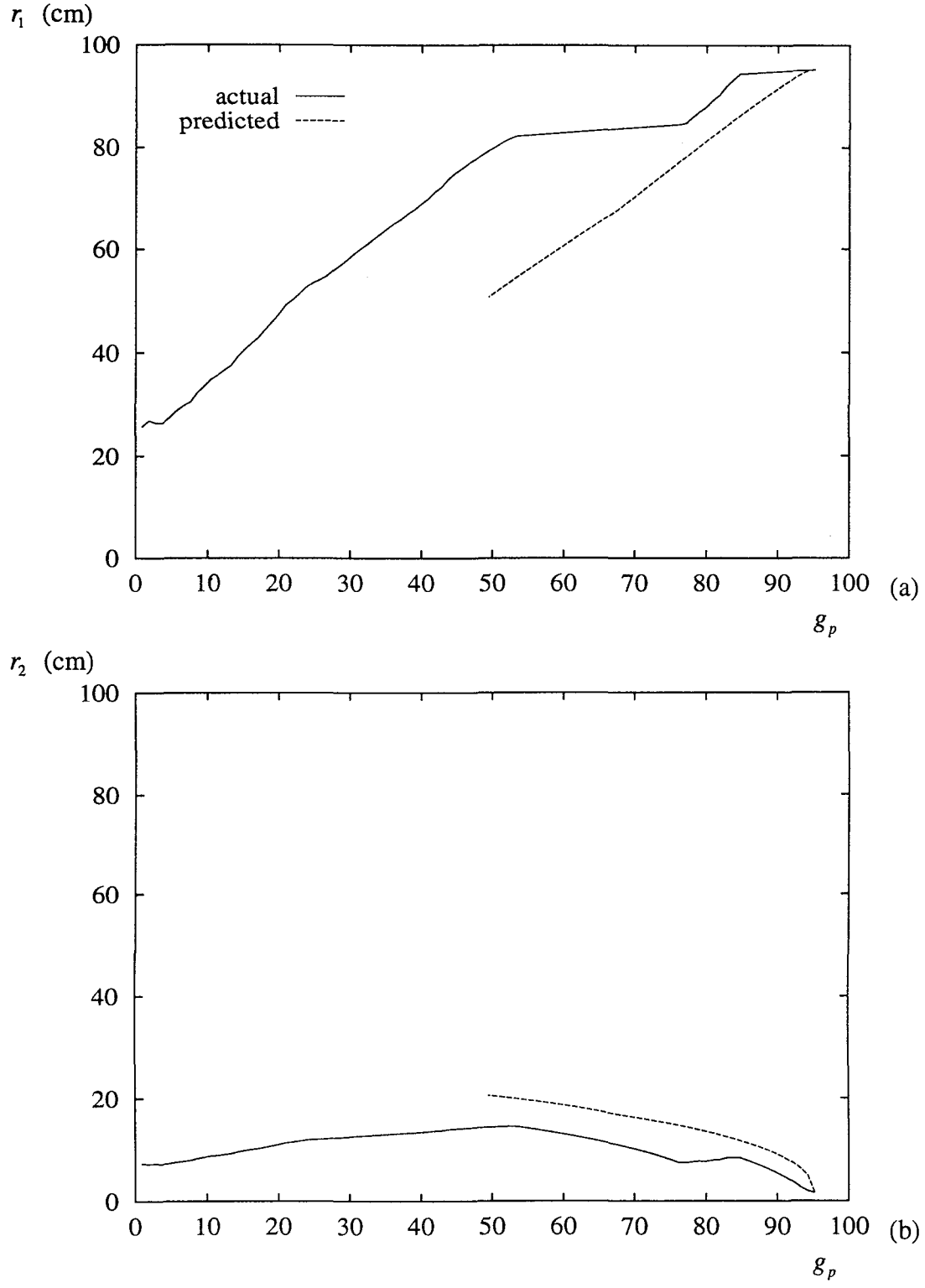

Fig. 5.17 Predicted vs. actual maximum Pseudo Energy Radius (T_1=2.0 sec, T_2=0.5 sec, Mexico City Earthquake).

5.6 Remarks and Conclusions

This section concentrates on the effects that can be expected when two structures are separated by a gap smaller than critical. Throughout the development of this work pounding is assumed to occur between floor slabs. That is, the effects of pounding along the height of a column are not investigated since that is an extremely hazardous situation, and should always be avoided.

Numerical simulations were carried out to observe some of the trends in the response when pounding occurs. Three type of input motions were considered: sinusoidal, narrow band (Mexico City earthquake), and broad band input (Taft earthquake). The analysis were carried out using the deterministic mathematical model briefly described in Section 3.5.

Results for the sinusoidal input motion indicated the clear dependence of the relative periods of the structures to fundamental period of the ground motion, and the ratio of the actual gap to the critical gap size. Large amplifications on the response of one of the structures were observed when the other is at a resonant period with the input motion.

For sinusoidal inputs, two critical periods for the input motions were identified. This periods increase the total amount of energy in the system. They correspond to the non-linear resonating periods for the pounding system. Structures in these conditions will experience large amplifications in the response, and a strategy for retrofit should be developed. The next section presents possible pounding mitigation techniques that can be implemented for such structures.

The numerical simulations for the Mexico City earthquake showed the same trends observed for the sinusoidal input. These results reflect the similarities of the input motion with a sinusoidal input. On the other hand, the numerical simulations for the Taft earthquake showed no clear trends, due to the wider frequency content of this earthquake.

To estimate pounding effects in adjacent structures, a simple method with little computational effort was developed. The method assumes that a single hit occurs between the structures,

determines the state at the onset of pounding, and using the rules of stereomechanical pounding, calculates the post-impact state of the structures.

To present the simple single hit methodology to estimate pounding effects, the concept of a Pseudo Energy Radius was introduced, where such radius as related to the maximum elastic structural (potential plus kinetic) energy. Using this concept, each structure, depending upon its period, reaches a different Pseudo Energy Radius for a given earthquake motion. Therefore, the Pseudo Energy Radius may be provided in a spectrum form.

Assuming that a single hit occurs when the structures move at the maximum Pseudo Energy Radius, the state at onset of pounding is calculated by backtracking from the onset of critical pounding, that is the onset of pounding when the actual gap equals the critical gap. Using the formulas for stereomechanical pounding the new maximum Pseudo Energy Radius for each system is calculated, considering the degree of inelasticity expected at the pounding, interface, and the relative mass of the structures.

The single hit methodology could be extended to multiple hit situations when the effects of the ground motion in the energy level of the structure is known. An approximate estimate of multiple pounding interactions could be made ignoring the effects of the input motion between successive hits. The use of this extension is discouraged until further studies reveal the effects of the input motion and its phase to the response on the energy levels, without numerical integration of the response.

The accurate or approximate analysis of the pounding effects will indicate if the amplifications expected, that are not likely to have been considered in the original designs, exceed the capacity of the structural members, or yield undesirable response characteristics. In such cases, some pounding mitigation technique must be implemented. Section 6 describes the mitigation techniques that can be implemented in this structures.

SECTION 6
POUNDING MITIGATION TECHNIQUES

6.1 Introduction

Once pounding effects in the structures has been quantified, using the mathematical models suggested in Section 3.5, or the approximate single hit methodology described in Section 5.5, structural amplifications may prove to be a serious hazard to their integrity. In these cases, the use of some type of pounding mitigation technique is necessary.

The pounding mitigation techniques may be classified in three broad groups: link elements, bumper damper elements, and supplemental energy dissipation elements. General description of how each group reduces pounding effects, without description of actual damper elements available, is included. Advantages and disadvantages inherent to each group are discussed.

All of the techniques can be modeled using the mathematical models described in Valles (1995). However, the effectiveness of bumper dampers and supplemental energy dissipating elements may be approximately evaluated using the concepts presented in Section 5.5.

6.2 Link Elements

The use of elastic links between the structures as a pounding mitigation technique was first introduced by Westermo (1989). Preliminary studies by him indicated that some reduction may be obtained, although some amplification will be observed in the stiffer structure. He indicated that in some cases the forces in the link elements could be of the same order of magnitude as the base shears. Later, numerical simulations by Filiatrault and Folz (1992), indicated that reductions are possible when the structures are linked with an energy dissipating device. However, the authors indicated that a change in the failure mechanism was observed due to the presence of the link.

Linking adjacent buildings has a number of disadvantages, including the high forces in the link, the fact that the dynamic characteristics and the design failure mechanisms are changed, and the uncertainties inherent when two structures of different characteristics must become one. Nevertheless, if those problems are solved, linking two structures will reduce the possibility of pounding interactions. If an energy dissipation device is used between the two structures, pounding will occur if the stroke of the element is not sufficient.

Linking two adjacent buildings effectively couples the motion of the two. Therefore, when linear elastic links are used, the analysis may be carried out using most of the available structural analysis software. The three mathematical formulations described in Section 3.5 include a Kelvin type link element, but other rheological models may be easily incorporated. Deterministic or probabilistic simulations can be carried out using the programs developed by Valles (1995) to assess the effectiveness of link elements as a pounding mitigation system. Results are to be compared to the no pounding and pounding solutions before retrofit.

In general, linking two adjacent buildings may not be an adequate solution if the buildings belong to different owners, since important technical and political problems may arise. In general, it will not be advisable to link buildings of completely different dynamic response characteristics, or buildings built under different design considerations, time periods, or intended for different use.

Although the analysis of linked structures may be simple, the design of the retrofitted system may become a cumbersome task. Unless all the inherent differences in the structures can be adequately handled, the use of other pounding mitigation techniques is suggested.

6.3 Bumper Damper Elements

The use of bumper dampers is considered as a possible pounding mitigation technique. Under bumper damper elements, all energy dissipation devices available that can be placed between the

structures, but connected only to one of them, are considered. Bumper dampers are therefore energy dissipation links that are activated when the gap is closed.

The response of two structures with bumper damper elements may be studied using the deterministic or hybrid models described in Section 3.5, or any of the available non-linear structural analysis software that includes a gap element. If the program developed is used, the parameters of the Impact Kelvin model may be modified to simulate the response of the damper element.

When the bumper damper element is such that an Impact Kelvin element is not a good representation of it, a different rheological model for the element may readily be incorporated in the program. Otherwise, a macroscopic approach to modeling the effects of the damper using a coefficient of restitution may be adopted. Such equivalent coefficient of restitution may vary depending on the relative velocity of the floors at the onset of pounding, however, a variable coefficient of restitution can easily be incorporated in the formulation.

The presence of the bumper damper element will reduce the impulsive forces transmitted from one structure to the other. If the element provides only stiffness the impulse loads will still be reduced since the impacting bodies will encounter a spring element reducing the kinetic energies of the structure before the stroke of the element is reached, at which point the full pounding of the masses will take place, but the impacting velocities will be smaller (see Fig. 6.1). Note that although the velocities at the onset of pounding are smaller, the linear spring will increase the velocities after pounding, but the high frequency accelerations observed will be reduced.

As the stiffness in the linear spring increases the reduction in the pounding velocities will be greater, however, a very stiff element will induce pounding like effects when activated. A gradual transition, as shown in Fig. 6.2 will reduce the high frequency accelerations since a smoother transition is selected. Note that if a linear spring is used no energy dissipation will take place and the overall macroscopic results will not change.

A simple physical analogy may be used to clarify the effect of a linear bumper spring between two colliding structures. Consider a ball rolling with velocity v_0 on a smooth surface that hits a wall elastically (see Fig. 6.3a), after hitting the wall the ball will move away from the wall with the same velocity. However, since the velocity drastically changed in a short period of time, the ball will be subjected to a large acceleration. Consider now that a distance s before the wall a frictionless ramp begins (see Fig. 6.3b). In this case part of the kinetic energy will be converted to potential, reducing the velocities at the onset of impact and consequently reducing the acceleration level at the instant of impact.

Continuing further with the analogy, if a gradually increasing slope is provided (see Fig. 6.3c), no actual impact will occur and a smooth transition from the approaching velocity (v_o) to the separating velocity ($-v_0$) will take place, and the acceleration will be smaller. Therefore, although the macroscopic effects are not affected by the ramp, the acceleration experienced by the ball will be reduced due to the presence of the ramp. Note that for small ramps, small s, or high initial velocities, the transition in velocity will take place in a small fraction of time, inducing therefore large accelerations. For high initial velocities, or small ramp sizes (stroke of spring), the presence of the ramp will have no effect on the acceleration levels.

Therefore, for pounding problems, a linear spring element acting as a bumper damper is not an adequate solution. Some energy dissipation must be provided in the bumper element to dissipate the energy transfer, reducing pounding effects in the structures. Using the physical analogy presented earlier, the addition of energy dissipation may be interpreted as friction, while a non-linear spring may be thought of as different ramps for loading and unloading.

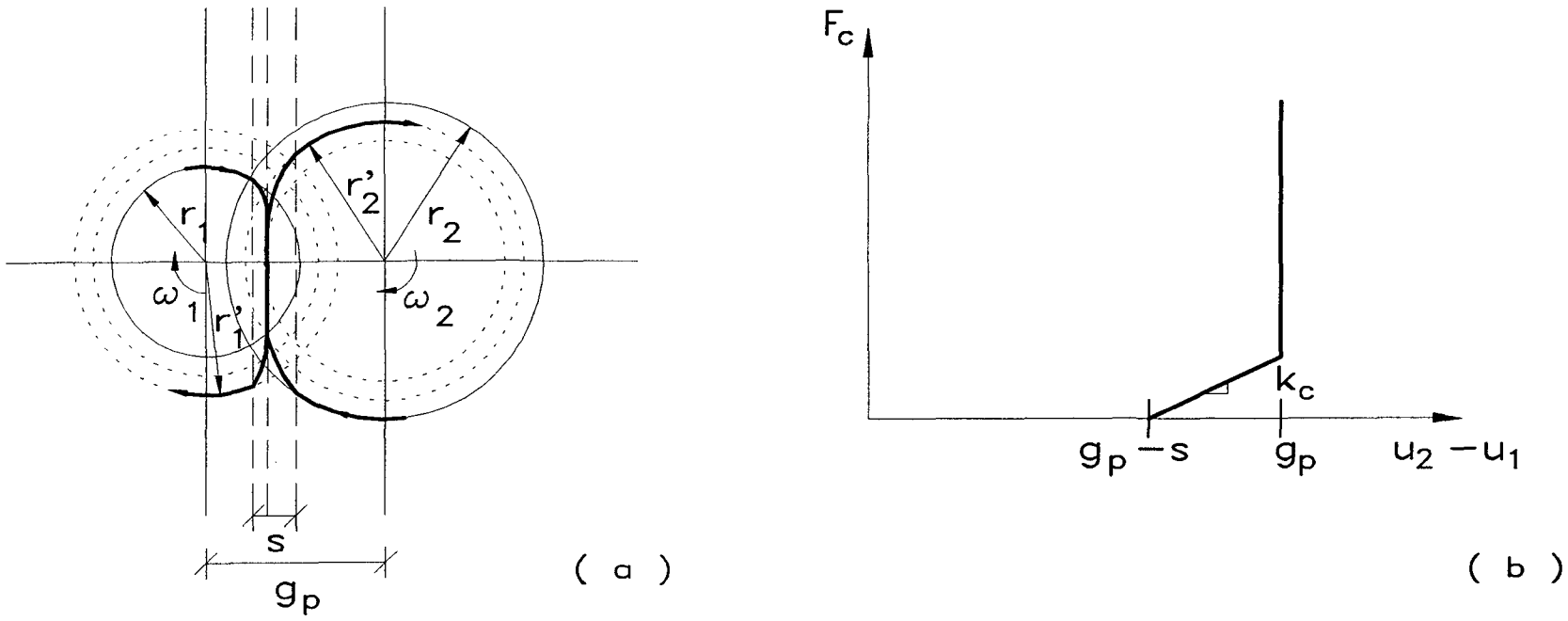

Fig. 6.1 Effects of a linear spring bumper damper element.

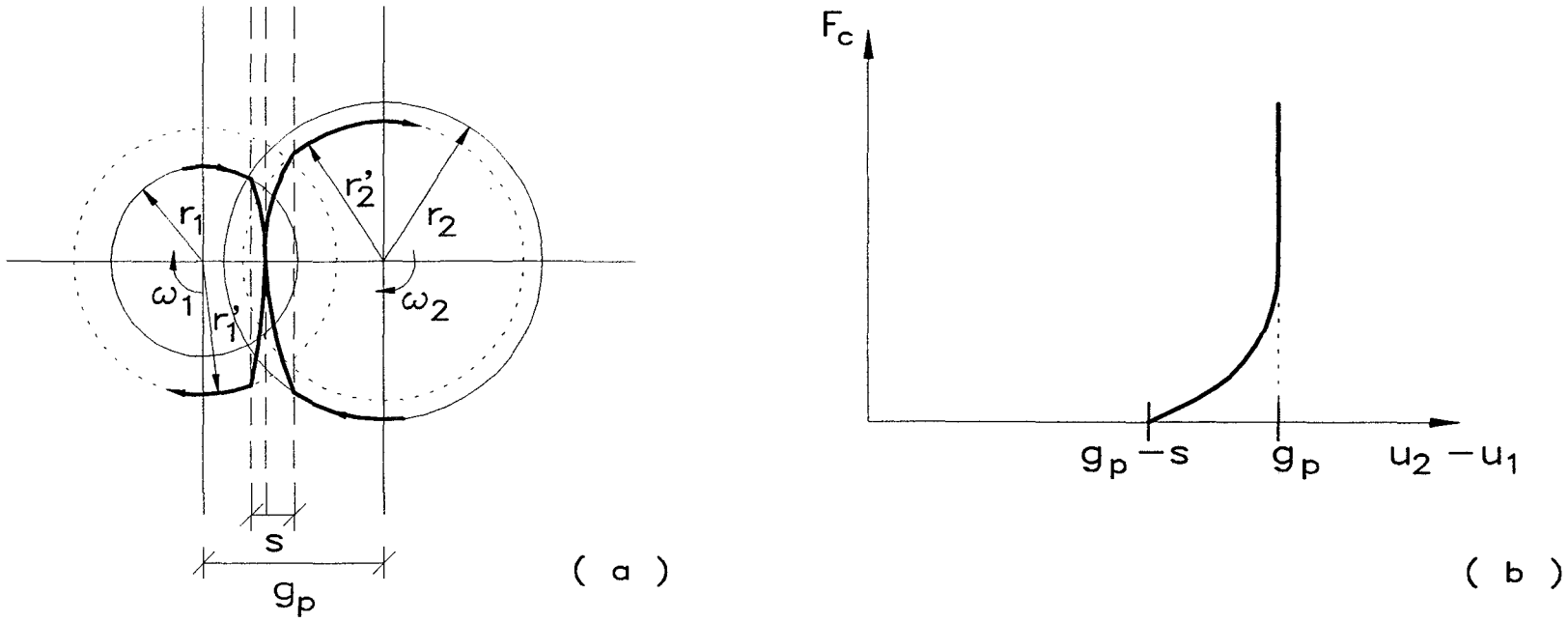

Fig. 6.2 Effects of a strain hardening elastic spring bumper damper element.

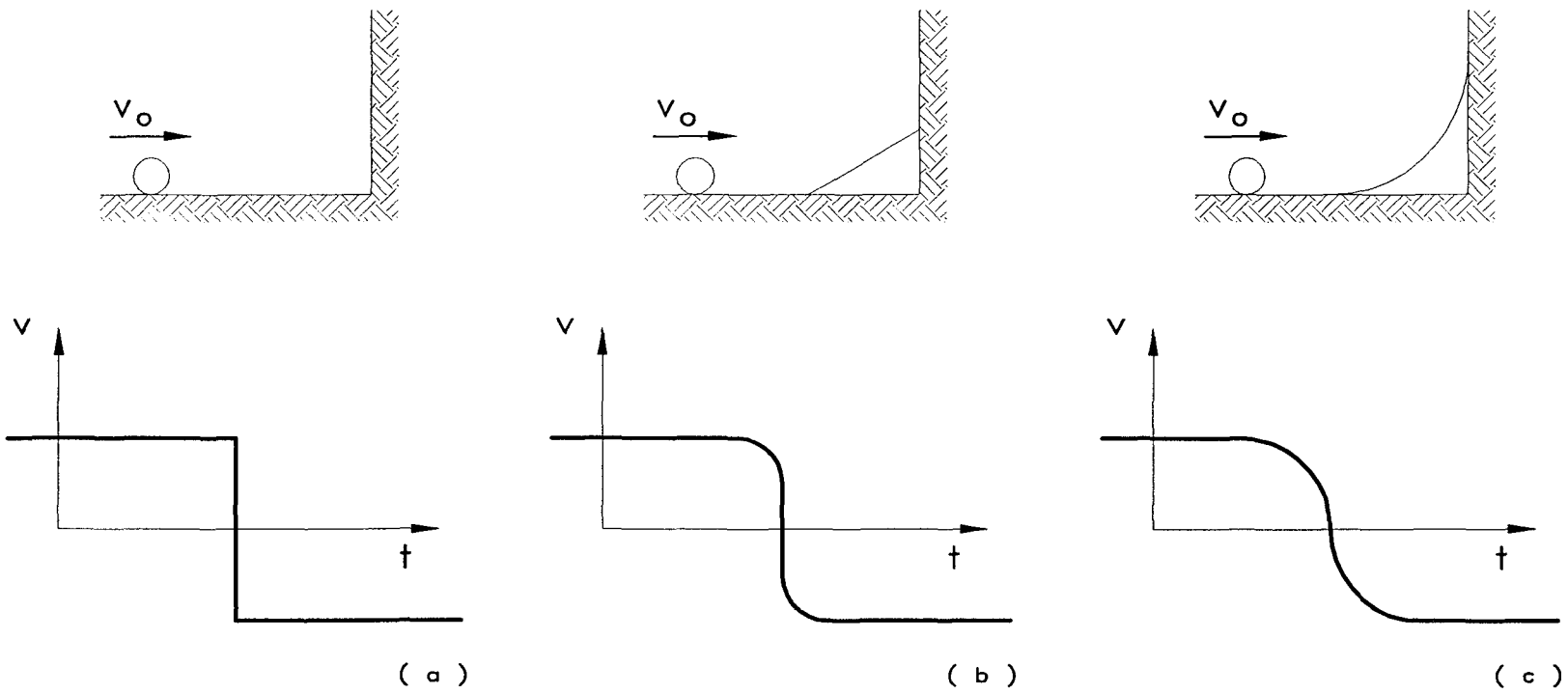

Fig. 6.3 Ball analogy for the response of an elastic bumper damper element.

When viscous damping devices are used as bumper damper elements, some elastic stiffness should also be provided to return the damper to the original position. Fluid viscous dampers can provide such characteristics when specially designed (Reinhorn et al., 1995). This will prevent the gap from becoming larger after each impact, and that the full damper stroke is still usable for subsequent impacts. Note that non-linear elements will show an increase in the gap size after each hit, gradually reducing the available stroke of the damper. Unless a single hit is expected to take place, the bumper damper element should be capable of sustaining repeated impacts without significant degradation.

Using the simplified, single hit, methodology for evaluating pounding effects, the effectiveness of bumper damper elements may be estimated. A bumper damper will provide some energy dissipation to the transfer energy, that can be related to a smaller coefficient of restitution, resulting in smaller amplifications in the response of the structures. Smaller coefficients of restitution will be linked to greater energy dissipation, and smaller amplification effects in the colliding structures (see Fig. 6.4). Fig. 6.5 shows the amplifications in velocity of structure one for different velocity ratios and coefficients of restitution, when the colliding bodies have the same mass. Note that a smaller coefficient of restitution will produce smaller amplifications in the post-impact velocities.

It should be noted that, in general, the coefficient of restitution for bumper damper elements is a function of the relative velocities at the onset of pounding:

$$e = e\left(\dot{u}_1 - \dot{u}_2\right) \tag{6.1}$$

the restitution coefficient dependence on the relative impacting velocities may be found from test data, from a drop test at different impact velocities (drop heights), or from numerical simulations if a rheological model for the element is available. The simple Kelvin or Impact Kelvin models show no variation of the equivalent coefficient of restitution with the impact velocity (see Section 3.3).

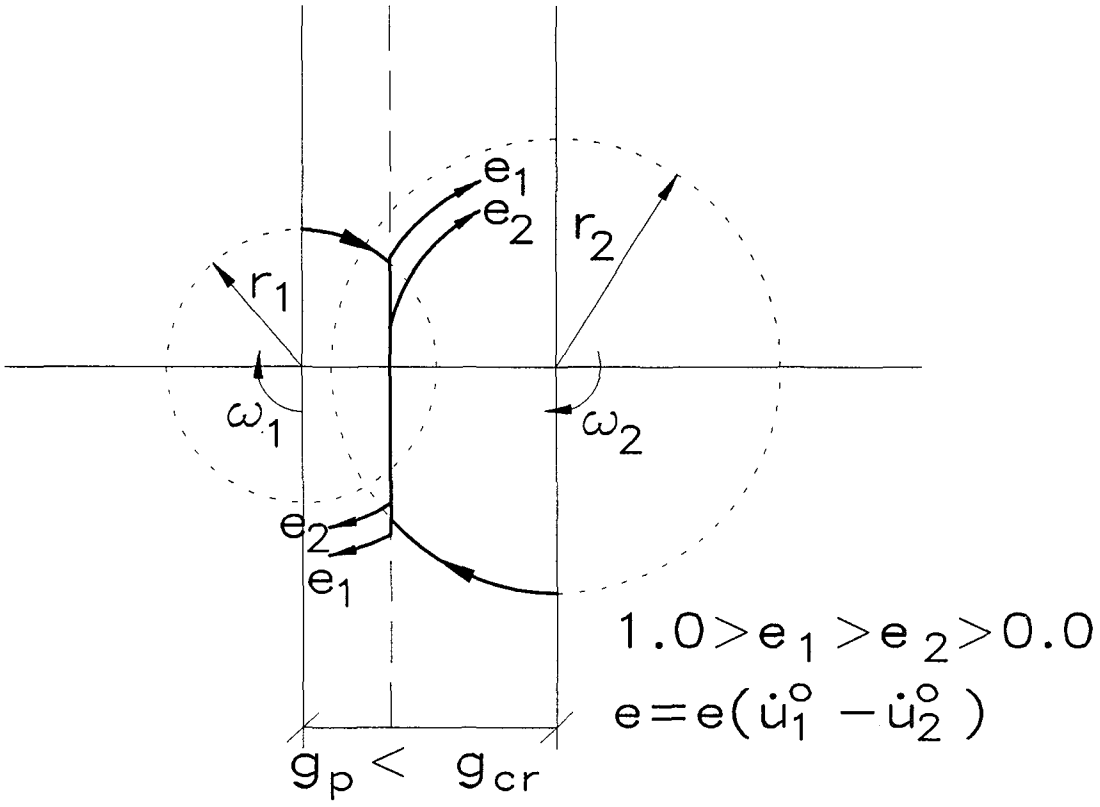

Fig. 6.4 Influence of the coefficient of restitution in post-impact conditions using the Pseudo Energy Radius representation.

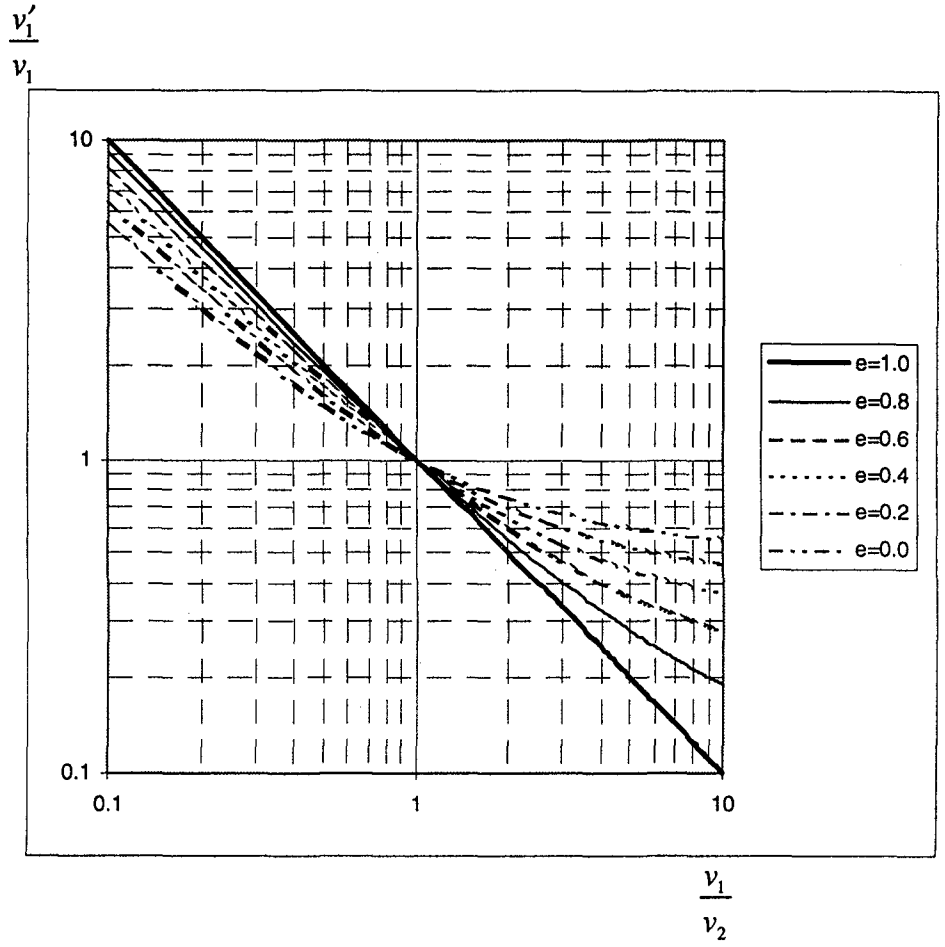

Fig. 6.5 Velocity amplification variation for different velocity ratios at pounding onset ($m_1 = m_2$).

6.4 Supplemental Energy Dissipation

The use of supplemental energy dissipation devices in the buildings has been proposed by Kasai et al. (1993b) as an effective method to reduce the probability of pounding. Using supplemental energy dissipation devices reduces the maximum lateral deflections of the building. The reduced lateral deflections will imply a smaller critical gap:

$$g_{cr} = \sqrt{u_1^2 + u_2^2 - 2u_1 u_2 \rho} \tag{6.2}$$

Furthermore, if supplemental damping is provided in both structures, they will tend to respond in phase, which implies a higher correlation coefficient, and leads to a further reduction of the critical gap size.

Using the phase plane representation introduced in Section 5.5 to estimate pounding effects, it is possible to calculate the amount of supplemental damping required to avoid pounding. Consider the case where only one of the structures is to be retrofitted using supplemental damping (see Fig. 6.6). Under these conditions, r_1 and r_2 will denote the pseudo energy radius of the structures before retrofit. Using Eq. 6.2 yields a critical gap g_{cr} greater then the actual gap g_p:

$$g_p < g_{cr} = \sqrt{r_1^2 + r_2^2 - 2r_1 r_2 \rho} \tag{6.3}$$

Supplemental damping is provided so that the actual gap equals the new retrofitted critical gap $(g_{cr})_r$:

$$g_p = (g_{cr})_r = \sqrt{r_1^2 + r_{2r}^2 - 2r_1 r_{2r} \rho} \tag{6.4}$$

Solving for the retrofitted pseudo energy radius of structure 2 (r_{2r}) yields a quadratic equation with solution:

$$r_{2r} = r_1 \rho - \sqrt{r_1^2 \rho^2 + g_p^2 - r_1^2} \tag{6.5}$$

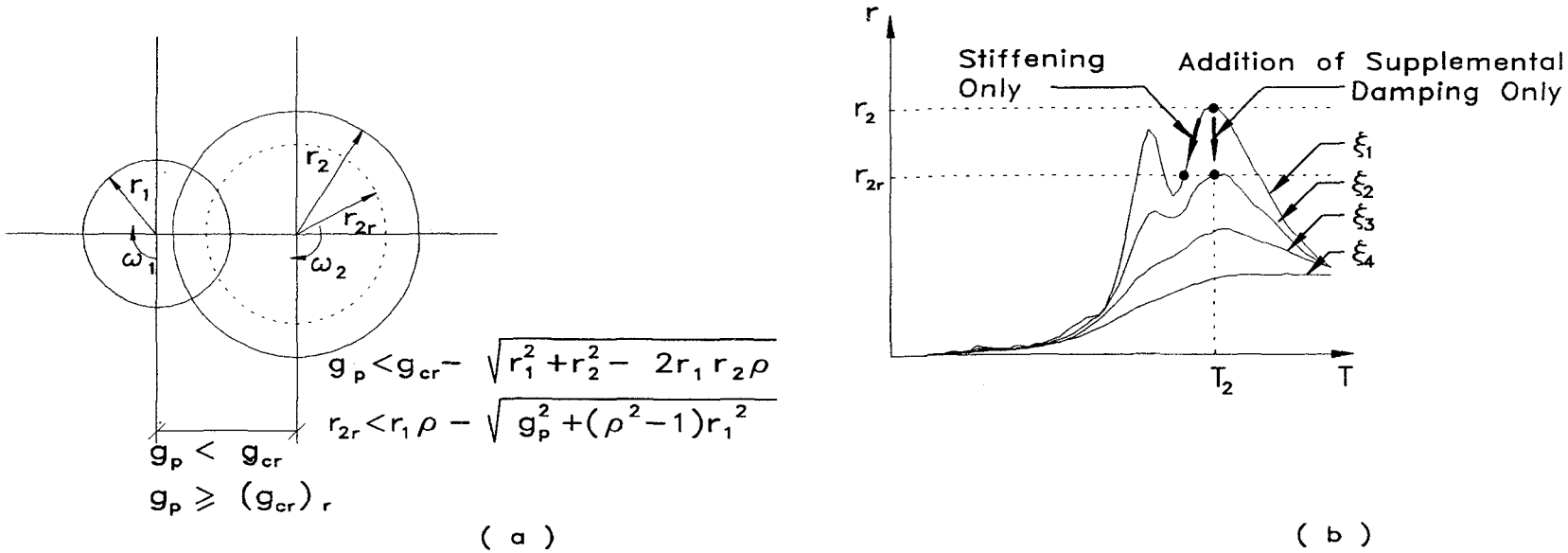

Fig. 6.6 Minimum supplemental damping to avoid pounding interactions.

The new retrofitted pseudo energy radius for structure 2 may be achieved by combining stiffening and adding supplemental damping (see Fig. 6.6). Reducing the maximum displacements by stiffening only is also a possible pounding prevention solution. Note that the value of the correlation coefficient should be recalculated to reflect the new response of the retrofitted structure. Using supplemental damping only will lead to bigger correlation coefficients, therefore a conservative estimate may be carried out using the original value before retrofit. However, when the solution involves some stiffening also, the new correlation coefficient may become smaller, leading to unconservative estimates in the maximum allowable pseudo energy radius to avoid impact.

So far, the use of supplemental energy dissipating elements has been discussed for pounding prevention, however, pounding mitigation is also efficiently achieved with such devices. Although the reduction in the maximum energy levels provided may not be sufficient to avoid pounding, the amplification effects in the structures will be smaller. The reduced pounding effects may be estimated using the simplified single hit approach, as described in Section 5.5.

The use of supplemental energy dissipation in structures is an efficient method to reduce or eliminate pounding effects in adjacent structures, and at the same time improve the performance of the buildings. Link elements may reduce the response of one structure and eliminate pounding, but will increase the response of the adjacent one and modify the demand distribution in both buildings. Bumper damper elements are designed to reduce transfer energy during pounding interactions. On the other hand, supplemental energy dissipation devices will benefit the response of the structures and eliminate or reduce pounding effects.

Energy dissipation elements used for pounding mitigation may be combined with bumper elements to further decrease pounding effects in structures. A combined application will provide supplemental energy dissipation in the structures and at the contact interface. Preliminary estimates on the effectiveness of the combined implementation may be carried out using the simplified single hit methodology introduced in Section 5.5, with the considerations for studying bumper damper elements described in Section 6.3.

Refined non-linear time history analysis for the supplemental energy dissipation, or the combined solution, can be carried out using the deterministic or hybrid models described in Section 3.5, or other non-linear time history analysis program with the capability of modeling two structures, and have the formulation for gap elements. Preliminary sizing of the dampers may be carried out using the simple analysis described earlier.

6.5 Remarks and Conclusions

Section 6 studied the possible pounding mitigation techniques available to retrofit buildings prone to large amplifications due to impact interactions. Pounding mitigation techniques may be classified in three groups: link elements, bumper damper elements, and supplemental energy dissipation elements.

Link elements are used to connect two adjacent buildings at one or multiple locations throughout the height. The use of link elements eliminates the possibility of pounding, however, the response of the buildings may be considerably modified. Some level of retrofit in the structures may have to be carried out to accommodate for the new force distributions. Furthermore, linking two structures of different structural systems or floor plans may promote torsional response. The analysis of this type of retrofit may be calculated using standard linear analysis software, if both structures, and the link, are expected to respond linearly. The use of link elements as a pounding mitigation technique may encounter serious problems when connecting buildings belonging to different owners, different dynamic properties, different structural system, built using different design criteria, etc.

Bumper damper elements are used between two adjacent structures to dissipate part of the transfer energy during pounding interactions. Bumper damper elements must be dissipative to reduce pounding accelerations and forces during contact. This type of element may be modeled using a rheological model, or through the use of a coefficient of restitution. The effectiveness of this system may be approximately evaluated, for gaps close to critical, using the simplified single hit methodology for pounding effects estimation presented in Section 5.

The use of supplemental energy dissipating devices in the structures provides an effective pounding prevention or mitigation technique. The supplemental damping in the structure may be tuned to reduce the structures response and mitigate or eliminate pounding interactions. By reducing the Pseudo Energy Radius, concept introduced in Section 5, the critical gap is also reduced. Furthermore, if both structures are damped, they will tend to respond in phase with the input motion, leading to a higher correlation coefficient, and a further reduction in the critical gap.

Tuning the amount of supplemental damping can yield a critical gap greater than the actual gap, or reduce the maximum Pseudo Energy Radius and pounding effects. The effectiveness of this system can approximately be estimated using the simplified single hit methodology presented in Section 5.

The use of supplemental energy dissipating devices is the preferred pounding mitigation technique since the structural response of the buildings is improved and pounding effects are reduced. When this solution is used in conjunction with bumper damper elements, further reductions in the pounding effects may be achieved.

The response of structures with link elements may be investigated using the three mathematical models described by Valles (1995). The implementation of bumper damper elements or supplemental energy dissipating elements may be studied using the deterministic and hybrid models.

The results and observations from the critical gap computation (Section 4), estimation of pounding effects (Section 5), pounding mitigation techniques (Section 6), and pounding analysis methods (Section 3) are summarized in Section 7, to provide general concepts and methodologies for the evaluation of pounding problems.

SECTION 7
DESIGN RECOMMENDATIONS

7.1 Introduction

The present section summarizes the relevant observations and design procedures presented in previous sections. The results and methodologies are intended to be used as design guidelines to evaluate, prevent or mitigate pounding effects. For further details on the derivations, assumptions or methodologies, refer to Sections 3 through 6.

This section briefly summarizes the approaches to pounding prevention adopted in building codes in different countries of the world. Then, the suggested methodology, extended from the Double Difference Combination rule introduced by Kasai, is presented. The simplified single hit methodology for estimating pounding effects is outlined. Later, the pounding mitigation techniques available are presented, and some simple guidelines for their evaluations are discussed. Finally, the section ends with a brief description of the mathematical models introduced by Valles (1995) for a detailed pounding analysis.

7.2 Survey of Building Code Requirements for Building Separations

A group of building codes were reviewed to investigate the criteria adopted in different seismic regions, with different design practices, to avoid undesirable pounding interactions between adjacent structures. The survey indicated that providing for a sufficient clear distance between buildings is the commonly adopted strategy to avoid pounding. During the survey only one building code, from Venezuela, was found to allow for some degree of pounding, if the forces exerted do not threaten the integrity of the structures. However, no guidelines for estimating such effects were given.

A review of building code recommendations identified four general expressions used to specify a minimum separation between two adjacent buildings:

$$g_p \geq \text{factor (sum of displacements)} \tag{7.1}$$

$$g_p \geq \text{coefficient (height)} \tag{7.2}$$

$$g_p \geq \text{fixed distance} \tag{7.3}$$

$$g_p \geq \text{SRSS (displacement)} \tag{7.4}$$

The first formula corresponds to a factored Absolute Sum of the maximum displacements of the structures. The second formula relates the minimum gap with a maximum interstory drift ratio. In the Mexico City building code Eqs. 7.2 and 7.1 are combined to take into account rotations at the foundation. Eq. 7.3 is generally specified as a minimum for construction purposes. Finally, the last formula takes into account that the maximum displacements in the structures will not occur at the same instant in time.

Of all the formulas adopted by different building codes, Eq. 7.4 provides the best estimate when the gap is compared to results from actual time history simulations. However, the SRSS rule yields very conservative results when the period of the structures are similar.

In the following paragraphs a summary of the mayor findings in the research project are presented to provide engineers with improved tools to estimate pounding effects in structures, with simple calculation procedures to estimate the critical gap in linear and bilinear structures, with an approximate and simple methodology to estimate pounding effects, with guidelines for the preliminary design of pounding mitigation devices, and mathematical models for the analysis of such devices.

7.3 Building Separation to Avoid Pounding

Providing a sufficient gap to avoid pounding interactions between structures is the most commonly accepted strategy in current building codes. The theory and assumptions to derive the procedure described herein is presented in Section 4, and Appendices A and B.

Critical gap (g_{cr}) is the minimum gap necessary between two structures to avoid pounding interaction. The critical gap is calculated according to the following procedures (see Fig. 7.1):

1.- From the elastic displacement design spectra and the fundamental periods of the structures (T_1 and T_2), calculate the maximum elastic displacements of the structures (u_{1e} and u_{2e}).

2.- Classify the input motion as a broad or narrow band process, and determine its predominant period, depending on the soil conditions at the building site.

3.- Using the amplification charts for bilinear oscillators provided in the Appendix B, determine the amplification coefficients a_{b1} and a_{b2} to calculate the inelastic displacements of the structures:

$$u_1 = a_{b1} u_{1e} \tag{7.5}$$

$$u_2 = a_{b2} u_{2e} \tag{7.6}$$

For linear systems use:

$$a_{b1} = a_{b2} = 1.0 \tag{7.7}$$

4.- Using the correlation coefficient charts for linear or bilinear systems provided in the Appendix B, determine the correlation coefficient ρ.

5.- Calculate the critical gap size according to:

$$g_{cr} = \sqrt{u_1^2 + u_2^2 - 2u_1 u_2 \rho} \tag{7.8}$$

If the structures have different damping ratios, different maximum ductility, or different force reduction factors, using the lowest value of the correlation coefficient is suggested for a conservative estimate of the critical gap. Otherwise, a detailed analysis of the correlation coefficient should be carried out.

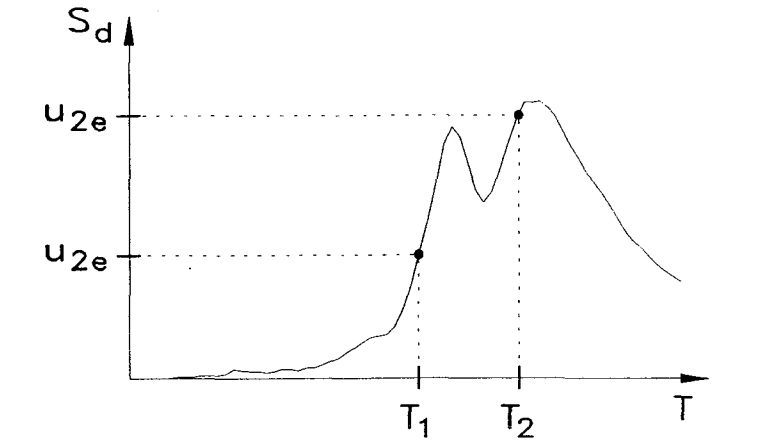

(a)

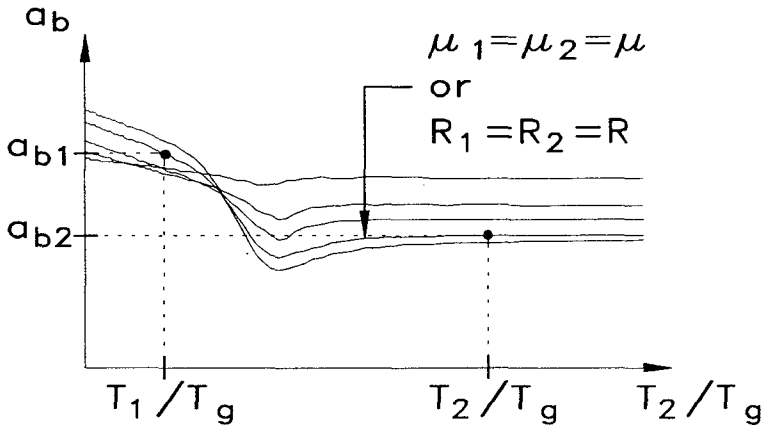

(b)

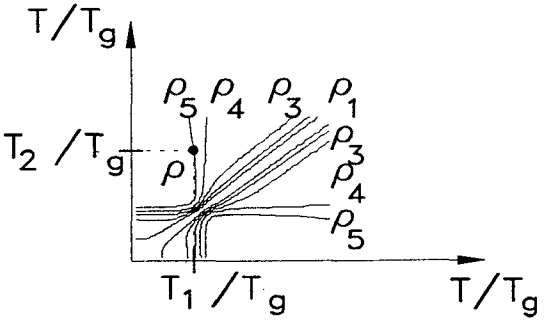

(c)

$$u_1 = a_{b1}\, u_{1e}$$

$$u_2 = a_{b2}\, u_{2e}$$

$$g_p = \sqrt{u_1^2 + u_2^2 - 2u_1u_2\rho}$$

(d)

Fig. 7.1 Methodology for critical gap computation.

The correlation coefficient plots are presented using contour lines. Although linear interpolation may be carried out, it is advisable to round down the final value for the correlation coefficient, to avoid underestimating the critical gap, and take into account uncertainties inherent in the actual fundamental periods of structural vibration, and input motion.

Using the methodology outlined earlier may lead to small values for the critical gap between structures of similar structural periods. In such cases a minimum gap should be observed for construction considerations.

Soil structure interaction is to be included for structures on soft soil conditions. In this case, the critical gap will include the contribution from rotation at the foundation (see Fig. 7.2):

$$\begin{aligned} g_{cr}^2 = {} & u_1^2 + h^2\theta_1^2 + u_2^2 + h^2\theta_2^2 + 2hu_1\theta_1\rho_{u1\theta1} + 2hu_2\theta_2\rho_{u2\theta2} \\ & -2u_1u_2\rho_{u1u2} - 2hu_1\theta_2\rho_{u1\theta2} - 2hu_2\theta_1\rho_{u2\theta1} - 2h^2\theta_1\theta_2\rho_{\theta1\theta2} \end{aligned} \tag{7.9}$$

where u_1 and u_2 are the maximum structural deflections, θ_1 and θ_2 are the maximum foundation rotations, $\rho_{u1\theta_1}$ is the correlation coefficient between the displacement u_1 and the rotation θ_1, etc.

7.4 Approximate Evaluation of Pounding Effects

The evaluation of pounding effects is of importance when studying adjacent existing buildings separated by a gap less than critical. A detailed description of the theory and assumptions of the methodology presented herein is included in Section 5.

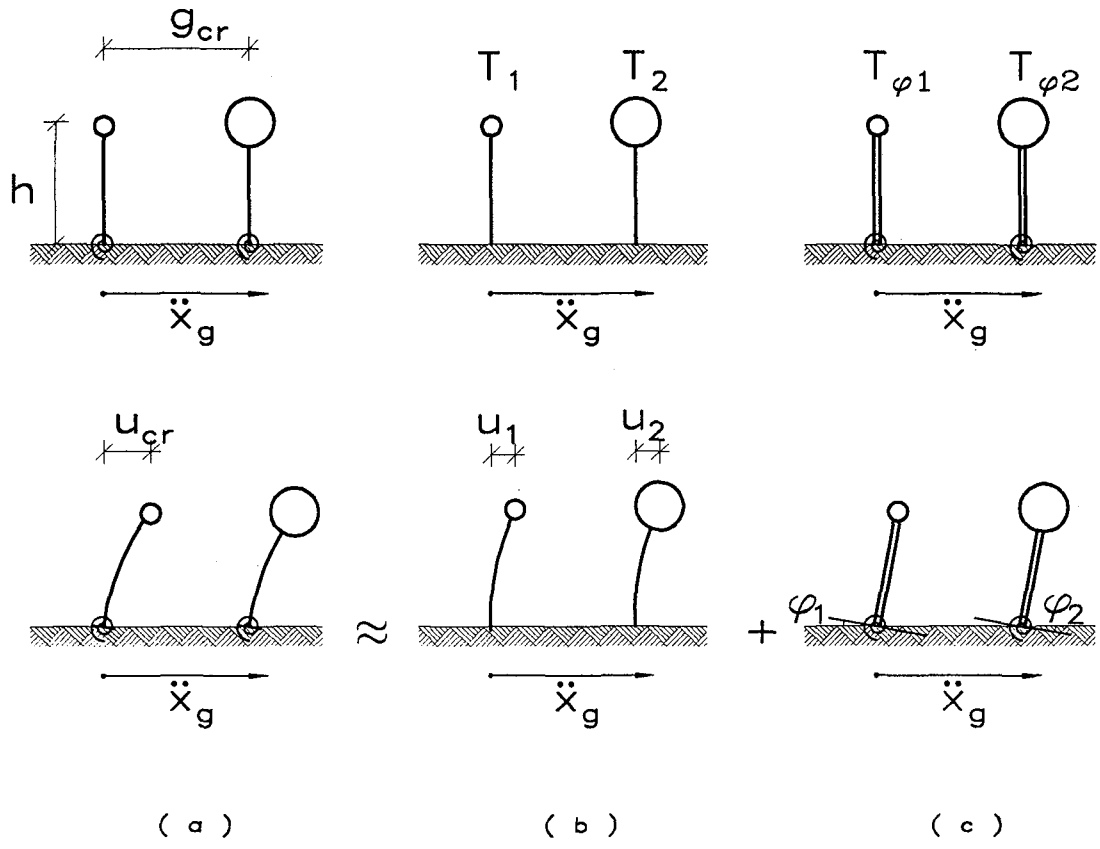

Fig. 7.2 Adjacent structures with flexible foundations.

Pounding effects in adjacent structures may be estimated using the simplified single hit assumption, only when the actual gap is only slightly smaller than the critical gap. The critical gap (g_{cr}) is to be calculated according to the methodology presented in Section 7.3.

The pounding effects in adjacent structures are determined according to the following procedures (see Fig. 7.3):

1.- Determine the critical gap from Section 7.3.

2.- Using a pseudo energy radius design spectrum determine the corresponding pseudo energy radius for each structure (r_1 and r_2):

$$r = \sqrt{\frac{2E_e}{m\omega^2}}$$

Where E_e is then maximum sum of the kinetic and potential energies, m is the mass of the structure, and ω its fundamental frequency.

3.- Calculate the angles at the onset of critical pounding assuming the actual gap is equal to the critical gap:

$$\cos\alpha_1 = \frac{-c_b + \sqrt{c_b^2 - 4C_aC_b}}{2C_a} \tag{7.10}$$

$$\cos\alpha_2 = \frac{g_{cr}}{r_2} - \frac{r_1}{r_2}\cos\alpha_1 \tag{7.11}$$

where:

$$C_a = \frac{r_1^2}{r_2^2}\left(1 - \frac{\omega_1^2}{\omega_2^2}\right) \tag{7.12a}$$

$$C_b = -2\frac{g_{cr}r_1}{r_2^2} \tag{7.12b}$$

$$C_c = \frac{r_1^2\omega_1^2}{r_2^2\omega_2^2} - 1 + \frac{g_{cr}^2}{r_2^2} \tag{7.12c}$$

4.- Find the time at which actual pounding occurs for the two possible impact conditions:

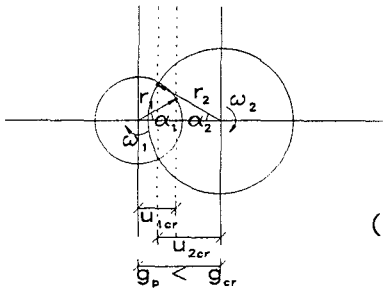

(a)

$$t = t_{cr} = 0$$

$$\cos\alpha_1 = \frac{-c_b + \sqrt{c_b^2 - 4c_a c_c}}{2c_a}$$

$$\cos\alpha_2 = \frac{g_{cr}}{r_2} - \frac{r_1}{r_2}\cos\alpha_1$$

where:

$$c_a = \frac{r_1^2}{r_2^2}\left(1 - \frac{\omega_1^2}{\omega_2^2}\right)$$

$$c_b = -2\frac{g_{cr} r_1}{r_2^3}$$

$$c_c = \frac{r_1^2\omega_1^2}{r_2^2\omega_2^2} - 1 + \frac{g_{cr}^2}{r_2^2}$$

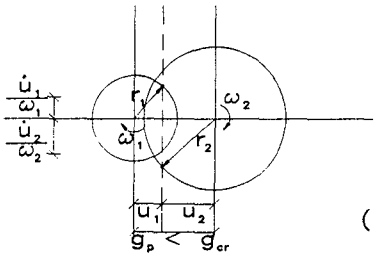

(b)

$$t = t_p < t_{cr}$$

Case A:

$$g_p - r_1\cos(-\omega_1 t_{pa} + \alpha_1) - r_2\cos(\omega_2 t_{pa} + \alpha_2) = 0$$

$$u_1 = r_1\cos(-\omega_1 t_{pa} + \alpha_1)$$

$$\dot{u}_1 = r_1\omega_1\sin(-\omega_1 t_{pa} + \alpha_1)$$

$$u_2 = -r_2\cos(\omega_2 t_{pa} + \alpha_2)$$

$$\dot{u}_2 = r_2\omega_2\sin(\omega_2 t_{pa} + \alpha_2)$$

Case B:

$$g_p - r_1\cos(\omega_1 t_{pa} + \alpha_1) - r_2\cos(-\omega_2 t_{pa} + \alpha_2) = 0$$

$$u_1 = r_1\cos(\omega_1 t_{pa} + \alpha_1)$$

$$\dot{u}_1 = -r_1\omega_1\sin(\omega_1 t_{pa} + \alpha_1)$$

$$u_2 = -r_2\cos(-\omega_2 t_{pa} + \alpha_2)$$

$$\dot{u}_2 = -r_2\omega_2\sin(-\omega_2 t_{pa} + \alpha_2)$$

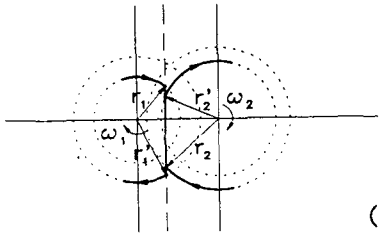

(c)

$$t = t_p^+$$

$$\dot{u}_1' = \dot{u}_1 - (1+e)\frac{m_2(\dot{u}_1 - \dot{u}_2)}{m_1 + m_2}$$

$$\dot{u}_2' = \dot{u}_2 + (1+e)\frac{m_1(\dot{u}_1 - \dot{u}_2)}{m_1 + m_2}$$

$$r_1' = \sqrt{u_1^2 + \left(\frac{\dot{u}_1'}{\omega_1}\right)^2}$$

$$r_2' = \sqrt{u_2^2 + \left(\frac{\dot{u}_2'}{\omega_2}\right)^2}$$

Fig. 7.3 Single hit methodology for pounding effects estimation.

a) Case A (positive velocities at critical pounding onset):

Calculate the negative root (t_{pa}) closest to zero for the function:.

$$f_{gp}(t_{pa}) = g_p - r_1 \cos(-\omega_1 t_{pa} + \alpha_1) - r_2 \cos(\omega_2 t_{pa} + \alpha_2) = 0 \tag{7.13}$$

b) Case B (negative velocities at critical pounding onset):

Calculate the negative root (t_{pb}) closest to zero for the function:

$$f_{gp}(t_{pb}) = g_p - r_1 \cos(\omega_1 t_{pb} + \alpha_1) - r_2 \cos(-\omega_2 t_{pb} + \alpha_2) = 0 \tag{7.14}$$

5.- Determine the state for each structure at the onset of pounding according to:

a) Case A:

$$u_1 = r_1 \cos(-\omega_1 t_{pa} + \alpha_1) \tag{7.15a}$$

$$\dot{u}_1 = r_1 \omega_1 \sin(-\omega_1 t_{pa} + \alpha_1) \tag{7.15b}$$

$$u_2 = -r_2 \cos(\omega_2 t_{pa} + \alpha_2) \tag{7.15c}$$

$$\dot{u}_2 = r_2 \omega_2 \sin(\omega_2 t_{pa} + \alpha_2) \tag{7.15d}$$

b) Case B:

$$u_1 = r_1 \cos(-\omega_1 t_{pb} + \alpha_1) \tag{7.16a}$$

$$\dot{u}_1 = -r_1 \omega_1 \sin(\omega_1 t_{pb} + \alpha_1) \tag{7.16b}$$

$$u_2 = -r_2 \cos(-\omega_2 t_{pb} + \alpha_2) \tag{7.16c}$$

$$\dot{u}_2 = -r_2 \omega_2 \sin(-\omega_2 t_{pb} + \alpha_2) \tag{7.16d}$$

6.- Using the formulas for stereomechanical pounding, calculate for each case the post-impact velocities:

$$\dot{u}_1' = \dot{u}_1 - (1+e)\frac{m_2(\dot{u}_1 - \dot{u}_2)}{m_1 + m_2} \tag{7.17a}$$

$$\dot{u}_2' = \dot{u}_2 + (1+e)\frac{m_1(\dot{u}_1 - \dot{u}_2)}{m_1 + m_2} \tag{7.17b}$$

where m_1 and m_2 are the masses of the colliding floors in structure 1 and 2 respectively, and e is the coefficient of restitution to account for energy dissipation

during impact. A coefficient of restitution of one is used for elastic impacts, while a value of zero is used for perfectly plastic impacts.

7.- Calculate, for each case, the post-impact pseudo energy radius according to:

$$r_1' = \sqrt{u_1^2 + \left(\frac{\dot{u}_1'}{\omega_1}\right)^2} \tag{7.18a}$$

$$r_2' = \sqrt{u_2^2 + \left(\frac{\dot{u}_2'}{\omega_2}\right)^2} \tag{7.18b}$$

8.- Determine the maximum post-impact Pseudo Energy Radius for each structure. The ratio of the maximum post-impact energy radius to the original yields an estimate of the amplifications in the maximum structural displacements and velocities.

The methodology outlined uses a simplified approach to the problem, and yields adequate results only for a range of critical gap sizes. A number of simulations when compared to the approximate predictions indicate that the simplified method provides a reasonably good estimates for the range:

$$0.8 g_{cr} < g_p < g_{cr} \tag{7.19}$$

Below this range the predictions are not as reliable.

When the structures are subjected to a narrow band input motion, the following recommendations should be observed:

- When one of the structures has a period close to resonance, severe amplifications will take place in the adjacent structure. This situation should be avoided by reducing the response of the resonating structure.
- When the input motion coincide with the critical periods described in Section 5.2:

$$T_{cr1} \approx 2\pi\sqrt{\frac{m_1}{k_1 + k_2}} \tag{7.20a}$$

$$T_{cr2} \approx 2\pi\sqrt{\frac{m_1 + m_2}{k_1 + k_2}} \tag{7.20b}$$

the amplification factors may be larger than the results from the simplified single hit analysis due to build-up the response from successive pounding interactions from a

resonant non-linear condition. In this situation, perform a second hit analysis by marching forward in time and determine the effects of a new impact.

7.5 Pounding Mitigation Techniques

Pounding effects may impose severe structural demands to the impacting structures. In some cases the level of forces exerted may be larger than the available capacity in the structures. Some type of pounding mitigation techniques will be of interest if these conditions arise.

A number of pounding mitigation devices have been proposed, and can be broadly classified in three groups: link elements, bumper damper elements, and supplemental energy dissipating elements.

Link elements are used to connect two buildings to eliminate pounding interaction. This method effectively eliminates pounding by combining two structural systems into one. However, high forces are often transmitted through the link when structures of different dynamic properties are connected. Forces in the link have been found, for extreme cases, to be on the order of magnitude of the structural base shears. The addition of the link elements have the important disadvantage that the design forces in the structure are completely altered, and will often lead to column and beam strengthening to resist the new system of forces. Furthermore, important difficulties may be encountered when two structures, belonging to different owners, built with different materials, with different design criteria, under different force levels, are connected to respond as one.

Retrofit solutions using link elements should be analyzed using a linear or non-linear structural analysis programs, depending on the expected link and structural response characteristics, to determinate the change in the global response characteristics, as well as the local stress concentrations at the vicinity of the link connection.

Bumper damper elements consists of link elements that are activated when a gap is closed. Such elements should be dissipative to reduce the energy transfer during pounding and reduce high frequency acceleration pulses. This type of pounding mitigation technique may be analyzed incorporating its rheological model into a non-linear analysis program, or considering only the macroscopic effects using a coefficient of restitution approach.

Preliminary estimates on the effectiveness of bumper damper elements may be obtained using the simplified single hit methodology described in Section 7.4 (see Fig. 7.4). In this case, a bumper damper element will provide a smaller value for the coefficient of restitution e, leading to smaller amplifications of the Pseudo Energy Radius. The coefficient of restitution for the bumper damper elements may vary depending on the relative approaching velocity at pounding onset.

Supplemental energy dissipation devices have been proposed as a third possible pounding mitigation technique. Using this solution, the response of one or both of the structures is modified to reduce their maximum lateral deflections. Depending on the level of additional damping supplied, this solution may be used to prevent pounding from occurring, or to reduce pounding effects.

When supplemental energy dissipation is provided as a pounding prevention measure, the retrofitted new maximum displacements (or Pseudo Energy Radius) must yield a critical gap smaller than the actual gap g_p. When only one structure is retrofitted, the maximum retrofitted Pseudo Energy Radius (displacement) may be calculated from:

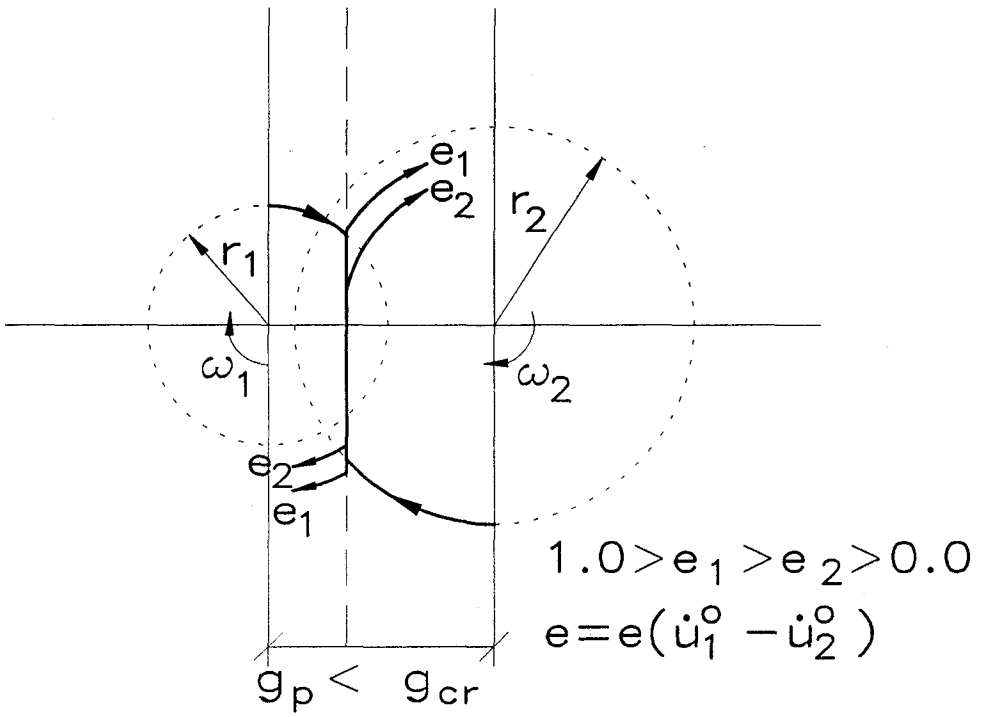

Fig. 7.4 Preliminary estimate of bumper damper effectiveness.

$$r_{2r} = r_1\rho - \sqrt{r_1^2\rho^2 + g_p^2 - r_1^2} \tag{7.21}$$

where ρ is the correlation coefficient from the plots in Appendix B, g_p is the actual gap, and r_1 is the Pseudo Energy Radius of the other structure. Using r_{2r} in the design spectrum will provide an estimate of the stiffening and supplemental damping necessary (see Fig. 7.5).

When supplemental energy dissipation is provided only as a pounding mitigation solution, the effectiveness may be measured using the simplified single hit methodology outlined in Section 7.4. This pounding mitigation technique may be combined with the use of bumper damper elements to reduce energy transfer during pounding interactions.

Of the three pounding mitigation techniques presented, the supplemental energy dissipation device is the most efficient, since not only the pounding effects are reduced, but the structural performance is also improved.

7.6 Analysis of Pounding Effects and Mitigation Techniques

To perform a detailed analysis of pounding effects and pounding mitigation effectiveness, three modeling techniques can be used: deterministic, probabilistic or hybrid mathematical models. Each modeling technique is briefly described in Section 3.5.

The deterministic model calculates the time history response of the structures when subjected to a given acceleration record. This model can estimate the effects of pounding interactions, and study the response of linked structures, with bumper damper, or with supplemental energy dissipating devices.

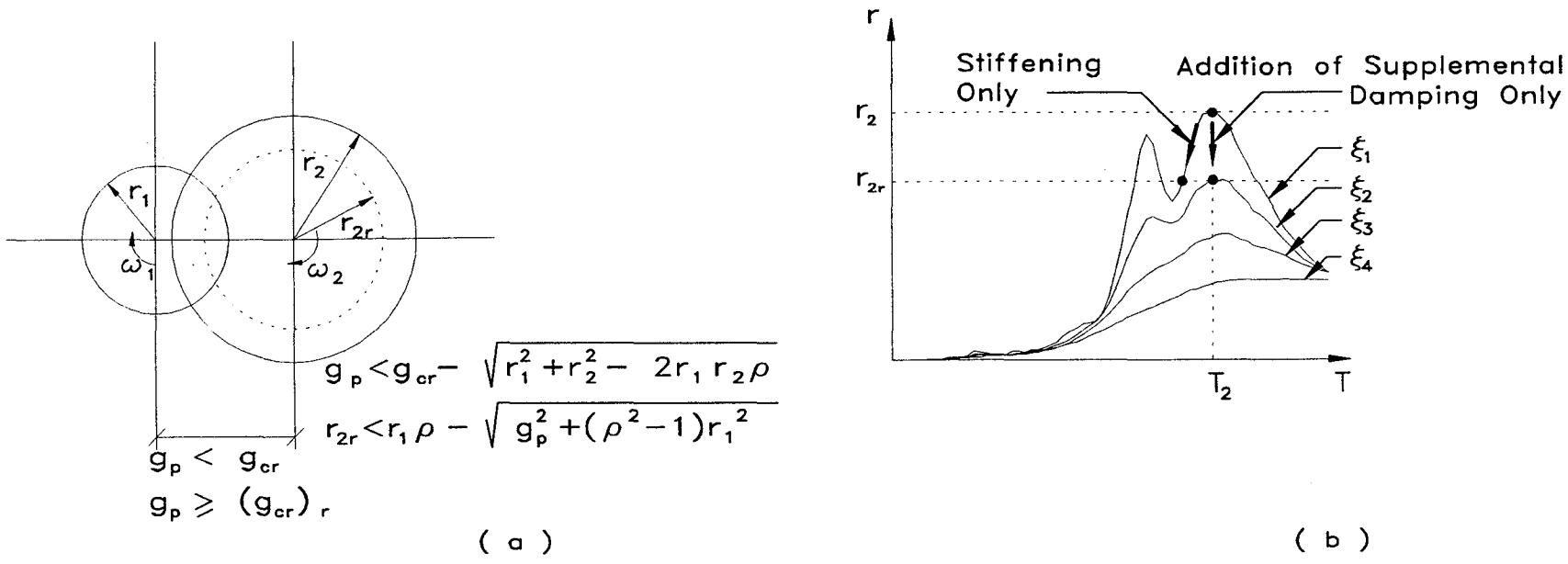

Fig. 7.5 Preliminary estimate of supplemental damping for pounding prevention.

The probabilistic model provides a stochastic description of the structural response for a stochastic input. This model can be used to estimate the statistics of the response for linked structures, or structures with supplemental energy dissipation devices. This model is not capable of calculating the response to pounding interactions.

The hybrid model combines both of the previous models. Input for this model consists of an acceleration record, an evolutionary power spectrum, and a maximum probability of pounding. This model can be used to estimate the effects of pounding interactions, and study the response of linked structures, with bumper dampers, or with supplemental energy dissipation devices.

SECTION 8
SUMMARY AND CONCLUSIONS

Pounding between adjacent structures subjected to dynamic excitations was investigated. After a review of the current state of the art, and some initial formulations of the structural problem, four major research objectives were identified and carried out. The research objectives were: (*i*) to determine the critical gap to avoid pounding (see Section 4); (*ii*) to estimate pounding effects in buildings separated by a gap smaller than critical (see Section 5); (*iii*) to describe possible pounding mitigation techniques, for buildings prone to high amplifications (see Section 6); and (*iv*) to summarize the results and observations from the previous three objectives in a comprehensive form that could be used by design engineers (see Section 7). The methodology necessary to accomplish such objectives are presented in Section 3.

State of the art review:

Pounding damage has been observed in most of the strong earthquakes affecting large metropolitan areas. Structures resting on soft soil conditions are more likely to pound due to the flexibility of their foundation. Pounding damage observed during the Mexico City earthquake may have been influenced by the flexible friction pile systems commonly used for mid-height buildings in the lake zone.

Pounding damage during the moderate 1989 Loma Prieta earthquake indicated that severe damage could take place during a strong earthquake in the San Francisco Bay area. More recently, the 1994 Northridge earthquake induced observable pounding interactions between bridge decks, or decks and abutments.

Two modeling approaches can be used to study pounding effects: stereomechanical and piece-wise linear impact. The former method calculates the post-impact velocities of the system based on the velocities at the onset of impact, the relative masses, and a coefficient of restitution that

measures the degree of plasticity induced at the interface. The later uses a rheological model that is activated when the gap between the structures is closed. This piece-wise linear impact model has been more extensively used by researchers in the field.

Studies by previous researchers provided valuable insight into the response of single-degree-of-freedom structures to: harmonic, actual earthquake excitations, and white noise input motions. Some studies have been published for the response of multi-degree-of-freedom structures to actual earthquake motions. The studies identified the major parameters that affect pounding response of structures: the gap size, the relative masses of the impacting floors, the fundamental periods of vibration, and the characteristics at the interface.

An attempt to estimate pounding effects using a simple formulation was proposed assuming a linear variation of the kinetic energy. Such an assumption covers only a range of possible combinations, namely, when the adjacent structure is very stiff. There is a need to formulate a simple methodology to estimate pounding effects for a wider range of applicability.

Part of the literature available on pounding deals with possible pounding mitigation techniques. Using published research on the combination of model responses by Der Kiureghian (1980), Kasai introduced the Double Difference Combination (DDC) rule to calculate the critical gap to avoid pounding (Jeng et al., 1992). Using a set of formulas to calculate an effective period and critical damping ratio, Jeng et al. (1992) extended the DDC rule to bilinear or degrading structures. The formulas were obtained from curve-fitting the results from numerical simulations. Since the input motion considered is a white noise process, and due to possible restrictions in the applicability of formulas derived using curve fitting, the critical gap for bilinear structures subjected to filtered white noise inputs should be determined.

Link elements have been proposed for pounding mitigation, with the disadvantage that high forces in the link may be observed, and that the structural response is considerably modified due to the presence of the link. The use of supplemental energy dissipation throughout the structures has been proposed to limit structural deflections and reduce pounding forces. Supplemental

energy dissipation in the structures has also been proposed for pounding mitigation. Available pounding mitigation techniques must be described, and their effectiveness determined.

Preliminary observations:

Energy is transferred from one structure to the other during pounding. This energy transfer produces an increase of the input energy level in one structure, and a reduction in the other. Part of the transfer energy is dissipated at the contact interface when pounding is not elastic. When pounding exhibits some level of plasticity or viscosity, the transfer energy released by one structure will not equal the transfer energy received by the other.

Although pounding is a non-linear problem, if the structures are linear, and a piece-wise linear element is used to model contact, scaling of the response for a different ground acceleration level is possible from a previous analysis, provided that the gap in the original analysis is scaled. That is, the response of the system with gap g_o and input motion $c_g \ddot{x}_g$, where c_g is a constant, may be obtained by multiplying by c_g the solution of the system with input motion $\ddot{x}_g$ and initial gap g_o / c_g. This observation makes it possible to generalize results from a given intensity of input to any intensity, provided that the gap is properly scaled.

A modified Kelvin element is introduced for impact problems. The proposed Impact Kelvin element contains a viscous element that is only active for approaching velocities. This model exhibits more realistic response characteristics than the traditional Kelvin element: the forces at the interface always tend to separate the masses, and never oppose separation; and, for greater damping constants, the duration of contact decreases. Both models may be related to an equivalent coefficient of restitution. The use of the Impact Kelvin element is suggested over the traditional Kelvin element.

Studying a continuous system subjected to a velocity pulse, at different locations, provides dynamic influence lines for displacements or shears. Such dynamic influence lines will identify critical pounding stories for which amplifications are greater or smaller. Pounding effects can be

separated in global and local, depending on the number of modes considered in the solution. Considering all modes will describe local sharp peaks in the response affecting small localized portions of the structure. Considering only a few of the first modes, the global response can be studied. Local and global effects should be checked during pounding interactions.

Several pounding mitigation techniques have been proposed. The addition of supplemental damping reduces the maximum displacements, and promotes in phase response. Linking adjacent structures eliminates pounding interactions but may drastically modify the dynamic response characteristics.

Modeling of structural pounding:

Two impact models were used: stereomechanical and piece-wise linear impact. The equations for the energy transfer in both models were derived. A Kelvin element was used as a link element, while an Impact Kelvin element was used for the piece-wise linear contact element.

Three mathematical formulations were developed: a deterministic, a probabilistic, and a hybrid formulation. Two computer programs were developed, one for deterministic and hybrid studies, and other for probabilistic studies. Structural stiffness data for the deterministic and hybrid models was be provided in terms of a stiffness matrix and bilinear or trilinear shear type elements. Structural stiffness data for the probabilistic model was linear. The Newmark-Beta method was reformulated to incorporate significant changes in the global stiffness and damping matrices.

The deterministic model studies the response of the system to a given history of ground motion accelerations. The probabilistic model studies the statistics of the response and the confidence of no pounding to an evolutionary power spectrum. This model does not incorporate pounding effects. The hybrid model studies the response to a given ground motion record, but uses prediction theory to determine pounding based on a probability limit.

Critical gap size:

Building code considerations for pounding were reviewed. Providing a sufficient distance between the structures is the commonly adopted criteria for pounding design. Critical gap to avoid pounding is specified in terms of the sum of the maximum displacements, or a percentage of the height, or a fixed quantity, or a SRSS combination of the response. Only one code allows for some level of pounding when the effects are not threatening to the stability of structures.

The absolute sum in maximum displacements assumes that the maximum response occurs in both structures at the same time but with opposite sign. This assumption yields conservative results in most cases, especially when the structures have similar periods. Combining the maximum displacements assumes that there is no correlation between the response of the structures. This approach leads to conservative estimates of the critical gap size when some correlation between responses is observed, for example for structures with similar periods, or with a high damping ratio. A percentage of the total height to determine the critical gap can account for a limit in the maximum interstory drift, however, implicitly uses the sum of the absolute maximums. This approach can also account for rotations at the foundation. Finally, a fixed quantity for the minimum gap will ensure sufficient clearance during construction.

Introducing the effect of the correlation coefficient (ρ) in the formula for the critical gap, the Double Difference Combination rule was introduced by Kasai. The absolute sum of displacements and SRSS rules are particular cases for negatively correlated process (ρ=-1) or uncorrelated process (ρ=0), respectively. Kasai suggested the use of the formula for the correlation coefficient derived by Der Kiureghian for linear structures subjected to white noise input.

Kasai and Jagiasi extended Der Kiureghian's correlation coefficient formula to bilinear or degrading structures by introducing an effective period and critical damping ratio. Formulas for the effective values were derived by interpolating the results from a large number of numerical simulations. Using statistical linearization an improved correlation coefficient can be derived for bilinear structures.

The correlation coefficient for bilinear structures subjected to filtered white noise input was calculated using statistical linearization. Broad band and narrow band inputs were considered to simulate Taft earthquake types, or Mexico City earthquake types, respectively. The correlation coefficient was calculated from the stationary solution. A more precise estimate for earthquake inputs could be obtained if the evolutionary solution is studied, however, a time function envelope of the filtered white noise input should be defined.

Two approaches to define the yield displacement of the bilinear oscillator are used: for a maximum probable ductility (μ), that is, for a ductility level with a predetermined maximum allowable probability of being exceeded; and for a reduction factor (R) from a maximum probable elastic demand level, that is, an elastic demand with a predetermined maximum allowable probability of being exceeded divided by a reduction factor. The former approach uses an iterative procedure to determine the yield displacement, while the later reduces the results from an initial elastic run. The predetermined maximum allowable probability levels should be set to a comparable risk level similar to the one inherent in the building code design spectra.

Using the improved correlation coefficient, the Double Difference Combination rule may be used to calculate the critical gap to avoid pounding. The formulation can be extended to include rotation at the foundation, or multi-degree-of-freedom structures.

The critical gap is defined for a given design peak ground acceleration. A larger intensity motion will require a larger critical gap, while a smaller intensity will require a smaller clear distance to avoid pounding. For existing structures, with gap smaller than critical, the maximum peak ground acceleration without inducing pounding can be determined.

Pounding effects:

Evaluation of pounding effects is of interest in structures separated by a gap less than critical. Structures with insufficient gap to avoid pounding are common in densely populated metropolitan areas.

Only pounding occurring between floor slabs is studied, since pounding occurring along the height of a column produce a large stress concentration that can severely threaten the integrity of the columns. This situation should be avoided, or special elements must be provided to transfer the impact loads to the adjacent floors.

Using a narrow band input, general trends in the response were identified. Two critical periods for the input motion exist that correspond to a resonant pounding response. For an input period in the neighborhood of one of the critical periods, the total input energy of the system increases. Similarly, two periods for the input motion yielding the greater reduction of the total input energy were identified. This periods correspond to the fundamental periods of the structures. For an input motion with period in the vicinity of the fundamental period of one of the structure the total input energy of the system is reduced since pounding transfers energy between the structures reducing the energy of the otherwise resonating structure. Transfer energy is maximum in this situation, with energy being transferred from the otherwise resonating structure to the other.

Four distinct trends are observed when the influence of the gap size on the total input energy is studied for the narrow band input case. When the period of the input motion coincides with one of the two critical periods, a dramatic increase in the total energy is observed for gap sizes only slightly smaller than critical. Amplification effects tend to be gradually less important as the gap size approaches zero. The second characteristic trend is observed when the period of the input motion lies between the largest critical period, and the period of either structure. In this condition, the amplification of the total input energy gradually increases as the gap size reduces. Maximum amplifications are observed for gaps close to zero. The third characteristic trend is observed when the period of the input motion approximately coincides with the period of the more flexible structure. In this case, a gradual decrease of the total input energy is observed as the gap size is reduced, and greater rate of reduction is observed for smaller gap sizes. The last characteristic trend is observed when the period of the input motion approximately coincides with the period of the stiffer structure. In this case, a large decrease is observed for gaps slightly smaller than critical.

Similar trends in the response were observed when the 1985 Mexico City earthquake was used. The similarities in the response are due to the similarity of the Mexico City earthquake with a sinusoidal motion. No clear trends were observed when the Taft earthquake was studied. The observed response is a direct consequence of the lack of a distinguishable trend in the input motion.

A large number of parameters influence the pounding response of structures. Therefore, it is difficult to identify the influence of all parameters and provide a quantitative estimate of the pounding response. Only a qualitative description of the influence of each parameter may be determined for narrow band input motions. The six sets of parameters that greatly influence pounding response are: the characteristics of the earthquake motion, the fundamental periods of the structures, damping and hysteretic characteristics, the mass of the colliding floors, the actual gap as a fraction of the critical gap, and the degree of elasticity or energy dissipation that can be expected to take place at the pounding interface.

The deterministic or hybrid models introduced can be used to determine the amplifications in the response of the structures due to pounding, for a given set of parameters. A simple method based on a single hit event was developed to estimate pounding effects for gap sizes close to critical. The method is considerably less computationally demanding.

The single hit methodology introduces the concept of a Pseudo Energy Radius to describe the elastic energy level of the structures. The Pseudo Energy Radius provides a measure that can be directly compared to maximum deflections or gap sizes. Using the Pseudo Energy Radius representation, and the critical gap computation, one will observe that some overlapping in the energy levels is possible without inducing pounding interactions.

The single hit methodology assumes that pounding takes place at the maximum energy level imposed by the earthquake. The state at pounding onset is determined by backtracking in time from the critical pounding onset. The method yields good approximation of the amplification for

gaps close to critical. The method provides a simple graphical representation that can be easily understood.

The single hit methodology will not yield reliable results for gap sizes considerably smaller than the critical gap, or for cases when multiple hits may occur. Furthermore, some non-linear resonance may take place.

Pounding mitigation techniques:

Pounding mitigation techniques are necessary when pounding effects exceed the structural capacity or a maximum serviceability limit. Often buildings with sensitive computer equipment will require stringent limits to the maximum allowable acceleration levels.

Three pounding mitigation techniques have been proposed: link elements, bumper damper elements, or supplemental energy dissipation devices. Link elements connect two adjacent buildings, effectively eliminating the possibility of pounding interactions. However, the presence of the link may considerably alter the load paths considered in the original analysis. Some level of retrofit is necessary to withstand the new distribution of forces in the structure. Forces in the links may be of the same order of magnitude as the base shears when the structures have different dynamic response characteristics. Furthermore, the stiffer structure will be subjected to higher forces.

Linking adjacent buildings with different response characteristics may promote torsional effects. Furthermore, serious political and technical problems may be encountered when linking structures that belong to different owners, were built using different design criteria, made of different materials, built for different use or with different importance levels.

Bumper damper elements dissipate the energy transferred between the structures during pounding interactions. Linear spring elements will only reduce the maximum acceleration but will not dissipate the transfer energy unless the bumper damper elements have some viscous or linear characteristics. Bumper damper elements can be modeled using a coefficient of restitution.

The equivalent coefficient of restitution may be dependent on the relative velocity at pounding onset. The effectiveness of bumper damper elements can be estimated using the single hit methodology introduced in Section 6.

Supplemental energy dissipation devices can be used in one or both structures to reduce their deflections, and reduce the critical gap size. This retrofit technique can be used to reduce or eliminate pounding effects, depending on the amount of additional damping supplied. The critical gap maximum response formula can be used to determine the amount of damping required for the retrofitted structure. Using a response spectra for various damping ratios, the minimum damping ratio to avoid pounding can be estimated. When both structures are retrofitted using energy dissipation devices, in phase response is promoted, leading to a further reduction in the critical gap size.

Reduced pounding effects in supplemental energy dissipation solutions can be estimated using the single hit methodology introduced in Section 6. This mitigation technique is preferred since it reduces pounding effects and improves structural response. The retrofit techniques may be combined with the use of bumper damper elements to further reduce pounding effects.

General observations:

Bridges and base isolated structures are also prone to pounding. Bridges will experience pounding when the clear gap in the seat of decks is closed, or when the device that prevents the decks from becoming unseated is activated. Isolated structures can experience pounding when the building hits the retaining wall at the foundation level, or when a fail-safe mechanism is activated.

SECTION 9

REFERENCES

1. Al-Hussaini, T.M., Zayas, V.A., and Constantinou, M.C. (1994), "Seismic isolation of multi-story frame structures with friction pendulum isolators," Report No. NCEER-94-0007, National Center for Earthquake Engineering Research, State University of New York at Buffalo.
2. American Iron and Steel Institute (1975), "Earthquakes: Agadir, Morocco; Skopje, Yugoslavia; Anchorage, Alaska; Caracas, Venezuela," American Iron and Steel Institute.
3. Anagnostopoulos, S.A. (1988), "Pounding of buildings is series during earthquakes," Earthquake Engineering and Structural Dynamics, Vol. 16, pp. 443-456.
4. Anagnostopoulos, S.A., and Spiliopoulos, K.V. (1990), "Analysis of building pounding due to earthquake," Structural Dynamics, Vol. 1, Eds. W.B. Kratzig et al., A.A. Balkema, Rotterdam, pp. 479-484.
5. Anagnostopoulos, S.A., and Spiliopoulos, K.V. (1992), "An investigation of earthquake induced pounding between adjacent buildings," Earthquake Engineering and Structural Dynamics, Vol. 21, pp. 289-302.
6. Applied Technology Council (1987), "Evaluating the seismic resistance of existing buildings," ATC-14, Redwood City, California.
7. Arnold, C. (1989), "Architectural considerations," The Seismic Design Handbook, Edited by F. Naeim, Structural Engineering Series, Van Nostrand Reinhold, New York.
8. Baber, T.T., and Noori, M.N. (1985), "Random vibration of degrading, pinching systems," Journal of Engineering Mechanics, ASCE, Vol. 111, No. 8, pp. 1010-1026.
9. Baber, T.T., and Wen, Y.-K. (1979), "Stochastic equivalent linearization for hysteretic, degrading, multistory structures," Structural Research Series No. 471, University of Illinois at Urbana-Champaing, Illinois.
10. Baber, T.T., and Wen, Y.-K. (1981), "Random vibration of hysteretic, degrading systems," Journal of Engineering Mechanics, ASCE, Vol. 107, No. EM6, pp. 1069-1087.
11. Bernal, D. (1991), "Locating events in step-by-step integration of equations of motion," Journal of Structural Engineering, ASCE, Vol. 117, No. 2, pp. 530-545, 1991.
12. Bertero, V.V., and Collins, R.G. (1973), "Investigation of the failures of the Olive View stairtowers during the San Fernando earthquake and their implications on seismic design," Report No. EERC 73-26, University of California, Berkeley, CA.
13. Bertero, V.V. (1986), "Observations on structural pounding," The Mexico City Earthquakes-1985: Factors Involved and Lessons Learned, Edited by M. A. Cassaro and E. Martínez-Romero, ASCE, pp. 264-278.

14. Bertero, V.V., and Uang, C.-M. (1992), "Issues and future directions in the use of an energy approach for seismic-resistant design of structures," Nonlinear Seismic Analysis and Design of Reinforced Concrete Buildings, Ed. by P. Fajfar and H. Krawinkler, Elsevier Applied Science, New York.

15. Blevins, R.D. (1979), "Formulas for natural frequency and mode shape," Van Nostrand Reinhold Co., New York.

16. Bracci, J.M. (1992), "Experimental and analytical study of seismic damage and retrofit of lightly reinforced concrete structures in low seismicity zones," Ph.D. Dissertation, State University of New York, Buffalo.

17. Carney, J.F., and Yeh, C. (1991), "Viscoplastic response of clamped beams under impact loading," Journal of Structural Engineering, ASCE, Vol. 117, No. 12, pp. 3680-3697.

18. Chaudhary, A.B., and Bathe, K.-J. (1986), "A solution method for static and dynamic analysis of three-dimensional contact problems with friction," Computers and Structures, Vol. 24, No. 6, pp. 855-873.

19. Chua, G.S., Pacheco, B.M., Fujino, Y., and Ito, M. (1990), "Classical impact damper and pendulum impact damper for potential civil engineering application," Structural Eng./Earthquake Eng., Vol. 7, No. 1, pp. 101s-112s.

20. Clough, R.W., and Penzien, J. (1993), "Dynamics of structures," Second Edition, McGraw-Hill Inc., New York.

21. Corotis, R.B., Vanmarcke, E.H., and Cornell, C.A. (1972), "First passage of nonstationary random processes," Journal of Engineering Mechanics, ASCE, Vol. 98, No. EM2, pp. 401-414.

22. Davis, R.O. (1992), "Pounding of buildings modeled by impact oscillator," Earthquake Engineering and Structural Dynamics, Vol. 21, pp. 253-274.

23. Den Hartog, J.P., and Heiles, R.M. (1936), "Forced vibration in nonlinear systems with various combinations of linear springs," Journal of Applied Mechanics, Vol. 3, pp. 127-130.

24. Der Kiureghian, A. (1979), "On response of structures to stationary excitation," Report No. UCB/EERC-79/32, Earthquake Engineering Research Center, University of California, Berkeley, CA, December.

25. Der Kiureghian, A. (1980), "A response spectrum method for random vibrations," Report No. UCB/EERC-80/15, Earthquake Engineering Research Center, University of California, Berkeley, CA, June.

26. Earthquake Engineering Research Institute (1979), "Thessaloniki, Greece earthquake: June 20, 1978," Reconnaissance Report, EERI, Edited by J. A. Blume and M. H. Stauduhar, Berkeley, CA, January.

27. Earthquake Engineering Research Institute (1980), "The 1976 Tangshan, China earthquake," Papers presented at the 2nd U.S. National Conference on Earthquake Engineering held at Stanford University in 1979.

28. Earthquake Engineering Research Institute (1995), "The Hyogo-Ken Nanbu Earthquake: January 17, 1995," Preliminary Reconnaissance Report EERI 95-04, Edited by C.D. Comartin, M. Greene and S. K. Tubbesing, Berkeley, CA, February.

29. EEFIT (1986), "The Mexican earthquake of 19th September 1985: A field report by EEFIT," Printed by Milford Printers Limited, West Bridgford, Nottingham.

30. Ellis, G.W., Srinivasan, M., and Cakmak, A.S. (1990), "A program to generate site dependent time histories: EQGEN," Technical Report NCEER-90-0009, National Center for Earthquake Engineering Research, State University of New York at Buffalo, January.

31. Filiatrault, A., and Folz, B. (1992), "Nonlinear earthquake response of structurally interconnected buildings," Canadian Journal of Civil Engineering, Vol. 19, pp. 560-572.

32. Fundación ICA (1988), "Experiencias derivadas de los sismos de septiembre de 1985," Noriega Editores, Ed. Limusa, México (in Spanish).

33. Ghali, A., and Neville, A.M. (1989), "Structural analysis: a unified classical and matrix approach," Third Edition, Chapman and Hall, New York.

34. Goldsmith, W. (1960), "Impact: the theory and physical behavior of colliding solids," Edward Arnold Publishers Ltd., London, U.K.

35. Hasofer, A.M., and Petocz, P. (1978), "The envelope of an oscillatory process and its upcrossings," Journal of Applied Advanced Probability, Vol. 10, pp. 711-716.

36. Humar, J.L. (1990), "Dynamics of Structures," Prentice Hall, New Jersey.

37. International Association for Earthquake Engineering (1988), "Earthquake Resistant Regulations, a world list 1988," Tokyo, Japan, July.

38. Jeng, V., Kasai, K., and Maison, B.F. (1992), "A spectral difference method to estimate building separations to avoid pounding," Earthquake Spectra, Vol. 8, No. 2, pp. 201-223.

39. Jing, H.-S., and Sheu, K.-C. (1990), "Exact stationary solutions of the random response of a single-degree-of-freedom vibro-impact system," Journal of Sound and Vibration, Vol. 141, No. 3, pp. 363-373.

40. Jing, H.-S., and Young, M. (1990), "Random response of a single-degree-of-freedom vibro-impact system with clearance," Earthquake Engineering and Structural Dynamics, Vol. 19, pp. 789-798.

41. Jing, H.-S., and Young, M. (1991), "Impact interactions between two vibration systems under random excitation," Earthquake Engineering and Structural Dynamics, Vol. 20, pp. 667-681.

42. Kasai, K., Maison, B.F., and Patel, D.J. (1990), "An earthquake analysis for buildings subjected to a type of pounding," Proceedings of Fourth U.S. National Conference on Earthquake Engineering, May 20-24, Vol. 2, pp. 289-298.

43. Kasai, K., and Maison, B.F. (1991a), "Observations of structural pounding damage from 1989 Loma Prieta earthquake," Proc. 6th Canadian Conference on Earthquake Engineering, Toronto, pp. 735-742.

44. Kasai, K., and Maison, B.F. (1991b), "Structural pounding damage," Loma Prieta Earthquake Reconnaissance Report, Chapter 6, Structural Engineers Association of California, pp. 91-112.

45. Kasai, K., Maison, B.F., Jeng, V., Patel, D.J., and Patel, P.C. (1991c), "A study on earthquake pounding between adjacent structures," Proc. 6th Canadian Conference on Earthquake Engineering, Toronto, pp. 93-100.

46. Kasai, K., and Jagiasi, A.R. (1993a), "Building separation rules to avoid seismic pounding," Proc. Structural Congress, ASCE, Irvine, CA, pp. 199-204, April.

47. Kasai, K., Munshi, J.A., and Maison, B.F. (1993b), "Viscoelastic dampers for seismic pounding mitigation," Proc. Structural Congress, ASCE, Irvine, CA, pp. 730-735, April.

48. Key, S.W. (1986), "Improvements in transient dynamic time integration with application to spent nuclear shipping cask impact analysis," Finite Element Methods for Nonlinear Problems, Europe-U.S. Symposium, Trondheim, Norway, Editors Bergan, Bathe and Wunderlich, Ed. Springer, pp. 497-511.

49. Kleiber, M., Kotula, W., and Saran, M. (1986), "Dynamic quasi-bifurcations in structures subjected to step loadings," Finite Element Methods for Nonlinear Problems, Europe-U.S. Symposium, Trondheim, Norway, Editors Bergan, Bathe and Wunderlich, Ed. Springer, pp. 529-538.

50. Lee, S.K., and Kozin, F. (1986), "Bounded state control of structures with uncertain parameters," Dynamic Response of Structures, Hart G.C. and Nelson R.B. editors, ASCE, New York, pp. 788-794.

51. Lee, S.K., and Kozin, F. (1987), "Bounded state control of linear structures," Structural Control, Leipholz H.H.E. editor, Martinus Nijhoff, Amsterdam, pp. 387-407.

52. Li, G.X., Rand, R.H., and Moon, F.C. (1990), "Bifurcations and chaos in a forced zero-stiffness impact oscillator," International Journal of Non-Linear Mechanics, Vol. 25, No. 4, pp. 417-432.

53. Mahin, S.A., Bertero, V.V., Chopra, A.K., and Collins, R.G. (1976), "Response of the Olive View Hospital main building during the San Fernando earthquake," Report No. EERC 76-22, University of California, Berkeley, CA.

54. Maidanik, G. (1977), "Some elements in statistical energy analysis," Journal of Sound and Vibration, Vol. 52, No. 2, pp. 171-191.

55. Maison, B.F., and Kasai, K., (1988), "SLAM: A computer program for the analysis of structural pounding," June, Available from the National Information Service for Earthquake Engineering, University of California, Berkeley, CA.

56. Maison, B.F., and Kasai, K. (1990a), "Analysis for type of structural pounding," Journal of Structural Engineering, ASCE, Vol. 116, No. 4, pp. 957-977.

57. Maison, B.F., and Kasai, K. (1990b), "SLAM-2: A computer program for the analysis of structural pounding (extended version)," June, Available from the National Information Service for Earthquake Engineering, University of California, Berkeley, CA.

58. Maison, B.F., and Kasai, K. (1992), "Dynamics of pounding when two buildings collide," Earthquake Engineering and Structural Dynamics, Vol. 21, pp. 771-786.

59. Masri, S.F., Bekey, G.A., and Udwadia, F.E. (1980), "On-line pulse control of tall buildings," Structural Control, H.H.E. Leipholz editor, North Holland Publishing Company & SM Publications, pp. 471-491.

60. Masri, S.F., Bekey, G.A., and Caughey, T.K. (1981), "Optimum pulse control of flexible structures," Journal of Applied Mechanics, ASME, Vol. 48, September, pp. 619-626.

61. Masri, S.F., Bekey, G.A., and Caughey, T.K. (1982), "On-line control of nonlinear flexible structures," Journal of Applied Mechanics, ASME, Vol. 49, No. 4, December, pp. 871-884.

62. Mendoza, M.J., and Auvinet, G. (1988), "The Mexico city earthquake of September 19, 1985- Behavior of building foundations in Mexico city," Earthquake Spectra, EERI, Vol. 4, No. 4, pp. 835-853.

63. Miller, R.K. (1980), "Steady vibroimpact at a seismic joint between adjacent structures," Proc. 7th World Conference on Earthquake Engineering, Istanbul, Turkey, Vol. 6, pp. 57-64.

64. Miller, R.K., Masri, S.F., Dehghanyar, T.J., and Caughey, T.K. (1988), "Active vibration control of large civil structures," Journal of Engineering Mechanics, ASCE, Vol. 114, No. 9, September, pp.1542-1570.

65. Miranda, I., Ferencz, R.M., and Hughes, T.J.R. (1989), "An improved implicit-explicit time integration method for structural dynamics," Earthquake Engineering and Structural Dynamics, Vol. 18, pp. 643-653.

66. Mofflin, D.S., Olson, M.D., and Anderson, D.L. (1986), "Finite strip analysis of blast loaded plates," Finite Element Methods for Nonlinear Problems, Europe-U.S. Symposium, Trondheim, Norway, Editors Bergan, Bathe and Wunderlich, Ed. Springer, pp. 539-553.

67. Natsiavas, S. (1990), "Stability and bifurcation analysis for oscillators with motion limiting constraints," Journal of Sound and Vibration, Vol. 141, No. 1, pp. 97-102.

68. Newland, D.E. (1989), "Mechanical vibration analysis and computation," Longman Scientific and Technical, Copublished with John Wiley & Sons Inc., New York.

69. Newmark, N.M., and Rosenblueth, E. (1982), "Fundamentos de Ingeniería Sísmica," Ed. Diana, México (in Spanish).

70. Ödeen, S., and Lundberg, B. (1991), "Prediction of impact force by impulse response method," International Journal of Impact Engineering, Vol. 11, No. 2, pp. 149-158.

71. Owen, D.R.J., Liu, G.Q., and Li, X.-L. (1986), "Nonlinear dynamic analysis of shell structures using general single step algorithms," Finite Element Methods for Nonlinear Problems, Europe-U.S. Symposium, Trondheim, Norway, Editors Bergan, Bathe and Wunderlich, Ed. Springer, pp. 513-528.

72. Page, C.H. (1952), "Instantaneous power spectra," Journal of Applied Physics, Vol. 23, No. 1, pp. 103-106.

73. Papadrakakis, M., Mouzakis, H., Plevris, N., and Bitzarakis, S. (1991), "A Lagrange multiplier solution for pounding of buildings during earthquakes," Earthquake Engineering and Structural Dynamics, Vol. 20, pp. 981-998.

74. Papoulis, A. (1991), "Probability, random variables, and stochastic processes," McGraw-Hill, third edition.

75. Park, Y.J., Reinhorn, A.M., and Kunnath, S.K., (1987), "IDARC: Inelastic damage analysis of reinforced concrete frame-Shear Wall Structures." Technical Report NCEER-87-0008, NCEER, Suny at Buffalo.

76. Press, W.H., Teukolsky, S.A., Vetterling, W.T., and Flannery, B.P. (1992), "Numerical recipes in Fortran: the art of scientific computing," Second Edition, Cambridge University Press, New York.

77. Priestley, M.B. (1965), "Evolutionary spectra and non-stationary processes," Journal Royal Statistical Society B, Vol. 27, pp. 204-237.

78. Priestley, M.B. (1966), "Design relations for non-stationary processes," Journal Royal Statistical Society B, Vol. 28, pp. 228-240.

79. Priestley, M.B. (1967), "Power spectral analysis of non-stationary random processes," Journal of Sound and Vibration, Vol. 6, No. 1, pp. 86-97.

80. Priestley, M.B. (1992), "Spectral analysis and time series," Probability and mathematical statistics, Academic Press Limited, Seventh printing.

81. Priestley, M.B., and Tong, H. (1973), "On the analysis of bivariate non-stationary processes," Journal Royal Statistical Society B, Vol. 35, pp. 153-166.

82. Prucz, Z., Soong, T.T., and Reinhorn, A.M. (1984), "Pulse control of deep-water offshore structures," Preprint 84-012, ASCE Annual Convention, Atlanta, GA, May.

83. Prucz, Z., Soong, T.T., and Reinhorn, A.M. (1985), "An analysis of pulse control for simple mechanical systems," Journal of Dynamic Systems, Measurement and Control, ASME, Vol. 107, No. 2, June, pp. 123-131.

84. Psycharis, I.N. (1990), "Dynamic behavior of rocking two-block assemblies," Earthquake Engineering and Structural Dynamics, Vol. 19, pp. 555-575.

85. Reinhorn, A.M., Li, C., and Constantinou, M.C. (1995), "Experimental and analytical investigation of seismic retrofit of structures with supplemental damping, Part I: Fluid viscous damping devices," Report No. NCEER-95-0001, National Center for Earthquake Engineering Research, State University of New York, Buffalo.

86. Reinhorn, A.M., Manolis, G.D., and Wen, C.Y. (1987), "Active control of inelastic structures," Journal of Engineering Mechanics, ASCE, Vol. 113, No. 3, March, pp. 315-333.

87. Ríos, R., Alva, J., Zegarra, L., and Pfeiffer, E. (1986), "El terremoto de México del 19 de septiembre de 1985," Centro Regional de Sismología para America del Sur, Lima, Perú (in Spanish).

88. Roberts, J.B. (1965), "On the harmonic analysis of evolutionary random vibrations," Journal of Sound Vibration, Vol. 2, No. 3, pp. 336-352.

89. Roberts, J.B., and Spanos, P.D. (1990), "Random vibration and statistical linearization," John Wiley and Sons.

90. Rodellar, J., Barbat, A.H., and Martín-Sánchez, J.M. (1987), "Predictive control of structures," Journal of Engineering Mechanics, ASCE, Vol. 113, No. 6, June, pp. 797-812.

91. Rosenblueth, E., and Meli, R. (1986), "The 1985 earthquake: causes and effects in Mexico City," Concrete International, Vol. 8, No. 5, pp. 23-34.

92. Smith, C.E. (1991), "Predicting rebounds using rigid body dynamics," Transactions of the ASME, Vol. 58, pp. 754-758, September.

93. Soong, T.T. (1983), "Dynamics of a simple system subjected to random impact," The Shock and Vibration Bulletin, Bulletin 53, Part 2, pp. 125-129, 1983.

94. Soong, T.T. (1990), "Active structural control: theory and practice," Longman.

95. Scientific & Technical, Copublished in the U.S. with John Wiley & Sons Inc., New York.

96. Soong, T.T., and Grigoriu, M. (1992), "Random vibration of mechanical and structural systems," Prentice Hall.

97. Stafford Smith, B., and Coull, A. (1991), "Tall buildings: analysis and design," John Wiley & Sons Inc., New York.

98. Stavroulakis, G.E., and Abdalla, K.M. (1991), "Contact between adjacent structures," Journal of Structural Engineering, ASCE, Vol. 117, No. 10, pp. 2838-2850.

99. Stratta, J.L. (1987), "Manual for seismic design," Prentice Hall Inc., International Series in Civil Engineering and Engineering Mechanics, New Jersey.

100. Sues, R.H., Lavelle, F.M., and Westermo, B.D. (1991), "Research and development of an optimum device to reduce seismic structural pounding (summary volume)," ARA Final Report No. 5655, Prepared for National Science Foundation.

101. Szuladzinki, G., (1982), "Dynamics of structures and machinery: Problems and solutions," Wiley-interscience publication, John Wiley and Sons, New York.

102. Taylor, R.L., and Papadopoulos, P. (1993), "On a finite element method for dynamic contact/impact problems," International Journal for Numerical Methods in Engineering, Vol. 36, pp. 2123-2140.

103. Timoshenko, S., Young, D.H., and Weaver, W., (1974), "Vibration problems in engineering," 4 th edition, John Wiley and Sons, New York.

104. Uang, C.-M. (1991a), "Comparison of seismic force reduction factors used in USA and Japan," Earthquake Engineering and Structural Dynamics, Vol. 20, pp. 389-397.

105. Uang, C.-M. (1991b), "Establishing R (or Rw) and Cd factors for building seismic provisions," Journal of Structural Engineering, ASCE, Vol. 117, No. 1, pp. 19-28.

106. Uang, C.-M., and Bertero, V.V. (1988a), "Implications of recorded earthquake ground motions on seismic design of building structures," Report No. UCB/EERC-88/13, Earthquake Engineering Research Center, University of California, Berkeley, CA, November.

107. Uang, C.-M., and Bertero, V.V. (1988b), "Use of energy as a design criterion in earthquake-resistant design," Report No. UCB/EERC-88/18, Earthquake Engineering Research Center, University of California, Berkeley, CA, November.

108. Uang, C.-M., and Bertero, V.V. (1990), "Evaluation of seismic energy in structures," Earthquake Engineering and Structural Dynamics, Vol. 19, pp. 77-90.

109. Uang, C.-M., and Bertero, V.V. (1991), "UBC seismic serviceability regulations: a critical review," Journal of Structural Engineering, Vol. 117, No. 7, pp. 2055-2068.

110. Valles, R.E. (1995), "Evaluation, prevention and mitigation of pounding effects in building structures," Ph.D. Dissertation, Department of Civil Engineering, State University of New York at Buffalo, April.

111. Valles, R.E. (1994), "Manual for three parameter Hysteretic model: Subroutine DDNSTH," Internal Report, Dept. of Civil Engineering State University of New York at Buffalo.

112. Valles, R.E., Reinhorn, A.M., and Kunnath, S.K., (1992), "Seismic Evaluation of Lightweight RC flat plate building in region of low to moderate seismicity," Proceedings of the tenth world conference on Earthquake Engineering, 16-24 July, Madrid, Spain.

113. Van Mier, J.G.M., Pruijssers, A.F., Reinhardt, H.W., and Monnier, T. (1991), "Load-time response of colliding concrete bodies," Journal of Structural Engineering, ASCE, Vol. 117, No. 2, pp. 354-374.

114. Vanmarcke, E.H. (1972), "Properties of spectral moments with applications to random vibration," Journal of Engineering Mechanics, ASCE, Vol. 98, No. EM2, pp. 425-446.

115. Vanmarcke, E.H. (1975), "On the distribution of the first-passage time for normal stationary random processes," Journal of Applied Mechanics, ASME, pp. 215-220, March.

116. Wada, A., Shinozaki, Y., and Nakamura, N. (1984), "Collapse of building with expansion joints through collision caused by earthquake motion," Proc. 8th WCEE, San Francisco, Volume IV, pp. 855-862.

117. Wen, Y.-K. (1976), "Method for random vibration of hysteretic systems," Journal of Engineering Mechanics, ASCE, Vol. 102, No. EM2, pp. 249-263.

118. Westermo, B.D. (1989), "The dynamics of interstructural connection to prevent pounding," Earthquake Engineering and Structural Dynamics, Vol. 18, pp. 687-699.

119. Wilson, E.L., Der Kiureghian, A., and Bayo, E.P. (1981), "A replacement for the SRSS method in seismic analysis," Earthquake Engineering and Structural Dynamics, Vol. 9, pp. 187-194.

120. Wolf, J.P., and Skikerud, P.E. (1980), "Mutual pounding of adjacent structures during earthquakes," Nuclear Engineering and Design, Vol. 57, pp. 253-275.

121. Wolf, J.P., and Skikerud, P.E. (1980), "Mutual pounding of adjacent structures during earthquakes," Nuclear Engineering and Design, Vol. 57, pp. 253-275.

122. Yang, J.N., and Liu, S.C. (1981), "Distribution of maximum and statistical response spectra," Journal of Engineering Mechanics, ASCE, Vol. 107, No. EM6.

APPENDIX A

Statistical Models for Critical Gap Computations

The conclusions and observations from critical gap size based upon statistical models use the mathematical formulations presented in this Appendix. The response of two single degree of freedom systems is studied under four different conditions:

- Linear structures subjected to a White Noise input.
- Linear structures subjected to a Filtered White Noise input.
- Bilinear structures subjected to a White Noise input.
- Bilinear structures subjected to a Filtered White Noise input.

The governing equations for each case have the form:

$$\dot{\mathbf{X}} = \mathbf{G}\mathbf{X} + \mathbf{B}n(t) \tag{A.1}$$

Where $n(t)$ is a stationary white noise input process. The variance of the response obeys the differential equation (Roberts and Spanos, 1990):

$$\dot{\mathbf{V}} = \mathbf{G}\mathbf{V}^t + \mathbf{V}\mathbf{G}^t + \mathbf{D} \tag{A.2}$$

that for the stationary case simplifies to:

$$\mathbf{G}\mathbf{V}^t + \mathbf{V}\mathbf{G}^t + \mathbf{D} = \mathbf{0} \tag{A.3}$$

The matrix $\mathbf{G}$, depending on the model studied, may include some or all of the submatrices:

$$\mathbf{G}_{\mu\mu} = \begin{bmatrix} 0 & 1 & 0 & 0 \\ -\alpha_1\omega_1^2 & -2\xi_1\omega_1 & 0 & 0 \\ 0 & 0 & 0 & 1 \\ 0 & 0 & -\alpha_2\omega_2^2 & -2\xi_2\omega_2 \end{bmatrix} \tag{A.4a}$$

$$\mathbf{G}_{\mu\nu} = \begin{bmatrix} 0 & 0 \\ \omega_1^2(\alpha_1 - 1) & 0 \\ 0 & 0 \\ 0 & \omega_2^2(\alpha_2 - 1) \end{bmatrix} \tag{A.4b}$$

$$\mathbf{G}_{\mu x} = \begin{bmatrix} 0 & 0 \\ \omega_g^2/u_{y1} & 2\xi_g\omega_g/u_{y1} \\ 0 & 0 \\ \omega_g^2/u_{y2} & 2\xi_g\omega_g/u_{y2} \end{bmatrix} \tag{A.4c}$$

$$\mathbf{G}_{zu} = \begin{bmatrix} 0 & -c_1^e & 0 & 0 \\ 0 & 0 & 0 & -c_2^e \end{bmatrix} \tag{A.4d}$$

$$\mathbf{G}_{zz} = \begin{bmatrix} -k_1^e & 0 \\ 0 & -k_2^e \end{bmatrix} \tag{A.4e}$$

$$\mathbf{G}_{xx} = \begin{bmatrix} 0 & 1 \\ -\omega_g^2 & -2\xi_g\omega_g \end{bmatrix} \tag{A.4f}$$

Where:

ω_1, ω_2: Frequency of each structure.

ξ_1, ξ_2: Critical damping ratio for each structure.

α_1, α_2: Ratio of post-yielding tangent frequency to initial frequency for each structure.

u_1, u_2: Displacement for each structure.

u_{y1}, u_{y2}: Yield displacement for each structure.

μ_1, μ_2: Ductility for each structure.

ω_g: Frequency for ground filter.

ξ_g: Critical damping ratio for ground filter.

x_g: Displacement of ground filter.

For linear structures subjected to a white noise input:

$$\mathbf{G} = \mathbf{G}_{\mu\mu} \tag{A.5a}$$

$$\mathbf{X} = \begin{Bmatrix} u_1 \\ \dot{u}_1 \\ u_2 \\ \dot{u}_2 \end{Bmatrix} \tag{A.5b}$$

$$\mathbf{B} = \begin{Bmatrix} 0 \\ 1 \\ 0 \\ 1 \end{Bmatrix} \tag{A.5c}$$

$$\mathbf{D}_{ij} = \begin{cases} 2\pi S_0 & \text{for } i = j = 2,\ i = 2\ j = 4, i = 4\ j = 2, \text{ and } i = j = 4 \\ 0 & \text{otherwise} \end{cases} \tag{A.5d}$$

For linear structures subjected to a filtered white noise input:

$$\mathbf{G} = \begin{bmatrix} \mathbf{G}_{\mu\mu} & \mathbf{G}_{\mu x} \\ \mathbf{0} & \mathbf{G}_{xx} \end{bmatrix} \tag{A.6a}$$

$$\mathbf{X} = \begin{Bmatrix} u_1 \\ \dot{u}_1 \\ u_2 \\ \dot{u}_2 \\ x_g \\ \dot{x}_g \end{Bmatrix} \tag{A.6b}$$

$$\mathbf{B}_i = \begin{cases} 1 & \text{for } i = 6 \\ 0 & \text{otherwise} \end{cases} \tag{A.6c}$$

$$\mathbf{D}_{ij} = \begin{cases} 2\pi S_0 & \text{for } i = j = 6 \\ 0 & \text{otherwise} \end{cases} \tag{A.6d}$$

For bilinear structures subjected to a white noise input:

$$\mathbf{G} = \begin{bmatrix} \mathbf{G}_{\mu\mu} & \mathbf{G}_{\mu x} \\ \mathbf{G}_{x\mu} & \mathbf{G}_{xx} \end{bmatrix} \tag{A.7a}$$

$$\mathbf{X} = \begin{Bmatrix} \mu_1 \\ \dot{\mu}_1 \\ \mu_2 \\ \dot{\mu}_2 \\ z_1 \\ z_2 \end{Bmatrix} \tag{A.7b}$$

$$\mathbf{B}_i = \begin{cases} 1 & \text{for } i = 2 \text{ or } i = 4 \\ 0 & \text{otherwise} \end{cases} \tag{A.7c}$$

$$\mathbf{D}_{ij} = \begin{cases} 2\pi S_0 / u_{y1}^2 & \text{for } i = j = 2 \\ 2\pi S_0 / u_{y2}^2 & \text{for } i = j = 4 \\ 2\pi S_0 / (u_{y1} u_{y2}) & \text{for } i = 2 \; j = 4, \text{ or } i = 4 \; j = 2 \\ 0 & \text{otherwise} \end{cases} \tag{A.7d}$$

For bilinear structures subjected to a filtered white noise input:

$$\mathbf{G} = \begin{bmatrix} \mathbf{G}_{\mu\mu} & \mathbf{G}_{\mu z} & \mathbf{G}_{\mu x} \\ \mathbf{G}_{z\mu} & \mathbf{G}_{zz} & \mathbf{0} \\ \mathbf{0} & \mathbf{0} & \mathbf{G}_{xx} \end{bmatrix} \tag{A.8a}$$

$$\mathbf{X} = \begin{Bmatrix} \mu_1 \\ \dot{\mu}_1 \\ \mu_2 \\ \dot{\mu}_2 \\ z_1 \\ z_2 \\ x_g \\ \dot{x}_g \end{Bmatrix} \tag{A.8b}$$

$$\mathbf{B}_i = \begin{cases} 1 & \text{for } i = 8 \\ 0 & \text{otherwise} \end{cases} \tag{A.8c}$$

$$\mathbf{D}_{ij} = \begin{cases} 2\pi S_0 & \text{for } i = j = 8 \\ 0 & \text{otherwise} \end{cases} \tag{A.8d}$$

The stationary solution may be calculated by rearranging the covariance matrix in a vector form:

$$\mathbf{G'V'} = \mathbf{D'} \tag{A.9}$$

Where the variances of the response in vector form ($\mathbf{V'}$) are related to the covariance matrix. For the bilinear structures subjected to a filtered white noise input:

$$\mathbf{V} = \begin{bmatrix} \nu_{\mu_1\mu_1} & \nu_{\mu_1\dot{\mu}_1} & \nu_{\mu_1\mu_2} & \nu_{\mu_1\dot{\mu}_2} & \nu_{\mu_1 z_1} & \nu_{\mu_1 z_2} & \nu_{\mu_1 x_g} & \nu_{\mu_1 \dot{x}_g} \\ \nu_{\dot{\mu}_1\mu_1} & \nu_{\dot{\mu}_1\dot{\mu}_1} & \nu_{\dot{\mu}_1\mu_2} & \nu_{\dot{\mu}_1\dot{\mu}_2} & \nu_{\dot{\mu}_1 z_1} & \nu_{\dot{\mu}_1 z_2} & \nu_{\dot{\mu}_1 x_g} & \nu_{\dot{\mu}_1 \dot{x}_g} \\ \nu_{\mu_2\mu_1} & \nu_{\mu_2\dot{\mu}_1} & \nu_{\mu_2\mu_2} & \nu_{\mu_2\dot{\mu}_2} & \nu_{\mu_2 z_1} & \nu_{\mu_2 z_2} & \nu_{\mu_2 x_g} & \nu_{\mu_2 \dot{x}_g} \\ \nu_{\dot{\mu}_2\mu_1} & \nu_{\dot{\mu}_2\dot{\mu}_1} & \nu_{\dot{\mu}_2\mu_2} & \nu_{\dot{\mu}_2\dot{\mu}_2} & \nu_{\dot{\mu}_2 z_1} & \nu_{\dot{\mu}_2 z_2} & \nu_{\dot{\mu}_2 x_g} & \nu_{\dot{\mu}_2 \dot{x}_g} \\ \nu_{z_1\mu_1} & \nu_{z_1\dot{\mu}_1} & \nu_{z_1\mu_2} & \nu_{z_1\dot{\mu}_2} & \nu_{z_1 z_1} & \nu_{z_1 z_2} & \nu_{z_1 x_g} & \nu_{z_1 \dot{x}_g} \\ \nu_{z_2\mu_1} & \nu_{z_2\dot{\mu}_1} & \nu_{z_2\mu_2} & \nu_{z_2\dot{\mu}_2} & \nu_{z_2 z_1} & \nu_{z_2 z_2} & \nu_{z_2 x_g} & \nu_{z_2 \dot{x}_g} \\ \nu_{x_g\mu_1} & \nu_{x_g\dot{\mu}_1} & \nu_{x_g\mu_2} & \nu_{x_g\dot{\mu}_2} & \nu_{x_g z_1} & \nu_{x_g z_2} & \nu_{x_g x_g} & \nu_{x_g \dot{x}_g} \\ \nu_{\dot{x}_g\mu_1} & \nu_{\dot{x}_g\dot{\mu}_1} & \nu_{\dot{x}_g\mu_2} & \nu_{\dot{x}_g\dot{\mu}_2} & \nu_{\dot{x}_g z_1} & \nu_{\dot{x}_g z_2} & \nu_{\dot{x}_g x_g} & \nu_{\dot{x}_g \dot{x}_g} \end{bmatrix}$$

$$= \begin{bmatrix} \nu'_1 & 0 & \nu'_2 & \nu'_3 & \nu'_4 & \nu'_5 & \nu'_6 & \nu'_7 \\ 0 & \nu'_8 & \nu'_9 & \nu'_{10} & \nu'_{11} & \nu'_{12} & \nu'_{13} & \nu'_{14} \\ \nu'_2 & \nu'_9 & \nu'_{15} & 0 & \nu'_{16} & \nu'_{17} & \nu'_{18} & \nu'_{19} \\ \nu'_3 & \nu'_{10} & 0 & \nu'_{20} & \nu'_{21} & \nu'_{22} & \nu'_{23} & \nu'_{24} \\ \nu'_4 & \nu'_{11} & \nu'_{16} & \nu'_{21} & \nu'_{25} & \nu'_{26} & \nu'_{27} & \nu'_{28} \\ \nu'_5 & \nu'_{12} & \nu'_{17} & \nu'_{22} & \nu'_{26} & \nu'_{29} & \nu'_{30} & \nu'_{31} \\ \nu'_6 & \nu'_{13} & \nu'_{18} & \nu'_{23} & \nu'_{27} & \nu'_{30} & \nu'_{32} & 0 \\ \nu'_7 & \nu'_{14} & \nu'_{19} & \nu'_{24} & \nu'_{28} & \nu'_{31} & 0 & \nu'_{33} \end{bmatrix} \tag{A.10}$$

For the bilinear structures subjected to a filtered white noise input, the set of linear algebraic equations that result are:

$$-\alpha_1\omega_1^2\nu'_1 - (1-\alpha_1)\omega_1^2\nu'_4 + \frac{\omega_g^2}{u_{y1}}\nu'_6 + \frac{2\xi_g\omega_g}{u_{y1}}\nu'_7 + \nu'_8 = 0 \tag{A.11}$$

$$\nu'_3 + \nu'_9 = 0 \tag{A.12}$$

$$-\alpha_2\omega_2^2\nu'_2 - 2\xi_2\omega_2\nu'_3 - (1-\alpha_2)\omega_2^2\nu'_5 + \frac{\omega_g^2}{u_{y2}}\nu'_6 + \frac{2\xi_g\omega_g}{u_{y2}}\nu'_7 + \nu'_{10} = 0 \tag{A.13}$$

$$-k_1^e\nu'_4 + \nu'_{11} = 0 \tag{A.14}$$

$$-c_2^e\nu'_3 - k_2^e\nu'_5 + \nu'_{12} = 0 \tag{A.15}$$

$$\nu'_7 + \nu'_{13} = 0 \tag{A.16}$$

$$-\omega_g^2 v_6' - 2\xi_g\omega_g v_7' + v_{14}' = 0 \tag{A.17}$$

$$-4\xi_1\omega_1 v_8' - 2(1-\alpha_1)\omega_1^2 v_{11}' + \frac{2\omega_g^2}{u_{y1}} v_{13}' + \frac{4\xi_g\omega_g}{u_{y1}} v_{14}' = 0 \tag{A.18}$$

$$-\alpha_1\omega_1^2 v_2' - 2\xi_1\omega_1 v_9' + v_{10}' - (1-\alpha_1)\omega_1^2 v_{16}' + \frac{\omega_g^2}{u_{y1}} v_{18}' + \frac{2\xi_g\omega_g}{u_{y1}} v_{19}' = 0 \tag{A.19}$$

$$-\alpha_1\omega_1^2 v_3' - \alpha_2\omega_2^2 v_9' - 2(\xi_1\omega_1 + \xi_2\omega_2) v_{10}' - (1-\alpha_2)\omega_2^2 v_{12}' + \frac{\omega_g^2}{u_{y2}} v_{13}' + \frac{2\xi_g\omega_g}{u_{y2}} v_{14}' - (1-\alpha_1)\omega_1^2 v_{21}' + \frac{\omega_g^2}{u_{y1}} v_{23}' + \frac{2\xi_g\omega_g}{u_{y1}} v_{24}' = 0 \tag{A.20}$$

$$-\alpha_1\omega_1^2 v_4' - c_1^e v_8' - (k_1^e + 2\xi_1\omega_1) v_{11}' - (1-\alpha_1)\omega_1^2 v_{25}' + \frac{\omega_g^2}{u_{y1}} v_{27}' + \frac{2\xi_g\omega_g}{u_{y1}} v_{28}' = 0 \tag{A.21}$$

$$-\alpha_1\omega_1^2 v_5' - c_2^e v_{10}' - (k_2^e + 2\xi_1\omega_1) v_{12}' - (1-\alpha_1)\omega_1^2 v_{26}' + \frac{\omega_g^2}{u_{y1}} v_{30}' + \frac{2\xi_g\omega_g}{u_{y1}} v_{31}' = 0 \tag{A.22}$$

$$-\alpha_1\omega_1^2 v_6' + 2\xi_1\omega_1 v_{13}' + v_{14}' - (1-\alpha_1)\omega_1^2 v_{27}' + \frac{\omega_g^2}{u_{y1}} v_{32}' = 0 \tag{A.23}$$

$$-\alpha_1\omega_1^2 v_7' - \omega_g^2 v_{13}' - 2(\xi_1\omega_1 + \xi_g\omega_g) v_{14}' - (1-\alpha_1)\omega_1^2 v_{28}' + \frac{2\xi_g\omega_g}{u_{y1}} v_{33}' = 0 \tag{A.24}$$

$$-\alpha_2\omega_2^2 v_{15}' - (1-\alpha_2)\omega_2^2 v_{17}' + \frac{\omega_g^2}{u_{y2}} v_{18}' + \frac{2\xi_g\omega_g}{u_{y2}} v_{19}' + v_{20}' = 0 \tag{A.25}$$

$$-c_1^e v_9' - k_1^e v_{16}' + v_{21}' = 0 \tag{A.26}$$

$$-k_2^e v_{17}' + v_{22}' = 0 \tag{A.27}$$

$$v_{19}' + v_{23}' = 0 \tag{A.28}$$

$$-\omega_g^2 v_{18}' - 2\xi_g\omega_g v_{19}' + v_{24}' = 0 \tag{A.29}$$

$$-4\xi_2\omega_2 v'_{20} - 2(1-\alpha_2)\omega_2^2 v'_{22} + \frac{2\omega_g^2}{u_{y2}} v'_{23} + \frac{4\xi_g\omega_g}{u_{y2}} v'_{24} = 0 \tag{A.30}$$

$$-c_1^e v'_{10} - \alpha_2\omega_2^2 v'_{16} - (k_1^e + 2\xi_2\omega_2) v'_{21} - \alpha_2\omega_2^2 v'_{26} + \frac{\omega_g^2}{u_{y2}} v'_{27} + \frac{2\xi_g\omega_g}{u_{y2}} v'_{28} = 0 \tag{A.31}$$

$$-\alpha_2\omega_2^2 v'_{17} - c_2^e v'_{20} - (k_2^e + 2\xi_2\omega_2) v'_{22} - (1-\alpha_2)\omega_2^2 v'_{29} + \frac{\omega_g^2}{u_{y2}} v'_{30} + \frac{2\xi_g\omega_g}{u_{y2}} v'_{31} = 0 \tag{A.32}$$

$$-\alpha_2\omega_2^2 v'_{18} + v'_{24} - 2\xi_2\omega_2 v'_{23} - (1-\alpha_2)\omega_2^2 v'_{30} + \frac{\omega_g^2}{u_{y2}} v'_{32} = 0 \tag{A.33}$$

$$-\alpha_2\omega_2^2 v'_{19} - \omega_g^2 v'_{23} - 2(\xi_g\omega_g + \xi_2\omega_2) v'_{24} - (1-\alpha_2)\omega_2^2 v'_{31} + \frac{2\xi_g\omega_g}{u_{y2}} v'_{33} = 0 \tag{A.34}$$

$$-2c_1^e v'_{11} - 2k_1^e v'_{25} = 0 \tag{A.35}$$

$$-c_1^e v'_{12} - c_2^e v'_{21} - (k_1^e + k_2^e) v'_{26} = 0 \tag{A.36}$$

$$-c_1^e v'_{13} - k_1^e v'_{27} + v'_{28} = 0 \tag{A.37}$$

$$-c_1^e v'_{14} - \omega_g^2 v'_{27} - (k_1^e + 2\xi_g\omega_g) v'_{28} = 0 \tag{A.38}$$

$$-2c_2^e v'_{22} - 2k_2^e v'_{29} = 0 \tag{A.39}$$

$$-c_2^e v'_{23} - k_2^e v'_{30} + v'_{31} = 0 \tag{A.40}$$

$$-c_2^e v'_{24} - \omega_g^2 v'_{30} - (2\xi_g\omega_g + k_2^e) v'_{31} = 0 \tag{A.41}$$

$$-\omega_g^2 v'_{32} + v'_{33} = 0 \tag{A.42}$$

$$4\xi_g\omega_g v'_{33} = 2\pi S_0 \tag{A.43}$$

APPENDIX B

Plots for Correlation Coefficient

A series of correlation coefficient plots are presents in this appendix. The correlation coefficient ρ obtained from these plots are used in the estimation of the critical gap: g_{cr} (see Fig. 7.1):

$$g_{cr} = \sqrt{u_1^2 + u_2^2 - 2u_1 u_2 \rho} \tag{B.1}$$

as described in Section 4. Where u_1 and u_2 are the maximum expected inelastic displacements of structure 1 and 2, respectively. To obtain the inelastic displacements (u_1 and u_2), the values from the elastic displacement design spectra (u_{1e} and u_{2e}) to be multiplied by the inelastic displacement amplification factors (a_{b1} and a_{b2}) presented in Figs. B.1 to B.4.

The inelastic amplification factors (a_{b1} and a_{b2}) are calculated from the rate of the variance in displacements of the bilinear system to the variance in displacements of on elastic system with the same initial dynamic characteristics:

$$a_{bi} = \frac{\sigma_{\mu i} u_{yi}}{\sigma_{ue}} = \sqrt{\frac{E\{\mu_i^2\} u_{yi}^2}{E\{U_e^2\}}} \tag{B.2}$$

where $\sigma_{\mu i}$ is the standard deviation for the ductility of the bilinear structure "i", U_{yi} is the yield displacement of the bilinear structure "i", σ_{ue} is the standard deviation of the elastic structure "i".

The correlation coefficient (ρ) is calculated as the ratio of the cross variance in the inelastic displacement of the two bilinear structures, normalized by the product of the standard deviations:

$$\rho = \frac{E\{\mu_1 \mu_2\} u_{y1} u_{y2}}{\sqrt{E\{\mu_1^2\} E\{\mu_2^2\} u_{y1}^2 u_{y2}^2}} \tag{B.3}$$

where μ_1 and μ_2 are the ductility of the bilinear structures, and u_{y1} and u_{y2}, the corresponding yield displacements. Note that the yield displacements cancel in the equation.

The correlation coefficient is also used in the approximate calculation of pounding effects as described in Section 5.5. Furthermore, the correlation coefficient is also necessary for some of the preliminary estimates on the effectiveness of bumper dampers, as described in Section 6.3, and for initial estimates for the minimum damping or stiffness necessary to alter the dynamic characteristics of the systems and avoid pounding, as indicated in Section 6.4.

The set of plots presents herein may be classified according to the characteristics of the systems:

- Linear: five critical damping ratios are considered: 0.1%, 2%, 5%, 10% and 20%.
- Bilinear: a critical damping ratio of 2% is assigned to the structures. Two type of analysis are considered:
    a) Maximum probable ductility: five probable ductility are considered: 1, 1.5, 2, 3, and 4.
    b) Reduction factors from maximum probable elastic demand: five reduction factors were considered: 1, 1.5, 2, 3 and 4.

According to the frequency content of the input motion:

- Broad band: filtered white noise with a critical damping ratio in the filter of $\xi_g = 0.06$.
- Narrow band: filtered white noise with a critical damping ratio in the filter of $\xi_g = 0.05$.

The amplification plots are presented in Fig. B.1 to B.4, and the plots for the correlation coefficient are presented in Figs. B.5 to B.34 (see Table B.1). The correlation coefficient plots are presented with contour lines in as array of period of structure one to period of structure two, with the periods normalized to the predominant period of the input motion. Since only a few contour lines are shown, linear interpolation may be performed, although taking the lowest value of the neighboring contour lines is suggested.

Plots for different set of parameters may be generated according to the theory presented in Section 4.4 and Appendix A.

Elastic Systems						
	Ampl.	$\xi = 0.001$	$\xi = 0.02$	$\xi = 0.05$	$\xi = 0.10$	$\xi = 0.20$
Broad Band		B.5	B.6	B.7	B.8	B.9
Narrow Band		B.10	B.11	B.12	B.13	B.14
Bilinear Systems						
	Ampl.	$\mu = 1$	$\mu = 1.5$	$\mu = 2$	$\mu = 3$	$\mu = 4$
Broad Band	B.1	B.15	B.16	B.17	B.18	B.19
Narrow Band	B.2	B.20	B.21	B.22	B.23	B.24
Bilinear Systems						
	Ampl.	$R = 1$	$R = 1.5$	$R = 2$	$R = 3$	$R = 4$
Broad Band	B.3	B.25	B.26	B.27	B.28	B.29
Narrow Band	B.4	B.30	B.31	B.32	B.33	B.34

Table B.1 Summary of plots derived for different structural characteristics.

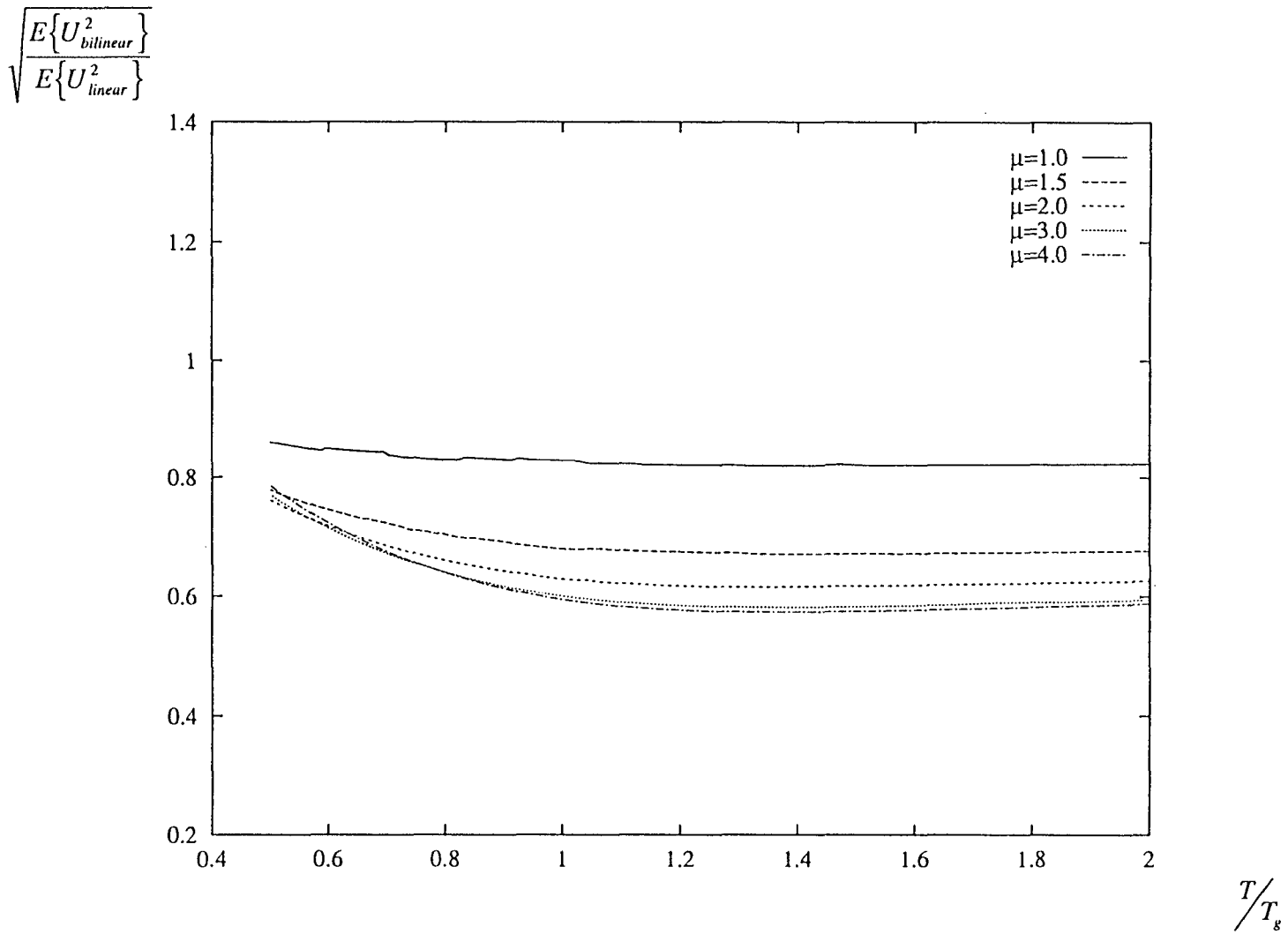

Fig. B.1 Amplification factor for broad band input and maximum probable ductility levels.

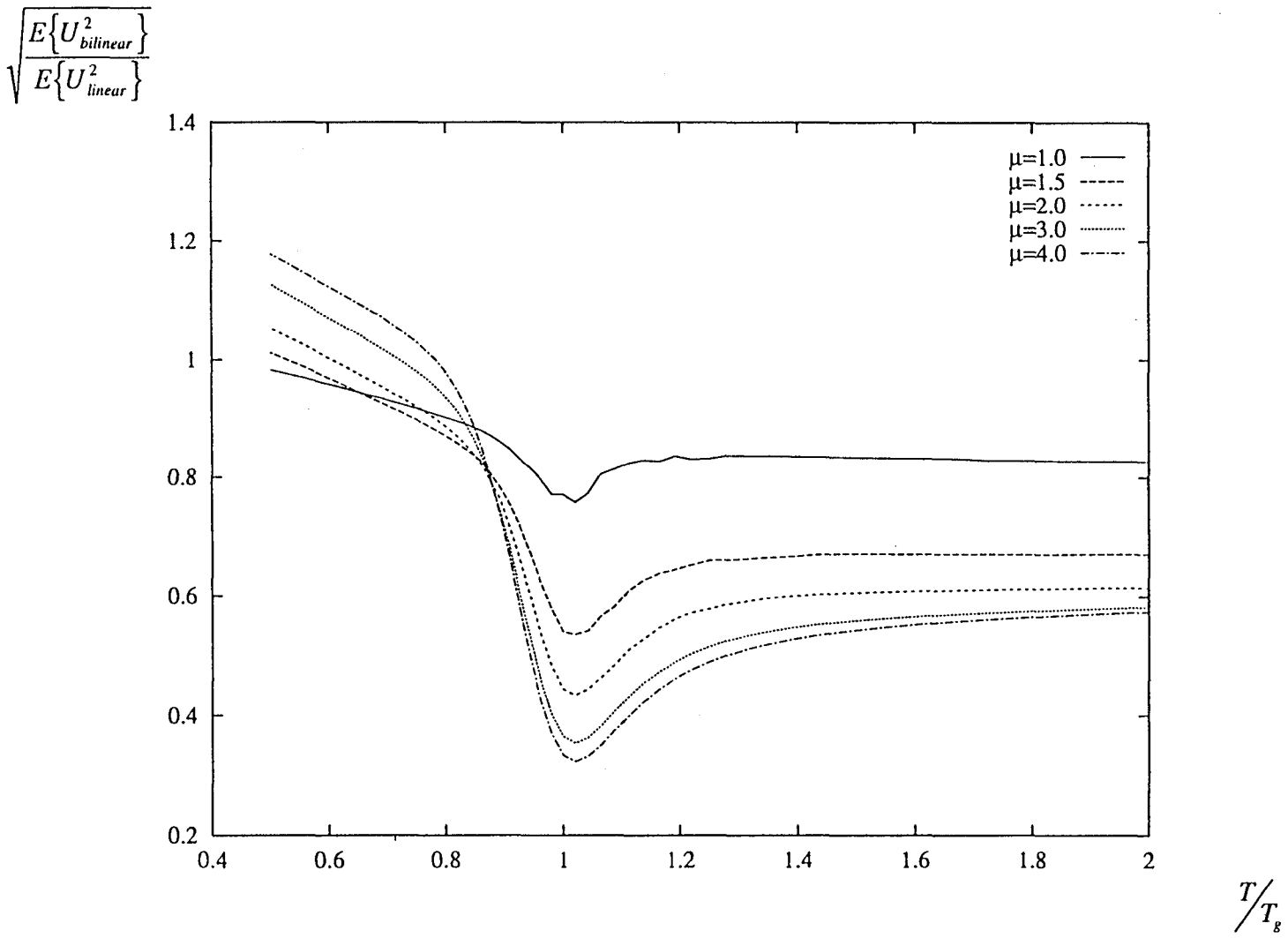

Fig. B.2 Amplification factor for narrow band input and maximum probable ductility levels.

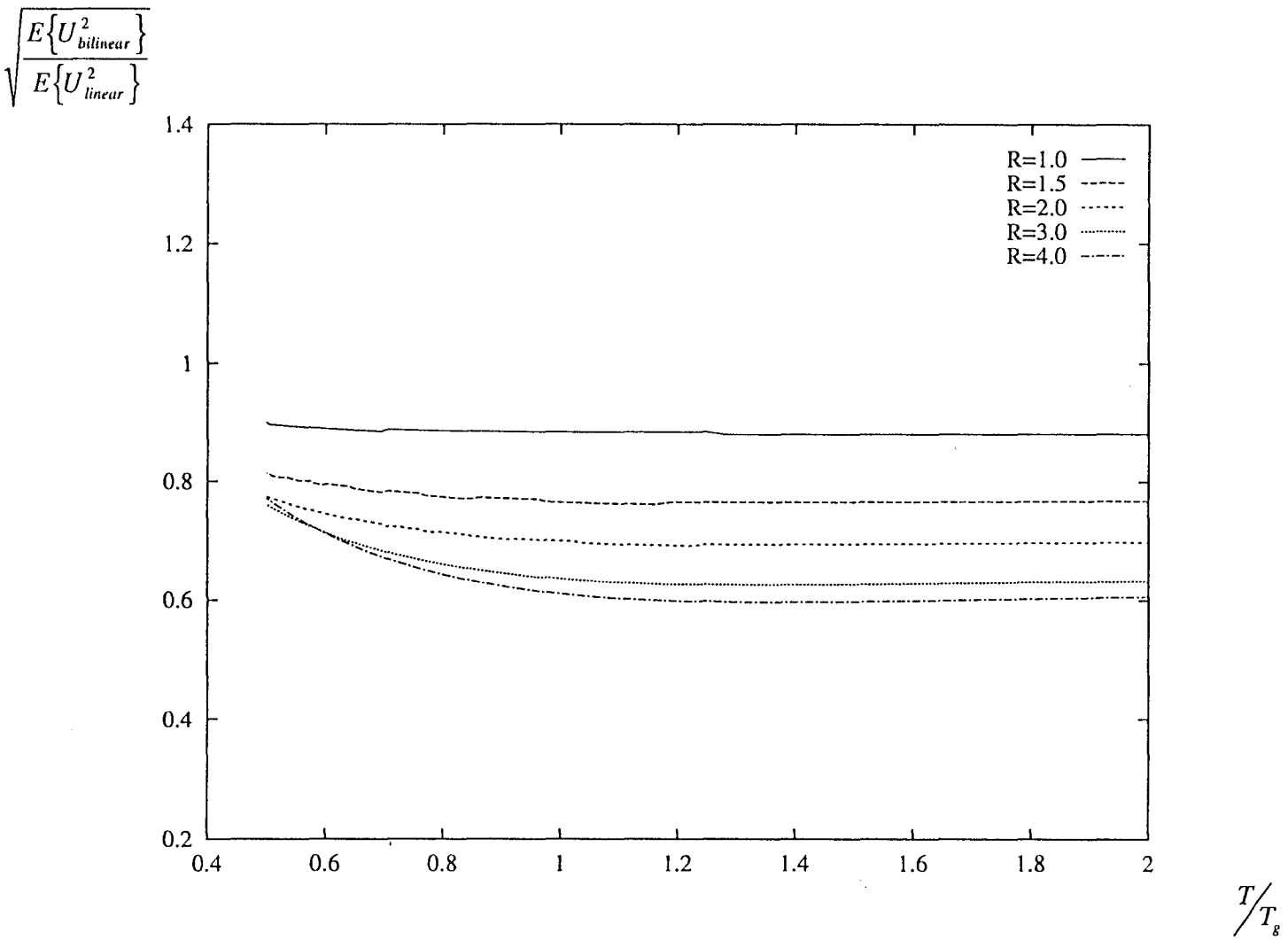

Fig. B.3 Amplification factor for broad band input and different reduction factors.

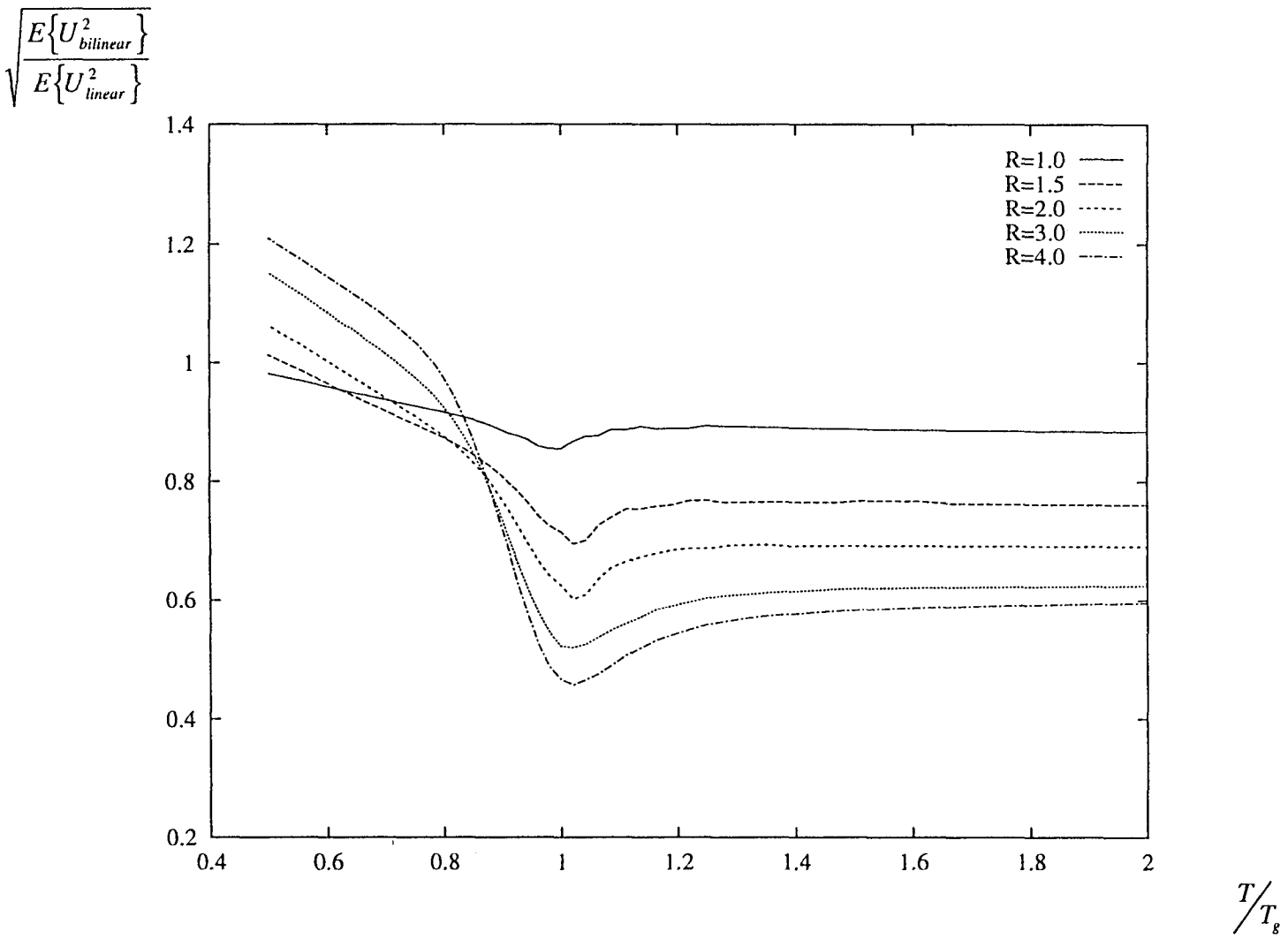

Fig. B.4 Amplification factor for narrow band input and different reduction factors.

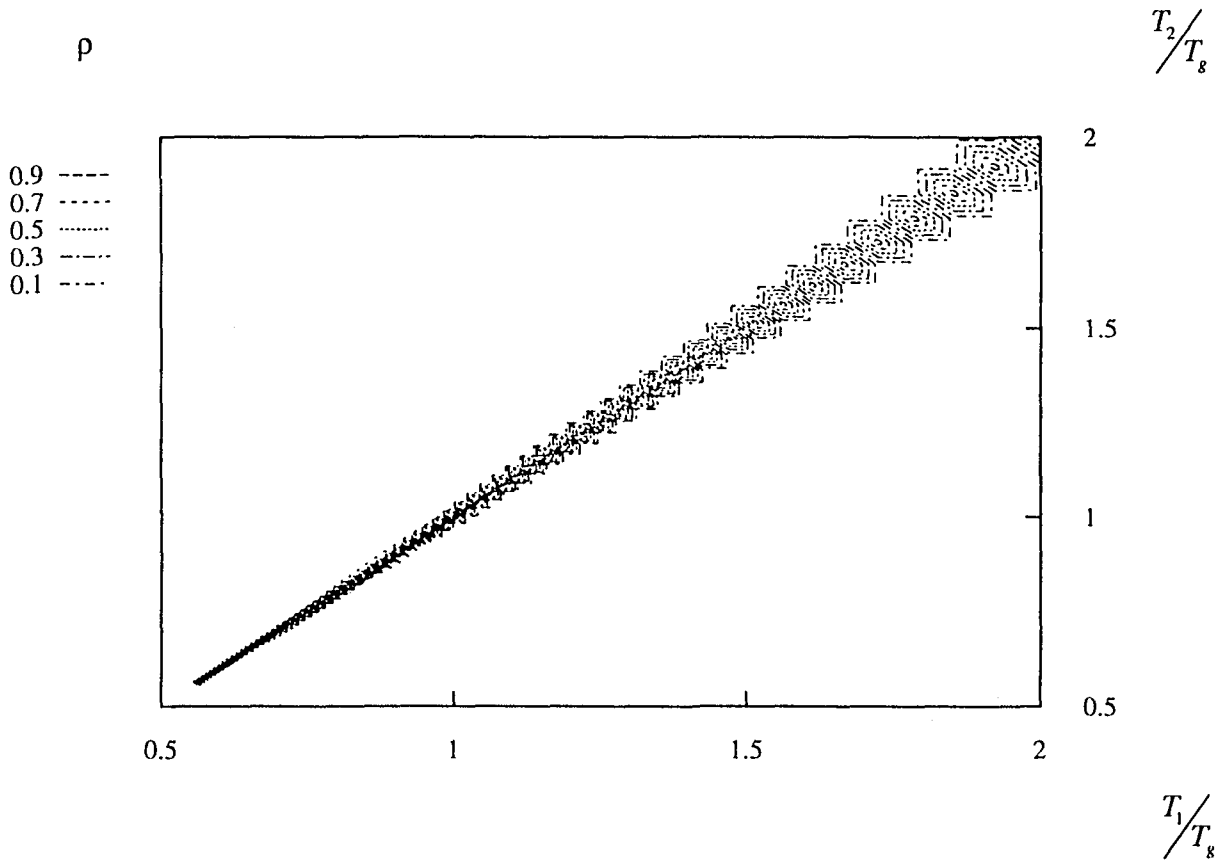

Fig. B.5 Correlation coefficient for elastic systems subjected to a broad band input ($\xi_1 = \xi_2 = 0.001$).

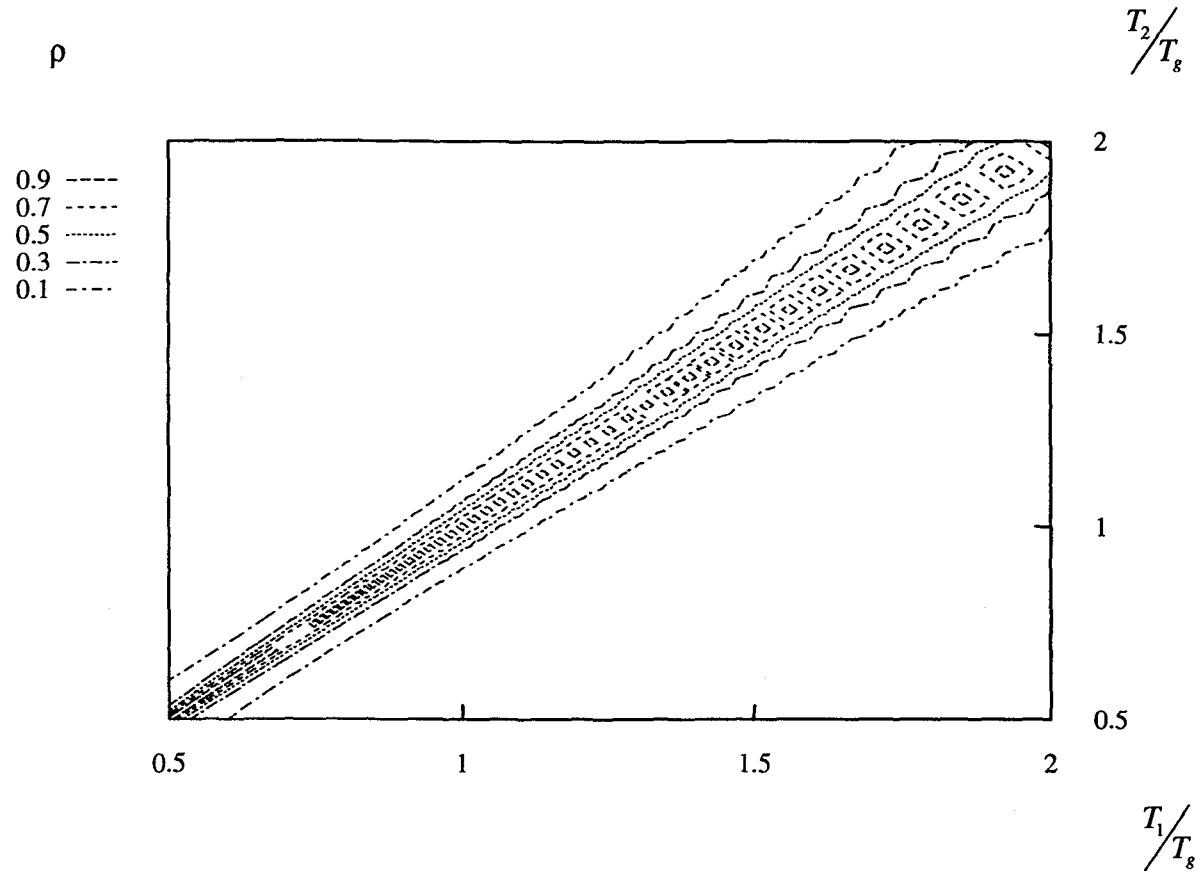

Fig. B.6 Correlation coefficient for elastic systems subjected to a broad band input ($\xi_1 = \xi_2 = 0.02$).

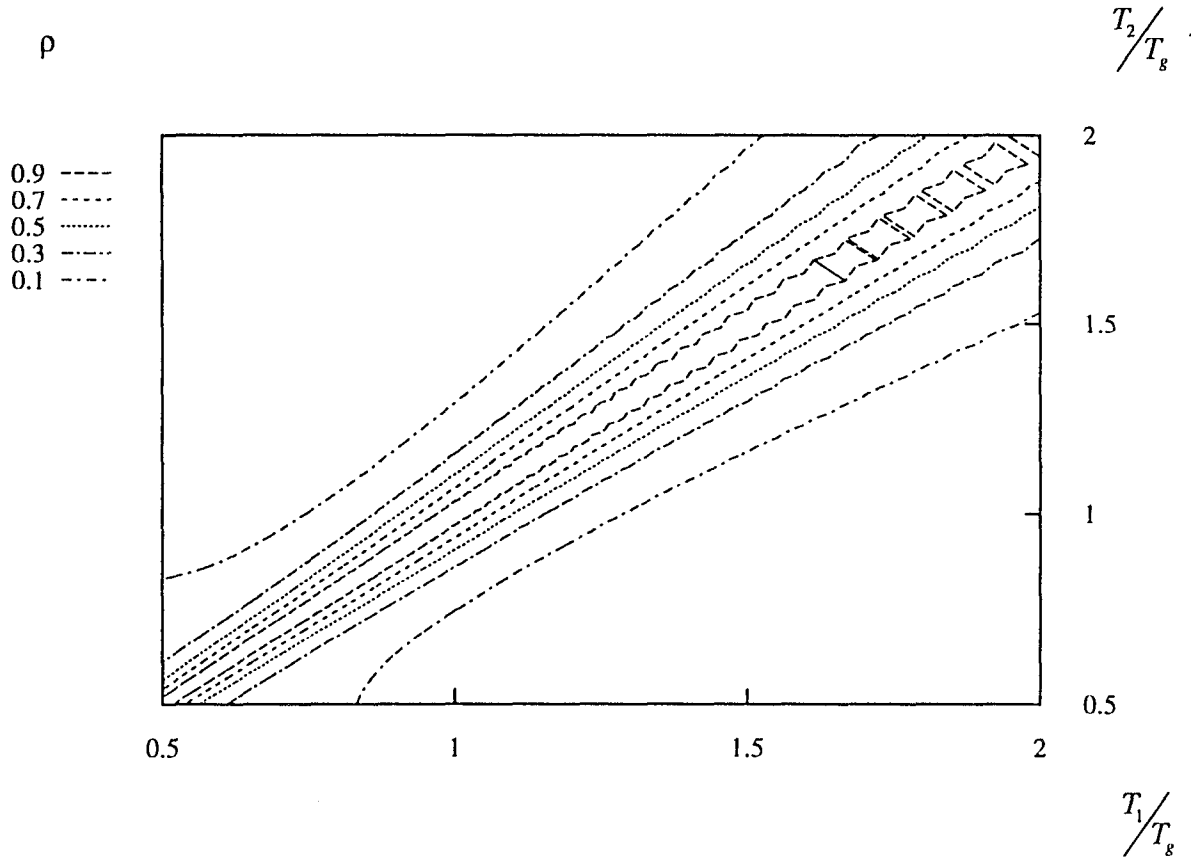

Fig. B.7 Correlation coefficient for elastic systems subjected to a broad band input ($\xi_1 = \xi_2 = 0.05$).

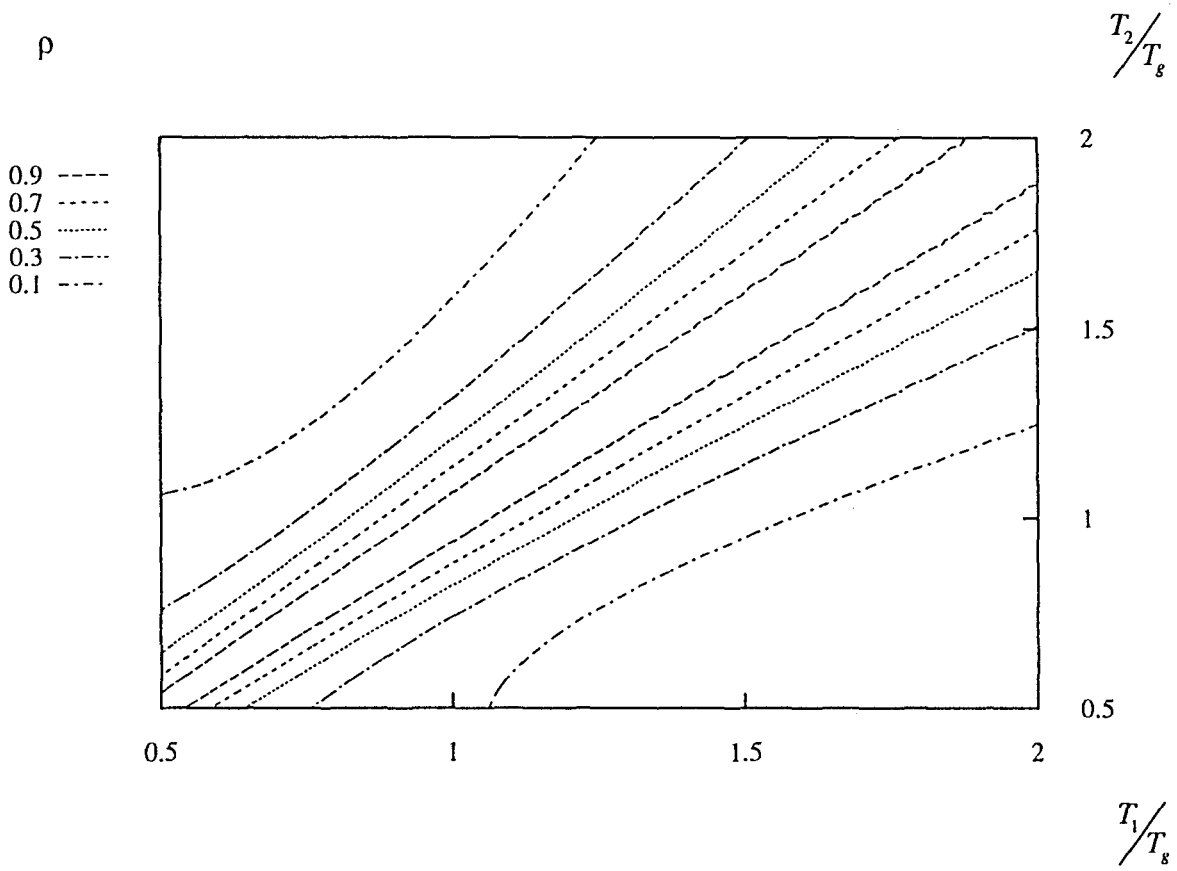

Fig. B.8 Correlation coefficient for elastic systems subjected to a broad band input ($\xi_1 = \xi_2 = 0.10$).

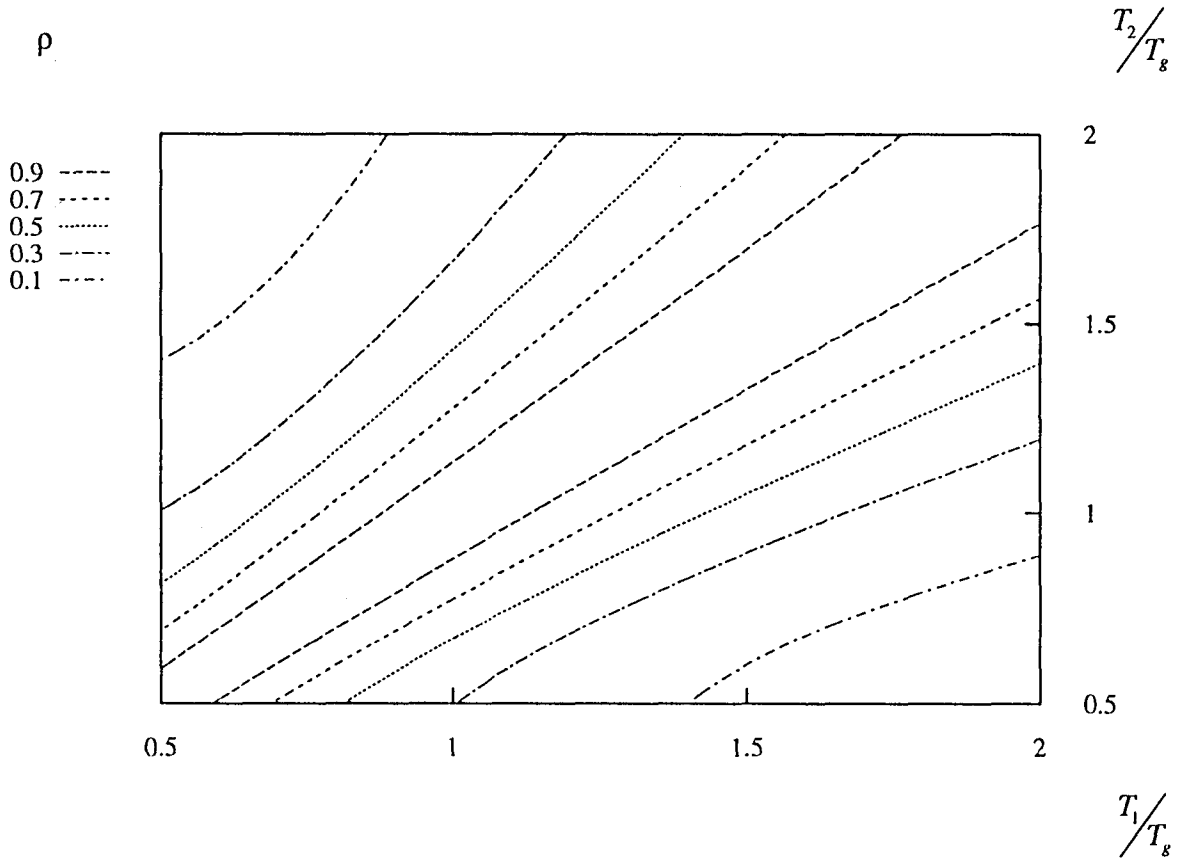

Fig. B.9 Correlation coefficient for elastic systems subjected to a broad band input ($\xi_1 = \xi_2 = 0.20$).

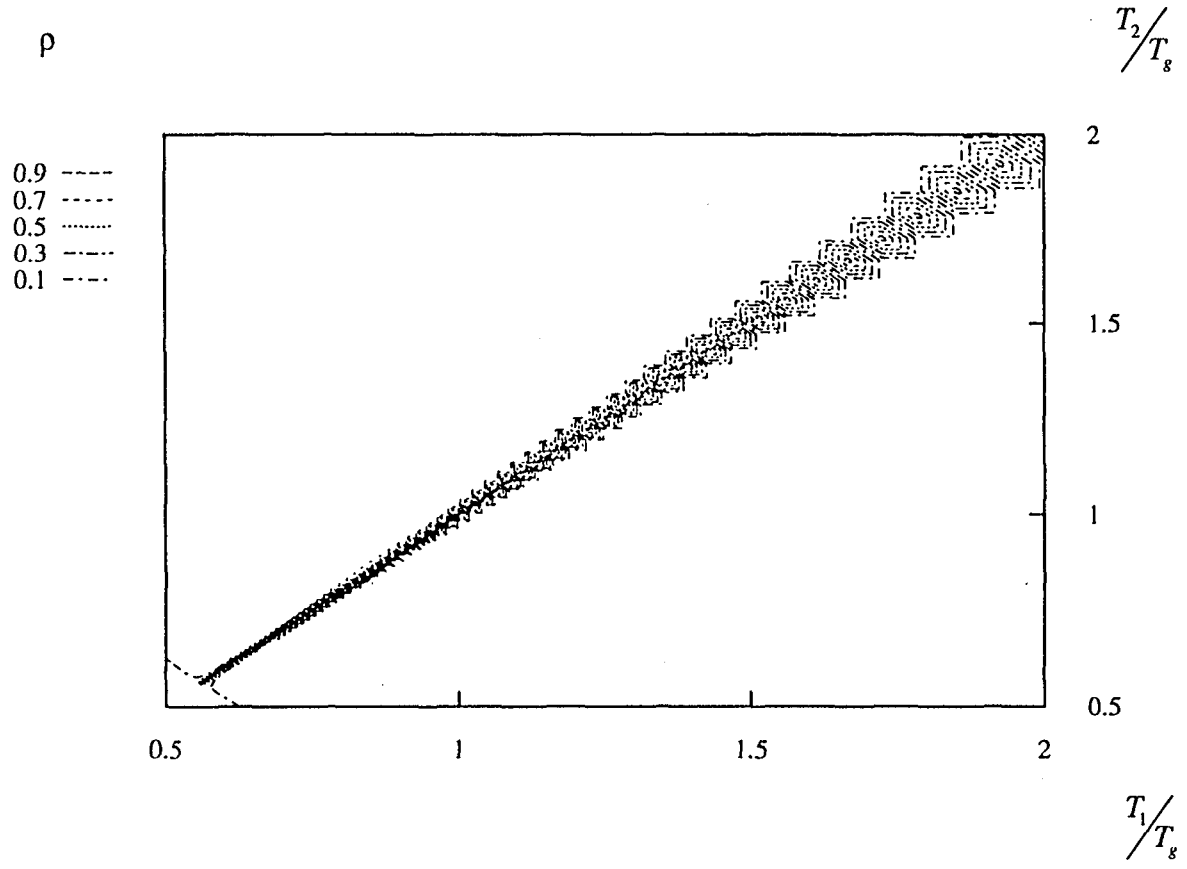

Fig. B.10 Correlation coefficient for elastic systems subjected to a narrow band input ($\xi_1 = \xi_2 = 0.001$).

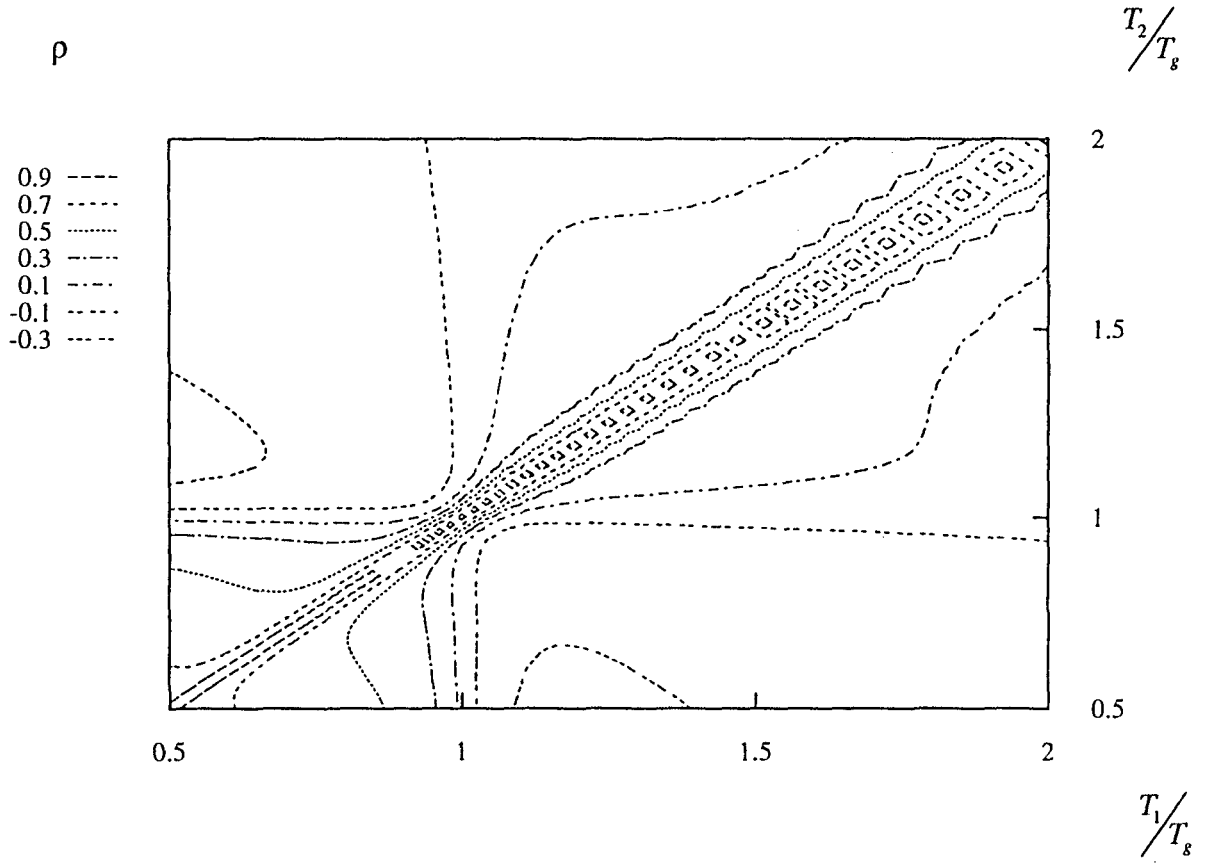

Fig. B.11 Correlation coefficient for elastic systems subjected to a narrow band input ($\xi_1 = \xi_2 = 0.02$).

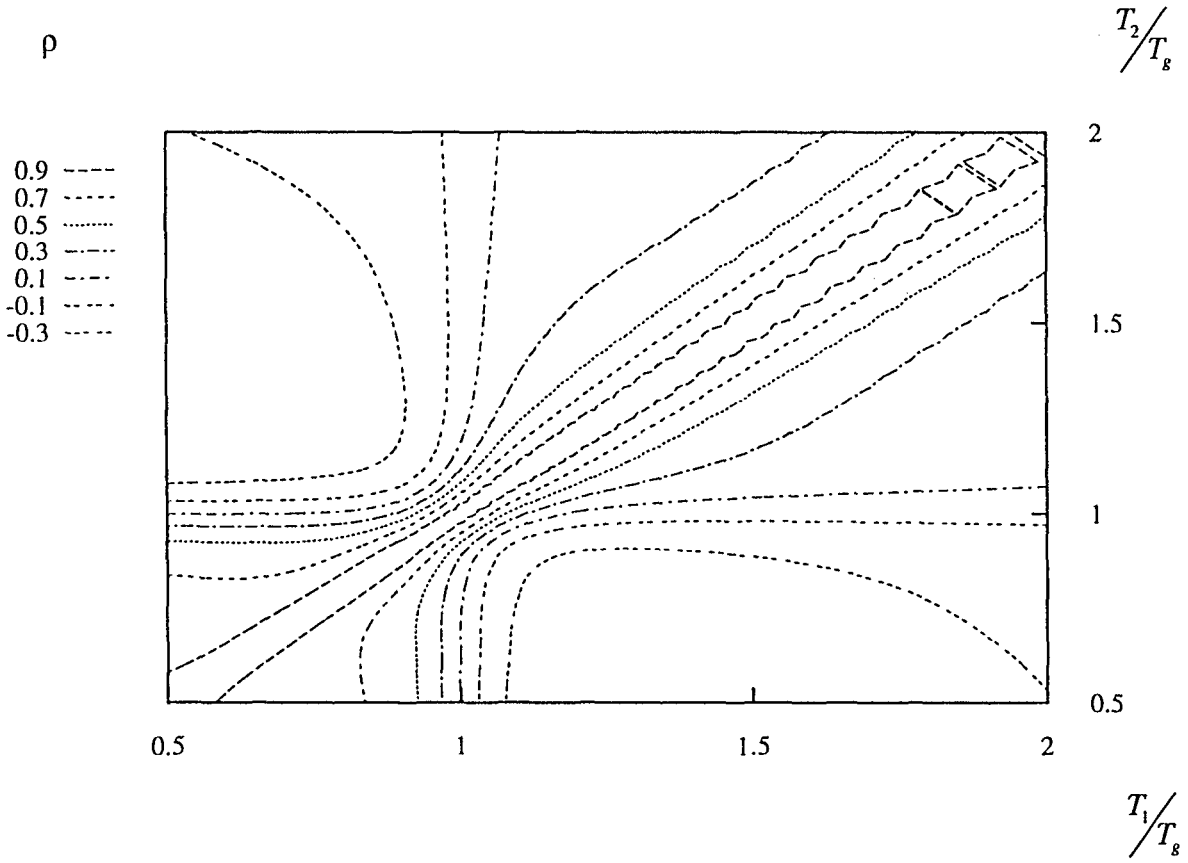

Fig. B.12 Correlation coefficient for elastic systems subjected to a narrow band input ($\xi_1 = \xi_2 = 0.05$).

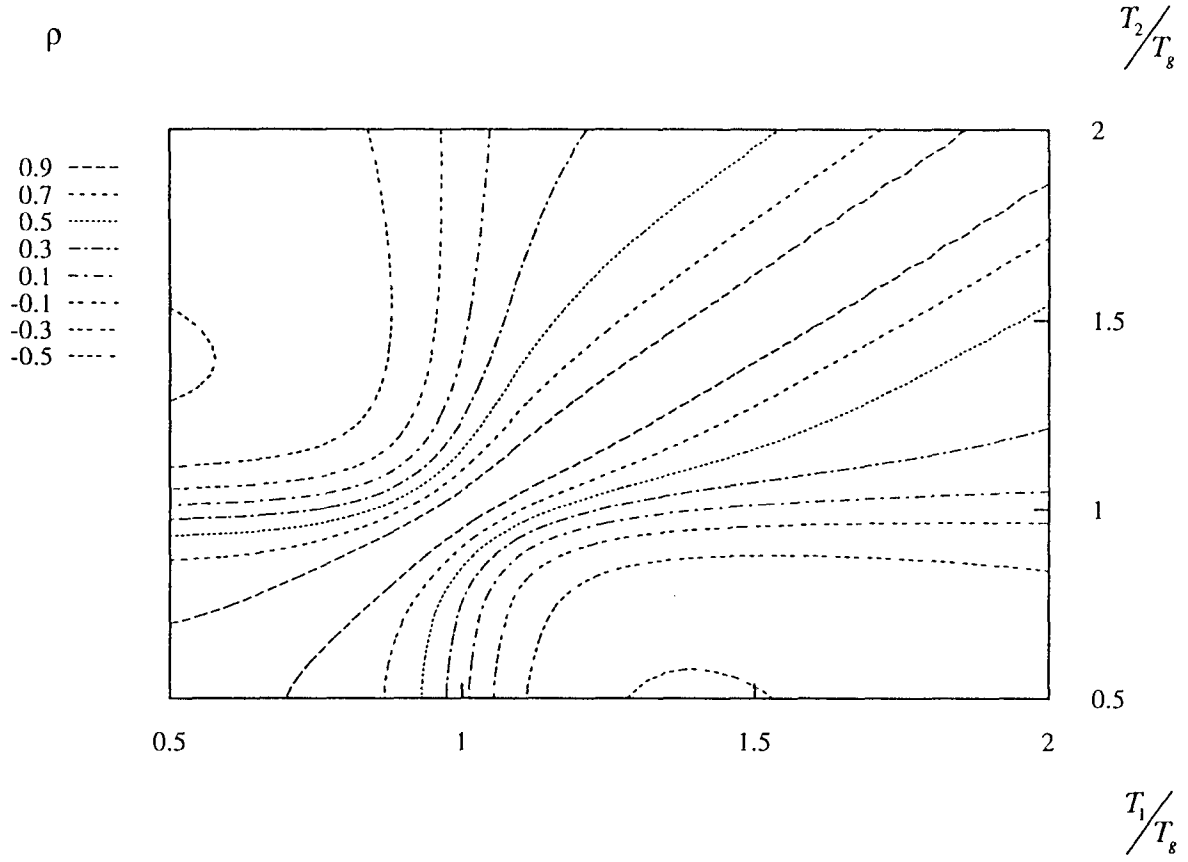

Fig. B.13 Correlation coefficient for elastic systems subjected to a narrow band input ($\xi_1 = \xi_2 = 0.10$).

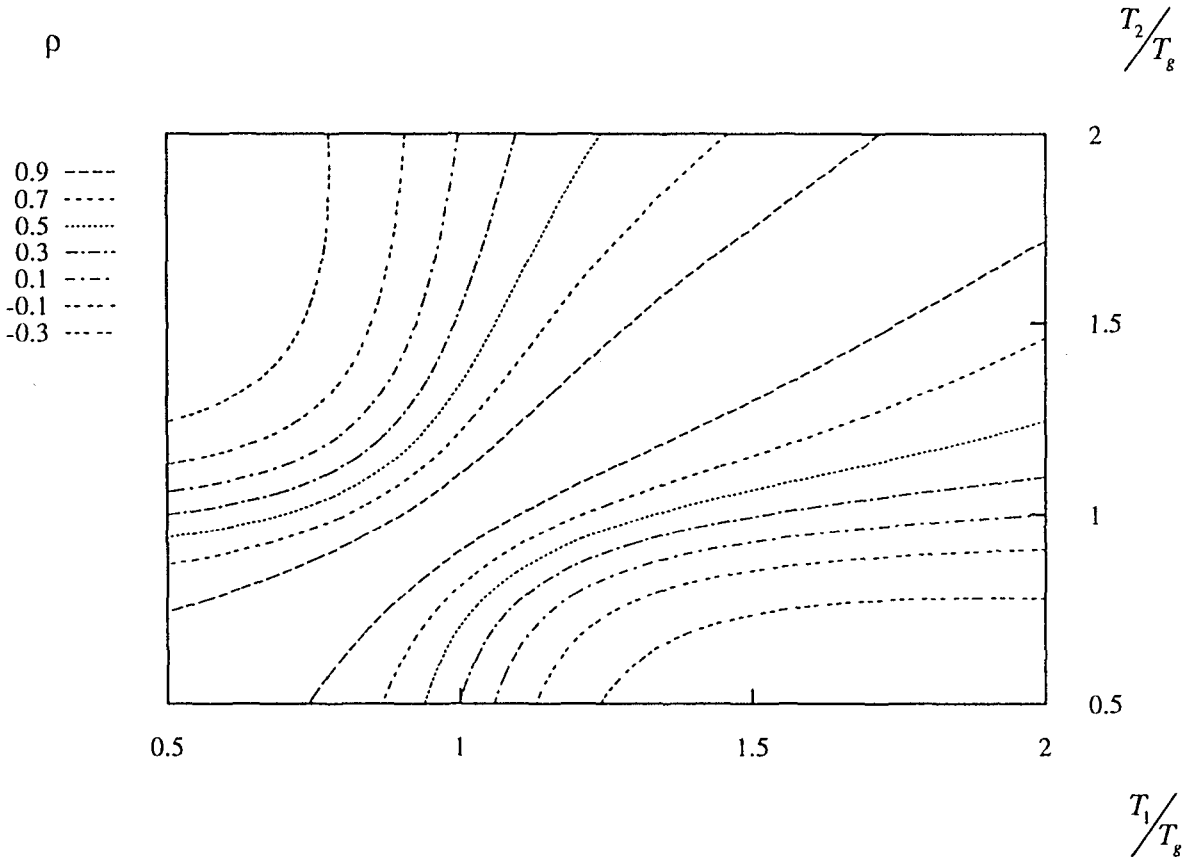

Fig. B.14 Correlation coefficient for elastic systems subjected to a narrow band input ($\xi_1 = \xi_2 = 0.20$).

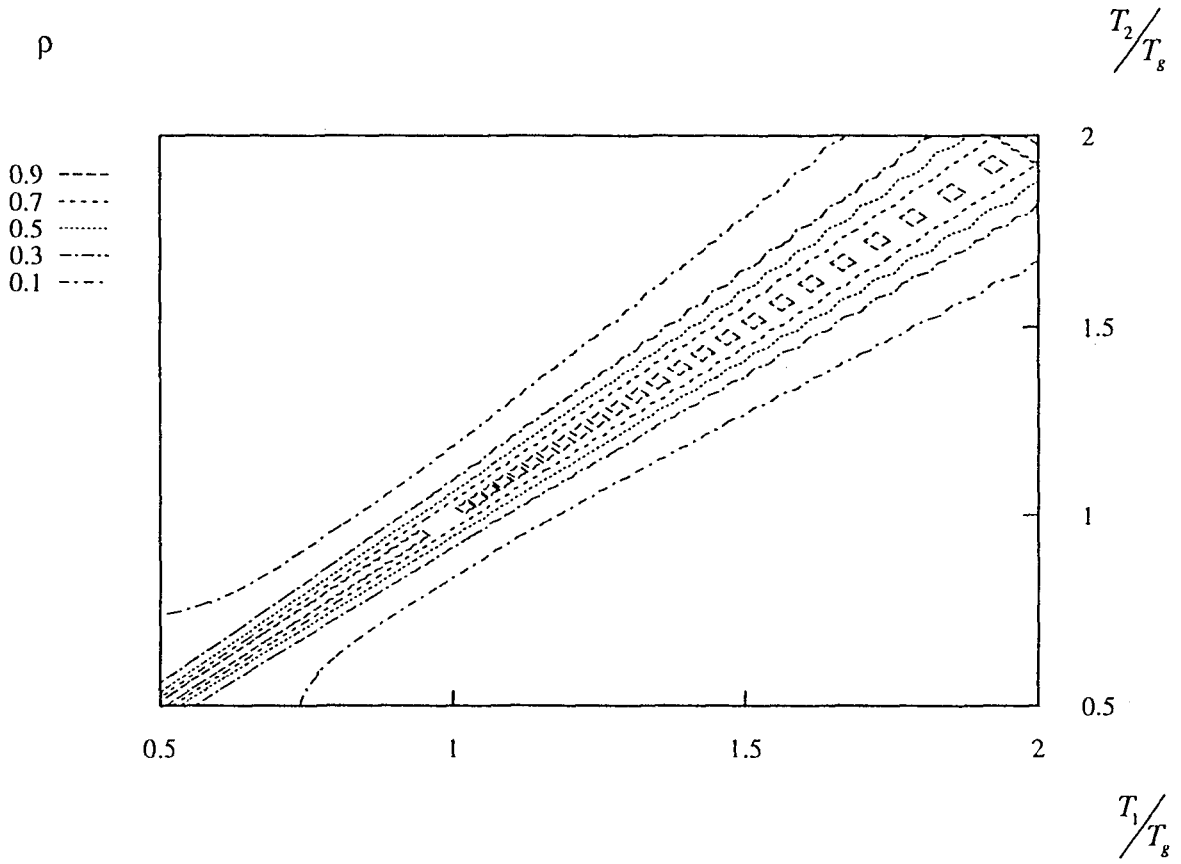

Fig. B.15 Correlation coefficient for bilinear systems subjected to a broad band input ($\mu_1 = \mu_2 = 1$).

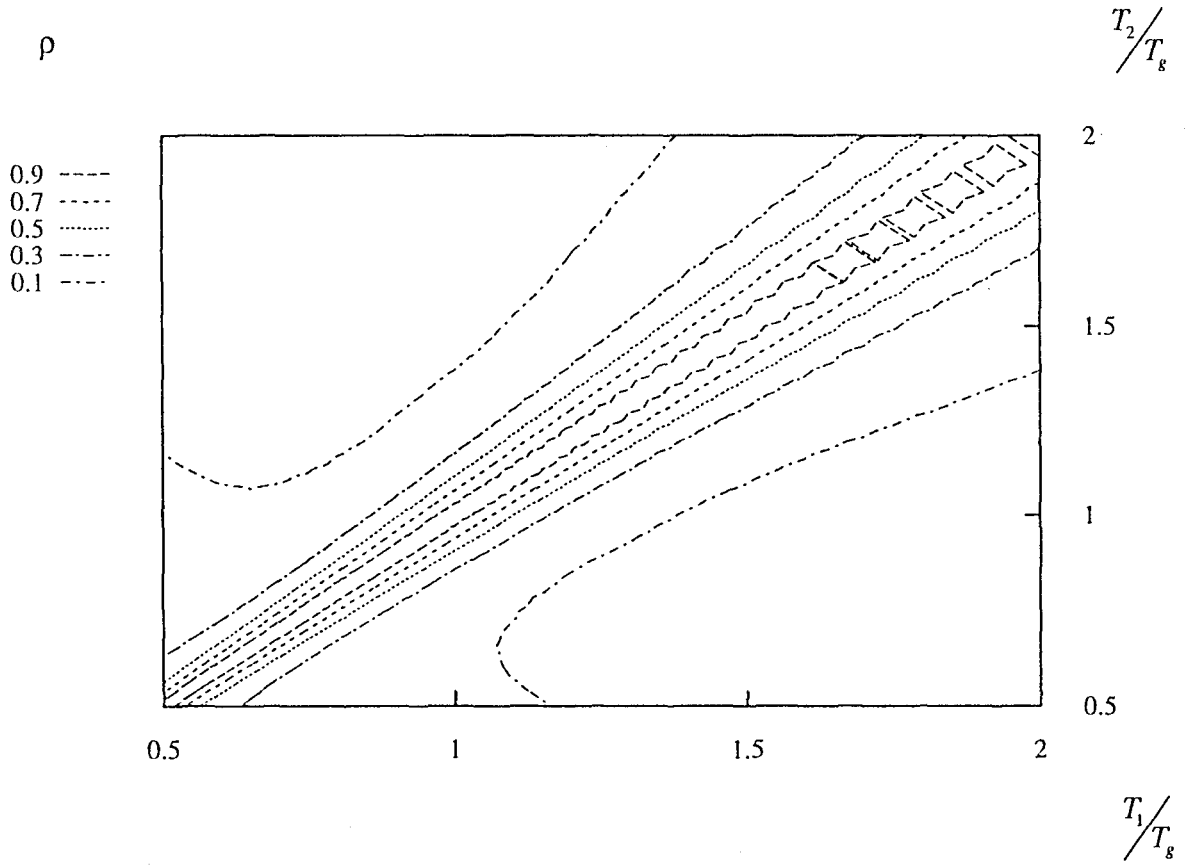

Fig. B.16 Correlation coefficient for bilinear systems subjected to a broad band input ($\mu_1 = \mu_2 = 1.5$).

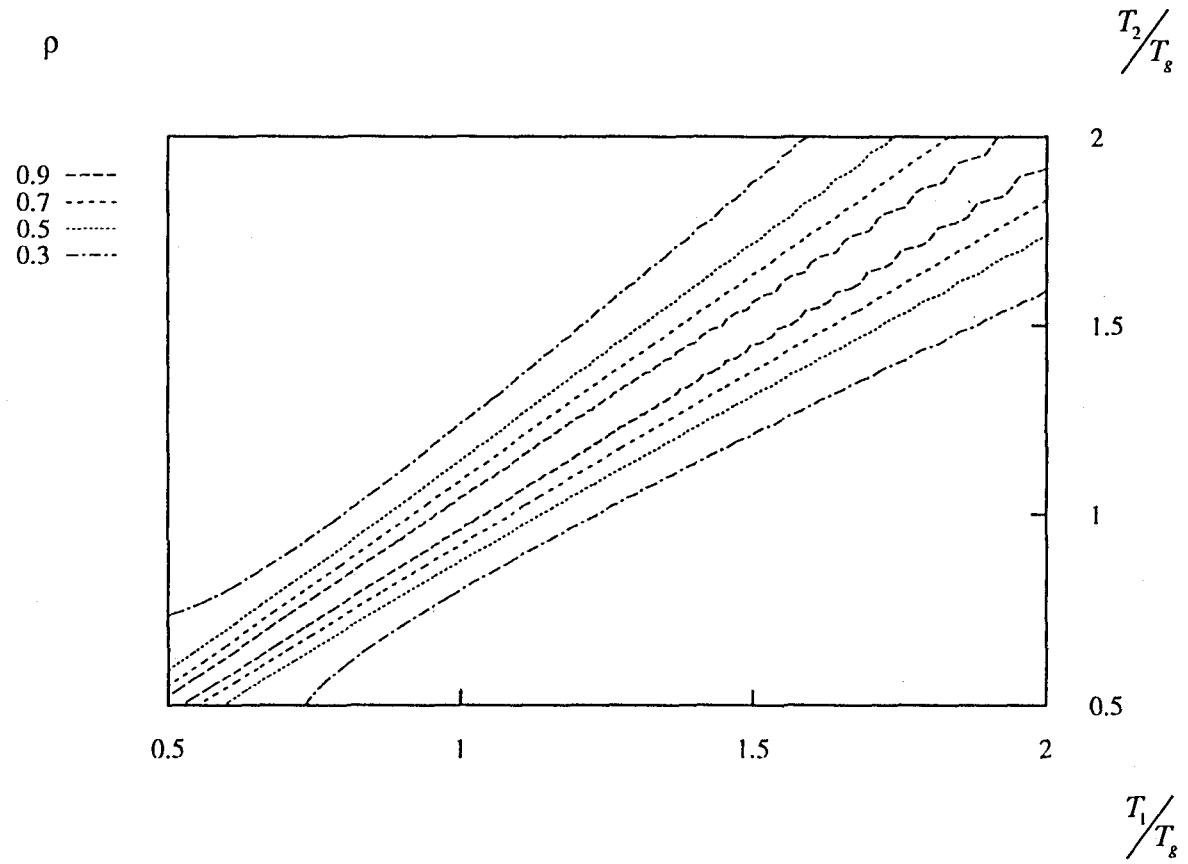

Fig. B.17 Correlation coefficient for bilinear systems subjected to a broad band input ($\mu_1 = \mu_2 = 2$).

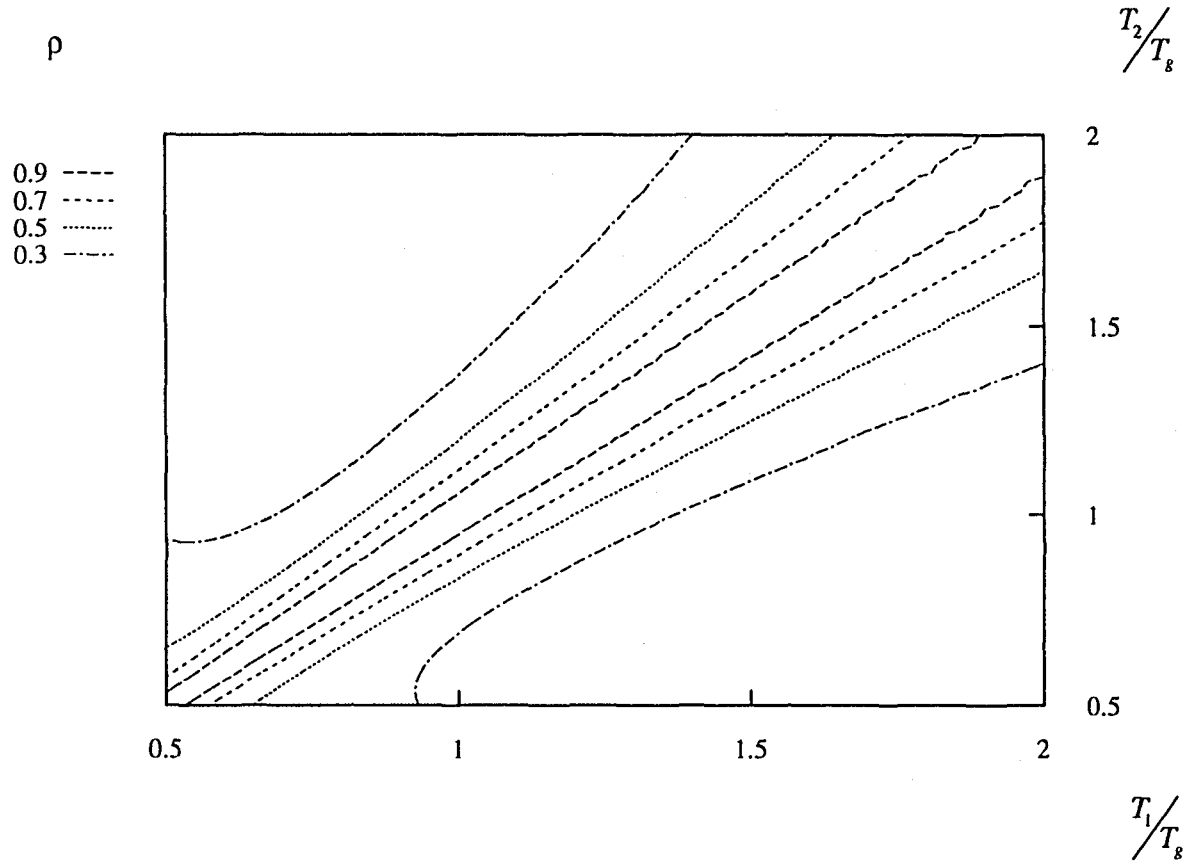

Fig. B.18 Correlation coefficient for bilinear systems subjected to a broad band input ($\mu_1 = \mu_2 = 3$).

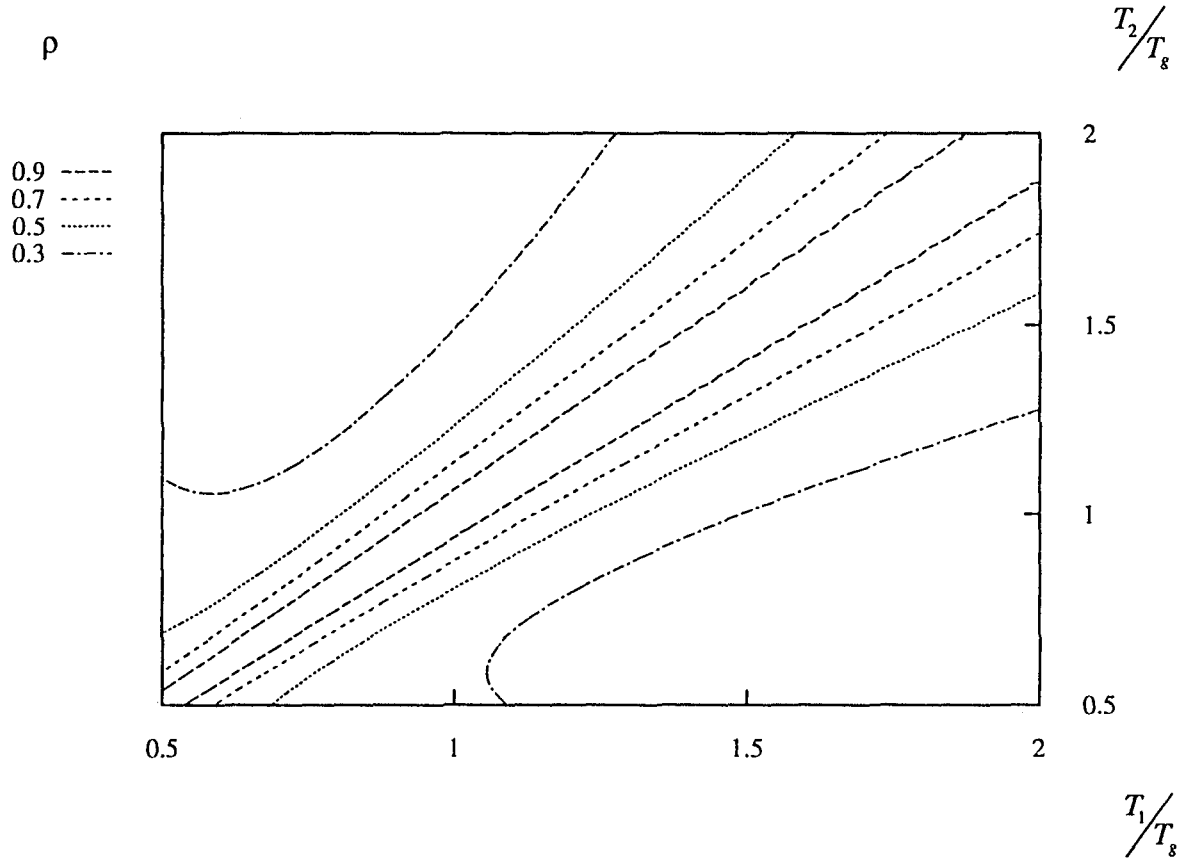

Fig. B.19 Correlation coefficient for bilinear systems subjected to a broad band input ($\mu_1 = \mu_2 = 4$).

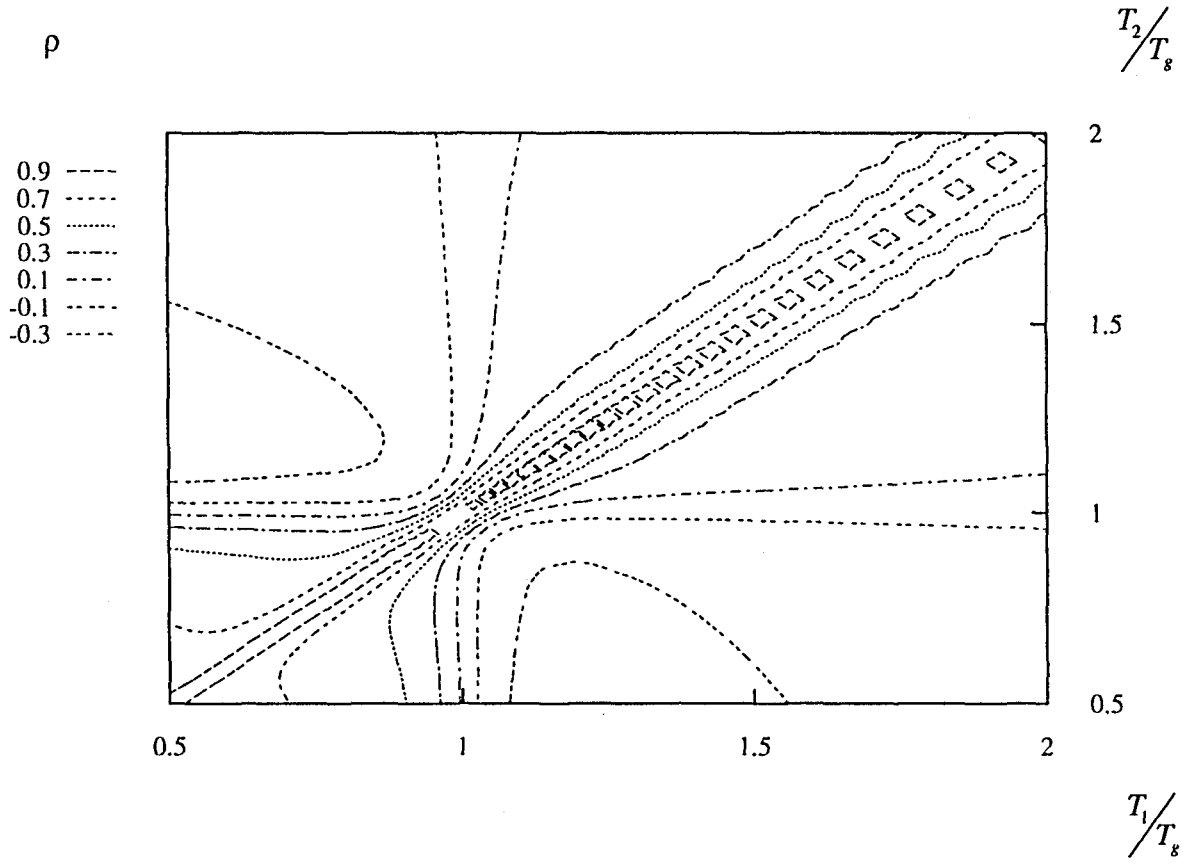

Fig. B.20 Correlation coefficient for bilinear systems subjected to a narrow band input ($\mu_1 = \mu_2 = 1$).

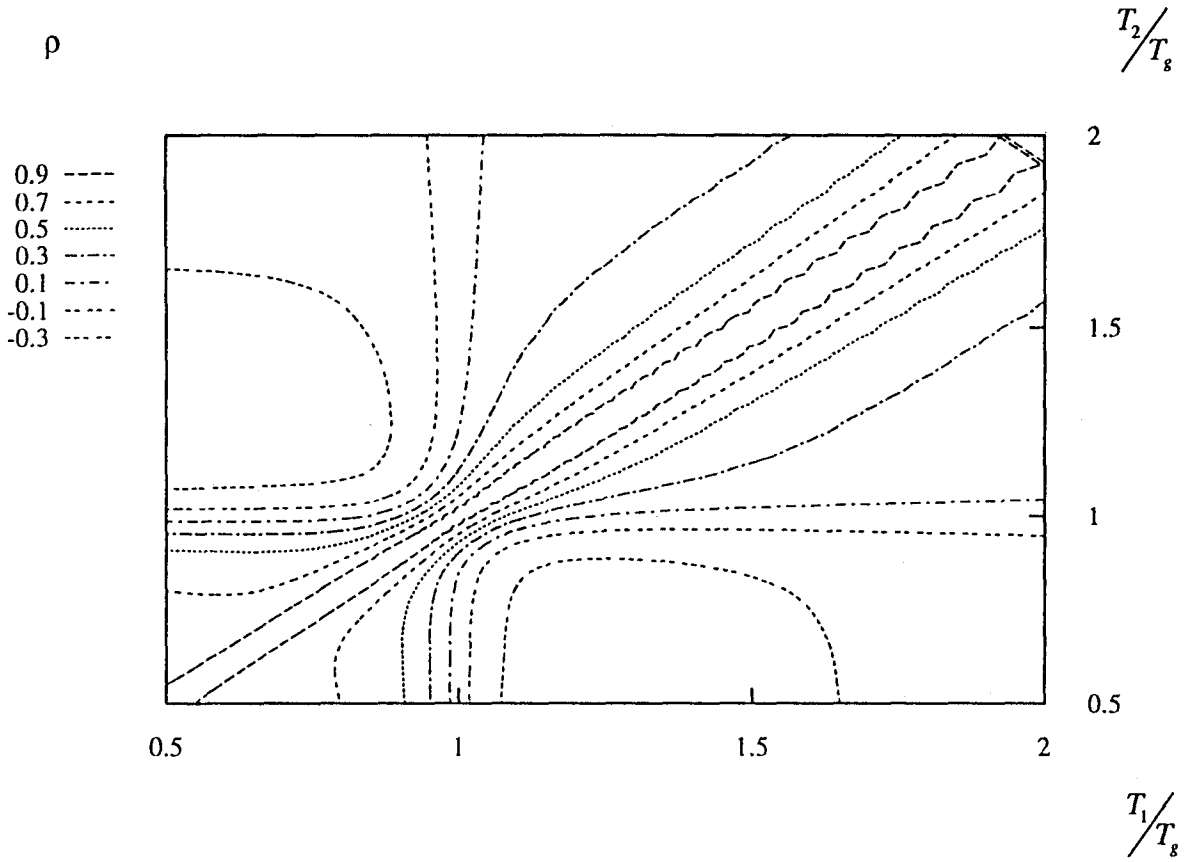

Fig. B.21 Correlation coefficient for bilinear systems subjected to a narrow band input ($\mu_1 = \mu_2 = 1.5$).

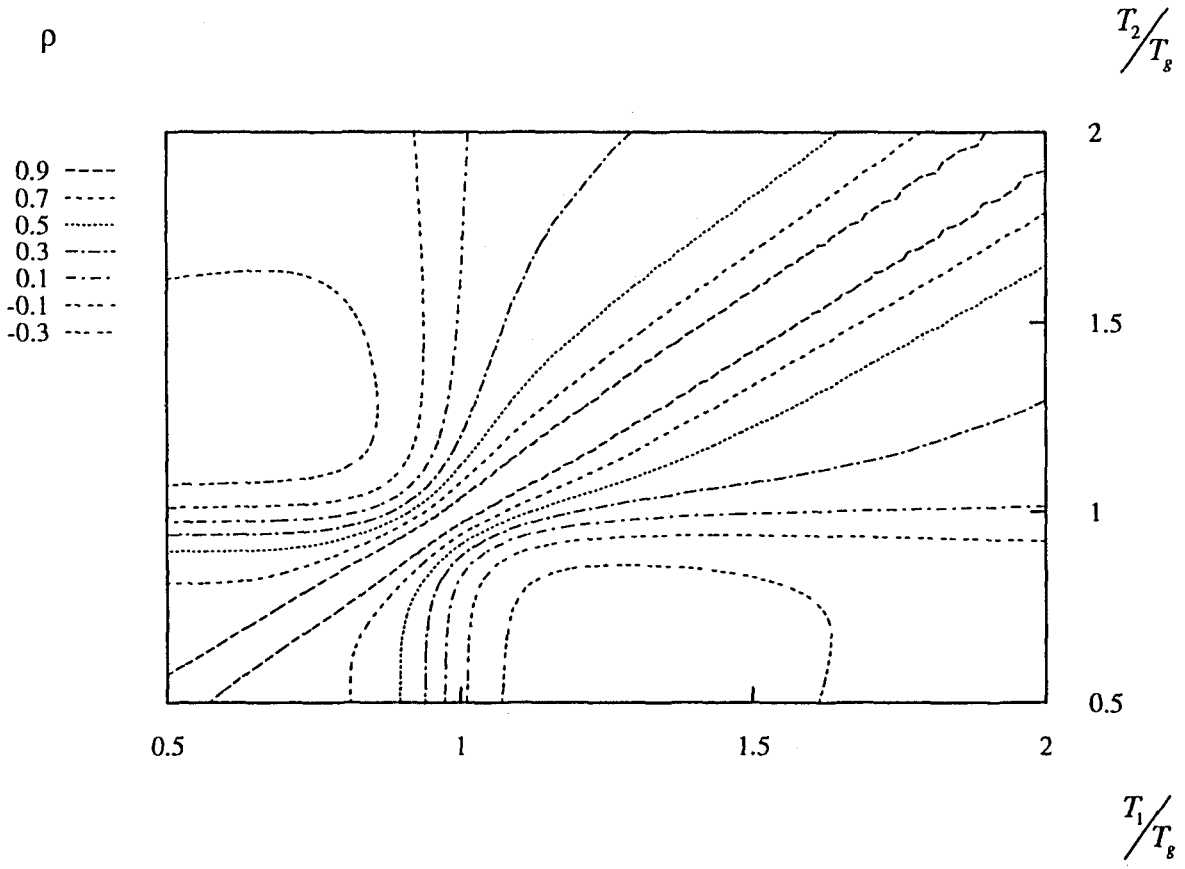

Fig. B.22 Correlation coefficient for bilinear systems subjected to a narrow band input ($\mu_1 = \mu_2 = 2$).

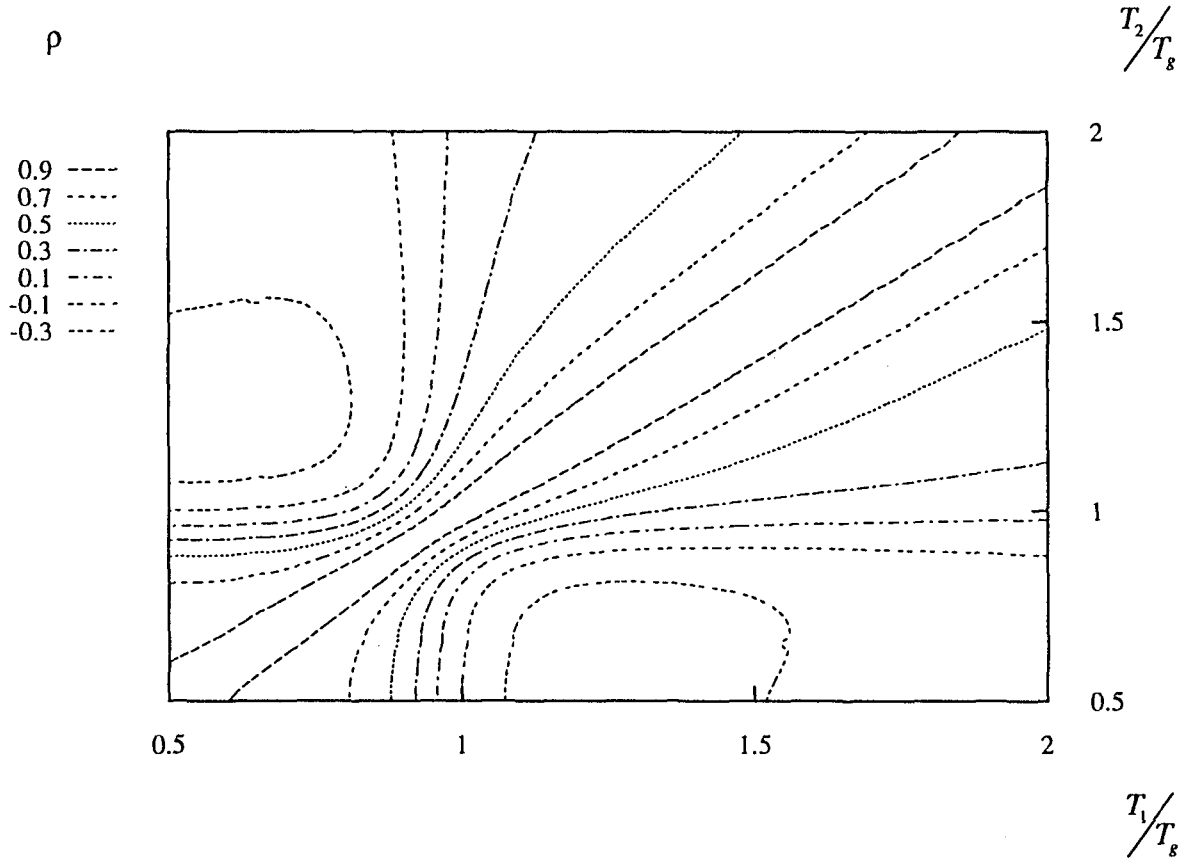

Fig. B.23 Correlation coefficient for bilinear systems subjected to a narrow band input ($\mu_1 = \mu_2 = 3$).

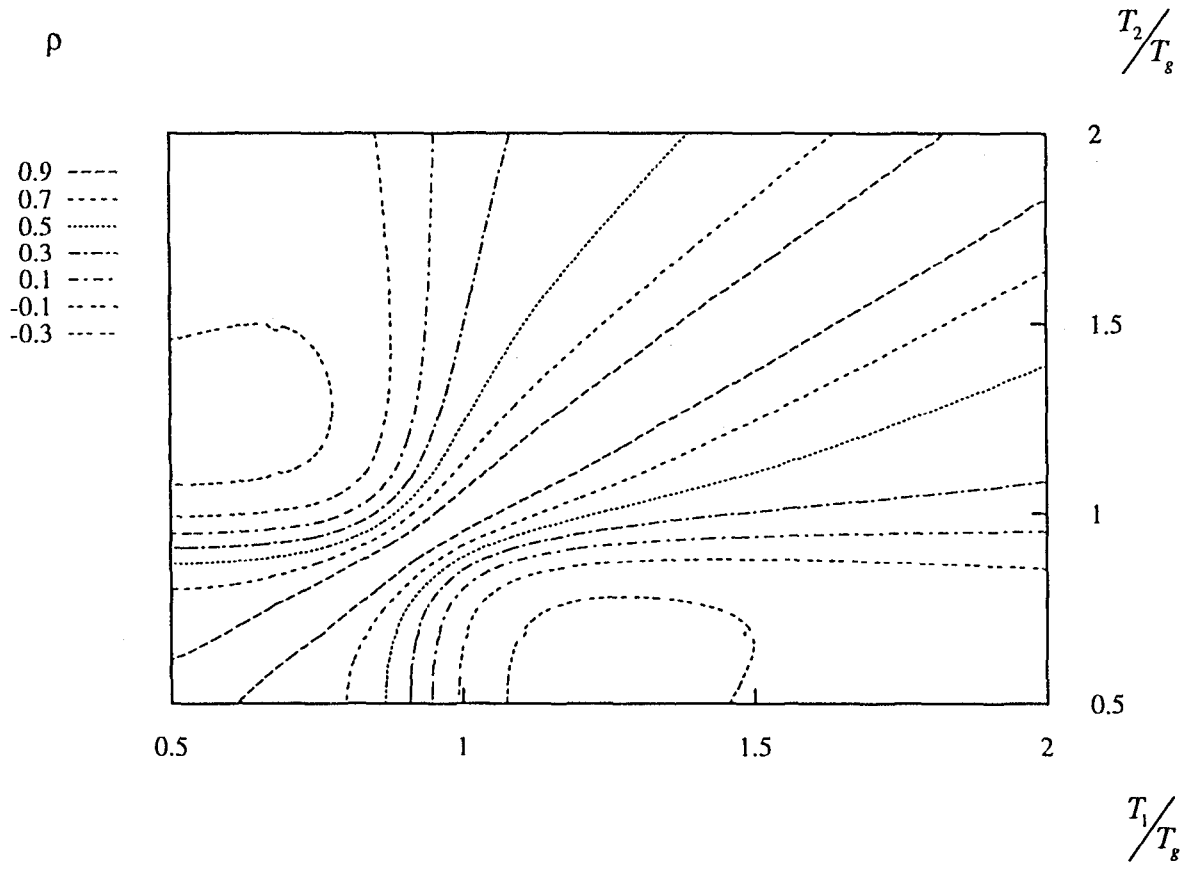

Fig. B.24 Correlation coefficient for bilinear systems subjected to a narrow band input ($\mu_1 = \mu_2 = 4$).

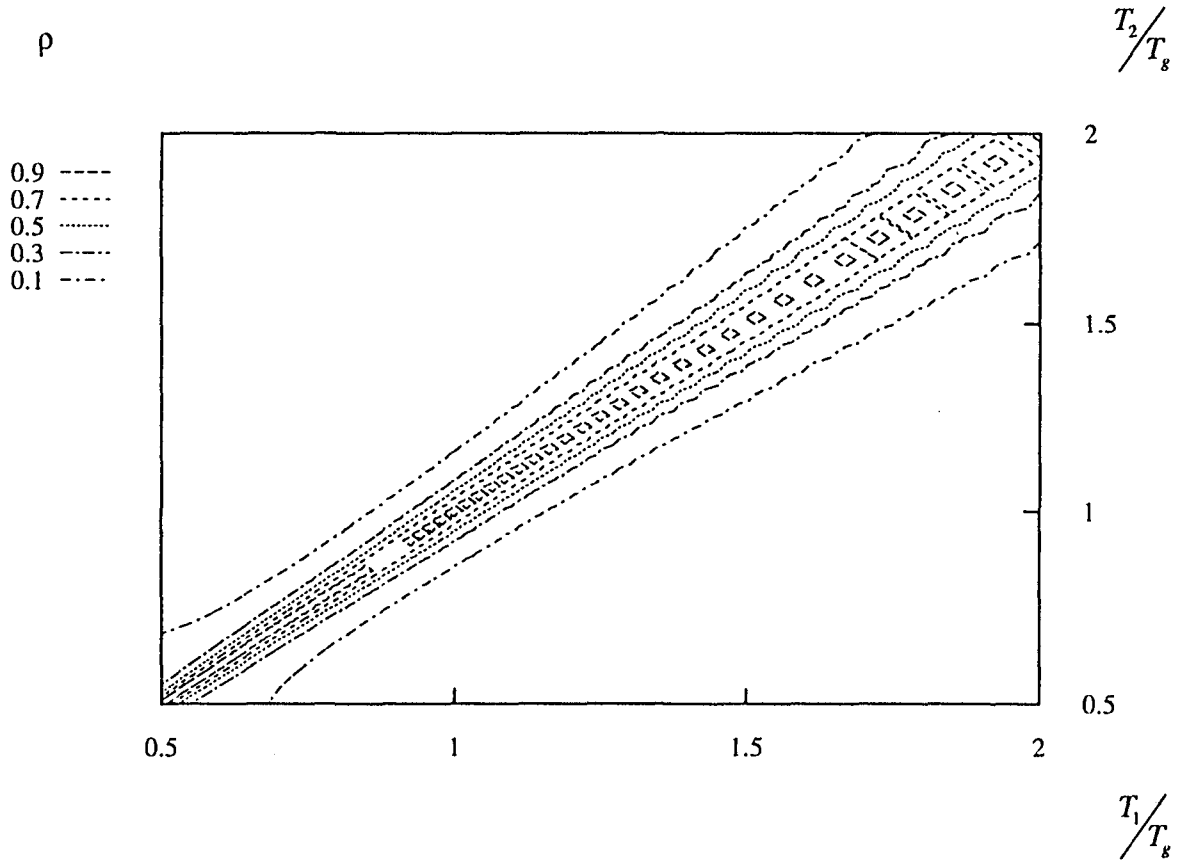

Fig. B.25 Correlation coefficient for bilinear systems subjected to a broad band input ($R_1 = R_2 = 1$).

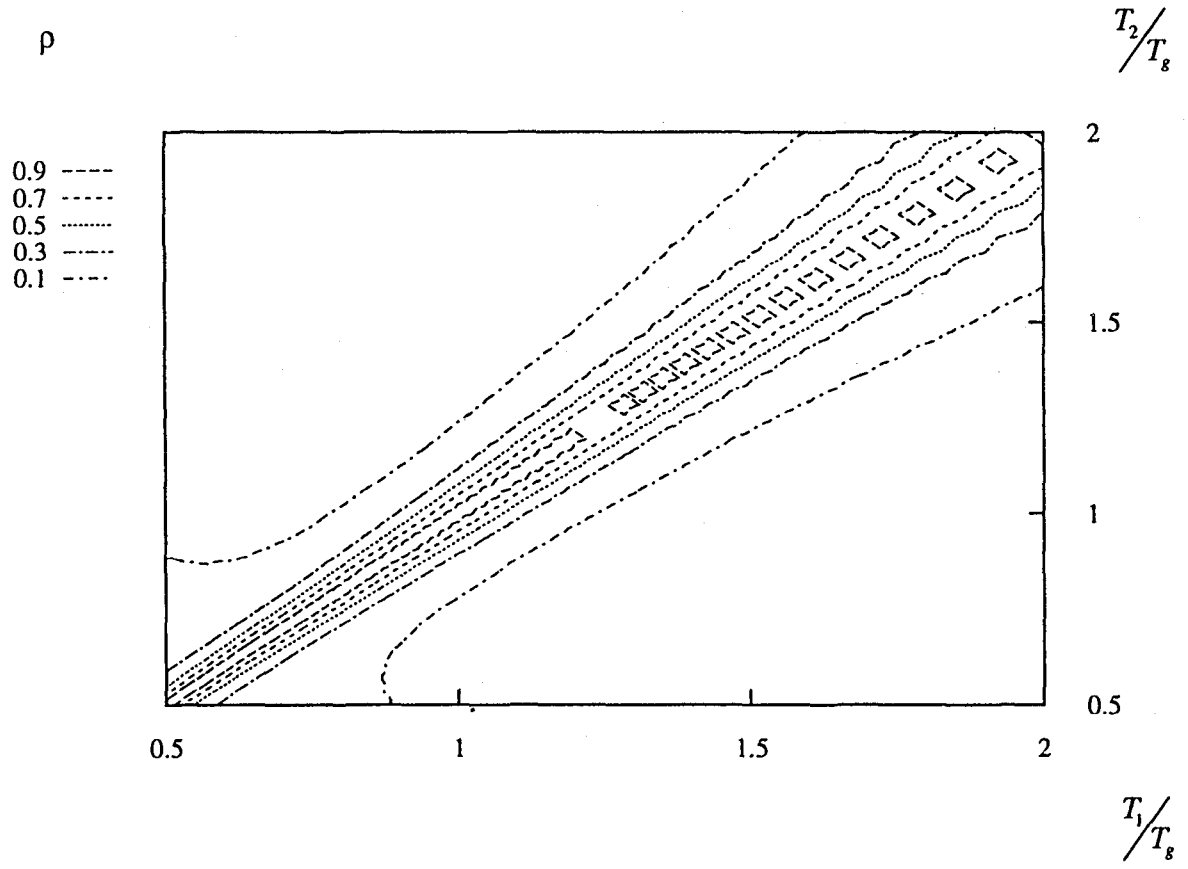

Fig. B.26 Correlation coefficient for bilinear systems subjected to a broad band input ($R_1 = R_2 = 1.5$).

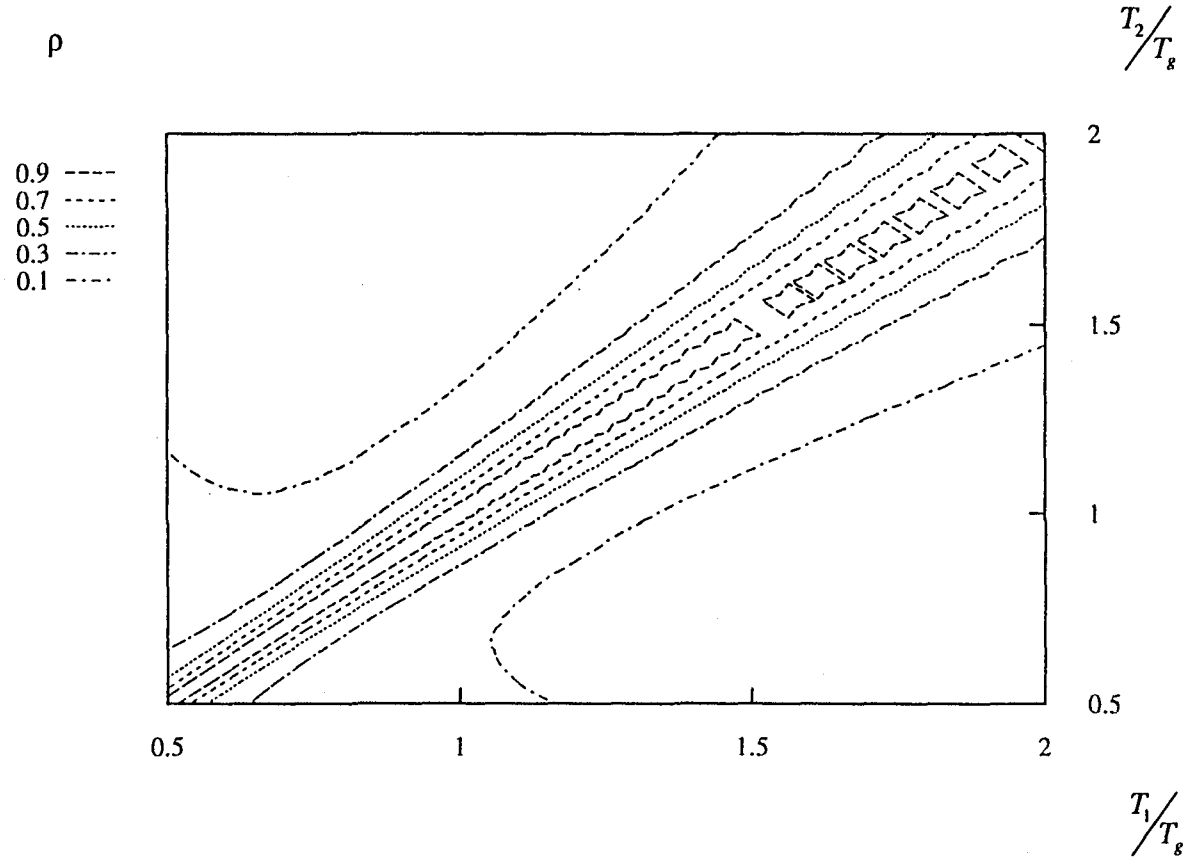

Fig. B.27 Correlation coefficient for bilinear systems subjected to a broad band input ($R_1 = R_2 = 2$).

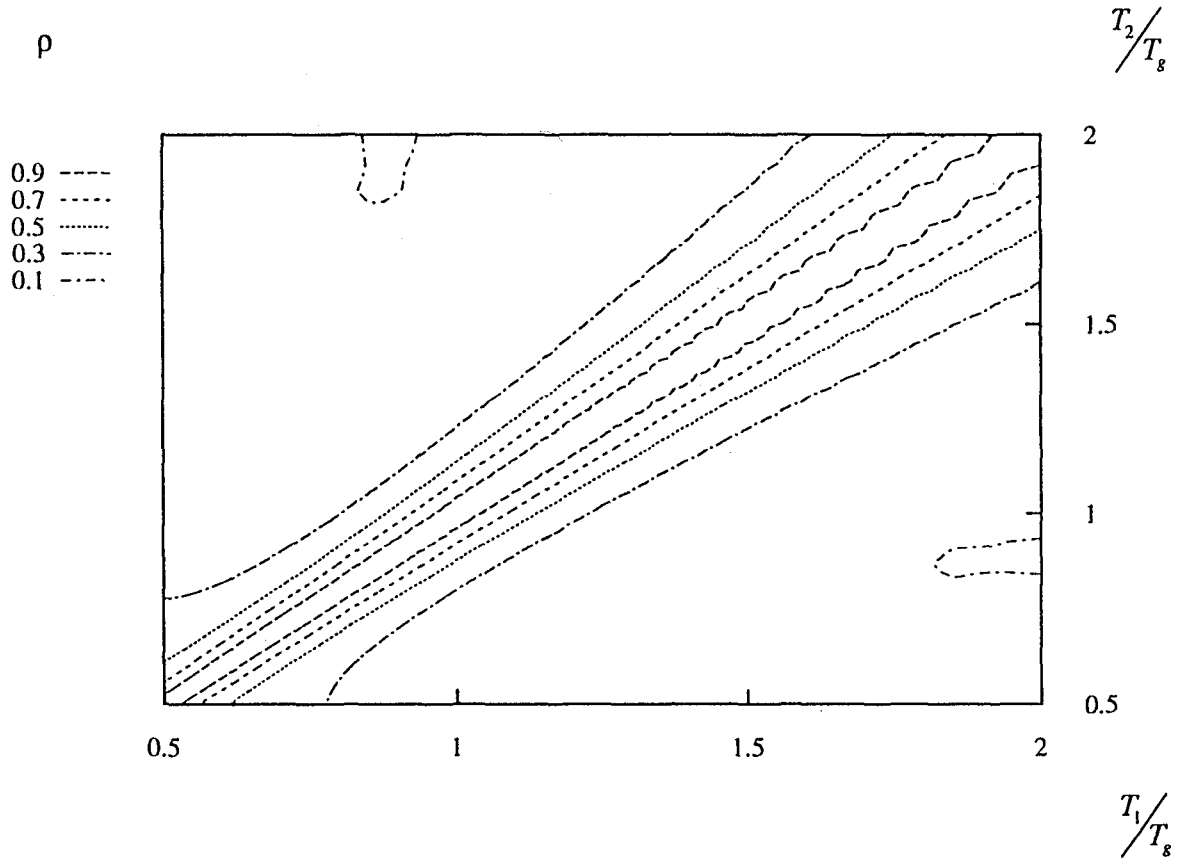

Fig. B.28 Correlation coefficient for bilinear systems subjected to a broad band input ($R_1 = R_2 = 3$).

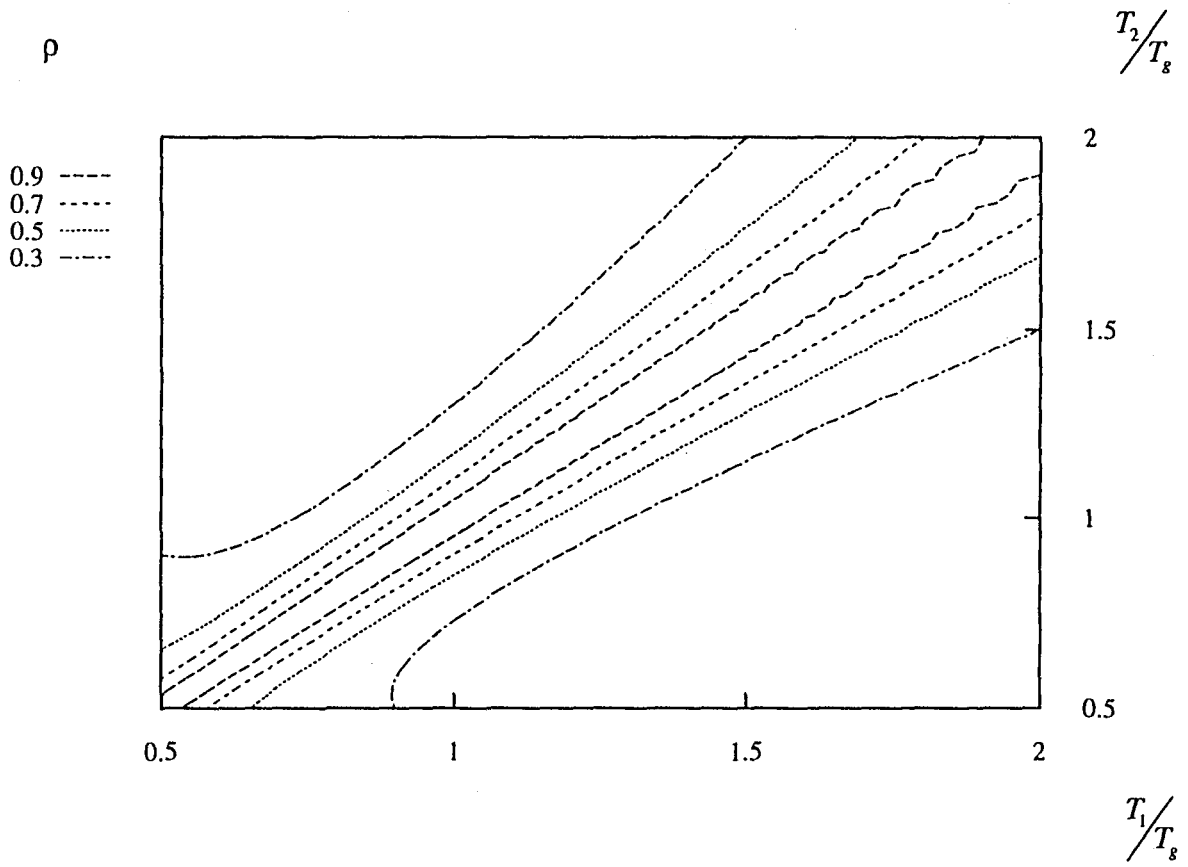

Fig. B.29 Correlation coefficient for bilinear systems subjected to a broad band input ($R_1 = R_2 = 4$).

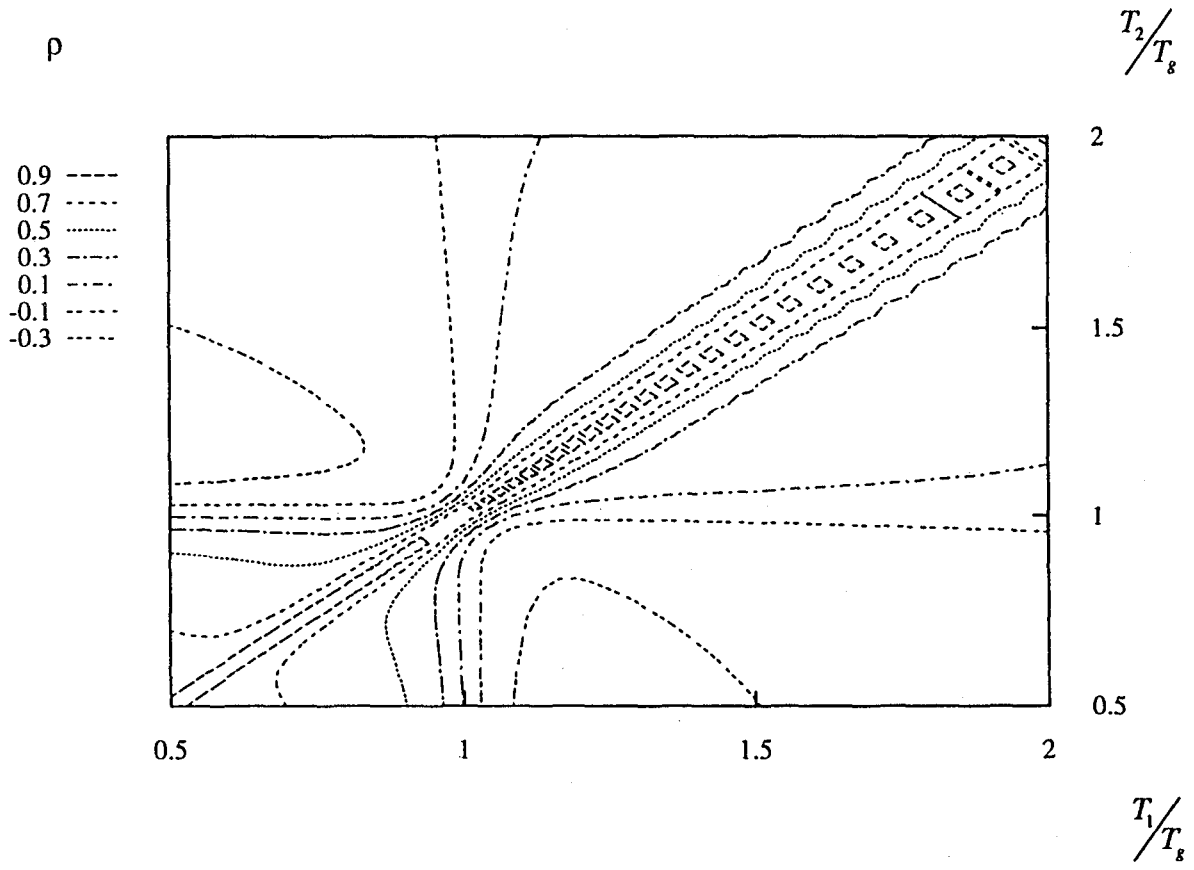

Fig. B.30 Correlation coefficient for bilinear systems subjected to a narrow band input ($R_1 = R_2 = 1$).

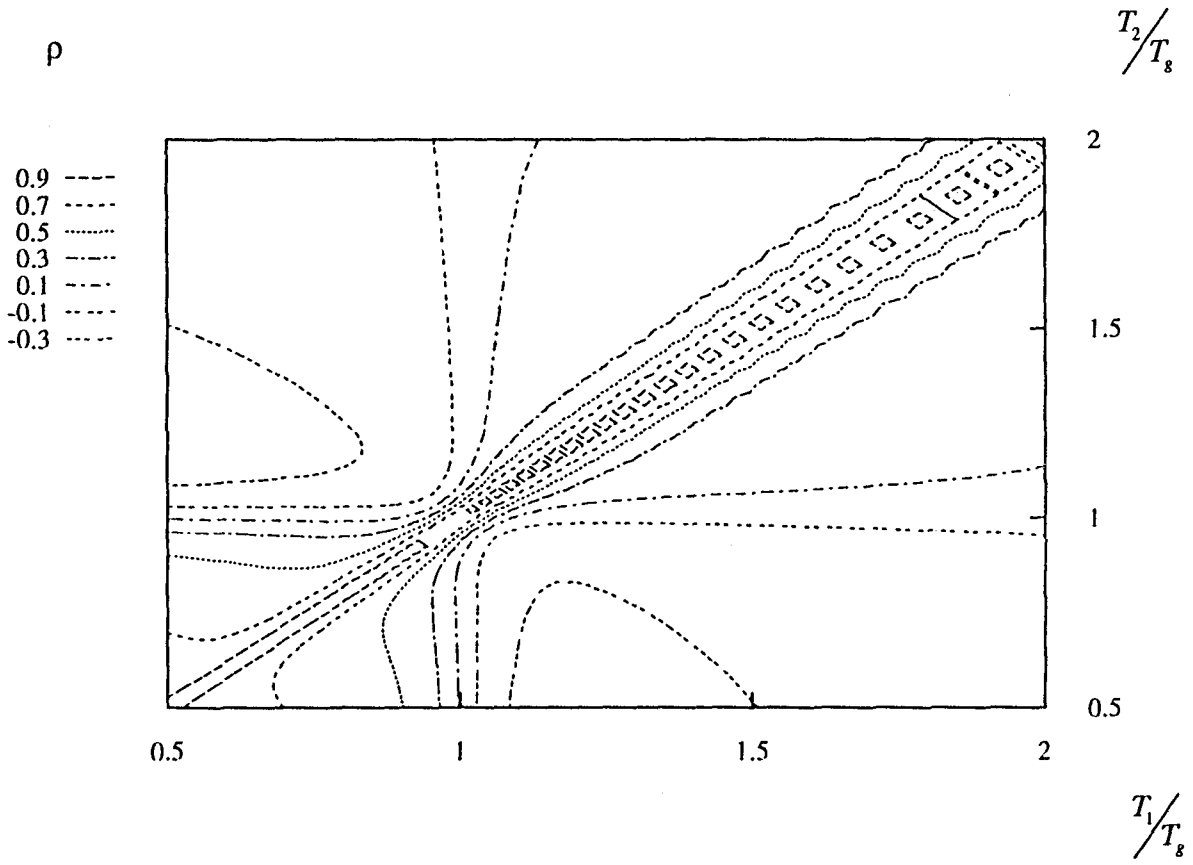

Fig. B.31 Correlation coefficient for bilinear systems subjected to a narrow band input ($R_1 = R_2 = 1.5$).

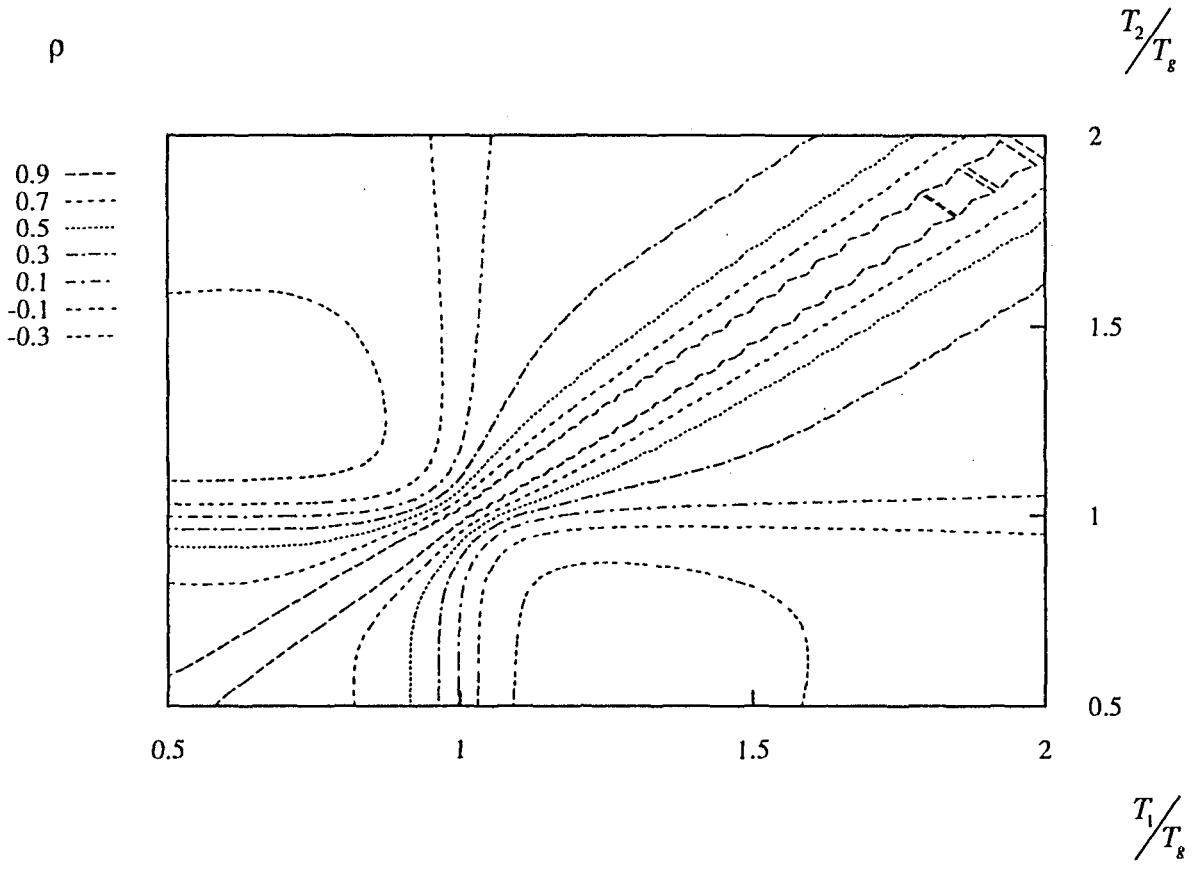

Fig. B.32 Correlation coefficient for bilinear systems subjected to a narrow band input ($R_1 = R_2 = 2$).

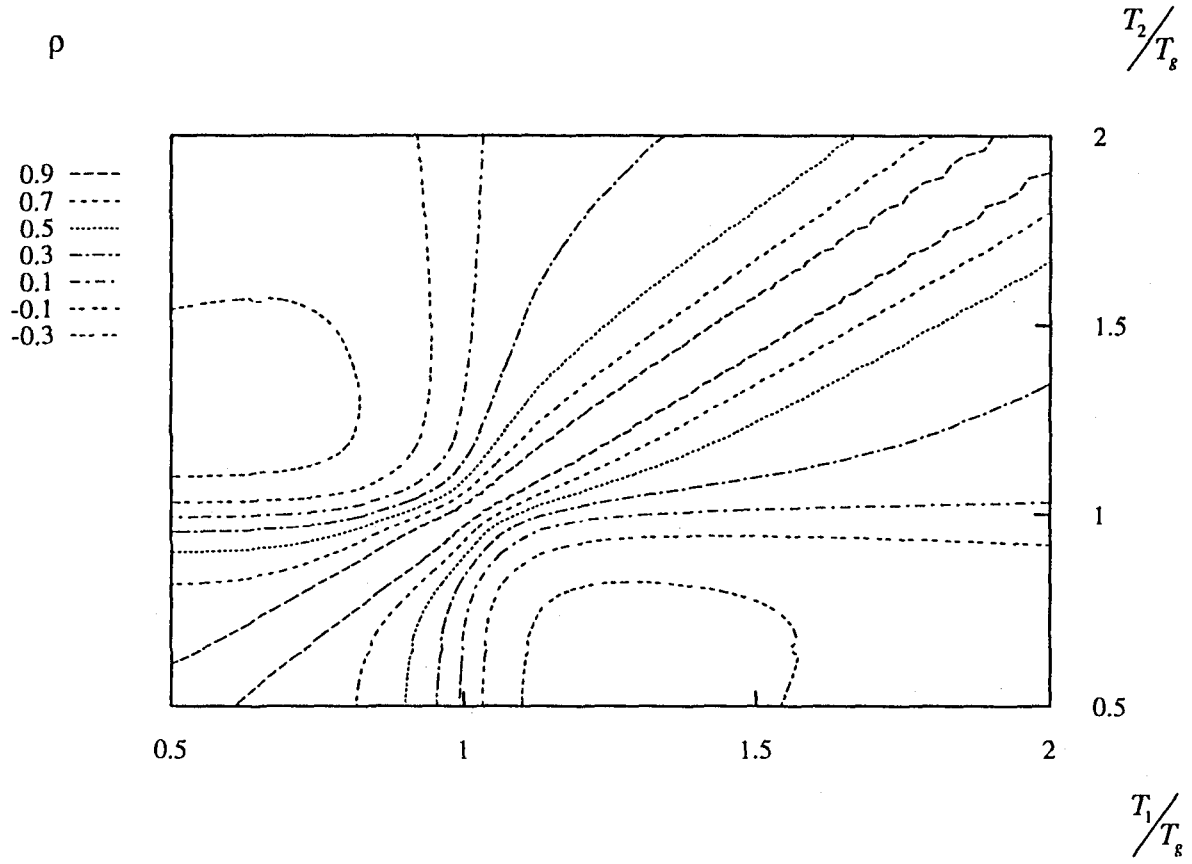

Fig. B.33 Correlation coefficient for bilinear systems subjected to a narrow band input ($R_1 = R_2 = 3$).

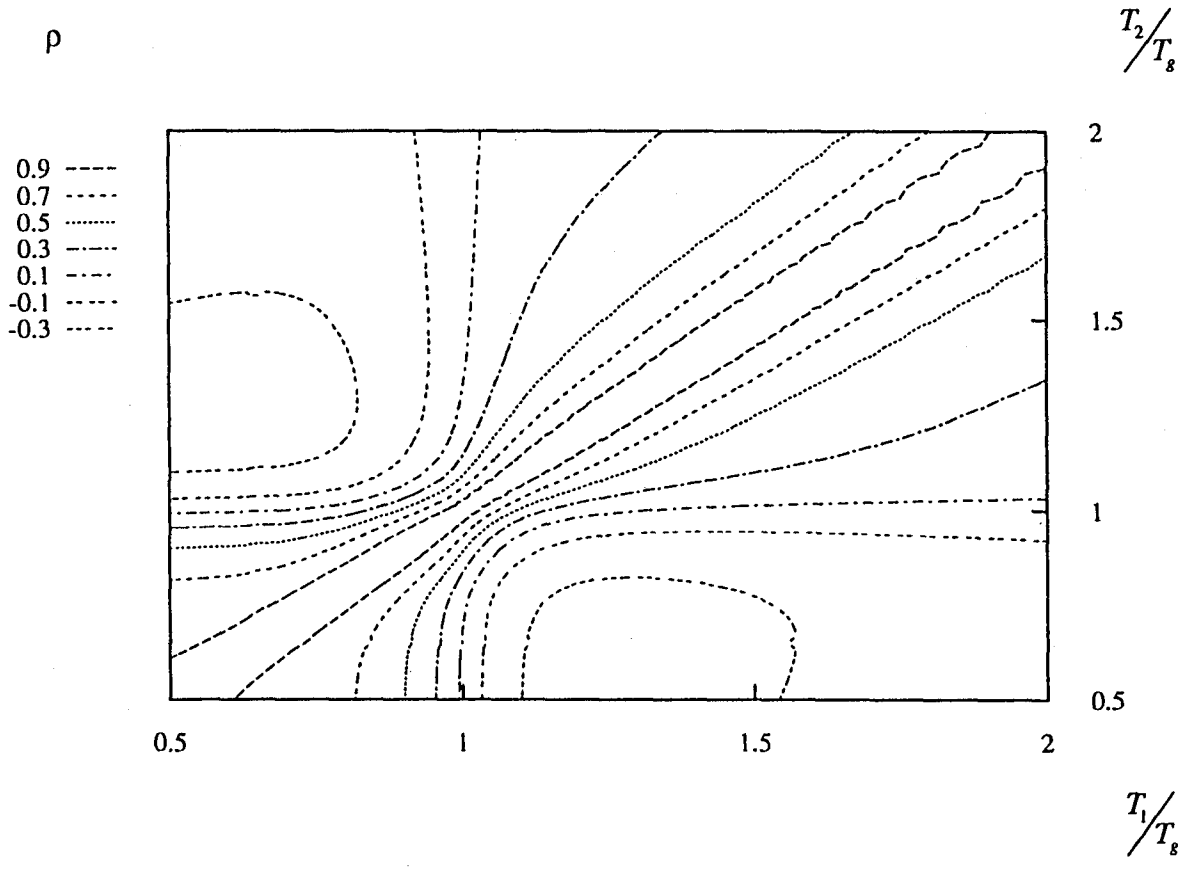

Fig. B.34 Correlation coefficient for bilinear systems subjected to a narrow band input ($R_1 = R_2 = 4$).

NATIONAL CENTER FOR EARTHQUAKE ENGINEERING RESEARCH
LIST OF TECHNICAL REPORTS

The National Center for Earthquake Engineering Research (NCEER) publishes technical reports on a variety of subjects related to earthquake engineering written by authors funded through NCEER. These reports are available from both NCEER Publications and the National Technical Information Service (NTIS). Requests for reports should be directed to NCEER Publications, National Center for Earthquake Engineering Research, State University of New York at Buffalo, Red Jacket Quadrangle, Buffalo, New York 14261. Reports can also be requested through NTIS, 5285 Port Royal Road, Springfield, Virginia 22161. NTIS accession numbers are shown in parenthesis, if available.

NCEER-87-0001 "First-Year Program in Research, Education and Technology Transfer," 3/5/87, (PB88-134275, A04, MF-A01).

NCEER-87-0002 "Experimental Evaluation of Instantaneous Optimal Algorithms for Structural Control," by R.C. Lin, T.T. Soong and A.M. Reinhorn, 4/20/87, (PB88-134341, A04, MF-A01).

NCEER-87-0003 "Experimentation Using the Earthquake Simulation Facilities at University at Buffalo," by A.M. Reinhorn and R.L. Ketter, to be published.

NCEER-87-0004 "The System Characteristics and Performance of a Shaking Table," by J.S. Hwang, K.C. Chang and G.C. Lee, 6/1/87, (PB88-134259, A03, MF-A01). This report is available only through NTIS (see address given above).

NCEER-87-0005 "A Finite Element Formulation for Nonlinear Viscoplastic Material Using a Q Model," by O. Gyebi and G. Dasgupta, 11/2/87, (PB88-213764, A08, MF-A01).

NCEER-87-0006 "Symbolic Manipulation Program (SMP) - Algebraic Codes for Two and Three Dimensional Finite Element Formulations," by X. Lee and G. Dasgupta, 11/9/87, (PB88-218522, A05, MF-A01).

NCEER-87-0007 "Instantaneous Optimal Control Laws for Tall Buildings Under Seismic Excitations," by J.N. Yang, A. Akbarpour and P. Ghaemmaghami, 6/10/87, (PB88-134333, A06, MF-A01). This report is only available through NTIS (see address given above).

NCEER-87-0008 "IDARC: Inelastic Damage Analysis of Reinforced Concrete Frame - Shear-Wall Structures," by Y.J. Park, A.M. Reinhorn and S.K. Kunnath, 7/20/87, (PB88-134325, A09, MF-A01). This report is only available through NTIS (see address given above).

NCEER-87-0009 "Liquefaction Potential for New York State: A Preliminary Report on Sites in Manhattan and Buffalo," by M. Budhu, V. Vijayakumar, R.F. Giese and L. Baumgras, 8/31/87, (PB88-163704, A03, MF-A01). This report is available only through NTIS (see address given above).

NCEER-87-0010 "Vertical and Torsional Vibration of Foundations in Inhomogeneous Media," by A.S. Veletsos and K.W. Dotson, 6/1/87, (PB88-134291, A03, MF-A01). This report is only available through NTIS (see address given above).

NCEER-87-0011 "Seismic Probabilistic Risk Assessment and Seismic Margins Studies for Nuclear Power Plants," by Howard H.M. Hwang, 6/15/87, (PB88-134267, A03, MF-A01). This report is only available through NTIS (see address given above).

NCEER-87-0012 "Parametric Studies of Frequency Response of Secondary Systems Under Ground-Acceleration Excitations," by Y. Yong and Y.K. Lin, 6/10/87, (PB88-134309, A03, MF-A01). This report is only available through NTIS (see address given above).

NCEER-87-0013 "Frequency Response of Secondary Systems Under Seismic Excitation," by J.A. HoLung, J. Cai and Y.K. Lin, 7/31/87, (PB88-134317, A05, MF-A01). This report is only available through NTIS (see address given above).

NCEER-87-0014 "Modelling Earthquake Ground Motions in Seismically Active Regions Using Parametric Time Series Methods," by G.W. Ellis and A.S. Cakmak, 8/25/87, (PB88-134283, A08, MF-A01). This report is only available through NTIS (see address given above).

NCEER-87-0015 "Detection and Assessment of Seismic Structural Damage," by E. DiPasquale and A.S. Cakmak, 8/25/87, (PB88-163712, A05, MF-A01). This report is only available through NTIS (see address given above).

NCEER-87-0016 "Pipeline Experiment at Parkfield, California," by J. Isenberg and E. Richardson, 9/15/87, (PB88-163720, A03, MF-A01). This report is available only through NTIS (see address given above).

NCEER-87-0017 "Digital Simulation of Seismic Ground Motion," by M. Shinozuka, G. Deodatis and T. Harada, 8/31/87, (PB88-155197, A04, MF-A01). This report is available only through NTIS (see address given above).

NCEER-87-0018 "Practical Considerations for Structural Control: System Uncertainty, System Time Delay and Truncation of Small Control Forces," J.N. Yang and A. Akbarpour, 8/10/87, (PB88-163738, A08, MF-A01). This report is only available through NTIS (see address given above).

NCEER-87-0019 "Modal Analysis of Nonclassically Damped Structural Systems Using Canonical Transformation," by J.N. Yang, S. Sarkani and F.X. Long, 9/27/87, (PB88-187851, A04, MF-A01).

NCEER-87-0020 "A Nonstationary Solution in Random Vibration Theory," by J.R. Red-Horse and P.D. Spanos, 11/3/87, (PB88-163746, A03, MF-A01).

NCEER-87-0021 "Horizontal Impedances for Radially Inhomogeneous Viscoelastic Soil Layers," by A.S. Veletsos and K.W. Dotson, 10/15/87, (PB88-150859, A04, MF-A01).

NCEER-87-0022 "Seismic Damage Assessment of Reinforced Concrete Members," by Y.S. Chung, C. Meyer and M. Shinozuka, 10/9/87, (PB88-150867, A05, MF-A01). This report is available only through NTIS (see address given above).

NCEER-87-0023 "Active Structural Control in Civil Engineering," by T.T. Soong, 11/11/87, (PB88-187778, A03, MF-A01).

NCEER-87-0024 "Vertical and Torsional Impedances for Radially Inhomogeneous Viscoelastic Soil Layers," by K.W. Dotson and A.S. Veletsos, 12/87, (PB88-187786, A03, MF-A01).

NCEER-87-0025 "Proceedings from the Symposium on Seismic Hazards, Ground Motions, Soil-Liquefaction and Engineering Practice in Eastern North America," October 20-22, 1987, edited by K.H. Jacob, 12/87, (PB88-188115, A23, MF-A01).

NCEER-87-0026 "Report on the Whittier-Narrows, California, Earthquake of October 1, 1987," by J. Pantelic and A. Reinhorn, 11/87, (PB88-187752, A03, MF-A01). This report is available only through NTIS (see address given above).

NCEER-87-0027 "Design of a Modular Program for Transient Nonlinear Analysis of Large 3-D Building Structures," by S. Srivastav and J.F. Abel, 12/30/87, (PB88-187950, A05, MF-A01). This report is only available through NTIS (see address given above).

NCEER-87-0028 "Second-Year Program in Research, Education and Technology Transfer," 3/8/88, (PB88-219480, A04, MF-A01).

NCEER-88-0001 "Workshop on Seismic Computer Analysis and Design of Buildings With Interactive Graphics," by W. McGuire, J.F. Abel and C.H. Conley, 1/18/88, (PB88-187760, A03, MF-A01). This report is only available through NTIS (see address given above).

NCEER-88-0002 "Optimal Control of Nonlinear Flexible Structures," by J.N. Yang, F.X. Long and D. Wong, 1/22/88, (PB88-213772, A06, MF-A01).

NCEER-88-0003 "Substructuring Techniques in the Time Domain for Primary-Secondary Structural Systems," by G.D. Manolis and G. Juhn, 2/10/88, (PB88-213780, A04, MF-A01).

NCEER-88-0004 "Iterative Seismic Analysis of Primary-Secondary Systems," by A. Singhal, L.D. Lutes and P.D. Spanos, 2/23/88, (PB88-213798, A04, MF-A01).

NCEER-88-0005 "Stochastic Finite Element Expansion for Random Media," by P.D. Spanos and R. Ghanem, 3/14/88, (PB88-213806, A03, MF-A01).

NCEER-88-0006 "Combining Structural Optimization and Structural Control," by F.Y. Cheng and C.P. Pantelides, 1/10/88, (PB88-213814, A05, MF-A01).

NCEER-88-0007 "Seismic Performance Assessment of Code-Designed Structures," by H.H-M. Hwang, J-W. Jaw and H-J. Shau, 3/20/88, (PB88-219423, A04, MF-A01). This report is only available through NTIS (see address given above).

NCEER-88-0008 "Reliability Analysis of Code-Designed Structures Under Natural Hazards," by H.H-M. Hwang, H. Ushiba and M. Shinozuka, 2/29/88, (PB88-229471, A07, MF-A01). This report is only available through NTIS (see address given above).

NCEER-88-0009 "Seismic Fragility Analysis of Shear Wall Structures," by J-W Jaw and H.H-M. Hwang, 4/30/88, (PB89-102867, A04, MF-A01).

NCEER-88-0010 "Base Isolation of a Multi-Story Building Under a Harmonic Ground Motion - A Comparison of Performances of Various Systems," by F-G Fan, G. Ahmadi and I.G. Tadjbakhsh, 5/18/88, (PB89-122238, A06, MF-A01). This report is only available through NTIS (see address given above).

NCEER-88-0011 "Seismic Floor Response Spectra for a Combined System by Green's Functions," by F.M. Lavelle, L.A. Bergman and P.D. Spanos, 5/1/88, (PB89-102875, A03, MF-A01).

NCEER-88-0012 "A New Solution Technique for Randomly Excited Hysteretic Structures," by G.Q. Cai and Y.K. Lin, 5/16/88, (PB89-102883, A03, MF-A01).

NCEER-88-0013 "A Study of Radiation Damping and Soil-Structure Interaction Effects in the Centrifuge," by K. Weissman, supervised by J.H. Prevost, 5/24/88, (PB89-144703, A06, MF-A01).

NCEER-88-0014 "Parameter Identification and Implementation of a Kinematic Plasticity Model for Frictional Soils," by J.H. Prevost and D.V. Griffiths, to be published.

NCEER-88-0015 "Two- and Three- Dimensional Dynamic Finite Element Analyses of the Long Valley Dam," by D.V. Griffiths and J.H. Prevost, 6/17/88, (PB89-144711, A04, MF-A01).

NCEER-88-0016 "Damage Assessment of Reinforced Concrete Structures in Eastern United States," by A.M. Reinhorn, M.J. Seidel, S.K. Kunnath and Y.J. Park, 6/15/88, (PB89-122220, A04, MF-A01). This report is only available through NTIS (see address given above).

NCEER-88-0017 "Dynamic Compliance of Vertically Loaded Strip Foundations in Multilayered Viscoelastic Soils," by S. Ahmad and A.S.M. Israil, 6/17/88, (PB89-102891, A04, MF-A01).

NCEER-88-0018 "An Experimental Study of Seismic Structural Response With Added Viscoelastic Dampers," by R.C. Lin, Z. Liang, T.T. Soong and R.H. Zhang, 6/30/88, (PB89-122212, A05, MF-A01). This report is available only through NTIS (see address given above).

NCEER-88-0019 "Experimental Investigation of Primary - Secondary System Interaction," by G.D. Manolis, G. Juhn and A.M. Reinhorn, 5/27/88, (PB89-122204, A04, MF-A01).

NCEER-88-0020 "A Response Spectrum Approach For Analysis of Nonclassically Damped Structures," by J.N. Yang, S. Sarkani and F.X. Long, 4/22/88, (PB89-102909, A04, MF-A01).

NCEER-88-0021 "Seismic Interaction of Structures and Soils: Stochastic Approach," by A.S. Veletsos and A.M. Prasad, 7/21/88, (PB89-122196, A04, MF-A01). This report is only available through NTIS (see address given above).

NCEER-88-0022 "Identification of the Serviceability Limit State and Detection of Seismic Structural Damage," by E. DiPasquale and A.S. Cakmak, 6/15/88, (PB89-122188, A05, MF-A01). This report is available only through NTIS (see address given above).

NCEER-88-0023 "Multi-Hazard Risk Analysis: Case of a Simple Offshore Structure," by B.K. Bhartia and E.H. Vanmarcke, 7/21/88, (PB89-145213, A05, MF-A01).

NCEER-88-0024 "Automated Seismic Design of Reinforced Concrete Buildings," by Y.S. Chung, C. Meyer and M. Shinozuka, 7/5/88, (PB89-122170, A06, MF-A01). This report is available only through NTIS (see address given above).

NCEER-88-0025 "Experimental Study of Active Control of MDOF Structures Under Seismic Excitations," by L.L. Chung, R.C. Lin, T.T. Soong and A.M. Reinhorn, 7/10/88, (PB89-122600, A04, MF-A01).

NCEER-88-0026 "Earthquake Simulation Tests of a Low-Rise Metal Structure," by J.S. Hwang, K.C. Chang, G.C. Lee and R.L. Ketter, 8/1/88, (PB89-102917, A04, MF-A01).

NCEER-88-0027 "Systems Study of Urban Response and Reconstruction Due to Catastrophic Earthquakes," by F. Kozin and H.K. Zhou, 9/22/88, (PB90-162348, A04, MF-A01).

NCEER-88-0028 "Seismic Fragility Analysis of Plane Frame Structures," by H.H-M. Hwang and Y.K. Low, 7/31/88, (PB89-131445, A06, MF-A01).

NCEER-88-0029 "Response Analysis of Stochastic Structures," by A. Kardara, C. Bucher and M. Shinozuka, 9/22/88, (PB89-174429, A04, MF-A01).

NCEER-88-0030 "Nonnormal Accelerations Due to Yielding in a Primary Structure," by D.C.K. Chen and L.D. Lutes, 9/19/88, (PB89-131437, A04, MF-A01).

NCEER-88-0031 "Design Approaches for Soil-Structure Interaction," by A.S. Veletsos, A.M. Prasad and Y. Tang, 12/30/88, (PB89-174437, A03, MF-A01). This report is available only through NTIS (see address given above).

NCEER-88-0032 "A Re-evaluation of Design Spectra for Seismic Damage Control," by C.J. Turkstra and A.G. Tallin, 11/7/88, (PB89-145221, A05, MF-A01).

NCEER-88-0033 "The Behavior and Design of Noncontact Lap Splices Subjected to Repeated Inelastic Tensile Loading," by V.E. Sagan, P. Gergely and R.N. White, 12/8/88, (PB89-163737, A08, MF-A01).

NCEER-88-0034 "Seismic Response of Pile Foundations," by S.M. Mamoon, P.K. Banerjee and S. Ahmad, 11/1/88, (PB89-145239, A04, MF-A01).

NCEER-88-0035 "Modeling of R/C Building Structures With Flexible Floor Diaphragms (IDARC2)," by A.M. Reinhorn, S.K. Kunnath and N. Panahshahi, 9/7/88, (PB89-207153, A07, MF-A01).

NCEER-88-0036 "Solution of the Dam-Reservoir Interaction Problem Using a Combination of FEM, BEM with Particular Integrals, Modal Analysis, and Substructuring," by C-S. Tsai, G.C. Lee and R.L. Ketter, 12/31/88, (PB89-207146, A04, MF-A01).

NCEER-88-0037 "Optimal Placement of Actuators for Structural Control," by F.Y. Cheng and C.P. Pantelides, 8/15/88, (PB89-162846, A05, MF-A01).

NCEER-88-0038 "Teflon Bearings in Aseismic Base Isolation: Experimental Studies and Mathematical Modeling," by A. Mokha, M.C. Constantinou and A.M. Reinhorn, 12/5/88, (PB89-218457, A10, MF-A01). This report is available only through NTIS (see address given above).

NCEER-88-0039 "Seismic Behavior of Flat Slab High-Rise Buildings in the New York City Area," by P. Weidlinger and M. Ettouney, 10/15/88, (PB90-145681, A04, MF-A01).

NCEER-88-0040 "Evaluation of the Earthquake Resistance of Existing Buildings in New York City," by P. Weidlinger and M. Ettouney, 10/15/88, to be published.

NCEER-88-0041 "Small-Scale Modeling Techniques for Reinforced Concrete Structures Subjected to Seismic Loads," by W. Kim, A. El-Attar and R.N. White, 11/22/88, (PB89-189625, A05, MF-A01).

NCEER-88-0042 "Modeling Strong Ground Motion from Multiple Event Earthquakes," by G.W. Ellis and A.S. Cakmak, 10/15/88, (PB89-174445, A03, MF-A01).

NCEER-88-0043 "Nonstationary Models of Seismic Ground Acceleration," by M. Grigoriu, S.E. Ruiz and E. Rosenblueth, 7/15/88, (PB89-189617, A04, MF-A01).

NCEER-88-0044 "SARCF User's Guide: Seismic Analysis of Reinforced Concrete Frames," by Y.S. Chung, C. Meyer and M. Shinozuka, 11/9/88, (PB89-174452, A08, MF-A01).

NCEER-88-0045 "First Expert Panel Meeting on Disaster Research and Planning," edited by J. Pantelic and J. Stoyle, 9/15/88, (PB89-174460, A05, MF-A01). This report is only available through NTIS (see address given above).

NCEER-88-0046 "Preliminary Studies of the Effect of Degrading Infill Walls on the Nonlinear Seismic Response of Steel Frames," by C.Z. Chrysostomou, P. Gergely and J.F. Abel, 12/19/88, (PB89-208383, A05, MF-A01).

NCEER-88-0047 "Reinforced Concrete Frame Component Testing Facility - Design, Construction, Instrumentation and Operation," by S.P. Pessiki, C. Conley, T. Bond, P. Gergely and R.N. White, 12/16/88, (PB89-174478, A04, MF-A01).

NCEER-89-0001 "Effects of Protective Cushion and Soil Compliancy on the Response of Equipment Within a Seismically Excited Building," by J.A. HoLung, 2/16/89, (PB89-207179, A04, MF-A01).

NCEER-89-0002 "Statistical Evaluation of Response Modification Factors for Reinforced Concrete Structures," by H.H-M. Hwang and J-W. Jaw, 2/17/89, (PB89-207187, A05, MF-A01).

NCEER-89-0003 "Hysteretic Columns Under Random Excitation," by G-Q. Cai and Y.K. Lin, 1/9/89, (PB89-196513, A03, MF-A01).

NCEER-89-0004 "Experimental Study of `Elephant Foot Bulge' Instability of Thin-Walled Metal Tanks," by Z-H. Jia and R.L. Ketter, 2/22/89, (PB89-207195, A03, MF-A01).

NCEER-89-0005 "Experiment on Performance of Buried Pipelines Across San Andreas Fault," by J. Isenberg, E. Richardson and T.D. O'Rourke, 3/10/89, (PB89-218440, A04, MF-A01). This report is available only through NTIS (see address given above).

NCEER-89-0006 "A Knowledge-Based Approach to Structural Design of Earthquake-Resistant Buildings," by M. Subramani, P. Gergely, C.H. Conley, J.F. Abel and A.H. Zaghw, 1/15/89, (PB89-218465, A06, MF-A01).

NCEER-89-0007 "Liquefaction Hazards and Their Effects on Buried Pipelines," by T.D. O'Rourke and P.A. Lane, 2/1/89, (PB89-218481, A09, MF-A01).

NCEER-89-0008 "Fundamentals of System Identification in Structural Dynamics," by H. Imai, C-B. Yun, O. Maruyama and M. Shinozuka, 1/26/89, (PB89-207211, A04, MF-A01).

NCEER-89-0009 "Effects of the 1985 Michoacan Earthquake on Water Systems and Other Buried Lifelines in Mexico," by A.G. Ayala and M.J. O'Rourke, 3/8/89, (PB89-207229, A06, MF-A01).

NCEER-89-R010 "NCEER Bibliography of Earthquake Education Materials," by K.E.K. Ross, Second Revision, 9/1/89, (PB90-125352, A05, MF-A01). This report is replaced by NCEER-92-0018.

NCEER-89-0011 "Inelastic Three-Dimensional Response Analysis of Reinforced Concrete Building Structures (IDARC-3D), Part I - Modeling," by S.K. Kunnath and A.M. Reinhorn, 4/17/89, (PB90-114612, A07, MF-A01).

NCEER-89-0012 "Recommended Modifications to ATC-14," by C.D. Poland and J.O. Malley, 4/12/89, (PB90-108648, A15, MF-A01).

NCEER-89-0013 "Repair and Strengthening of Beam-to-Column Connections Subjected to Earthquake Loading," by M. Corazao and A.J. Durrani, 2/28/89, (PB90-109885, A06, MF-A01).

NCEER-89-0014 "Program EXKAL2 for Identification of Structural Dynamic Systems," by O. Maruyama, C-B. Yun, M. Hoshiya and M. Shinozuka, 5/19/89, (PB90-109877, A09, MF-A01).

NCEER-89-0015 "Response of Frames With Bolted Semi-Rigid Connections, Part I - Experimental Study and Analytical Predictions," by P.J. DiCorso, A.M. Reinhorn, J.R. Dickerson, J.B. Radziminski and W.L. Harper, 6/1/89, to be published.

NCEER-89-0016 "ARMA Monte Carlo Simulation in Probabilistic Structural Analysis," by P.D. Spanos and M.P. Mignolet, 7/10/89, (PB90-109893, A03, MF-A01).

NCEER-89-P017 "Preliminary Proceedings from the Conference on Disaster Preparedness - The Place of Earthquake Education in Our Schools," Edited by K.E.K. Ross, 6/23/89, (PB90-108606, A03, MF-A01).

NCEER-89-0017 "Proceedings from the Conference on Disaster Preparedness - The Place of Earthquake Education in Our Schools," Edited by K.E.K. Ross, 12/31/89, (PB90-207895, A012, MF-A02). This report is available only through NTIS (see address given above).

NCEER-89-0018 "Multidimensional Models of Hysteretic Material Behavior for Vibration Analysis of Shape Memory Energy Absorbing Devices, by E.J. Graesser and F.A. Cozzarelli, 6/7/89, (PB90-164146, A04, MF-A01).

NCEER-89-0019 "Nonlinear Dynamic Analysis of Three-Dimensional Base Isolated Structures (3D-BASIS)," by S. Nagarajaiah, A.M. Reinhorn and M.C. Constantinou, 8/3/89, (PB90-161936, A06, MF-A01). This report has been replaced by NCEER-93-0011.

NCEER-89-0020 "Structural Control Considering Time-Rate of Control Forces and Control Rate Constraints," by F.Y. Cheng and C.P. Pantelides, 8/3/89, (PB90-120445, A04, MF-A01).

NCEER-89-0021 "Subsurface Conditions of Memphis and Shelby County," by K.W. Ng, T-S. Chang and H-H.M. Hwang, 7/26/89, (PB90-120437, A03, MF-A01).

NCEER-89-0022 "Seismic Wave Propagation Effects on Straight Jointed Buried Pipelines," by K. Elhmadi and M.J. O'Rourke, 8/24/89, (PB90-162322, A10, MF-A02).

NCEER-89-0023 "Workshop on Serviceability Analysis of Water Delivery Systems," edited by M. Grigoriu, 3/6/89, (PB90-127424, A03, MF-A01).

NCEER-89-0024 "Shaking Table Study of a 1/5 Scale Steel Frame Composed of Tapered Members," by K.C. Chang, J.S. Hwang and G.C. Lee, 9/18/89, (PB90-160169, A04, MF-A01).

NCEER-89-0025 "DYNA1D: A Computer Program for Nonlinear Seismic Site Response Analysis - Technical Documentation," by Jean H. Prevost, 9/14/89, (PB90-161944, A07, MF-A01). This report is available only through NTIS (see address given above).

NCEER-89-0026 "1:4 Scale Model Studies of Active Tendon Systems and Active Mass Dampers for Aseismic Protection," by A.M. Reinhorn, T.T. Soong, R.C. Lin, Y.P. Yang, Y. Fukao, H. Abe and M. Nakai, 9/15/89, (PB90-173246, A10, MF-A02).

NCEER-89-0027 "Scattering of Waves by Inclusions in a Nonhomogeneous Elastic Half Space Solved by Boundary Element Methods," by P.K. Hadley, A. Askar and A.S. Cakmak, 6/15/89, (PB90-145699, A07, MF-A01).

NCEER-89-0028 "Statistical Evaluation of Deflection Amplification Factors for Reinforced Concrete Structures," by H.H.M. Hwang, J-W. Jaw and A.L. Ch'ng, 8/31/89, (PB90-164633, A05, MF-A01).

NCEER-89-0029 "Bedrock Accelerations in Memphis Area Due to Large New Madrid Earthquakes," by H.H.M. Hwang, C.H.S. Chen and G. Yu, 11/7/89, (PB90-162330, A04, MF-A01).

NCEER-89-0030 "Seismic Behavior and Response Sensitivity of Secondary Structural Systems," by Y.Q. Chen and T.T. Soong, 10/23/89, (PB90-164658, A08, MF-A01).

NCEER-89-0031 "Random Vibration and Reliability Analysis of Primary-Secondary Structural Systems," by Y. Ibrahim, M. Grigoriu and T.T. Soong, 11/10/89, (PB90-161951, A04, MF-A01).

NCEER-89-0032 "Proceedings from the Second U.S. - Japan Workshop on Liquefaction, Large Ground Deformation and Their Effects on Lifelines, September 26-29, 1989," Edited by T.D. O'Rourke and M. Hamada, 12/1/89, (PB90-209388, A22, MF-A03).

NCEER-89-0033 "Deterministic Model for Seismic Damage Evaluation of Reinforced Concrete Structures," by J.M. Bracci, A.M. Reinhorn, J.B. Mander and S.K. Kunnath, 9/27/89, (PB91-108803, A06, MF-A01).

NCEER-89-0034 "On the Relation Between Local and Global Damage Indices," by E. DiPasquale and A.S. Cakmak, 8/15/89, (PB90-173865, A05, MF-A01).

NCEER-89-0035 "Cyclic Undrained Behavior of Nonplastic and Low Plasticity Silts," by A.J. Walker and H.E. Stewart, 7/26/89, (PB90-183518, A10, MF-A01).

NCEER-89-0036 "Liquefaction Potential of Surficial Deposits in the City of Buffalo, New York," by M. Budhu, R. Giese and L. Baumgrass, 1/17/89, (PB90-208455, A04, MF-A01).

NCEER-89-0037 "A Deterministic Assessment of Effects of Ground Motion Incoherence," by A.S. Veletsos and Y. Tang, 7/15/89, (PB90-164294, A03, MF-A01).

NCEER-89-0038 "Workshop on Ground Motion Parameters for Seismic Hazard Mapping," July 17-18, 1989, edited by R.V. Whitman, 12/1/89, (PB90-173923, A04, MF-A01).

NCEER-89-0039 "Seismic Effects on Elevated Transit Lines of the New York City Transit Authority," by C.J. Costantino, C.A. Miller and E. Heymsfield, 12/26/89, (PB90-207887, A06, MF-A01).

NCEER-89-0040 "Centrifugal Modeling of Dynamic Soil-Structure Interaction," by K. Weissman, Supervised by J.H. Prevost, 5/10/89, (PB90-207879, A07, MF-A01).

NCEER-89-0041 "Linearized Identification of Buildings With Cores for Seismic Vulnerability Assessment," by I-K. Ho and A.E. Aktan, 11/1/89, (PB90-251943, A07, MF-A01).

NCEER-90-0001 "Geotechnical and Lifeline Aspects of the October 17, 1989 Loma Prieta Earthquake in San Francisco," by T.D. O'Rourke, H.E. Stewart, F.T. Blackburn and T.S. Dickerman, 1/90, (PB90-208596, A05, MF-A01).

NCEER-90-0002 "Nonnormal Secondary Response Due to Yielding in a Primary Structure," by D.C.K. Chen and L.D. Lutes, 2/28/90, (PB90-251976, A07, MF-A01).

NCEER-90-0003 "Earthquake Education Materials for Grades K-12," by K.E.K. Ross, 4/16/90, (PB91-251984, A05, MF-A05). This report has been replaced by NCEER-92-0018.

NCEER-90-0004 "Catalog of Strong Motion Stations in Eastern North America," by R.W. Busby, 4/3/90, (PB90-251984, A05, MF-A01).

NCEER-90-0005 "NCEER Strong-Motion Data Base: A User Manual for the GeoBase Release (Version 1.0 for the Sun3)," by P. Friberg and K. Jacob, 3/31/90 (PB90-258062, A04, MF-A01).

NCEER-90-0006 "Seismic Hazard Along a Crude Oil Pipeline in the Event of an 1811-1812 Type New Madrid Earthquake," by H.H.M. Hwang and C-H.S. Chen, 4/16/90, (PB90-258054, A04, MF-A01).

NCEER-90-0007 "Site-Specific Response Spectra for Memphis Sheahan Pumping Station," by H.H.M. Hwang and C.S. Lee, 5/15/90, (PB91-108811, A05, MF-A01).

NCEER-90-0008 "Pilot Study on Seismic Vulnerability of Crude Oil Transmission Systems," by T. Ariman, R. Dobry, M. Grigoriu, F. Kozin, M. O'Rourke, T. O'Rourke and M. Shinozuka, 5/25/90, (PB91-108837, A06, MF-A01).

NCEER-90-0009 "A Program to Generate Site Dependent Time Histories: EQGEN," by G.W. Ellis, M. Srinivasan and A.S. Cakmak, 1/30/90, (PB91-108829, A04, MF-A01).

NCEER-90-0010 "Active Isolation for Seismic Protection of Operating Rooms," by M.E. Talbott, Supervised by M. Shinozuka, 6/8/9, (PB91-110205, A05, MF-A01).

NCEER-90-0011 "Program LINEARID for Identification of Linear Structural Dynamic Systems," by C-B. Yun and M. Shinozuka, 6/25/90, (PB91-110312, A08, MF-A01).

NCEER-90-0012 "Two-Dimensional Two-Phase Elasto-Plastic Seismic Response of Earth Dams," by A.N. Yiagos, Supervised by J.H. Prevost, 6/20/90, (PB91-110197, A13, MF-A02).

NCEER-90-0013 "Secondary Systems in Base-Isolated Structures: Experimental Investigation, Stochastic Response and Stochastic Sensitivity," by G.D. Manolis, G. Juhn, M.C. Constantinou and A.M. Reinhorn, 7/1/90, (PB91-110320, A08, MF-A01).

NCEER-90-0014 "Seismic Behavior of Lightly-Reinforced Concrete Column and Beam-Column Joint Details," by S.P. Pessiki, C.H. Conley, P. Gergely and R.N. White, 8/22/90, (PB91-108795, A11, MF-A02).

NCEER-90-0015 "Two Hybrid Control Systems for Building Structures Under Strong Earthquakes," by J.N. Yang and A. Danielians, 6/29/90, (PB91-125393, A04, MF-A01).

NCEER-90-0016 "Instantaneous Optimal Control with Acceleration and Velocity Feedback," by J.N. Yang and Z. Li, 6/29/90, (PB91-125401, A03, MF-A01).

NCEER-90-0017 "Reconnaissance Report on the Northern Iran Earthquake of June 21, 1990," by M. Mehrain, 10/4/90, (PB91-125377, A03, MF-A01).

NCEER-90-0018 "Evaluation of Liquefaction Potential in Memphis and Shelby County," by T.S. Chang, P.S. Tang, C.S. Lee and H. Hwang, 8/10/90, (PB91-125427, A09, MF-A01).

NCEER-90-0019 "Experimental and Analytical Study of a Combined Sliding Disc Bearing and Helical Steel Spring Isolation System," by M.C. Constantinou, A.S. Mokha and A.M. Reinhorn, 10/4/90, (PB91-125385, A06, MF-A01). This report is available only through NTIS (see address given above).

NCEER-90-0020 "Experimental Study and Analytical Prediction of Earthquake Response of a Sliding Isolation System with a Spherical Surface," by A.S. Mokha, M.C. Constantinou and A.M. Reinhorn, 10/11/90, (PB91-125419, A05, MF-A01).

NCEER-90-0021 "Dynamic Interaction Factors for Floating Pile Groups," by G. Gazetas, K. Fan, A. Kaynia and E. Kausel, 9/10/90, (PB91-170381, A05, MF-A01).

NCEER-90-0022 "Evaluation of Seismic Damage Indices for Reinforced Concrete Structures," by S. Rodriguez-Gomez and A.S. Cakmak, 9/30/90, PB91-171322, A06, MF-A01).

NCEER-90-0023 "Study of Site Response at a Selected Memphis Site," by H. Desai, S. Ahmad, E.S. Gazetas and M.R. Oh, 10/11/90, (PB91-196857, A03, MF-A01).

NCEER-90-0024 "A User's Guide to Strongmo: Version 1.0 of NCEER's Strong-Motion Data Access Tool for PCs and Terminals," by P.A. Friberg and C.A.T. Susch, 11/15/90, (PB91-171272, A03, MF-A01).

NCEER-90-0025 "A Three-Dimensional Analytical Study of Spatial Variability of Seismic Ground Motions," by L-L. Hong and A.H.-S. Ang, 10/30/90, (PB91-170399, A09, MF-A01).

NCEER-90-0026 "MUMOID User's Guide - A Program for the Identification of Modal Parameters," by S. Rodriguez-Gomez and E. DiPasquale, 9/30/90, (PB91-171298, A04, MF-A01).

NCEER-90-0027 "SARCF-II User's Guide - Seismic Analysis of Reinforced Concrete Frames," by S. Rodriguez-Gomez, Y.S. Chung and C. Meyer, 9/30/90, (PB91-171280, A05, MF-A01).

NCEER-90-0028 "Viscous Dampers: Testing, Modeling and Application in Vibration and Seismic Isolation," by N. Makris and M.C. Constantinou, 12/20/90 (PB91-190561, A06, MF-A01).

NCEER-90-0029 "Soil Effects on Earthquake Ground Motions in the Memphis Area," by H. Hwang, C.S. Lee, K.W. Ng and T.S. Chang, 8/2/90, (PB91-190751, A05, MF-A01).

NCEER-91-0001 "Proceedings from the Third Japan-U.S. Workshop on Earthquake Resistant Design of Lifeline Facilities and Countermeasures for Soil Liquefaction, December 17-19, 1990," edited by T.D. O'Rourke and M. Hamada, 2/1/91, (PB91-179259, A99, MF-A04).

NCEER-91-0002 "Physical Space Solutions of Non-Proportionally Damped Systems," by M. Tong, Z. Liang and G.C. Lee, 1/15/91, (PB91-179242, A04, MF-A01).

NCEER-91-0003 "Seismic Response of Single Piles and Pile Groups," by K. Fan and G. Gazetas, 1/10/91, (PB92-174994, A04, MF-A01).

NCEER-91-0004 "Damping of Structures: Part 1 - Theory of Complex Damping," by Z. Liang and G. Lee, 10/10/91, (PB92-197235, A12, MF-A03).

NCEER-91-0005 "3D-BASIS - Nonlinear Dynamic Analysis of Three Dimensional Base Isolated Structures: Part II," by S. Nagarajaiah, A.M. Reinhorn and M.C. Constantinou, 2/28/91, (PB91-190553, A07, MF-A01). This report has been replaced by NCEER-93-0011.

NCEER-91-0006 "A Multidimensional Hysteretic Model for Plasticity Deforming Metals in Energy Absorbing Devices," by E.J. Graesser and F.A. Cozzarelli, 4/9/91, (PB92-108364, A04, MF-A01).

NCEER-91-0007 "A Framework for Customizable Knowledge-Based Expert Systems with an Application to a KBES for Evaluating the Seismic Resistance of Existing Buildings," by E.G. Ibarra-Anaya and S.J. Fenves, 4/9/91, (PB91-210930, A08, MF-A01).

NCEER-91-0008 "Nonlinear Analysis of Steel Frames with Semi-Rigid Connections Using the Capacity Spectrum Method," by G.G. Deierlein, S-H. Hsieh, Y-J. Shen and J.F. Abel, 7/2/91, (PB92-113828, A05, MF-A01).

NCEER-91-0009 "Earthquake Education Materials for Grades K-12," by K.E.K. Ross, 4/30/91, (PB91-212142, A06, MF-A01). This report has been replaced by NCEER-92-0018.

NCEER-91-0010 "Phase Wave Velocities and Displacement Phase Differences in a Harmonically Oscillating Pile," by N. Makris and G. Gazetas, 7/8/91, (PB92-108356, A04, MF-A01).

NCEER-91-0011 "Dynamic Characteristics of a Full-Size Five-Story Steel Structure and a 2/5 Scale Model," by K.C. Chang, G.C. Yao, G.C. Lee, D.S. Hao and Y.C. Yeh," 7/2/91, (PB93-116648, A06, MF-A02).

NCEER-91-0012 "Seismic Response of a 2/5 Scale Steel Structure with Added Viscoelastic Dampers," by K.C. Chang, T.T. Soong, S-T. Oh and M.L. Lai, 5/17/91, (PB92-110816, A05, MF-A01).

NCEER-91-0013 "Earthquake Response of Retaining Walls; Full-Scale Testing and Computational Modeling," by S. Alampalli and A-W.M. Elgamal, 6/20/91, to be published.

NCEER-91-0014 "3D-BASIS-M: Nonlinear Dynamic Analysis of Multiple Building Base Isolated Structures," by P.C. Tsopelas, S. Nagarajaiah, M.C. Constantinou and A.M. Reinhorn, 5/28/91, (PB92-113885, A09, MF-A02).

NCEER-91-0015 "Evaluation of SEAOC Design Requirements for Sliding Isolated Structures," by D. Theodossiou and M.C. Constantinou, 6/10/91, (PB92-114602, A11, MF-A03).

NCEER-91-0016 "Closed-Loop Modal Testing of a 27-Story Reinforced Concrete Flat Plate-Core Building," by H.R. Somaprasad, T. Toksoy, H. Yoshiyuki and A.E. Aktan, 7/15/91, (PB92-129980, A07, MF-A02).

NCEER-91-0017 "Shake Table Test of a 1/6 Scale Two-Story Lightly Reinforced Concrete Building," by A.G. El-Attar, R.N. White and P. Gergely, 2/28/91, (PB92-222447, A06, MF-A02).

NCEER-91-0018 "Shake Table Test of a 1/8 Scale Three-Story Lightly Reinforced Concrete Building," by A.G. El-Attar, R.N. White and P. Gergely, 2/28/91, (PB93-116630, A08, MF-A02).

NCEER-91-0019 "Transfer Functions for Rigid Rectangular Foundations," by A.S. Veletsos, A.M. Prasad and W.H. Wu, 7/31/91, to be published.

NCEER-91-0020 "Hybrid Control of Seismic-Excited Nonlinear and Inelastic Structural Systems," by J.N. Yang, Z. Li and A. Danielians, 8/1/91, (PB92-143171, A06, MF-A02).

NCEER-91-0021 "The NCEER-91 Earthquake Catalog: Improved Intensity-Based Magnitudes and Recurrence Relations for U.S. Earthquakes East of New Madrid," by L. Seeber and J.G. Armbruster, 8/28/91, (PB92-176742, A06, MF-A02).

NCEER-91-0022 "Proceedings from the Implementation of Earthquake Planning and Education in Schools: The Need for Change - The Roles of the Changemakers," by K.E.K. Ross and F. Winslow, 7/23/91, (PB92-129998, A12, MF-A03).

NCEER-91-0023 "A Study of Reliability-Based Criteria for Seismic Design of Reinforced Concrete Frame Buildings," by H.H.M. Hwang and H-M. Hsu, 8/10/91, (PB92-140235, A09, MF-A02).

NCEER-91-0024 "Experimental Verification of a Number of Structural System Identification Algorithms," by R.G. Ghanem, H. Gavin and M. Shinozuka, 9/18/91, (PB92-176577, A18, MF-A04).

NCEER-91-0025 "Probabilistic Evaluation of Liquefaction Potential," by H.H.M. Hwang and C.S. Lee," 11/25/91, (PB92-143429, A05, MF-A01).

NCEER-91-0026 "Instantaneous Optimal Control for Linear, Nonlinear and Hysteretic Structures - Stable Controllers," by J.N. Yang and Z. Li, 11/15/91, (PB92-163807, A04, MF-A01).

NCEER-91-0027 "Experimental and Theoretical Study of a Sliding Isolation System for Bridges," by M.C. Constantinou, A. Kartoum, A.M. Reinhorn and P. Bradford, 11/15/91, (PB92-176973, A10, MF-A03).

NCEER-92-0001 "Case Studies of Liquefaction and Lifeline Performance During Past Earthquakes, Volume 1: Japanese Case Studies," Edited by M. Hamada and T. O'Rourke, 2/17/92, (PB92-197243, A18, MF-A04).

NCEER-92-0002 "Case Studies of Liquefaction and Lifeline Performance During Past Earthquakes, Volume 2: United States Case Studies," Edited by T. O'Rourke and M. Hamada, 2/17/92, (PB92-197250, A20, MF-A04).

NCEER-92-0003 "Issues in Earthquake Education," Edited by K. Ross, 2/3/92, (PB92-222389, A07, MF-A02).

NCEER-92-0004 "Proceedings from the First U.S. - Japan Workshop on Earthquake Protective Systems for Bridges," Edited by I.G. Buckle, 2/4/92, (PB94-142239, A99, MF-A06).

NCEER-92-0005 "Seismic Ground Motion from a Haskell-Type Source in a Multiple-Layered Half-Space," A.P. Theoharis, G. Deodatis and M. Shinozuka, 1/2/92, to be published.

NCEER-92-0006 "Proceedings from the Site Effects Workshop," Edited by R. Whitman, 2/29/92, (PB92-197201, A04, MF-A01).

NCEER-92-0007 "Engineering Evaluation of Permanent Ground Deformations Due to Seismically-Induced Liquefaction," by M.H. Baziar, R. Dobry and A-W.M. Elgamal, 3/24/92, (PB92-222421, A13, MF-A03).

NCEER-92-0008 "A Procedure for the Seismic Evaluation of Buildings in the Central and Eastern United States," by C.D. Poland and J.O. Malley, 4/2/92, (PB92-222439, A20, MF-A04).

NCEER-92-0009 "Experimental and Analytical Study of a Hybrid Isolation System Using Friction Controllable Sliding Bearings," by M.Q. Feng, S. Fujii and M. Shinozuka, 5/15/92, (PB93-150282, A06, MF-A02).

NCEER-92-0010 "Seismic Resistance of Slab-Column Connections in Existing Non-Ductile Flat-Plate Buildings," by A.J. Durrani and Y. Du, 5/18/92, (PB93-116812, A06, MF-A02).

NCEER-92-0011 "The Hysteretic and Dynamic Behavior of Brick Masonry Walls Upgraded by Ferrocement Coatings Under Cyclic Loading and Strong Simulated Ground Motion," by H. Lee and S.P. Prawel, 5/11/92, to be published.

NCEER-92-0012 "Study of Wire Rope Systems for Seismic Protection of Equipment in Buildings," by G.F. Demetriades, M.C. Constantinou and A.M. Reinhorn, 5/20/92, (PB93-116655, A08, MF-A02).

NCEER-92-0013 "Shape Memory Structural Dampers: Material Properties, Design and Seismic Testing," by P.R. Witting and F.A. Cozzarelli, 5/26/92, (PB93-116663, A05, MF-A01).

NCEER-92-0014 "Longitudinal Permanent Ground Deformation Effects on Buried Continuous Pipelines," by M.J. O'Rourke, and C. Nordberg, 6/15/92, (PB93-116671, A08, MF-A02).

NCEER-92-0015 "A Simulation Method for Stationary Gaussian Random Functions Based on the Sampling Theorem," by M. Grigoriu and S. Balopoulou, 6/11/92, (PB93-127496, A05, MF-A01).

NCEER-92-0016 "Gravity-Load-Designed Reinforced Concrete Buildings: Seismic Evaluation of Existing Construction and Detailing Strategies for Improved Seismic Resistance," by G.W. Hoffmann, S.K. Kunnath, A.M. Reinhorn and J.B. Mander, 7/15/92, (PB94-142007, A08, MF-A02).

NCEER-92-0017 "Observations on Water System and Pipeline Performance in the Limón Area of Costa Rica Due to the April 22, 1991 Earthquake," by M. O'Rourke and D. Ballantyne, 6/30/92, (PB93-126811, A06, MF-A02).

NCEER-92-0018 "Fourth Edition of Earthquake Education Materials for Grades K-12," Edited by K.E.K. Ross, 8/10/92, (PB93-114023, A07, MF-A02).

NCEER-92-0019 "Proceedings from the Fourth Japan-U.S. Workshop on Earthquake Resistant Design of Lifeline Facilities and Countermeasures for Soil Liquefaction," Edited by M. Hamada and T.D. O'Rourke, 8/12/92, (PB93-163939, A99, MF-E11).

NCEER-92-0020 "Active Bracing System: A Full Scale Implementation of Active Control," by A.M. Reinhorn, T.T. Soong, R.C. Lin, M.A. Riley, Y.P. Wang, S. Aizawa and M. Higashino, 8/14/92, (PB93-127512, A06, MF-A02).

NCEER-92-0021 "Empirical Analysis of Horizontal Ground Displacement Generated by Liquefaction-Induced Lateral Spreads," by S.F. Bartlett and T.L. Youd, 8/17/92, (PB93-188241, A06, MF-A02).

NCEER-92-0022 "IDARC Version 3.0: Inelastic Damage Analysis of Reinforced Concrete Structures," by S.K. Kunnath, A.M. Reinhorn and R.F. Lobo, 8/31/92, (PB93-227502, A07, MF-A02).

NCEER-92-0023 "A Semi-Empirical Analysis of Strong-Motion Peaks in Terms of Seismic Source, Propagation Path and Local Site Conditions, by M. Kamiyama, M.J. O'Rourke and R. Flores-Berrones, 9/9/92, (PB93-150266, A08, MF-A02).

NCEER-92-0024 "Seismic Behavior of Reinforced Concrete Frame Structures with Nonductile Details, Part I: Summary of Experimental Findings of Full Scale Beam-Column Joint Tests," by A. Beres, R.N. White and P. Gergely, 9/30/92, (PB93-227783, A05, MF-A01).

NCEER-92-0025 "Experimental Results of Repaired and Retrofitted Beam-Column Joint Tests in Lightly Reinforced Concrete Frame Buildings," by A. Beres, S. El-Borgi, R.N. White and P. Gergely, 10/29/92, (PB93-227791, A05, MF-A01).

NCEER-92-0026 "A Generalization of Optimal Control Theory: Linear and Nonlinear Structures," by J.N. Yang, Z. Li and S. Vongchavalitkul, 11/2/92, (PB93-188621, A05, MF-A01).

NCEER-92-0027 "Seismic Resistance of Reinforced Concrete Frame Structures Designed Only for Gravity Loads: Part I - Design and Properties of a One-Third Scale Model Structure," by J.M. Bracci, A.M. Reinhorn and J.B. Mander, 12/1/92, (PB94-104502, A08, MF-A02).

NCEER-92-0028 "Seismic Resistance of Reinforced Concrete Frame Structures Designed Only for Gravity Loads: Part II - Experimental Performance of Subassemblages," by L.E. Aycardi, J.B. Mander and A.M. Reinhorn, 12/1/92, (PB94-104510, A08, MF-A02).

NCEER-92-0029 "Seismic Resistance of Reinforced Concrete Frame Structures Designed Only for Gravity Loads: Part III - Experimental Performance and Analytical Study of a Structural Model," by J.M. Bracci, A.M. Reinhorn and J.B. Mander, 12/1/92, (PB93-227528, A09, MF-A01).

NCEER-92-0030 "Evaluation of Seismic Retrofit of Reinforced Concrete Frame Structures: Part I - Experimental Performance of Retrofitted Subassemblages," by D. Choudhuri, J.B. Mander and A.M. Reinhorn, 12/8/92, (PB93-198307, A07, MF-A02).

NCEER-92-0031 "Evaluation of Seismic Retrofit of Reinforced Concrete Frame Structures: Part II - Experimental Performance and Analytical Study of a Retrofitted Structural Model," by J.M. Bracci, A.M. Reinhorn and J.B. Mander, 12/8/92, (PB93-198315, A09, MF-A03).

NCEER-92-0032 "Experimental and Analytical Investigation of Seismic Response of Structures with Supplemental Fluid Viscous Dampers," by M.C. Constantinou and M.D. Symans, 12/21/92, (PB93-191435, A10, MF-A03).

NCEER-92-0033 "Reconnaissance Report on the Cairo, Egypt Earthquake of October 12, 1992," by M. Khater, 12/23/92, (PB93-188621, A03, MF-A01).

NCEER-92-0034 "Low-Level Dynamic Characteristics of Four Tall Flat-Plate Buildings in New York City," by H. Gavin, S. Yuan, J. Grossman, E. Pekelis and K. Jacob, 12/28/92, (PB93-188217, A07, MF-A02).

NCEER-93-0001 "An Experimental Study on the Seismic Performance of Brick-Infilled Steel Frames With and Without Retrofit," by J.B. Mander, B. Nair, K. Wojtkowski and J. Ma, 1/29/93, (PB93-227510, A07, MF-A02).

NCEER-93-0002 "Social Accounting for Disaster Preparedness and Recovery Planning," by S. Cole, E. Pantoja and V. Razak, 2/22/93, (PB94-142114, A12, MF-A03).

NCEER-93-0003 "Assessment of 1991 NEHRP Provisions for Nonstructural Components and Recommended Revisions," by T.T. Soong, G. Chen, Z. Wu, R-H. Zhang and M. Grigoriu, 3/1/93, (PB93-188639, A06, MF-A02).

NCEER-93-0004 "Evaluation of Static and Response Spectrum Analysis Procedures of SEAOC/UBC for Seismic Isolated Structures," by C.W. Winters and M.C. Constantinou, 3/23/93, (PB93-198299, A10, MF-A03).

NCEER-93-0005 "Earthquakes in the Northeast - Are We Ignoring the Hazard? A Workshop on Earthquake Science and Safety for Educators," edited by K.E.K. Ross, 4/2/93, (PB94-103066, A09, MF-A02).

NCEER-93-0006 "Inelastic Response of Reinforced Concrete Structures with Viscoelastic Braces," by R.F. Lobo, J.M. Bracci, K.L. Shen, A.M. Reinhorn and T.T. Soong, 4/5/93, (PB93-227486, A05, MF-A02).

NCEER-93-0007 "Seismic Testing of Installation Methods for Computers and Data Processing Equipment," by K. Kosar, T.T. Soong, K.L. Shen, J.A. HoLung and Y.K. Lin, 4/12/93, (PB93-198299, A07, MF-A02).

NCEER-93-0008 "Retrofit of Reinforced Concrete Frames Using Added Dampers," by A. Reinhorn, M. Constantinou and C. Li, to be published.

NCEER-93-0009 "Seismic Behavior and Design Guidelines for Steel Frame Structures with Added Viscoelastic Dampers," by K.C. Chang, M.L. Lai, T.T. Soong, D.S. Hao and Y.C. Yeh, 5/1/93, (PB94-141959, A07, MF-A02).

NCEER-93-0010 "Seismic Performance of Shear-Critical Reinforced Concrete Bridge Piers," by J.B. Mander, S.M. Waheed, M.T.A. Chaudhary and S.S. Chen, 5/12/93, (PB93-227494, A08, MF-A02).

NCEER-93-0011 "3D-BASIS-TABS: Computer Program for Nonlinear Dynamic Analysis of Three Dimensional Base Isolated Structures," by S. Nagarajaiah, C. Li, A.M. Reinhorn and M.C. Constantinou, 8/2/93, (PB94-141819, A09, MF-A02).

NCEER-93-0012 "Effects of Hydrocarbon Spills from an Oil Pipeline Break on Ground Water," by O.J. Helweg and H.H.M. Hwang, 8/3/93, (PB94-141942, A06, MF-A02).

NCEER-93-0013 "Simplified Procedures for Seismic Design of Nonstructural Components and Assessment of Current Code Provisions," by M.P. Singh, L.E. Suarez, E.E. Matheu and G.O. Maldonado, 8/4/93, (PB94-141827, A09, MF-A02).

NCEER-93-0014 "An Energy Approach to Seismic Analysis and Design of Secondary Systems," by G. Chen and T.T. Soong, 8/6/93, (PB94-142767, A11, MF-A03).

NCEER-93-0015 "Proceedings from School Sites: Becoming Prepared for Earthquakes - Commemorating the Third Anniversary of the Loma Prieta Earthquake," Edited by F.E. Winslow and K.E.K. Ross, 8/16/93, (PB94-154275, A16, MF-A02).

NCEER-93-0016 "Reconnaissance Report of Damage to Historic Monuments in Cairo, Egypt Following the October 12, 1992 Dahshur Earthquake," by D. Sykora, D. Look, G. Croci, E. Karaesmen and E. Karaesmen, 8/19/93, (PB94-142221, A08, MF-A02).

NCEER-93-0017 "The Island of Guam Earthquake of August 8, 1993," by S.W. Swan and S.K. Harris, 9/30/93, (PB94-141843, A04, MF-A01).

NCEER-93-0018 "Engineering Aspects of the October 12, 1992 Egyptian Earthquake," by A.W. Elgamal, M. Amer, K. Adalier and A. Abul-Fadl, 10/7/93, (PB94-141983, A05, MF-A01).

NCEER-93-0019 "Development of an Earthquake Motion Simulator and its Application in Dynamic Centrifuge Testing," by I. Krstelj, Supervised by J.H. Prevost, 10/23/93, (PB94-181773, A-10, MF-A03).

NCEER-93-0020 "NCEER-Taisei Corporation Research Program on Sliding Seismic Isolation Systems for Bridges: Experimental and Analytical Study of a Friction Pendulum System (FPS)," by M.C. Constantinou, P. Tsopelas, Y-S. Kim and S. Okamoto, 11/1/93, (PB94-142775, A08, MF-A02).

NCEER-93-0021 "Finite Element Modeling of Elastomeric Seismic Isolation Bearings," by L.J. Billings, Supervised by R. Shepherd, 11/8/93, to be published.

NCEER-93-0022 "Seismic Vulnerability of Equipment in Critical Facilities: Life-Safety and Operational Consequences," by K. Porter, G.S. Johnson, M.M. Zadeh, C. Scawthorn and S. Eder, 11/24/93, (PB94-181765, A16, MF-A03).

NCEER-93-0023 "Hokkaido Nansei-oki, Japan Earthquake of July 12, 1993, by P.I. Yanev and C.R. Scawthorn, 12/23/93, (PB94-181500, A07, MF-A01).

NCEER-94-0001 "An Evaluation of Seismic Serviceability of Water Supply Networks with Application to the San Francisco Auxiliary Water Supply System," by I. Markov, Supervised by M. Grigoriu and T. O'Rourke, 1/21/94, (PB94-204013, A07, MF-A02).

NCEER-94-0002 "NCEER-Taisei Corporation Research Program on Sliding Seismic Isolation Systems for Bridges: Experimental and Analytical Study of Systems Consisting of Sliding Bearings, Rubber Restoring Force Devices and Fluid Dampers," Volumes I and II, by P. Tsopelas, S. Okamoto, M.C. Constantinou, D. Ozaki and S. Fujii, 2/4/94, (PB94-181740, A09, MF-A02 and PB94-181757, A12, MF-A03).

NCEER-94-0003 "A Markov Model for Local and Global Damage Indices in Seismic Analysis," by S. Rahman and M. Grigoriu, 2/18/94, (PB94-206000, A12, MF-A03).

NCEER-94-0004 "Proceedings from the NCEER Workshop on Seismic Response of Masonry Infills," edited by D.P. Abrams, 3/1/94, (PB94-180783, A07, MF-A02).

NCEER-94-0005 "The Northridge, California Earthquake of January 17, 1994: General Reconnaissance Report," edited by J.D. Goltz, 3/11/94, (PB193943, A10, MF-A03).

NCEER-94-0006 "Seismic Energy Based Fatigue Damage Analysis of Bridge Columns: Part I - Evaluation of Seismic Capacity," by G.A. Chang and J.B. Mander, 3/14/94, (PB94-219185, A11, MF-A03).

NCEER-94-0007 "Seismic Isolation of Multi-Story Frame Structures Using Spherical Sliding Isolation Systems," by T.M. Al-Hussaini, V.A. Zayas and M.C. Constantinou, 3/17/94, (PB193745, A09, MF-A02).

NCEER-94-0008 "The Northridge, California Earthquake of January 17, 1994: Performance of Highway Bridges," edited by I.G. Buckle, 3/24/94, (PB94-193851, A06, MF-A02).

NCEER-94-0009 "Proceedings of the Third U.S.-Japan Workshop on Earthquake Protective Systems for Bridges," edited by I.G. Buckle and I. Friedland, 3/31/94, (PB94-195815, A99, MF-A06).

NCEER-94-0010 "3D-BASIS-ME: Computer Program for Nonlinear Dynamic Analysis of Seismically Isolated Single and Multiple Structures and Liquid Storage Tanks," by P.C. Tsopelas, M.C. Constantinou and A.M. Reinhorn, 4/12/94, (PB94-204922, A09, MF-A02).

NCEER-94-0011 "The Northridge, California Earthquake of January 17, 1994: Performance of Gas Transmission Pipelines," by T.D. O'Rourke and M.C. Palmer, 5/16/94, (PB94-204989, A05, MF-A01).

NCEER-94-0012 "Feasibility Study of Replacement Procedures and Earthquake Performance Related to Gas Transmission Pipelines," by T.D. O'Rourke and M.C. Palmer, 5/25/94, (PB94-206638, A09, MF-A02).

NCEER-94-0013 "Seismic Energy Based Fatigue Damage Analysis of Bridge Columns: Part II - Evaluation of Seismic Demand," by G.A. Chang and J.B. Mander, 6/1/94, (PB95-18106, A08, MF-A02).

NCEER-94-0014 "NCEER-Taisei Corporation Research Program on Sliding Seismic Isolation Systems for Bridges: Experimental and Analytical Study of a System Consisting of Sliding Bearings and Fluid Restoring Force/Damping Devices," by P. Tsopelas and M.C. Constantinou, 6/13/94, (PB94-219144, A10, MF-A03).

NCEER-94-0015 "Generation of Hazard-Consistent Fragility Curves for Seismic Loss Estimation Studies," by H. Hwang and J-R. Huo, 6/14/94, (PB95-181996, A09, MF-A02).

NCEER-94-0016 "Seismic Study of Building Frames with Added Energy-Absorbing Devices," by W.S. Pong, C.S. Tsai and G.C. Lee, 6/20/94, (PB94-219136, A10, A03).

NCEER-94-0017 "Sliding Mode Control for Seismic-Excited Linear and Nonlinear Civil Engineering Structures," by J. Yang, J. Wu, A. Agrawal and Z. Li, 6/21/94, (PB95-138483, A06, MF-A02).

NCEER-94-0018 "3D-BASIS-TABS Version 2.0: Computer Program for Nonlinear Dynamic Analysis of Three Dimensional Base Isolated Structures," by A.M. Reinhorn, S. Nagarajaiah, M.C. Constantinou, P. Tsopelas and R. Li, 6/22/94, (PB95-182176, A08, MF-A02).

NCEER-94-0019 "Proceedings of the International Workshop on Civil Infrastructure Systems: Application of Intelligent Systems and Advanced Materials on Bridge Systems," Edited by G.C. Lee and K.C. Chang, 7/18/94, (PB95-252474, A20, MF-A04).

NCEER-94-0020 "Study of Seismic Isolation Systems for Computer Floors," by V. Lambrou and M.C. Constantinou, 7/19/94, (PB95-138533, A10, MF-A03).

NCEER-94-0021 "Proceedings of the U.S.-Italian Workshop on Guidelines for Seismic Evaluation and Rehabilitation of Unreinforced Masonry Buildings," Edited by D.P. Abrams and G.M. Calvi, 7/20/94, (PB95-138749, A13, MF-A03).

NCEER-94-0022 "NCEER-Taisei Corporation Research Program on Sliding Seismic Isolation Systems for Bridges: Experimental and Analytical Study of a System Consisting of Lubricated PTFE Sliding Bearings and Mild Steel Dampers," by P. Tsopelas and M.C. Constantinou, 7/22/94, (PB95-182184, A08, MF-A02).

NCEER-94-0023 "Development of Reliability-Based Design Criteria for Buildings Under Seismic Load," by Y.K. Wen, H. Hwang and M. Shinozuka, 8/1/94, (PB95-211934, A08, MF-A02).

NCEER-94-0024 "Experimental Verification of Acceleration Feedback Control Strategies for an Active Tendon System," by S.J. Dyke, B.F. Spencer, Jr., P. Quast, M.K. Sain, D.C. Kaspari, Jr. and T.T. Soong, 8/29/94, (PB95-212320, A05, MF-A01).

NCEER-94-0025 "Seismic Retrofitting Manual for Highway Bridges," Edited by I.G. Buckle and I.F. Friedland, published by the Federal Highway Administration (PB95-212676, A15, MF-A03).

NCEER-94-0026 "Proceedings from the Fifth U.S.-Japan Workshop on Earthquake Resistant Design of Lifeline Facilities and Countermeasures Against Soil Liquefaction," Edited by T.D. O'Rourke and M. Hamada, 11/7/94, (PB95-220802, A99, MF-E08).

NCEER-95-0001 "Experimental and Analytical Investigation of Seismic Retrofit of Structures with Supplemental Damping: Part 1 - Fluid Viscous Damping Devices," by A.M. Reinhorn, C. Li and M.C. Constantinou, 1/3/95, (PB95-266599, A09, MF-A02).

NCEER-95-0002 "Experimental and Analytical Study of Low-Cycle Fatigue Behavior of Semi-Rigid Top-And-Seat Angle Connections," by G. Pekcan, J.B. Mander and S.S. Chen, 1/5/95, (PB95-220042, A07, MF-A02).

NCEER-95-0003 "NCEER-ATC Joint Study on Fragility of Buildings," by T. Anagnos, C. Rojahn and A.S. Kiremidjian, 1/20/95, (PB95-220026, A06, MF-A02).

NCEER-95-0004 "Nonlinear Control Algorithms for Peak Response Reduction," by Z. Wu, T.T. Soong, V. Gattulli and R.C. Lin, 2/16/95, (PB95-220349, A05, MF-A01).

NCEER-95-0005 "Pipeline Replacement Feasibility Study: A Methodology for Minimizing Seismic and Corrosion Risks to Underground Natural Gas Pipelines," by R.T. Eguchi, H.A. Seligson and D.G. Honegger, 3/2/95, (PB95-252326, A06, MF-A02).

NCEER-95-0006 "Evaluation of Seismic Performance of an 11-Story Frame Building During the 1994 Northridge Earthquake," by F. Naeim, R. DiSulio, K. Benuska, A. Reinhorn and C. Li, to be published.

NCEER-95-0007 "Prioritization of Bridges for Seismic Retrofitting," by N. Basöz and A.S. Kiremidjian, 4/24/95, (PB95-252300, A08, MF-A02).

NCEER-95-0008 "Method for Developing Motion Damage Relationships for Reinforced Concrete Frames," by A. Singhal and A.S. Kiremidjian, 5/11/95, (PB95-266607, A06, MF-A02).

NCEER-95-0009 "Experimental and Analytical Investigation of Seismic Retrofit of Structures with Supplemental Damping: Part II - Friction Devices," by C. Li and A.M. Reinhorn, 7/6/95, (PB96-128087, A11, MF-A03).

NCEER-95-0010 "Experimental Performance and Analytical Study of a Non-Ductile Reinforced Concrete Frame Structure Retrofitted with Elastomeric Spring Dampers," by G. Pekcan, J.B. Mander and S.S. Chen, 7/14/95, (PB96-137161, A08, MF-A02).

NCEER-95-0011 "Development and Experimental Study of Semi-Active Fluid Damping Devices for Seismic Protection of Structures," by M.D. Symans and M.C. Constantinou, 8/3/95, (PB96-136940, A23, MF-A04).

NCEER-95-0012 "Real-Time Structural Parameter Modification (RSPM): Development of Innervated Structures," by Z. Liang, M. Tong and G.C. Lee, 4/11/95, (PB96-137153, A06, MF-A01).

NCEER-95-0013 "Experimental and Analytical Investigation of Seismic Retrofit of Structures with Supplemental Damping: Part III - Viscous Damping Walls," by A.M. Reinhorn and C. Li, 10/1/95, (PB96-176409, A11, MF-A03).

NCEER-95-0014 "Seismic Fragility Analysis of Equipment and Structures in a Memphis Electric Substation," by J-R. Huo and H.H.M. Hwang, (PB96-128087, A09, MF-A02), 8/10/95.

NCEER-95-0015 "The Hanshin-Awaji Earthquake of January 17, 1995: Performance of Lifelines," Edited by M. Shinozuka, 11/3/95, (PB96-176383, A15, MF-A03).

NCEER-95-0016 "Highway Culvert Performance During Earthquakes," by T.L. Youd and C.J. Beckman, available as NCEER-96-0015.

NCEER-95-0017 "The Hanshin-Awaji Earthquake of January 17, 1995: Performance of Highway Bridges," Edited by I.G. Buckle, 12/1/95, to be published.

NCEER-95-0018 "Modeling of Masonry Infill Panels for Structural Analysis," by A.M. Reinhorn, A. Madan, R.E. Valles, Y. Reichmann and J.B. Mander, 12/8/95.

NCEER-95-0019 "Optimal Polynomial Control for Linear and Nonlinear Structures," by A.K. Agrawal and J.N. Yang, 12/11/95, (PB96-168737, A07, MF-A02).

NCEER-95-0020 "Retrofit of Non-Ductile Reinforced Concrete Frames Using Friction Dampers," by R.S. Rao, P. Gergely and R.N. White, 12/22/95.

NCEER-95-0021 "Parametric Results for Seismic Response of Pile-Supported Bridge Bents," by G. Mylonakis, A. Nikolaou and G. Gazetas, 12/22/95, (PB97-100242, A12, MF-A03).

NCEER-95-0022 "Kinematic Bending Moments in Seismically Stressed Piles," by A. Nikolaou, G. Mylonakis and G. Gazetas, 12/23/95.

NCEER-96-0001 "Dynamic Response of Unreinforced Masonry Buildings with Flexible Diaphragms," by A.C. Costley and D.P. Abrams," 10/10/96.

NCEER-96-0002 "State of the Art Review: Foundations and Retaining Structures," by I. Po Lam, to be published.

NCEER-96-0003 "Ductility of Rectangular Reinforced Concrete Bridge Columns with Moderate Confinement," by N Wehbe, M. Saiidi, D. Sanders and B. Douglas, 11/7/96.

NCEER-96-0004 "Proceedings of the Long-Span Bridge Seismic Research Workshop," edited by I.G. Buckle and I.M. Friedland, to be published.

NCEER-96-0005 "Establish Representative Pier Types for Comprehensive Study: Eastern United States," by J. Kulicki and Z. Prucz, 5/28/96.

NCEER-96-0006 "Establish Representative Pier Types for Comprehensive Study: Western United States," by R. Imbsen, R.A. Schamber and T.A. Osterkamp, 5/28/96.

NCEER-96-0007 "Nonlinear Control Techniques for Dynamical Systems with Uncertain Parameters," by R.G. Ghanem and M.I. Bujakov, 5/27/96, (PB97-100259, A17, MF-A03).

NCEER-96-0008 "Seismic Evaluation of a 30-Year Old Non-Ductile Highway Bridge Pier and Its Retrofit," by J.B. Mander, B. Mahmoodzadegan, S. Bhadra and S.S. Chen, 5/31/96.

NCEER-96-0009 "Seismic Performance of a Model Reinforced Concrete Bridge Pier Before and After Retrofit," by J.B. Mander, J.H. Kim and C.A. Ligozio, 5/31/96.

NCEER-96-0010 "IDARC2D Version 4.0: A Computer Program for the Inelastic Damage Analysis of Buildings," by R.E. Valles, A.M. Reinhorn, S.K. Kunnath, C. Li and A. Madan, 6/3/96, (PB97-100234, A17, MF-A03).

NCEER-96-0011 "Estimation of the Economic Impact of Multiple Lifeline Disruption: Memphis Light, Gas and Water Division Case Study," by S.E. Chang, H.A. Seligson and R.T. Eguchi, 8/16/96.

NCEER-96-0012 "Proceedings from the Sixth Japan-U.S. Workshop on Earthquake Resistant Design of Lifeline Facilities and Countermeasures Against Soil Liquefaction, Edited by M. Hamada and T. O'Rourke, 9/11/96.

NCEER-96-0013 "Chemical Hazards, Mitigation and Preparedness in Areas of High Seismic Risk: A Methodology for Estimating the Risk of Post-Earthquake Hazardous Materials Release," by H.A. Seligson, R.T. Eguchi, K.J. Tierney and K. Richmond, 11/7/96.

NCEER-96-0014 "Response of Steel Bridge Bearings to Reversed Cyclic Loading," by J.B. Mander, D-K. Kim, S.S. Chen and G.J. Premus, 11/13/96.

NCEER-96-0015 "Highway Culvert Performance During Past Earthquakes," by T.L. Youd and C.J. Beckman, 11/25/96.

NCEER-97-0001 "Evaluation, Prevention and Mitigation of Pounding Effects in Building Structures," by R.E. Valles and A.M. Reinhorn, 2/20/97.